Estimating Regional Nitrous Oxide Emissions Using Isotopic Ratio Observations and a Bayesian Inverse Framework

by

Michael James McClellan

B.A. Chemistry
Carleton College, 2013

Submitted to the Department of Earth, Atmospheric, and Planetary Sciences in partial fulfillment of the requirements for the degree of

Doctor of Philosophy in Atmospheric Science

at the

MASSACHUSETTS INSTITUTE OF TECHNOLOGY

September 2018

© Massachusetts Institute of Technology 2018. All rights reserved.

Signature redacted

Author .....
Department of Earth, Atmospheric, and Planetary Sciences
August 15, 2018

Signature redacted

Certified by .....
Ronald G. Prinn
TEPCO Professor of Atmospheric Science
Thesis Supervisor

Signature redacted

Accepted by .....
Robert D. van der Hilst
Schlumberger Professor of Earth and Planetary Sciences
Head of Department

MASSACHUSETTS INSTITUTE OF TECHNOLOGY
SEP 11 2018
LIBRARIES
ARCHIVES

Estimating Regional Nitrous Oxide Emissions Using Isotopic Ratio Observations and a Bayesian Inverse Framework

by
Michael James McClellan

Submitted to the Department of Earth, Atmospheric, and Planetary Sciences
on August 15, 2018, in partial fulfillment of the
requirements for the degree of
Doctor of Philosophy in Atmospheric Science

Abstract

Atmospheric nitrous oxide (N_2O) significantly impacts Earth's climate due to its dual role as an inert potent greenhouse gas in the troposphere and as a reactive source of ozone-destroying nitrogen oxides in the stratosphere. Global atmospheric concentrations of N_2O, produced by natural and anthropogenic processes, continue to rise due to increases in emissions linked to human activity. The understanding of the impact of this gas is incomplete as there remain significant uncertainties in its global budget. The experiment described in this thesis, in which a global chemical transport model (MOZART-4), a fine-scale regional Lagrangian model (NAME), and new high-frequency atmospheric observations are combined, shows that uncertainty in N_2O emissions estimates can be reduced in areas with continuous monitoring of N_2O mole fraction and site-specific isotopic ratios.

Due to unique heavy-atom (^{15}N and ^{18}O) isotopic substitutions made by different N_2O sources, the measurement of N_2O isotopic ratios in ambient air can help identify the distribution and magnitude of distinct sources. The new Stheno-TILDAS continuous wave laser spectroscopy instrument developed at MIT, recently installed at the Mace Head Atmospheric Research Station in western Ireland, can produce high-frequency timelines of atmospheric N_2O isotopic ratios that can be compared to contemporaneous trends in correlative trace gas mole fractions and NAME-based statistical distributions of the origin of air sampled at the station. This combination leads to apportionment of the relative contribution from five major N_2O sectors in the European region (agriculture, oceans, natural soils, industry, and biomass burning) plus well-mixed air transported from long distances to the atmospheric N_2O measured at Mace Head.

Bayesian inverse modeling methods that compare N_2O mole fraction and isotopic ratio observations at Mace Head and at Dübendorf, Switzerland to simulated conditions produced using NAME and MOZART-4 lead to an optimized set of source-specific N_2O emissions estimates in the NAME Europe domain. Notably, this inverse modeling experiment leads to a significant decrease in uncertainty in summertime emissions for the four largest sectors in Europe, and shows that industrial and agricultural N_2O emissions in Europe are underestimated in inventories such as EDGAR v4.3.2. This experiment sets up future work that will be able to help constrain global estimates of N_2O emissions once additional isotopic observations are made in other global locations and integrated into the NAME-MOZART inverse modeling framework described in this thesis.

Thesis Supervisor: Ronald G. Prinn
Title: TEPCO Professor of Atmospheric Science

Acknowledgments

This work would not have been possible without the support of many people and external sources. This project was supported by NASA Grants NNX11AF17G and NNX16AC98G, and NSF Grant 0959280 MRI-I2, all to MIT. In my first year at MIT, I was generously supported by a Rasmussen Foundation Fellowship. The MIT Center for Global Change Science and the MIT Department of Earth, Atmospheric, and Planetary Sciences provided use of their facilities and additional support.

The most novel—and therefore most interesting—aspects of this thesis involve collecting and subsequently analyzing N_2O isotopic ratios at Mace Head, Ireland; an entire team of people were necessary to make this experiment happen. Eliza Harris (previously at MIT and EMPA, now at the University of Innsbruck) developed the first version of the Stheno-TILDAS analysis software, including the original scripts used to process data at Mace Head and similar data from EMPA. Her guidance over email during my summer at Mace Head (June-August 2014) was what enabled necessary "just-in-time" corrections to the Stheno-TILDAS operating procedure for accurate sampling of ambient air while there. In addition to being my two-time travel partner from Boston to Mace Head, Bill Olszewski provided crucial technical support at all points throughout the Stheno-TILDAS project, including the original development of the instrument and its rebuild efforts. Gerry Spain (National University of Ireland, Galway) provided critical instrumental support at Mace Head and facilitated many important aspects of my three-month stay in Ireland, including a long-term bike rental to help mitigate the fact that I was too young to rent a car in the Republic of Ireland. Alistair Manning (UK Met Office) and Anita Ganesan (University of Bristol) informed the interpretation of NAME surface sensitivity footprints, crucial tools for analyzing Stheno-TILDAS observations in the context of European N_2O emissions.

The members of my thesis defense committee have all provided guidance in specific areas, and my academic research experience has been richer due to the relationships I have built with each of them. Shuhei Ono helped secure initial funding for Stheno-TILDAS development, arranged for the delivery of key components to Mace Head in summer 2014, and provided feedback on instrument-based components of this experiment. Eri Saikawa (Emory University) shared many components of her inverse modeling experiment, published in 2014, that became the bedrock for all chemical transport model simulations conducted in this entire thesis. Matt Rigby (University of Bristol) provided invaluable advice for all inverse modeling components of this experiment. Susan Solomon has been a constant source of both specific information about the role of the stratosphere in the N_2O earth system, and general guidance on my potential to positively impact the world through scientific research. Ron Prinn, my advisor for this project, provided critical guidance throughout every step of the experiment, and I cannot thank him enough for the professional and personal support while at MIT.

There have also been many people who have made my experience at MIT outside of the classroom and laboratory special. My officemates throughout the years have made every day an adventure: Charles Gertler, Martin Wolf, Maria Zawadowicz, Sarvesh Garimella, Jimmy

Gasore, and everyone else who called 54-1320 "home" while I was there. I moved into a different apartment every year while at MIT, but that allowed me to find some truly exceptional roommates and life-long friends, especially Sam Silva, Devon Bracher, and Phoebe the Labrador Retriever. The MIT EAPS community, especially my fellow 2013 first-years Sandy Shedd and Erik Lindgren, helped bring a smile to my face during every ride on the Green Building elevators. I was honored to work alongside Eva Golos, Affi Maragh, Kyle Kotowick, and many other talented student leaders in my years of involvement with the Graduate Student Council. At two crucial turning points in my career thus far, Deborah Gross (my undergraduate research advisor at Carleton College) and Charles Ichoku (my summer mentor at NASA Goddard Space Flight Center) helped me gain clarity on uncertain areas of my future. My fellow baseball toolBOX project members, Colin Thackray, Dan Congreve, and Vince Agard helped steer me toward novel ways to apply my knowledge in science and engineering. And finally, I must extend wholehearted gratitude to my grandparents, parents, siblings, extended family, and "bonus" family (the Stills) for keeping me humble and keeping me motivated.

Contents

1 Introduction **19**
1.1 Problem Statement 22
1.2 Research Goals and Approach 26
1.2.1 Continuous *in situ* Observations 26
1.2.2 Regional Lagrangian Dispersion Models 27
1.2.3 Global Chemical Transport Models 29
1.2.4 Inverse Modeling with N_2O Isotopic Observations and Atmospheric Models 29
1.3 Summary of Major Thesis Findings 30

2 Nitrous Oxide and Isotopic Chemistry **33**
2.1 Physical Properties 33
2.2 Sources and Sinks 34
2.3 Stratospheric Sink and Lifetime 35
2.4 Radiative Impact and Ozone Depletion 36
2.5 Isotopic Chemistry 36
2.6 Isotopic Signatures in Sources 39
2.7 Isotopic Signatures from Stratospheric Sink 40
2.8 Uncertainty in N_2O Isotopic Ratios 43

3 Nitrous Oxide Isotopic Analysis **45**
3.1 Initial N_2O Isotopologue Measurements 46
3.1.1 Offline vs Online Analysis 46
3.1.2 Mass Spectrometry 47
3.1.3 Laser Spectroscopy 47
3.2 Isotopic N_2O Observations at Mace Head, Ireland using Stheno-TILDAS . . 48
3.2.1 Mace Head Atmospheric Research Station 48
3.2.2 Observations from 2010 49
3.2.3 North Atlantic Oscillation 49
3.3 Stheno-TILDAS Instrument 50
3.3.1 Experimental Procedure 53
3.4 Experimental Best Practices 54
3.4.1 Isotopic Standard Gases 55

3.4.2 Instrument Intercomparisons 55
3.5 Observations at Mace Head, Ireland (Summer 2014) 55
3.5.1 Interpretation of Stheno-TILDAS Timelines 57
3.5.2 Experimental Issues from 2014-2015 58
3.6 Future Operation of Stheno-TILDAS 58
3.7 Summary 59

4 Analysis of 2014-2015 Stheno-TILDAS Observations 61
4.1 Comparison to Past Analysis at MHD 62
4.2 Trace Gas Measurements 63
4.3 Source Attribution from Isotopic Composition Observations 66
4.4 NAME Inert Tracer Sensitivity "Footprints" 71
4.5 Source Attribution using NAME Lagrangian Footprints 73
4.6 Limitations of Event-Based Analysis 76
4.7 Summary 76

5 Global Atmospheric Chemical Transport Modeling 79
5.1 Chemical Transport Models 79
5.1.1 MOZART-4 Model 80
5.1.2 Input Data for MOZART-4 N_2O Modeling 80
5.1.3 Model Output Interpretation 81
5.2 Modeling Atmospheric N_2O 81
5.2.1 Meteorological Inputs 81
5.2.2 Initial Conditions 83
5.2.3 N_2O Emissions Estimates 83
5.2.4 Chemical Destruction of N_2O 84
5.2.5 Results from Saikawa et al. (2014) Extension to 2014-2015 85
5.3 Addition of Isotopic Chemistry 88
5.3.1 Isotopically Differentiated Initial Conditions 88
5.3.2 Isotopically Differentiated Emissions 89
5.3.3 Isotopically Differentiated Chemical Destruction 91
5.3.4 Spin-up with Isotopic Chemistry 92
5.3.5 MOZART-4 Simulated N_2O Isotopic Ratios in 2014-2015 93
5.4 Summary 98

6 Inverse Modeling 101
6.1 Bayesian Inverse Methodology 101
6.2 NAME-MOZART N_2O Isotopic Simulation 104
6.2.1 Input Data for NAME-MOZART N_2O Modeling 104
6.2.2 NAME-MOZART with Bulk N_2O Mole Fraction 105
6.2.3 Isotopically Differentiated NAME-MOZART 109
6.3 Inverse Modeling with NAME-MOZART 113
6.3.1 Inversion by Spatial Location 115

6.3.2 Inversion by Emissions Sector 118
6.4 Future Improvements to Inverse Modeling 129
6.5 Summary 132

7 Conclusions and Future Work **133**
7.1 Conclusions 133
7.2 Future Work 135
7.2.1 Observations 136
7.2.2 Global Forward Modeling 138
7.2.3 Global Inverse Modeling 138
7.3 Closing Thoughts 140

A Community Intercomparison Suite **149**
A.1 Simulation of Flight Data in West Africa 149

B Inversion by Source Sector Isotopic Signature **155**
B.1 Inversion Setup 155

List of Figures

1-1 "Nitrous oxide for a dental operation. Anaesthetics and their administration (1922)" `https://wellcomecollection.org/works/fh4j7zdr`. Copyrighted work available under Creative Commons Attribution only licence CC BY 4.0. 19

1-2 Surface mole fraction (ppb) of N_2O as measured at five AGAGE sites (with location and latitude), from 1978-2017 (Prinn et al., 2000, 2018) 20

1-3 Pictorial representations of nitrous oxide: structural formula identifying α and β nitrogen atoms, atoms depicted as red (oxygen) and blue (nitrogen) circles, and a simplified graphical representation of N_2O throughout this thesis . . . 21

1-4 Stratospheric photolysis and chemical destruction pathways for N_2O, with production of NO and $O(^1D)$ that can destroy ozone in direct and indirect subsequent reactions 21

1-5 Radiative forcing of N_2O and other well-mixed greenhouse gases, according IPCC AR5 (IPCC, 2013), including estimates of uncertainty and level of confidence in radiative effects; this latest report indicates an increasing importance in determining N_2O sources, as evidenced by the separation of N_2O from a group of "other" long-lived greenhouse gases in a similar figure from IPCC (2007). 22

1-6 Simplified graphical workflow of a Bayesian inverse experiment, in which the *a priori* emissions estimate is updated to better match observed conditions when used to drive a chemical transport model; this process continues until an "optimized" *a posteriori* emissions estimate is produced taking into account uncertainties in the observations and the prior emissions estimate 24

1-7 Summary of all processes influencing the isotopic ratios of atmospheric N_2O 25

1-8 Locations of AGAGE network stations and affiliated atmospheric observation stations contributing to a global network of trace gas mole fraction observations (`agage.mit.edu`; Prinn et al. (2018)) 27

1-9 Lagrangian dispersion in "forward" and "backward" modes, as illustrated in this cartoon of Lagrangian particle spread in both modes following the prevailing southeasterly wind conditions in this example 28

1-10 Creation of a Lagrangian surface sensitivity "footprint" from one Lagrangian plume released at Mace Head, Ireland 28

2-1 Latitude-altitude cross-section of photolysis (top) and $O(^1D)$ (bottom) reaction rates in April from Saikawa et al. (2014) 37
2-2 Regions of the electromagnetic spectrum in which N_2O absorbs and re-radiates 38
2-3 Pictorial representations of N_2O isotopologues 38
2-4 Equations used to calculate N_2O isotopic ratios (R) and "delta-values" 39
2-5 Isotopic ratios of N_2O as presented in *delta notation*, including a pictorial example of delta-value calculation based on whole-gas N_2O samples and a hypothetical N_2O isotopic standard 40
2-6 Ranges of site-specific ^{15}N and ^{18}O isotopic ratios for various N_2O sources impacting measurements at Mace Head, Ireland, including an average modeled estimate for measurements at Mace Head (after Potter (2011), Figure 3.5) . 41
2-7 Average isotopic ratios of sources of N_2O (Potter, 2011; Pérez et al., 2001; Whalen and Yoshinari, 1985) 42
2-8 Isotopic kinetic effects in each stratospheric destruction process of N_2O (Röckmann et al., 2001; Kaiser et al., 2002a) 42
2-9 Isotopic fractionation processes of N_2O lead to enrichment of heavy-substituted N_2O isotopologues compared to mean tropospheric N_2O (R_{std} of each isotopologue is equal to the mean isotopic ratio of tropospheric N_2O) 43

3-1 Location of the AGAGE station (Prinn et al., 2000) at Mace Head, Ireland (Google Maps) 48
3-2 CF-IRMS N_2O isotopic ratio observations from 2010 at MHD, adapted with permission from Potter (2011) Figure 4.3 50
3-3 North Atlantic Oscillation index (NAO, from NOAA Climate Prediction Center) three-month running mean with 2014-2015 and closest analogues highlighted (panel A), monthly averages for 2014-2015, 2011-2012, and 2007-2008 (panel B), and daily values for the same time periods (panel C) 51
3-4 Schematic of Stheno-TILDAS instrument (after (Harris et al., 2014), Figure 1) 52
3-5 Preconcentration and analysis procedure for Stheno-TILDAS 52
3-6 Standard experimental procedure for long-term sampling, including preconcentration, of ambient air (AA) and compressed air "drift" standard (CA) with Stheno-TILDAS 53
3-7 Timeline of N_2O isotopic ratios measured at MHD in the first year of Stheno-TILDAS operation; green points indicate actual measurements, the thick line indicates a 24-hour running mean, the translucent bounds represent the standard deviation of isotopic measurements of contemporaneously-measured compressed air "drift" standard, large purple points are daily average measurements of the "drift" standard, and yellow stars indicate the annual average of flask-based isotopic ratio observations made at MHD in 2010 (Potter et al., 2013) 56

4-1 Ranges of site-specific ^{15}N and ^{18}O isotopic ratios for various N_2O sources potentially impacting measurements at Mace Head, Ireland (adapted with permission from Potter (2011), Figure 3.5), with a simplified diagram of the $\delta 456$-$\delta 546$ phase space of source signatures (inset). 62
4-2 Timeline of N_2O isotopic ratios (Stheno-TILDAS), as described in Figure 3-7, and mole fractions of trace gases (Medusa and ECD) measured at MHD in the first year of Stheno-TILDAS operation in 2014-2015. The two highlighted regions, spanning 26 June-9 July 2014 and 26 January-9 February 2015 are analyzed in further detail in the following sections. 64
4-3 Stratospheric tracer mole fractions (AGAGE GC-ECD and Medusa) at MHD contemporaneous with Figure 4-2 65
4-4 Stheno-TILDAS N_2O isotopic ratios and trace gas measurements at MHD in the first highlighted region from Figure 4-2, with year-long average observations at MHD from 2010 represented by the yellow star (average of all flask samples from 2010 in Potter (2011)). Events marked by the letters A-E are notable events within the highlighted time window, each of which bears a provisional source assignment (or indication of well-mixed background air) based on N_2O isotopic ratios (see the inset from Figure 4-1) and trace gas mole fractions. 67
4-5 Stheno-TILDAS N_2O isotopic ratios and trace gas measurements at MHD in the second highlighted region from Figure 4-2, with year-long average observations at MHD from 2010 represented by the yellow star (average of all flask samples from 2010 in Potter (2011)). Events marked by the letters V-Z are notable events within the highlighted time window, each of which bears a provisional source assignment (or indication of well-mixed background air) based on N_2O isotopic ratios (see the inset from Figure 4-1) and trace gas mole fractions. 68
4-6 Calculation of sensitivity of NAME "footprints" and its relation to the matrix $\mathbf{H}$ used in Bayesian inverse methods, with $\mathbf{y}$ representing a vector of observations and $\mathbf{x}$ representing a vector of emissions, with i representing a particular time at which an observation is made and j representing a particular grid cell from which emissions originate 72
4-7 A sample NAME surface sensitivity "footprint" for MHD on 25 May 2014 . . 72
4-8 NAME emissions footprints calculated for 10 meters above ground level at MHD at events (A-E, V-Z) explored in Figures 4-4 and 4-5 74

5-1 Sample MERRA/GEOS-5 land mask for 1 January 2011, featuring surface gridboxes corresponding to land, water, and ice 82
5-2 N_2O mole fraction initial conditions at the surface for January 1, 2009, from the end of Saikawa et al. (2014) 84
5-3 Linear extrapolation of monthly optimized emissions for years outside of the original experiment ending in 2008 (Saikawa et al., 2014) 85

5-4 Optimized net N_2O flux estimates for 2008 (A) in January and (B) in July (Saikawa et al., 2014) 86
5-5 Meridionally averaged N_2O surface flux estimates from Figure 5-4 87
5-6 MOZART-4 simulated monthly average N_2O mole fraction in the grid box containing Mace Head (using GEOS-5 reanalysis meteorology), as compared to GC-ECD observations at the station in 2014-2015 87
5-7 Initial conditions for the first spin-up year for distribution of N_2O isotopic ratios from averaged *in situ* vertical profiles (Toyoda et al., 2013); ratios are applied equally in the zonal dimension to standard MOZART initial conditions for whole-gas N_2O at the spring equinox of 2011 89
5-8 MOZART-4 simulated surface N_2O mole fraction for March 1, 2011, the fields to which the isotopic ratios in Figure 5-7 are applied to create initial conditions for isotopically-differentiated MOZART-4 model runs) 90
5-9 Creation of isotopically differentiated emissions using optimized N_2O emissions (Saikawa et al., 2014) and mean isotopic signatures of N_2O sources (Potter, 2011; Pérez et al., 2001; Whalen and Yoshinari, 1985) 91
5-10 Procedure for advancing the spin-up phase of the N_2O isotopologue MOZART experiment, starting with the initial conditions described in Figure 5-7 and continuing with the model output, scaled to the initial surface concentration of N_2O from MOZART chemical forecasts 93
5-11 MOZART-4 surface (top) and zonal average (bottom; latitude-altitude plot) N_2O mole fraction on January 1, 2015 94
5-12 MOZART-4 surface (top) and zonal average (bottom; latitude-altitude plot) $\delta\mathbf{448}$ (per mil) on January 1, 2015 95
5-13 MOZART-4 surface (top) and zonal average (bottom; latitude-altitude plot) $\delta\mathbf{456}$ (per mil) on January 1, 2015 96
5-14 MOZART-4 surface (top) and zonal average (bottom; latitude-altitude plot) $\delta\mathbf{546}$ (per mil) on January 1, 2015 97

6-1 Formulation of the cost function J, which is minimized by finding the emissions estimate vector $\mathbf{x}$ that best explains the observations vector $\mathbf{y}$ given uncertainties within the matrices $\mathbf{R}$ and $\mathbf{P}$, using a linear model $\mathbf{H}$ 102
6-2 Simulated timeline of N_2O mole fraction (purple line) at Mace Head, Ireland in 2014-2015, separated into contribution from MOZART boundaries (red line) and contribution from surface emissions within the domain (space between red and purple lines, shaded green in April 2014) 105
6-3 N_2O mole fraction observations at Mace Head, Ireland, as measured using the AGAGE GC-ECD instrument 106
6-4 Prior emissions for inverse modeling, with sectors stacked to show net emissions (top) and separated by sector to show relative magnitude (bottom) . . 108
6-5 AGAGE GC-ECD N_2O mole fraction observations at Mace Head (top), NAME-MOZART simulated N_2O mole fraction (center; from Figure 6-2), and residual (bottom) 109

6-6 NAME-MOZART simulation of N_2O isotopic ratios and mole fraction, shown in the same time periods as Stheno-TILDAS observations in Figure 3-7; green points indicate simulated measurements, the thick line indicates a 24-hour running mean of simulated measurements, the translucent bounds represent the uncertainty in the simulated isotopic ratios 112

6-7 Basis functions for inversion of gridded bulk N_2O emissions, with four long-range sectors and a high-resolution (at the native NAME grid resolution) within continental Europe 114

6-8 Prior emissions estimate, posterior emissions estimate, prior-posterior difference, and uncertainty reduction for summer (JJA) N_2O emissions, using basis function from Figure 6-7 116

6-9 Prior emissions estimate, posterior emissions estimate, prior-posterior difference, and uncertainty reduction for winter (DJF) N_2O emissions, using basis function from Figure 6-7 117

6-10 Average seasonal NAME surface sensitivity "footprints" at Mace Head for periods with Stheno-TILDAS observations during Summer (JJA) 2014 and Winter (DJF) 2014-2015 118

6-11 Average seasonal NAME surface sensitivity "footprints" at Dübendorf for periods concurrent with Stheno-TILDAS observations during Summer (JJA) 2014 and Winter (DJF) 2014-2015 119

6-12 Prior emissions for inverse modeling within the NAME Europe domain from Figure 6-4, separated into the Europe subregion (top) and the rest-of-domain region (bottom) 121

6-13 NAME-MOZART inverse modeling results in the two regions for natural soil emissions, with geographic distribution of prior emissions (top), changes in magnitude (center), and changes in uncertainty (bottom) 123

6-14 NAME-MOZART inverse modeling results in the two regions for oceanic emissions, with geographic distribution of prior emissions (top), changes in magnitude (center), and changes in uncertainty (bottom) 124

6-15 NAME-MOZART inverse modeling results in the two regions for agricultural emissions, with geographic distribution of prior emissions (top), changes in magnitude (center), and changes in uncertainty (bottom) 125

6-16 NAME-MOZART inverse modeling results in the two regions for industrial emissions, with geographic distribution of prior emissions (top), changes in magnitude (center), and changes in uncertainty (bottom) 126

6-17 NAME-MOZART inverse modeling results in the two regions for biomass burning emissions, with geographic distribution of prior emissions (top), changes in magnitude (center), and changes in uncertainty (bottom) 127

6-18 Timeline of residual between Stheno-TILDAS N_2O isotopic ratio observations and NAME-MOZART simulations (orange representing simulation with *a priori* emissions estimates and purple representing simulation with *a posteriori* emissions estimates), with Stheno-TILDAS observation uncertainty in shown in shading (as in Figure 3-7) 129
6-19 Relative contribution to σ^2 from the four factors σ_M, σ_{RE}, σ_{SF}, and σ_{SIR} for the three N_2O isotopic ratios 131

7-1 Schematic of Bayesian inverse modeling methodology, including measured concentrations, modeled concentrations, an *a priori* emissions estimate, and an optimized *a posteriori* emissions estimate 139

A-1 Hypothetical flight tracks for a flight experiment on air quality in West Africa 150
A-2 Black carbon mass concentration timelines for flight tracks 1-3 at four altitudes on January 1 2015, as interpolated from MERRA black carbon fields 151
A-3 Aerosol optical depth timelines for flight tracks 1-5 on July 1 2015, as interpolated from Terra/Aqua column satellite retrievals 152

B-1 Changes in isotopic signature "delta values" for EDGAR/ocean/natural sectors over the entire Stheno-TILDAS observation period, with uncertainty reduction from prior to optimized estimates (Part 1) 157
B-2 Changes in isotopic signature "delta values" for EDGAR/ocean/natural sectors over the entire Stheno-TILDAS observation period, with uncertainty reduction from prior to optimized estimates (Part 2) 158

List of Tables

1.1 Estimates of total N_2O budget from IPCC AR5 (IPCC, 2013), with best estimate for each source type and associated uncertainty ranges in parentheses 23

2.1 EDGAR main anthropogenic N_2O source categories 35

3.1 Isotopic standards available for use in Stheno-TILDAS experiments at Mace Head, Ireland and at MIT 54

5.1 Resolution of NCEP/NCAR, MERRA, and GEOS-5 reanalysis meteorological datasets with variables needed to run MOZART-4 82

5.2 Fractionation factors φ for each N_2O chemical destruction process, drawn from Figure 2-8 92

6.1 Site-specific N_2O isotopic signatures for EDGAR anthropogenic industrial and agricultural sources (Harris et al., 2017), and for the remaining three source sectors (Potter, 2011); any isotopic ratios originally reported in terms of ^{15}N and Site Preference have been converted to δ**456** and δ**546** 111

Chapter 1

Introduction

Nitrous oxide (N_2O) is a significant trace gas in Earth's atmosphere that has a major effect on the planet's climate and the health of its stratospheric ozone layer. As with other major greenhouse gases in Earth's atmosphere—namely, carbon dioxide, methane, and ozone—nitrous oxide has significant natural and anthropogenic sources. The annual N_2O emission levels from natural biotic nitrification/denitrification processes in the soil and ocean (IPCC, 2007) have remained relatively constant over recent history, leading to a stable "background" contribution from natural sources to atmospheric N_2O mole fractions.

Figure 1-1: "Nitrous oxide for a dental operation. Anaesthetics and their administration (1922)" `https://wellcomecollection.org/works/fh4j7zdr`. Copyrighted work available under Creative Commons Attribution only licence CC BY 4.0.

Primary anthropogenic release of N_2O directly into the atmosphere, including from its use in medical (e.g. anesthesia, a common and long-time use, as shown in Figure 1-1) and culinary applications (e.g. foams and emulsions such as whipped cream), remains a relatively minor component of net annual N_2O emissions despite these applications representing perhaps the most common direct human interaction with N_2O in the Western world. Secondary anthropogenic emissions whereby N_2O is created in subsequent chemical processes, including from agriculture, nitrogen fertilizer use, biofuel burning, sewage treatment, manufacturing, transportation, and other industrial processes (IPCC, 2007; Janssens-Maenhout et al., 2017; EDGARv4.3.2, 2018) have significantly increased as these processes become progressively more important in maintaining modern quality-of-life expectations and in ensuring food security across the planet.

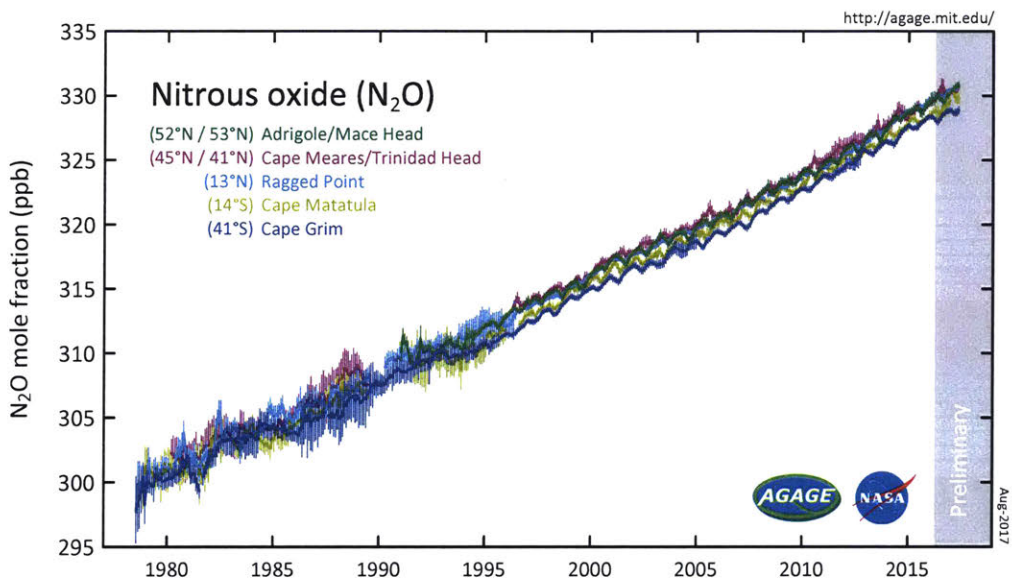

Figure 1-2: Surface mole fraction (ppb) of N_2O as measured at five AGAGE sites (with location and latitude), from 1978-2017 (Prinn et al., 2000, 2018)

The increasing primacy of anthropogenic N_2O emissions on the composition of Earth's atmosphere is made clear when comparing the global concentration of N_2O from pre-industrial levels of ~270 ppb to current-day concentrations of approximately 330 ppb (Toyoda et al., 2013; Prinn et al., 2016). Due to the preponderance of N_2O sources being located in the Northern Hemisphere, there is a significant latitudinal gradient in N_2O mole fractions, as seen in the various AGAGE global monitoring network stations in Figure 1-2. In addition, the measured N_2O concentrations feature seasonal variations due to variable activity of natural and anthropogenic N_2O sources (Liao et al., 2004); natural sources vary due to the timing

of biological processes and kinetic effects in production processes that change with conditions such as temperature, and anthropogenic sources largely respond to the intermittent schedules of agriculture and intentional biomass burning (Janssens-Maenhout et al., 2017; EDGARv4.3.2, 2018).

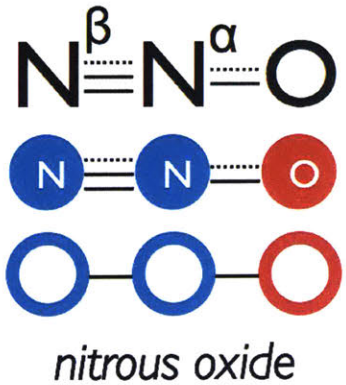

Figure 1-3: Pictorial representations of nitrous oxide: structural formula identifying α and β nitrogen atoms, atoms depicted as red (oxygen) and blue (nitrogen) circles, and a simplified graphical representation of N_2O throughout this thesis

Each molecule of N_2O released into the atmosphere has the capability to impact Earth's climate more strongly than molecules of other closely-monitored greenhouse gases due to the chemical inertness of N_2O in the troposphere leading to a long average lifetime in the atmosphere (Prather et al., 2015), and the region of infrared radiation in which N_2O absorbs and re-radiates (IPCC, 2007, 2013; Seinfeld and Pandis, 2006). In addition, chemical destruction of N_2O in the stratosphere creates nitrogen oxides (notably, NO and NO_2) that can catalytically deplete ozone in the stratospheric ozone layer (Ravishankara et al., 2009; IPCC, 2013); decreasing stratospheric ozone leads to increased incoming ultraviolet radiation impacting Earth's surface.

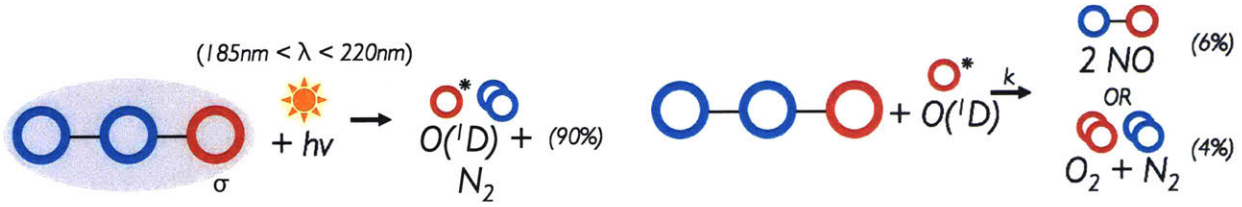

Figure 1-4: Stratospheric photolysis and chemical destruction pathways for N_2O, with production of NO and $O(^1D)$ that can destroy ozone in direct and indirect subsequent reactions

Because of the enhanced radiative forcing capacity on a *per-molecule basis* of N_2O compared to other greenhouse gases (IPCC, 2013), the linearly increasing concentration of atmospheric N_2O (Figure 1-2) threatens to further drive the radiative balance and climate of

Earth from its pre-industrial conditions. Therefore, close study of the rising concentrations and increasing emissions of N_2O are important aspects of a global goal to decrease the impact of greenhouse gases on Earth's atmosphere.

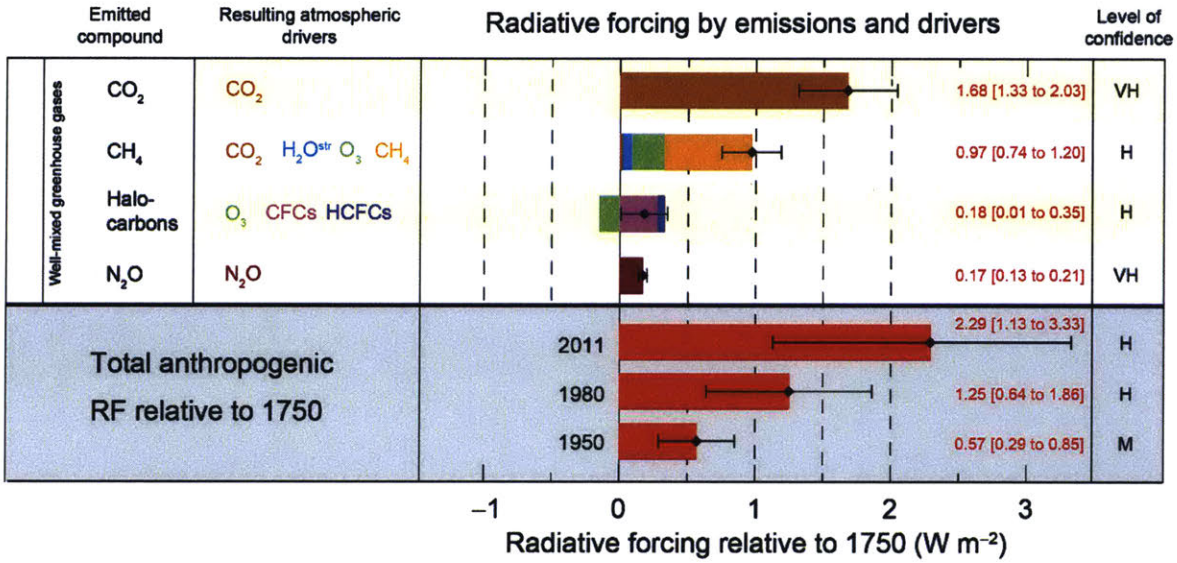

Figure 1-5: Radiative forcing of N_2O and other well-mixed greenhouse gases, according IPCC AR5 (IPCC, 2013), including estimates of uncertainty and level of confidence in radiative effects; this latest report indicates an increasing importance in determining N_2O sources, as evidenced by the separation of N_2O from a group of "other" long-lived greenhouse gases in a similar figure from IPCC (2007).

Accurate apportionment of N_2O source distributions can lead to identification of emerging sources and development of potential strategies for abatement of non-critical N_2O-emitting processes. A thorough understanding of N_2O budgets can inform policy in areas ranging from food security to global climate due to the indelible role of N_2O in many modern areas of life. Due to its ascendance as an increasingly important ozone-depleting greenhouse gas in Earth's atmosphere, all phases of the N_2O budget must be studied further in order to understand the role of this gas in the changing global Earth system.

1.1 Problem Statement

In order to develop abatement strategies for the impact of N_2O on Earth's climate, the magnitude and geographic distribution of its sources must be well understood. Estimates of N_2O emissions from various sectors have significant associated uncertainties; for example, agricultural sources are estimated to contribute 4.1 TgN/yr (1 TgN $\equiv$ 1.57 Tg N_2O) to the global N_2O budget (out of a total $\sim$18 TgN/yr), but the actual value may fall within the range of 1.7-4.8 TgN/yr (IPCC, 2013). Other significant sources of atmospheric N_2O

(Table 1.1) have similar margins of error, preventing robust source-specific N_2O abatement strategies from being developed and widely implemented.

Nitrous Oxide Budget, 2013	
Source name	*Flux (TgN yr^{-1})*
Anthropogenic Sources	
Agricultural soil	4.1 (1.7-4.8)
Rivers, coast, estuaries	0.6 (0.1-2.9)
Biomass/biofuel burning	0.7 (0.2-1.0)
Fossil fuels/industry	0.7 (0.2-1.8)
Surface deposition from atmosphere, re-release	0.6 (0.3-0.9)
Human sewage	0.2 (0.1-0.3)
Natural Sources	
Soil	6.6 (3.3-9.0)
Oceans	3.8 (1.8-9.4)
Atmospheric chemistry	0.6 (0.3-1.2)
Total	17.9 (8.0-31.3)

Table 1.1: Estimates of total N_2O budget from IPCC AR5 (IPCC, 2013), with best estimate for each source type and associated uncertainty ranges in parentheses

Emissions estimates of N_2O that contribute to the ranges in Table 1.1 are constructed in two major ways: *bottom-up* estimates in which reported (from industrial and governmental disclosures) and inferred (from activity maps and emissions factors, and process models such as DNDC, Giltrap et al. (2010)) source magnitudes and distributions are summed to provide a continuous global emissions profile (e.g. EDGAR and similar databases), and *top-down* estimates in which emissions are inferred from detailed analysis of changes in observed atmospheric concentrations (Nevison et al., 2007; Huang et al., 2008; Saikawa et al., 2014). Each method has its own assumptions that can bias and muddle the final results; the wide uncertainty ranges for the various N_2O sources in Table 1.1 are due to differences in the methods and source data sets used in various computational and observational experiments that make up the consensus "best estimates" by the Intergovernmental Panel on Climate Change (IPCC, 2013). The widespread, diffuse nature of global N_2O sources makes emissions apportionment particularly challenging.

Bottom-up estimates of N_2O emissions yield useful results alone, but can be especially helpful in constraining N_2O emissions when combined with results from atmospheric modeling experiments in a systematic manner. Effective combination of both *bottom-up* emissions inventories and observed atmospheric measurements is possible using Bayesian methods (Huang et al., 2008; Saikawa et al., 2014; Hirsch et al., 2006) that statistically constrain emissions estimates given observed mole fractions and results from an atmospheric chemical transport model (each weighted by their associated uncertainty). This combined Bayesian inverse framework has the potential of yielding precise high-resolution apportion-

ment of spatially-resolved N_2O emissions estimates given observed N_2O mole fractions.

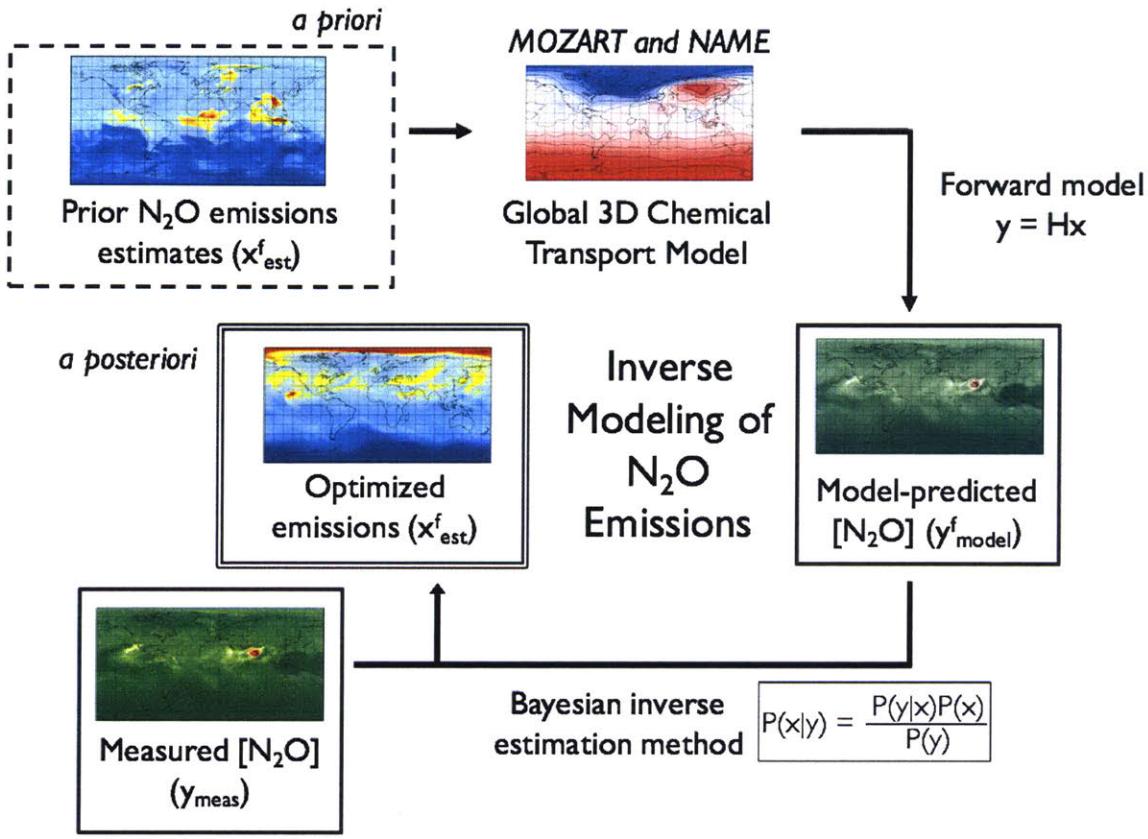

Figure 1-6: Simplified graphical workflow of a Bayesian inverse experiment, in which the *a priori* emissions estimate is updated to better match observed conditions when used to drive a chemical transport model; this process continues until an "optimized" *a posteriori* emissions estimate is produced taking into account uncertainties in the observations and the prior emissions estimate

Given a dense enough network of N_2O concentration measurements, chemical transport models (CTMs) can indicate regions from which measured parcels of N_2O-containing air may have originated, leading to preliminary assignment of N_2O emissions to particular source types. This framework, however, relies on the accuracy and precision of CTMs and is far from a hypothetical "ideal" case in which every molecule of N_2O bears a unique signature imparted by its source. Although individual N_2O molecules do not bear such a source-specific tag, every source of N_2O preferentially incorporates heavy isotopes of nitrogen (^{15}N) and oxygen (^{18}O) in ratios that differ from the mean isotopic ratios of N_2O in the atmosphere and from those of every other source (Denk et al., 2017).

In addition to isotopic signatures imparted by sources, isotopic effects in photolysis and chemical destruction of N_2O also lead to unique N_2O isotopic ratios. The only regions where N_2O is appreciably destroyed are located in the stratosphere and feature unblocked mid-to-far

ultraviolet (UV) radiation (185 nm< λ <220 nm (Röckmann et al., 2001)) or high concentrations of excited oxygen atoms ($O(^1D)$, the singlet-D first excited state of atomic oxygen). These N_2O destruction processes preferentially destroy N_2O molecules without "heavy-atom" ^{15}N or ^{18}O substitution, effectively depleting stratospheric air of "lighter" ^{14}N and ^{16}O atoms compared to N_2O found in the troposphere. When a parcel of air from the stratosphere enters the troposphere via dynamically-forced stratosphere-troposphere exchange, the isotopic signature of N_2O within this parcel depends on the duration and location of its journey through the stratosphere due to vertical and meridional gradients of UV photon density and $O(^1D)$ concentration, and thermal effects on the chemical kinetic rates (Kaiser et al., 2002b). As an air parcel spends more time in the high-altitude regions of the stratosphere, the overall concentration of N_2O decreases, but the remaining N_2O becomes relatively enriched in ^{15}N and ^{18}O (Röckmann et al., 2001; Kaiser et al., 2002a).

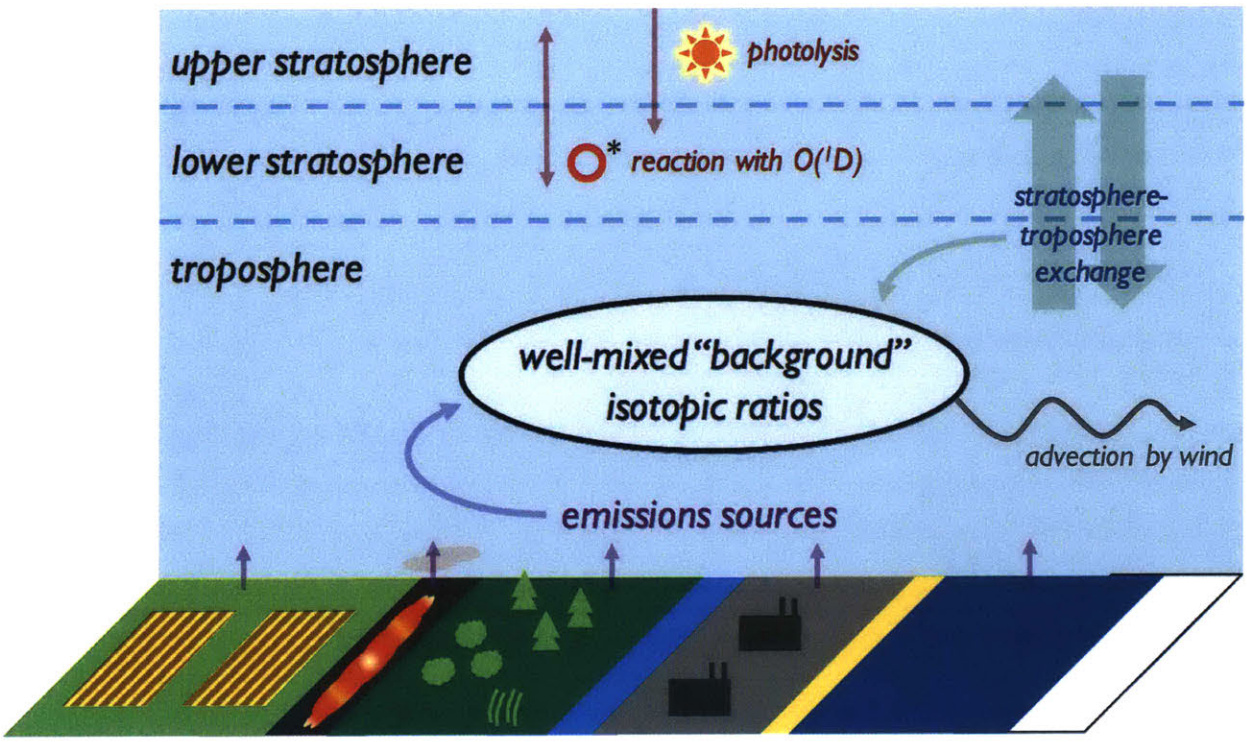

Figure 1-7: Summary of all processes influencing the isotopic ratios of atmospheric N_2O

Analysis of isotopic differentiation patterns in measured parcels of air in combination with concurrent CTM runs can identify source, sink, and transport dynamics at work and can allow for better apportionment of N_2O source types on both regional and global scales. Due to the inert nature of N_2O in the troposphere, the accuracy of a particular chemical transport model iteration (or "model run") relies chiefly on the accuracies of surface emissions, horizontal transport in the troposphere, vertical mixing of N_2O in stratosphere-troposphere exchange, and chemical and photolytic destruction processes in the high stratosphere (Figure 1-7).

In this experiment, isotopically-resolved chemical transport model simulations will be combined with *in situ* measurement of N_2O isotopic ratios in order to improve the current state of N_2O emissions estimates.

1.2 Research Goals and Approach

The continued increase in concentrations of atmospheric N_2O, largely due to anthropogenic agricultural and industrial processes (IPCC, 2013), motivates the need to identify the magnitude and global distribution of all N_2O sources. Bayesian inverse modeling experiments (Huang et al., 2008; Saikawa et al., 2014) have the capability of optimally comparing global N_2O isotopic ratio observations to outputs of well-conditioned chemical transport model experiments in order to produce N_2O emissions maps for each source type.

Due to the diffuse nature of N_2O sources–contrast the footprint of a single factory smokestack emitting large amounts of a particular gas to entire regions of monoculture agriculture emitting small amounts over a vast area–and the rapid mixing (Boering et al., 2004; Hintsa et al., 1998; Wofsy et al., 1994) of isotopically-enriched N_2O from stratospheric intrusions (Park et al., 2004; Kaiser et al., 2006), the effects of each constituent of the N_2O Earth system must be well constrained in order to realistically model the results from the many competing global factors. After a brief introduction of the factors that impact the isotopic chemistry of N_2O, this thesis introduces significant advances to isotopic N_2O inverse modeling through development of four experimental phases involving *in situ* measurements and atmospheric computational models, outlined below.

1.2.1 Continuous *in situ* Observations

Following the recent development Stheno-TILDAS (Harris et al., 2014), an instrument capable of making high-frequency measurements of N_2O isotopic ratios in remote locations, this thesis will introduce the results from the first field deployment of Stheno-TILDAS at the Mace Head Atmospheric Research Station (Mace Head, or abbreviated MHD) in western Ireland. Mace Head was chosen as the site for ongoing observations in the AGAGE (Prinn et al., 2016) global monitoring network (Figure 1-8) due to its unique meteorological conditions and proximity to continental Europe.

The synoptic situation at MHD features clean background air from the northern Atlantic Ocean about half of the time, polluted air from the UK and continental Europe 35% of the time, and stagnant air masses with local sources for the remaining fraction (Potter, 2011). This synoptic set-up is ideal for Stheno-TILDAS due to the contrast in conditions sampled with long-term trends influenced by the North Atlantic Oscillation dynamics (Chen and Prinn, 2005), and the potential to measure relatively undiluted stratospheric air as it mixes into the high-latitude troposphere in early spring (Potter, 2011; Nevison et al., 2007).

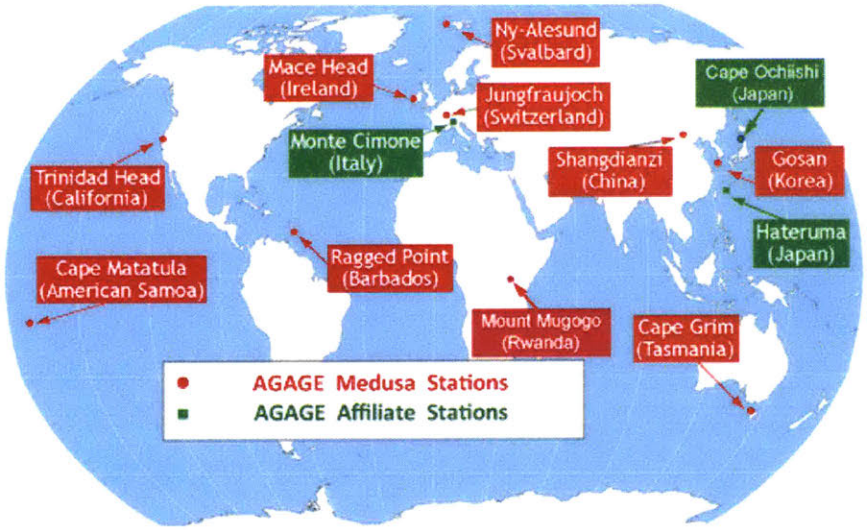

Figure 1-8: Locations of AGAGE network stations and affiliated atmospheric observation stations contributing to a global network of trace gas mole fraction observations (`agage.mit.edu`; Prinn et al. (2018))

The choice to deploy Stheno-TILDAS at Mace Head allows for the added benefit of co-located and contemporaneous measurements of numerous atmospheric trace gases at MHD as part of the AGAGE global network (Prinn et al., 2016, 2018). Mole fractions of these trace gases can be used to indicate differences between polluted, clean, and stagnant conditions (as indicated by elevated CO, CH_4, $CHBr_3$, and more). The two seasons in which Stheno-TILDAS was operating at MHD, summer 2014 and winter 2014-2015, provide a rich set of N_2O isotopic ratio data that can be compared to other trace gas measurements and supporting results from computational atmospheric models.

1.2.2 Regional Lagrangian Dispersion Models

For an understanding of the way in which regional and local emissions affect the observations made at one location (Croteau et al., 2010), Lagrangian dispersion models set up to simulate a geographic subset of the global domain (Manning et al., 2011) are one valuable tool. In a given model realization, a "plume" of inert particles are released from the location chosen at a particular time and tracked until they next strike the surface or leave the model domain. The particles move according to a set of three-dimensional meteorological fields provided to the model.

The models can be run in "forward" mode, in which air being released from the location of interest is tracked to see where it will most likely end up, or "backward" mode, in which the past origin of air sampled at the location of interest is estimated. By adding in parameterized turbulence and small perturbations to the initial release location and time, the particles end

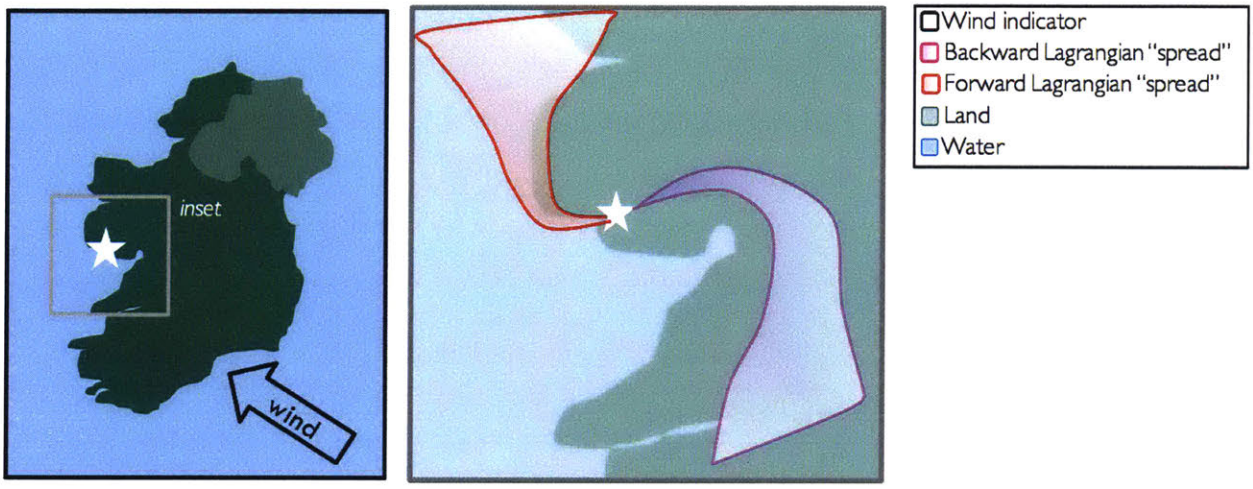

Figure 1-9: Lagrangian dispersion in "forward" and "backward" modes, as illustrated in this cartoon of Lagrangian particle spread in both modes following the prevailing southeasterly wind conditions in this example

up following significantly different trajectories; this allows for a statistical distribution of the most likely origin (or final) locations of individual parcels of air that are ultimately sampled (or released) at the model location.

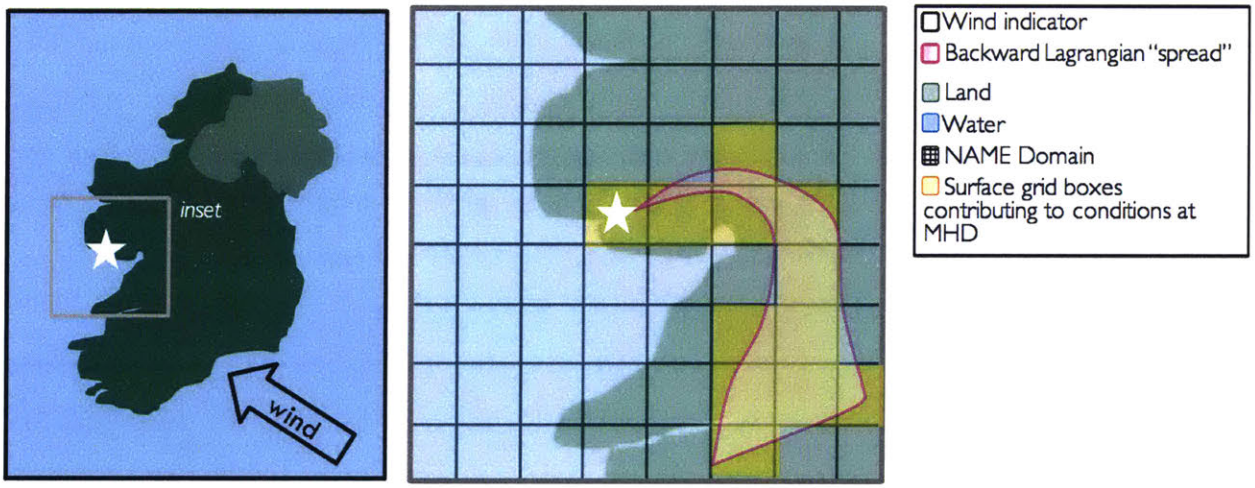

Figure 1-10: Creation of a Lagrangian surface sensitivity "footprint" from one Lagrangian plume released at Mace Head, Ireland

In this thesis, the only Lagrangian model results used are produced in the "backward" operation mode in order to better understand the locations and magnitudes of N_2O emissions in Europe. When run in "backward" mode, the sensitivity of observations at the location of interest to emissions from the surface can be visualized by "footprint" plots, as seen in a cartoon diagram of this result in Figure 1-10. The Lagrangian model chosen for this experi-

ment is NAME, the Numerical Atmospheric-dispersion Modelling Environment produced by the United Kingdom Met Office (Jones et al., 2007). The wealth of studies using NAME to help estimate emissions of greenhouse gases and air pollutants using data from the AGAGE network (Rigby et al., 2011, 2012; Manning et al., 2011)lends credibility to the choice of NAME in this experiment.

1.2.3 Global Chemical Transport Models

In order to understand the impact of well-mixed "background" air that is sampled at Mace Head on the N_2O isotopic ratios measured there, modeling tools with a larger domain than NAME must be employed. Global Chemical Transport Models (CTMs) such as the Model for Ozone and Related Tracers version 4 (MOZART-4), developed at the National Center for Atmospheric Research (NCAR) can be used to produce global three-dimensional mole fraction fields of chemicals of interest (Emmons et al., 2010); in this case, concentrations of N_2O and its isotopic analogues ("isotopologues") are modeled in the global domain.

Global CTMs are particularly useful in two major applications: standalone "forward modeling" to ascertain the connections between changes in N_2O emissions dynamics and large-scale global trends in N_2O mole fractions and isotopic ratios, and as components of Bayesian inverse methods in which an initial N_2O emissions distribution (*a priori* or prior estimate) and a forward model are used to determine an optimized emissions estimate that can best explain experimental observations.

1.2.4 Inverse Modeling with N_2O Isotopic Observations and Atmospheric Models

Stheno-TILDAS data from MHD show the capability of the instrument to observe short-term excursions from baseline N_2O isotopic ratios in events that sample enhanced contribution from particular N_2O sources more completely than is possible with infrequent flask-based sampling experiments (Potter, 2011). These events can be recreated in a computational framework combining high-resolution NAME model results in the European region and coarser MOZART-4 global model results as the "boundary walls" of the NAME Europe domain (Lunt et al., 2016). This setup allows for efficient use of computational resources, giving significantly enhanced time and spatial resolution in the areas of N_2O emission statistically most responsible for influencing N_2O mole fractions and isotopic ratios at Mace Head, Ireland.

By using a Bayesian inverse method, numerous model runs with slightly perturbed *a priori* N_2O emissions estimates are compared to the observations from Mace Head in order to determine the set of regional emissions that can best explain the N_2O GC-ECD mole fraction and Stheno-TILDAS isotopic ratio observations (a similar approach to the experiment

conducted by Rigby et al. (2012) for methane isotopic ratios). In order to further constrain European N_2O emissions estimates using NAME-MOZART, the N_2O isotopic ratio observations made by EMPA (the Swiss Federal Laboratories for Materials Science and Technology) at Dübendorf, Switzerland over the same timeframe as Stheno-TILDAS observations (Harris et al., 2017) can be added to the inverse modeling framework.

1.3 Summary of Major Thesis Findings

As described in the previous section, this thesis aims to incorporate atmospheric observations and computational models of N_2O isotopic ratios in order to further constrain source-specific N_2O emissions estimates (Yoshida and Matsuo, 1983). Steps toward this goal are described in more detail in the following chapters, with the main findings being:

- High-frequency N_2O isotopic ratio observations from Stheno-TILDAS show features whereby isotopic signatures from distinct sources are measured as excursions from well-mixed average "background" conditions
- Trace gas observations of molecules (CH_4, CO, $CHBr_3$) co-emitted with N_2O indicate enhanced sampling of anthropogenic and natural N_2O sources at various times
- Regional Lagrangian modeling near Mace Head using NAME creates surface emissions sensitivity "footprint" maps that support provisional N_2O source apportionment from N_2O isotopic ratio and AGAGE trace gas mole fraction observations
- Inclusion of N_2O isotopic chemistry in MOZART-4, a global chemical transport model, leads to a general understanding of global trends in N_2O isotopic ratios
- Bayesian inverse modeling combining N_2O isotopic ratio observations, NAME footprints, and MOZART-4 global N_2O isotopic ratio fields can lead to a reduction in uncertainty of source-specific N_2O emissions estimates

Continuing work will aim to incorporate additional experimental data that will allow for more precise simulation of global and regional N_2O isotopic chemistry. Notably, direct measurements of high-altitude air (Park et al., 2004; Toyoda et al., 2004, 2013) from flasks will help constrain the vertical site-specific (each ^{15}N position and ^{18}O) isotopic gradients of N_2O, and concentrated sampling of individual source sectors (Yano et al., 2014; Toyoda et al., 2005; Snider et al., 2009; Smemo et al., 2011; Popp et al., 2002; Mathieu et al., 2006; Frame et al., 2014; Ogawa and Yoshida, 2005; Toyoda et al., 2008; Acton and Baggs, 2011; Arévalo-Martínez et al., 2016; Breider et al., 2015; Bol et al., 2003; Harris et al., 2015; Park et al., 2011; Pérez et al., 2001; Whalen and Yoshinari, 1985; Yamulki et al., 2001) will reduce the uncertainty in the source-specific isotopic "signatures" of the various N_2O emissions sources (Table 1.1).

As evidenced by the recent abundance of published research on N_2O isotopic ratio modeling (McLinden et al., 2003; Snider et al., 2013; Morgan et al., 2004) and observation (Harris et al., 2017; Prokopiou et al., 2017; Sowers et al., 2002), numerous researchers around the world find great value of site-specific N_2O isotopic chemistry in helping constrain the greatly uncertain distribution of N_2O emissions sources. As Stheno-TILDAS continues to expand the spatial coverage of N_2O isotopic ratio observations through a combined high-frequency/flask sampling experiment, its future data will be a significant component of future isotopically differentiated modeling experiments of N_2O emissions.

Chapter 2

Nitrous Oxide and Isotopic Chemistry

This chapter will introduce the chemical species of interest in this thesis, nitrous oxide (N_2O). The chemical reactivity and radiative properties of this gas make it a particularly important component of Earth's atmosphere when considering its impact on a changing climate. The processes by which N_2O is produced and destroyed impart specific "signatures" in the heavy-atom (^{15}N and ^{18}O, as compared to more common "light" ^{14}N and ^{16}O) isotopic ratios of the molecule. Although these isotopic ratios do not lead to definitive identification of the original source of any particular molecule of N_2O, when combined with other measurements in ambient air, N_2O isotopic ratios can help elucidate the relative contributions of different N_2O sources sampled at a particular location.

2.1 Physical Properties

Nitrous oxide (N_2O) is a colorless gas that features an asymmetric arrangement of two nitrogen atoms and one oxygen atom. This N-N-O arrangement leads to a permanent dipole moment across the molecule, with the oxygen atom bearing a slight negative net atomic charge and the terminal nitrogen atom bearing a slight positive net atomic charge. The distribution of electrons across the two covalent bonds in the molecule leads to a non-integer bond order of 2.5 for the N-N bond and 1.5 for the N-O bond.

Following the nomenclature in organic chemistry for sequential atoms bonded to a functional group, the two nitrogen atoms are assigned Greek letter symbols increasing with distance from the oxygen atom (Figure 1-3): N(beta)-N(alpha)-O. This naming convention (Toyoda et al., 2013) is at odds with another common way of differentiating the two nitrogen atoms, in which the atoms are assigned numerical designations that descend with increasing distance from the oxygen atom (Bernath et al., 2017): N(1)-N(2)-O. In this thesis, the alpha/beta notation will be used when referring to the nitrogen atoms within the N_2O molecule.

2.2 Sources and Sinks

Nitrous oxide is released into the atmosphere from a wide variety of sources. Some, such as production from biotic processes in the ocean, are geographically diffuse and poorly constrained (Clough et al., 2007; Arévalo-Martínez et al., 2016; Babbin et al., 2015). Others, such as direct industrial use of N_2O as a food-grade aerosol propellant, are more precisely quantified but represent a vanishingly small fraction of the overall global N_2O emissions. Previous experiments with the goal of identifying magnitudes and distributions of global N_2O emissions (Saikawa et al., 2014) have focused on five main sectors: natural emissions from land, natural emissions from ocean, emissions from agricultural processes, industrial emissions, and biomass burning emissions.

Natural emissions of N_2O are difficult to ascertain directly from N_2O mole fraction measurements; therefore, a combination of bottom-up "inventory" methods and top-down "inverse modeling" methods are used to provide the best understanding of land-based and oceanic natural N_2O emissions. In the global inverse modeling experiment conducted by Saikawa et al. (2014), the authors used natural N_2O emissions produced by land process models and ocean biogeochemical models as the *a priori* basis for optimization in a Bayesian inverse modeling framework.

Further differentiation within anthropogenic emissions processes (agriculture, industry, and intentional biomass burning directly associated with human activity) is possible using the designations in the EDGAR database (Janssens-Maenhout et al., 2017), a joint project of the European Commission JRC Joint Research Centre and the Netherlands Environmental Assessment Agency (PBL). EDGAR (Emissions Database for Global Atmospheric Research) is a cooperative experiment that has produced inventory maps for major greenhouse gases, including N_2O. The most recent version of the EDGAR inventory, version 4.3.2 (EDGARv4.3.2, 2018) features maps of anthropogenic N_2O emissions, separated by the relevant industrial designations used by the IPCC in their reports, as described in Table 2.1.

EDGAR v4.3.2 emissions maps are available for N_2O in horizontal spatial resolution of 0.1 degrees latitude by 0.1 degrees longitude, with annual maps of emissions by sector produced for years between 1970-2012. In addition, EDGAR v4.3.2 features monthly emissions rates for the year 2010, allowing for a general understanding of seasonal trends in each of the various sectors. The detail in EDGAR v4.3.2, not only in spatial resolution but in monthly sector-specific trends and enhanced representation of emerging N_2O sectors, far exceeds the detail that was available to Saikawa et al. (2014) when EDGAR v4.1 was used as the basis for industrial and agricultural N_2O emissions in their inverse modeling experiment. This represents an opportunity for the inverse modeling results from that experiment to be revisited with improved input data sets such as seasonally-varying source-specific *a priori* emissions fields.

EDGAR Anthropogenic N_2O Emissions Sources		
Abbreviation	*Description*	*IPCC Code*
ENERGY	Power, Oil, and Energy Transformation	1A1-1A2
TRANS	Non-road transportation	1A3 (except 1A3b)
CARS	Road transportation	1A3b
HEAT	Heat and energy for buildings	1A4
INDUSTRY	Direct production and chemical processes	2 and 3
MANURE	Manure management	4B
AGSOIL	Agricultural soils	4D
AGBURN	Agricultural waste burning	4F
WASTE	Solid waste handling/incineration and waste water	6
INDIRECT	Indirect emissions from NOx and NH_3	4D3, 7B, 7C
FFFIRE	Fossil fuel fires	7A

Table 2.1: EDGAR main anthropogenic N_2O source categories

2.3 Stratospheric Sink and Lifetime

The long chemical lifetime (Prather et al., 2015; Ravishankara et al., 2009) of N_2O is largely due to the manners in which it is destroyed in the atmosphere. The two pathways for N_2O destruction are reaction with excited atomic oxygen ($O(^1D)$, leading to two different products) and photolysis by mid-far ultraviolet radiation. Each reaction is affected by temperature (Kaiser et al., 2002b) and photolysis is also controlled by the spectrum of ultraviolet radiation available (Kaiser et al., 2003).

$$N_2O + h\nu_{185-220nm} \xrightarrow{1} N_2 + O(^1D)$$

$$N_2O + O(^1D) \xrightarrow{2a} 2\,NO$$

$$N_2O + O(^1D) \xrightarrow{2b} N_2 + O_2$$

In the troposphere, the region of UV radiation (Figure 2-1, top) needed to photolyze N_2O is blocked overhead chiefly by the stratospheric ozone layer. Similarly, the concentration of $O(^1D)$ in the troposphere (Figure 2-1, bottom) is exceedingly small due to its

highly reactive nature and because the main production processes of $O(^1D)$ also require UV radiation to photolyze ozone, peroxides, and other oxygen-containing species (Seinfeld and Pandis, 2006).

The inertness of N_2O in the troposphere lends an estimated average lifetime of 116 $\pm$ 9 years (Prather et al., 2015). Estimates of the N_2O lifetime vary depending on the method used to calculate the value, spanning about 110 years to 175 years depending on the observations and models used (Prather et al., 2015). Regardless of the exact value of this lifetime, it is agreed to be significantly longer than those of other major greenhouse gases: the lifetime of CH_4 is estimated at 12.4 years and the lifetime of CFC-11 is estimated at 24.0 years; contrast these lifetimes to those of extremely inert gases such as CF_4 that have an estimated lifetime of 50,000 years (IPCC, 2013).

2.4 Radiative Impact and Ozone Depletion

The impact of atmospheric N_2O on the radiative balance of Earth is becoming increasingly important due to its linearly increasing atmospheric concentration, the wavelengths of its spectral absorption features, and its long chemical lifetime.

Each molecule of N_2O has an enhanced effect on Earth's radiative environment due to its absorption cross-section and the unsaturated characteristics of its infrared absorption bands; in contrast, each molecule of CO_2 that is emitted competes for radiation in regions of the electromagnetic spectrum that are relatively "saturated" by the large concentrations of competing absorbing chemical species (Seinfeld and Pandis, 2006).

In addition to the direct radiative effect that N_2O has on Earth's climate due to its infrared absorption, it can have an additional impact due to its destruction pathways in the stratosphere. Photolysis and chemical destruction by $O(^1D)$ can lead, directly or indirectly, to creation of nitrogen oxides (such as NO) that proceed to catalytically destroy stratospheric ozone (Ravishankara et al., 2009). Due to the altitudes at which N_2O is destroyed (Prather and Hsu, 2010), the nitrogen oxides produced can have immediate effect in the areas of greatest ozone mole fraction (Ravishankara et al., 2009). By destroying ozone in this region of the atmosphere, additional high-energy ultraviolet radiation can make its way through the rest of the atmosphere to the surface (IPCC, 2007, 2013; Ravishankara et al., 2009), leading to additional warming.

2.5 Isotopic Chemistry

In this experiment, the isotopic chemistry of nitrous oxide (N_2O) is explored in order to understand the emission of "whole-gas" (all molecules without regard to isotopic chemistry

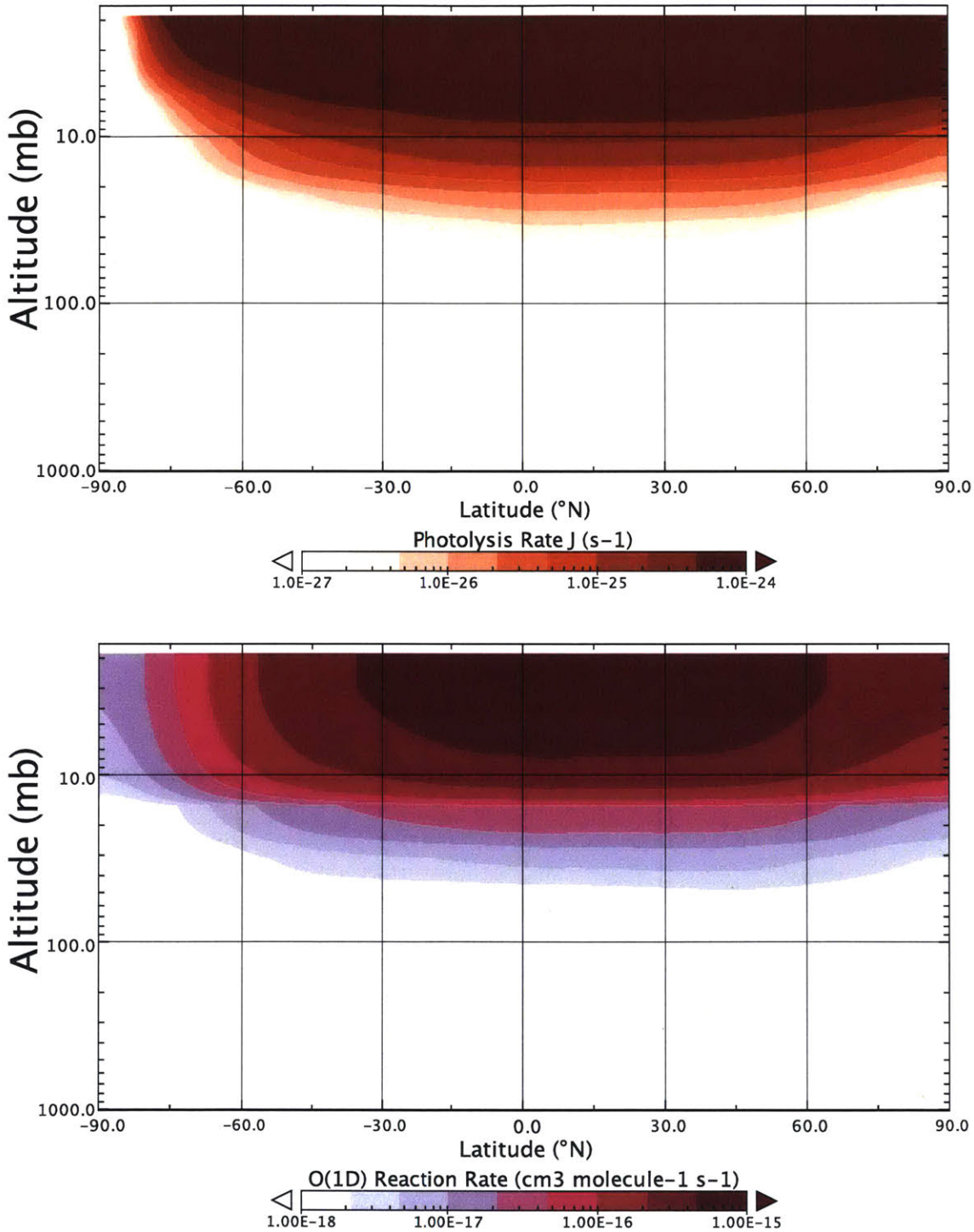

Figure 2-1: Latitude-altitude cross-section of photolysis (top) and O(^{1}D) (bottom) reaction rates in April from Saikawa et al. (2014)

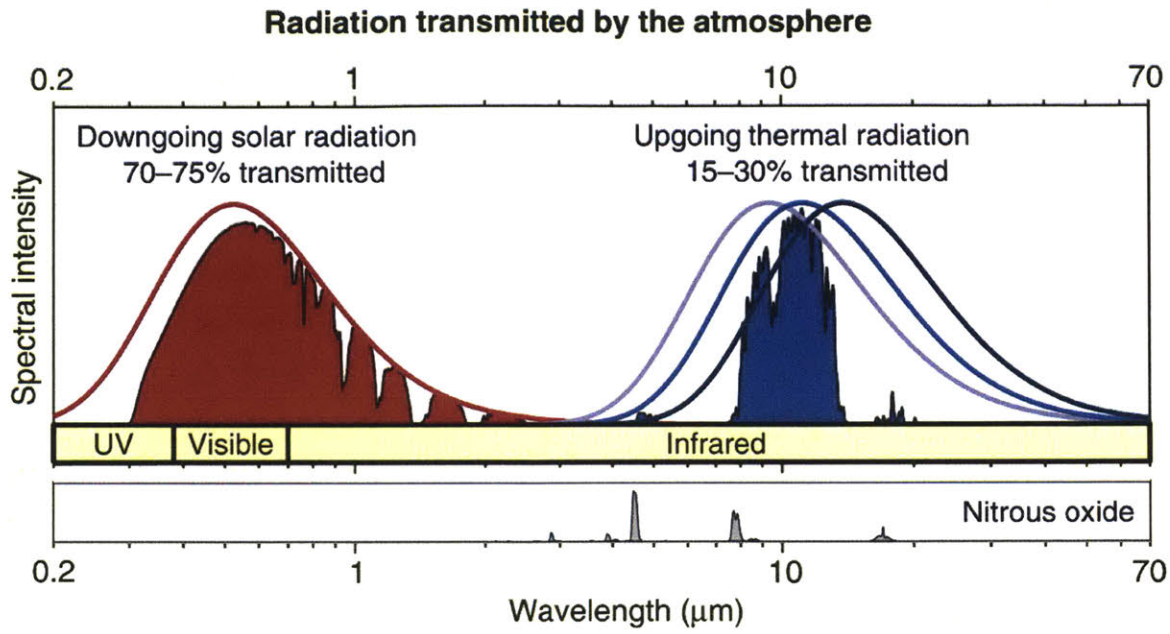

Figure 2-2: Regions of the electromagnetic spectrum in which N_2O absorbs and re-radiates

described below) N_2O. Isotopic ratios of N_2O may be assessed on a bulk basis in a given sample of N_2O, but heavy-atom isotopic substitutions occur on a discrete, *per-molecule* basis. Because ^{14}N and ^{16}O are the most common isotopes of nitrogen and oxygen atoms, respectively, the most common form of N_2O is $^{14}N^{14}N^{16}O$. The most common heavy-atom-substituted isotopic analogues, or **isotopologues**, of N_2O are $^{14}N^{15}N^{16}O$, $^{15}N^{14}N^{16}O$, and $^{14}N^{14}N^{18}O$.

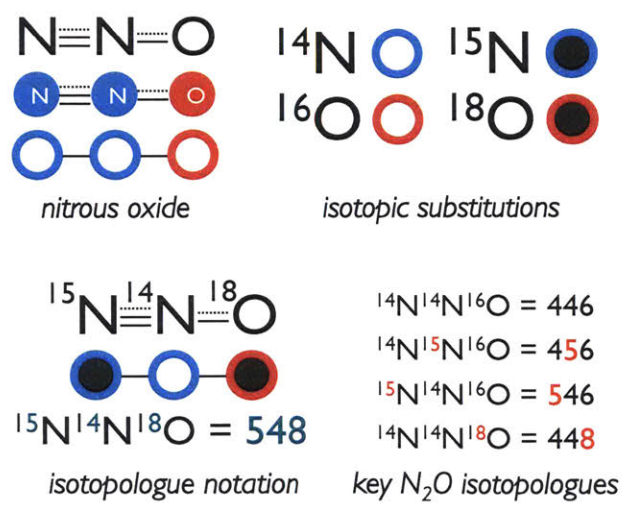

Figure 2-3: Pictorial representations of N_2O isotopologues

Doubly-substituted N_2O isotopologues (Schmidt and Johnson, 2015) and inclusion of ^{17}O in N_2O isotopologues (McLinden et al., 2003) are rare, and represent a vanishingly small number of molecules in a given sample of whole-gas N_2O; therefore, the four isotopologues outlined in Figure 2-3 are the only N_2O isotopologues considered in this experiment. When concentrations of *whole-gas* or *bulk* N_2O are required, they can be determined by analytical methods that do not differentiate N_2O isotopologues, or they can be calculated by summing the concentrations of all N_2O isotopologues.

As shown in Figure 2-3, each of the most common isotopologues of N_2O can be abbreviated by the mass number ones-place digit of each atom in order of the furthest nitrogen atom from the oxygen atom (N^{β}), the closest nitrogen atom to the oxygen atom (N^{α}), and the oxygen atom itself. Therefore, as in Figure 2-3, $^{15}N^{14}N^{16}O$ can be represented as **546**.

$$^{15}R^{\alpha} = [456]/[446] \qquad \delta^{15}N^{i} = (^{15}R^{i}_{sample} / {}^{15}R_{std}) - 1$$

$$^{15}R^{\beta} = [546]/[446] \qquad SP = \delta^{15}N^{\alpha} - \delta^{15}N^{\beta}$$

$$^{15}R = (^{15}R^{\alpha} + {}^{15}R^{\beta})/2 \qquad \text{(SP: site preference)}$$

$$^{18}R = [448]/[446] \qquad \delta^{18}O = (^{18}R_{sample} / {}^{18}R_{std}) - 1$$

isotopic ratios *delta notation*

Figure 2-4: Equations used to calculate N_2O isotopic ratios (R) and "delta-values"

In order to express the relative populations of N_2O isotopologues in a bulk sample, the "raw" isotope ratio (R) (Figure 2-4) and delta-value (δ) notation discussed in detail in Toyoda et al. (2013) will be used throughout this experiment (Figure 2-5). Isotope ratios (R) are calculated by comparing the number of molecules of "light" isotopologue **446** to the number of molecules of any given "heavy" isotopologue (**456**, **546**, or **448**). Delta-values (δ) involve comparing the measured isotopic ratios (R_{sample}) to the isotopic ratio of a widely-accepted standard (R_{std}). For N_2O, the most commonly used standards (Potter, 2011; Harris et al., 2014, 2017; Mohn et al., 2014) are ^{18}O in Vienna Standard Mean Ocean Water (VSMOW, $^{18}R_{VSMOW} = 0.0020052$) and ^{15}N in mean atmospheric nitrogen ($^{15}R_{N2} = 0.0036765$).

The delta-values calculated for the hypothetical sample in Figure 2-5 compare this sample to a "standard" of N_2O that has measurements both site-specific ^{15}N ratios and the ^{18}O ratio. In practice, each atom in N_2O is considered separately and compared to the appropriate ^{15}N and ^{18}O standards (in this experiment, VSMOW and mean atmospheric N_2).

2.6 Isotopic Signatures in Sources

The main source types of atmospheric N_2O, as listed in Table 1.1, are agriculture, natural land processes, industrial processes, biomass burning, and biotic processes in oceans and fresh water features. Each of these sources has a unique range of N_2O isotopic ratios (Figure

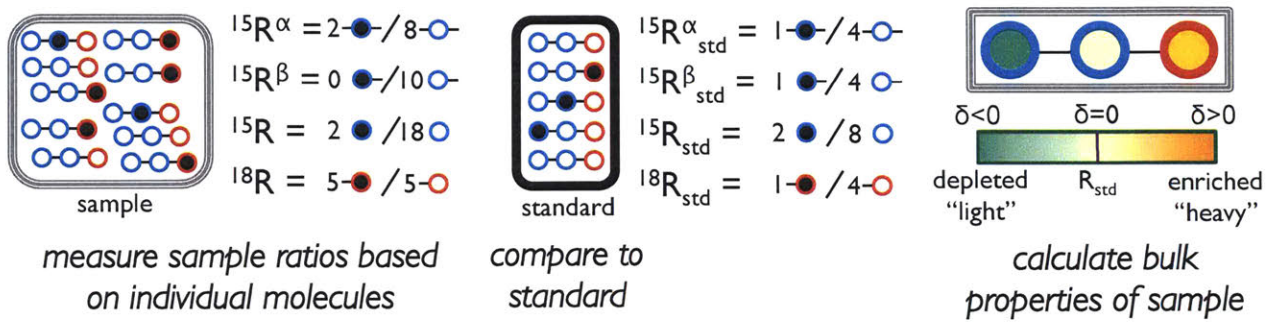

Figure 2-5: Isotopic ratios of N_2O as presented in *delta notation*, including a pictorial example of delta-value calculation based on whole-gas N_2O samples and a hypothetical N_2O isotopic standard

2-6) due to persistent heavy-atom enrichment or depletion inherent in the kinetics and thermodynamics of the production processes (for ^{15}N (Pérez et al., 2001)) or the mean isotopic ratios of water in the source region (for ^{18}O (Whalen and Yoshinari, 1985)).

Although ^{15}N isotopic source signatures span wide ranges (Figure 2-6) depending on the source type, on a global average basis, each source group remains mostly distinct from the rest. These ranges (Potter, 2011; Pérez et al., 2001; Whalen and Yoshinari, 1985) were distilled into the average values presented in Figure 2-7.

As global consumption patterns continue to change, however, these grouped mean isotopic ratios may continue to change. The increasing demands on agriculture to meet global food needs will continue to drive soil conditions from the "natural" state, as seen in Figure 2-6, to a "depleted" state in which additional nitrogen must be added to the soil to be used for agriculture (Mandernack et al., 2009; Acton and Baggs, 2011). Since N_2O can be created as a waste byproduct of inefficient nitrification and denitrification processes (Snider et al., 2013, 2009, 2012), addition of superstoichiometric amounts of nitrogen (in the form of ammonia, ammonium salts, or nitrates) to soils as fertilizer (Acton and Baggs, 2011) will lead to drastically enhanced emissions of N_2O as soil bacteria attempt to moderate the artificially-induced glut of available nitrogen (Pérez et al., 2001).

2.7 Isotopic Signatures from Stratospheric Sink

In addition to the isotopic signatures seen in distinct N_2O sources, another major driver in the overall isotopic chemistry of atmospheric N_2O is the enrichment of heavy-substituted N_2O isotopologues in the stratosphere due to kinetic effects (Kaiser et al., 2002a,b, 2006; Röckmann et al., 2001) in the two N_2O destruction pathways.

The stratospheric N_2O reactions introduced above and in Figure 1-4 do not all proceed

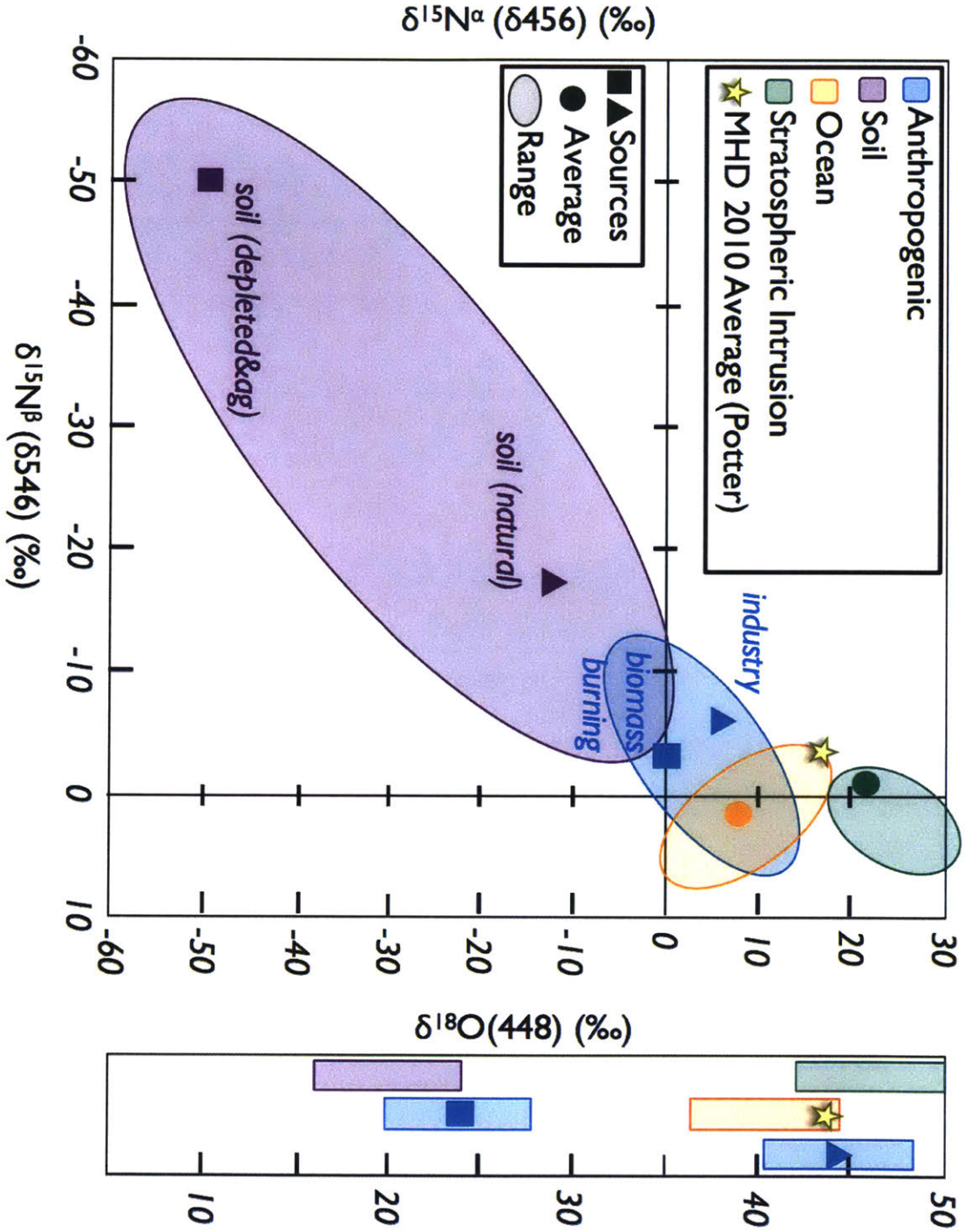

Figure 2-6: Ranges of site-specific ^{15}N and ^{18}O isotopic ratios for various N_2O sources impacting measurements at Mace Head, Ireland, including an average modeled estimate for measurements at Mace Head (after Potter (2011), Figure 3.5)

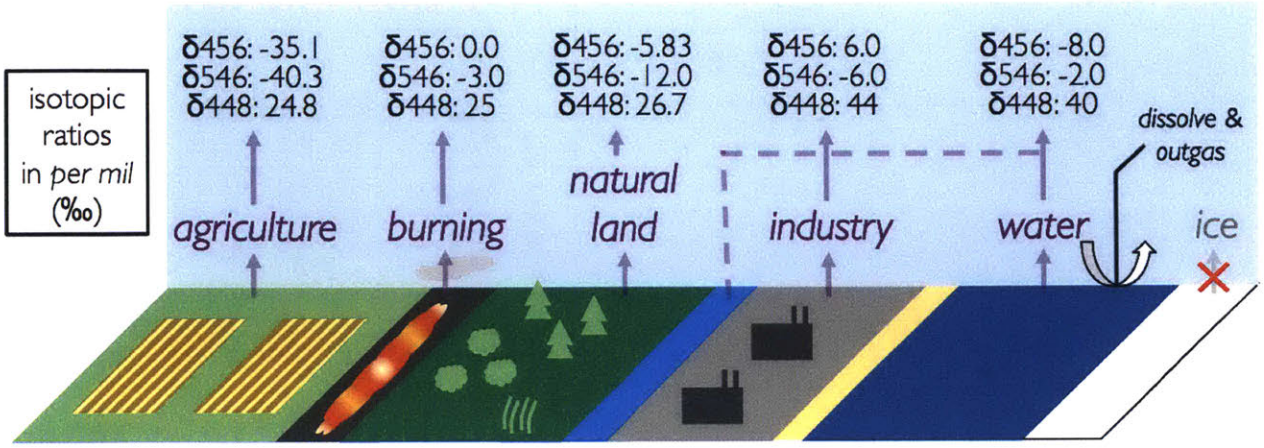

Figure 2-7: Average isotopic ratios of sources of N_2O (Potter, 2011; Pérez et al., 2001; Whalen and Yoshinari, 1985)

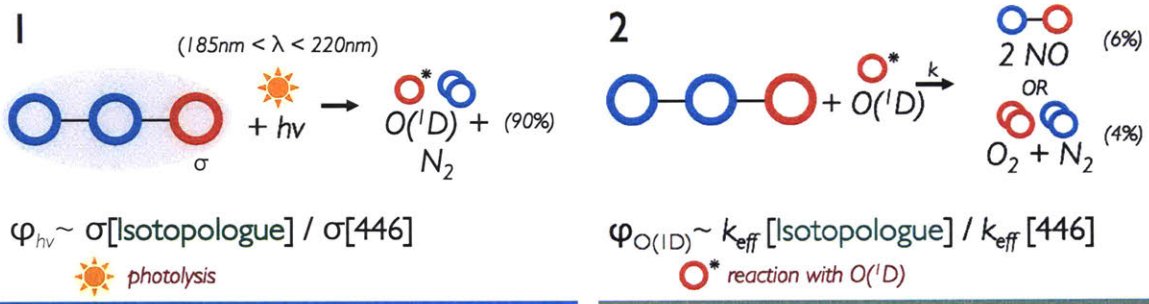

$\varphi_{h\nu} \sim \sigma$[Isotopologue] / σ[446]

photolysis

$\varphi_{O(1D)} \sim k_{eff}$ [Isotopologue] / k_{eff} [446]

reaction with $O(^1D)$

Isotope	ε_N (cross-section factor)	Fractionation Factor (φ)
446	0	1
546 ($^{15}N^{\beta}$)	-0.0214	0.9786
456 ($^{15}N^{\alpha}$)	-0.0512	0.9488
448 (^{18}O)	-0.0331	0.9669

Isotope	k_1 (to N_2+ O_2, s^{-1})	k_2 (to 2 NO, s^{-1})	Fractionation Factor (φ)
446	4.90×10^{-11}	6.70×10^{-11}	1
546 ($^{15}N^{\beta}$)	4.86×10^{-11}	6.64×10^{-11}	0.991
456 ($^{15}N^{\alpha}$)	4.89×10^{-11}	6.69×10^{-11}	0.998
448 (^{18}O)	4.84×10^{-11}	6.62×10^{-11}	0.986

Figure 2-8: Isotopic kinetic effects in each stratospheric destruction process of N_2O (Röckmann et al., 2001; Kaiser et al., 2002a)

at the same rate. On average, photolysis (Reaction 1 in Figure 2-8) accounts for 90% of stratospheric N_2O destruction (Röckmann et al., 2001), while reaction with $O(^1D)$ accounts for 10% of destruction (6% for Reaction 2a, 4% for Reaction 2b in Figure 2-8) (Kaiser et al., 2002a). In addition, each isotopologue of N_2O is destroyed at different rates (Figure 2-8) for each destruction process, leading to enrichment of ^{15}N and ^{18}O in stratospheric N_2O.

As shown in Figure 2-9, reaction with $O(^1D)$ slightly enriches all three atoms of N_2O, while photolysis drastically enriches $^{15}N^{\alpha}$ (**456**) compared to the modest enrichment of $^{15}N^{\beta}$ (**546**). Due to this distinct pattern, bulk measurements of ^{15}N are not sufficient to distin-

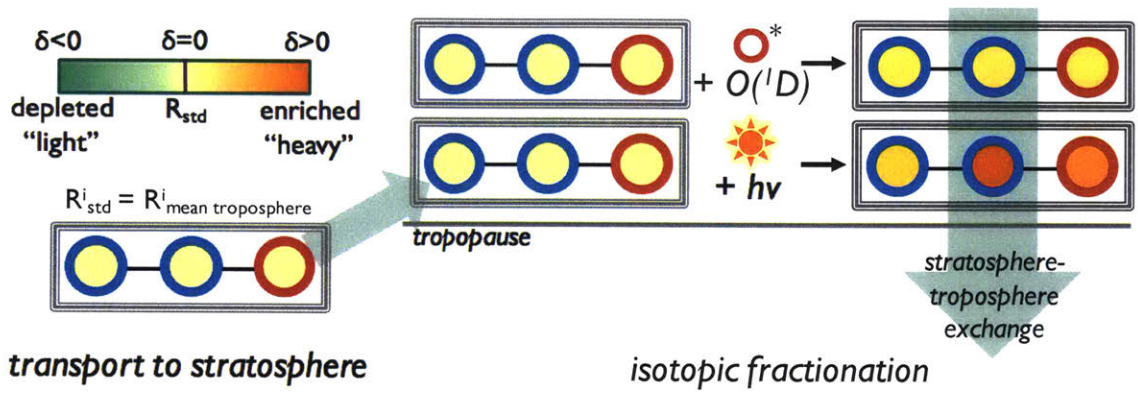

Figure 2-9: Isotopic fractionation processes of N_2O lead to enrichment of heavy-substituted N_2O isotopologues compared to mean tropospheric N_2O (R_{std} of each isotopologue is equal to the mean isotopic ratio of tropospheric N_2O)

guish N_2O sources or to provide evidence of stratosphere-troposphere exchange. Site-specific isotopic ratios of ^{15}N must be known in order to definitively identify an N_2O-containing stratospheric intrusion at the surface; certain ocean-based sources of N_2O have similar $^{15}N^{bulk}$ values (Yamagishi et al., 2007) to those from natural soil sources, but tend to be enriched in $^{15}N^{\beta}$ (**546**) instead of $^{15}N^{\alpha}$ (**456**).

2.8 Uncertainty in N_2O Isotopic Ratios

When combining the factors above that play a role in the N_2O isotopic ratios observed at the surface, any combination will involve multiple variables that have large amounts of uncertainty. Notably, the large ranges in all three site-specific isotopic ratios for N_2O sources (Figure 2-7) compound with uncertainties in the magnitudes and locations of bulk N_2O sources; this leads to large relative ranges for emissions of each N_2O isotopologue.

This theoretical uncertainty presents a great opportunity for additional targeted measurement of individual N_2O emissions sources to further constrain the ranges in which their site-specific ^{15}N and ^{18}O signatures fall. While N_2O isotopic observations in one location may be able to provide slight constraint on the average isotopic environment near the measurement sites, the dilution of multiple source signatures into well-mixed background air requires long-term N_2O isotopic observations in order to constrain emissions estimates by magnitude and source sector, as theoretically performed for methane using synthetic CH_4 "pseudodata" isotopic ratio observations in Rigby et al. (2012). The component experiments of this thesis will largely follow the procedure described by Rigby et al. (2012) in estimating source-specific N_2O emissions in Europe using observations from recent N_2O isotopic ratio observation campaigns.

Chapter 3

Nitrous Oxide Isotopic Analysis

This chapter will describe methods for measurement of N_2O isotopic ratios, and will introduce observations made using the Stheno-TILDAS instrument (Harris et al., 2014) at Mace Head, Ireland in 2014-2015. As with any other chemical measurement, there are many choices regarding instrumentation and procedure, each of which impacts the accuracy and precision of the resulting analysis. Early isotopic analysis of N_2O was solely conducted using mass spectrometry and highly controlled analysis of standard gases in order to account for the various confounding factors that result from ionization of N_2O, such as "ion scrambling" in which the terminal (β) nitrogen atom may end up as the nitrogen atom in the NO^- ion fragments analyzed by the mass spectrometer despite the original bond between the oxygen atom and the central (α) nitrogen atom. These "isotope ratio mass spectrometry" (IRMS) instruments often require a large permanent magnet to separate the ions being analyzed, reducing the capability of high-frequency *in situ* IRMS-based N_2O isotopic analysis.

Recent advances, notably in the field of compact laser-based optical spectroscopic instrumentation, have led to the ability to directly measure N_2O isotopic ratios without confounding factors inherent in mass spectrometry. In addition, the relatively small size of these instruments can enable their deployment to sites of interest where high-frequency N_2O isotopic observations can be made *in situ*. The Stheno-TILDAS continuous-wave laser spectroscopy instrument, built at MIT and described in detail by Harris et al. (2014), has shown that such high-frequency isotopic observations are feasible with its initial field deployment at the Mace Head Atmospheric Research Station in County Galway, Ireland. Other similar long-term N_2O isotopic analysis campaigns, such as that conducted in Dübendorf, Switzerland and described in Harris et al. (2017), show the value of high-frequency N_2O observations in helping constrain local, regional, and global estimates of N_2O emissions.

3.1 Initial N_2O Isotopologue Measurements

Depending on the desired future use of the data, there are many different instruments and experimental procedures for measuring N_2O isotopic ratios that can produce useful results. The first *in situ* measurements of N_2O isotopologues led to some improvements in understanding global and regional N_2O budgets, but early analytical methods (such as isotope ratio mass spectrometry, IRMS) had significant drawbacks including lack of site-specific ^{15}N differentiation (Yoshida and Matsuo, 1983) and ion rearrangement (Potter et al., 2013). However, due to the ubiquity of these instruments, many researchers and laboratories continue to make IRMS-based N_2O isotopic ratio measurements using analytical methods that can account for the drawbacks discussed above. Newer analytical methods performing analysis using optical spectroscopy avoid the need for these particular correction methods due to direct nondestructive measurement of isotopic ratios.

3.1.1 Offline vs Online Analysis

The first determination that must be made in making observations of N_2O isotopic ratios is whether the measurements will be made "offline" or "online", with the difference being whether the samples are collected in flasks and analyzed at a later date or directly analyzed from an inlet system.

There are two major advantages to flask collection and subsequent offline analysis of samples: there can be a large volume of air collected on which many replicate analyses can be performed, and samples can be collected from environments where it would not be feasible to deploy an instrument. The most significant advantage of direct online analysis is the capability of high-frequency sampling, leading to a timeline of data that can identify short-term pollution events and isotopic excursions that would be lost in an infrequent flask sampling schedule.

Due to the low mole fractions of N_2O isotopologues in ambient air, most N_2O isotopic ratio analyses require significant volumes of ambient air. Over a liter of ambient air is typically required for pre-concentration and optical analysis of N_2O isotopic ratios (Harris et al., 2014, 2017). Therefore, if a flask is filled with ambient air at high enough pressure to yield liters of air at standard conditions, additional precision can be gained by repeating the analysis on the same flask.

In some cases, offline analysis is the only feasible choice for making N_2O isotopic ratio measurements. In extremely remote areas that may not be able to serve N_2O isotopic instruments, whether due to difficulty of standard gas delivery or lack of personnel support, flasks could still be used to collect samples for subsequent analysis. For high-altitude sampling, whether on aircraft or balloon-based platforms, the size and delicacy of some instrumental components prohibits direct online analysis.

In an ideal experimental setup, combining online and offline analysis may provide the best possible outcome for any N_2O isotopic ratio instrument. Flask measurements from the same location as online analysis can be collected and compared to high-frequency online observations made at the same time in order to ensure comparability of both types of data. In addition, flasks could be collected from other locations and analyzed on a schedule that still supports near-continuous high-frequency sampling.

3.1.2 Mass Spectrometry

In order to produce measurements of site-specific N_2O isotopic ratios differentiating between the two ^{15}N positions on the molecule, mass spectrometry instruments typically monitor five instrumental response channels corresponding to the molecular ion N_2O^+ and the fragment ion NO^+. Depending on the presence of heavy ^{15}N or ^{18}O isotopes in these ions, the five mass-to-charge (m/z) ratios of 44/45/46 (N_2O^+) and 30/31 (NO^+) from ambient samples are compared to those of a known isotopic standard gas.

Although an analytical solution can be developed to calculate isotopic ratios from the instrumental response to these five ions (Potter et al., 2013), the uncertainty involved in obtaining a number of factors that describe the ionization "scrambling" by which the β-position nitrogen atom ends up in the NO^- ion fragment leads to a relatively poor theoretical limit on the precision of ambient air observations made using mass spectrometry. Continuing development of procedures for using mass spectrometry in N_2O isotopic analysis (Potter et al., 2013) show promise to mitigate some of the early experimental drawbacks (such as a lack of site specificity in ^{15}N measurement), but new laser-based optical instruments described in the following section are able to avoid issues of these types altogether.

3.1.3 Laser Spectroscopy

Optical analytical measurements of N_2O isotopic ratios are able to avoid many of the difficulties with mass spectrometry due to the non-destructive nature of optical spectroscopy. Instead of ionizing molecules of N_2O and analyzing the resulting fragments, optical spectroscopy uses the Beer-Lambert Law ($A = \epsilon * b * c$, where A is the measured absorbance, ϵ is a molar absorptivity coefficient at a particular wavelength, b is the path length of the cell, and c is the concentration of the absorbing species) to directly obtain concentrations of N_2O isotopologues from their absorption of specific infrared frequencies. Lasers are typically used to provide the light used by these instruments due to their coherence and narrow band of wavelengths, which allows for analysis of N_2O isotopologue absorption lines that may be closely grouped together.

The most significant limitations of optical analysis of N_2O isotopic ratios are the low mole fractions of heavy-substituted N_2O isotopologues in tropospheric air and the presence

of other gases (such as water vapor, CO, and CO_2) that absorb in the same regions of the infrared spectrum. In order to eliminate these confounding factors, a series of purification and pre-concentration steps may be employed in order for these instruments to be able to analyze relatively pure samples of N_2O.

3.2 Isotopic N_2O Observations at Mace Head, Ireland using Stheno-TILDAS

The observational portion of this thesis involves analysis of N_2O isotopologue concentrations at a remote atmospheric measurement station at Mace Head, Ireland. Mace Head (MHD) is member station of the AGAGE network (Prinn et al., 2000), which provides co-located and contemporaneous measurements of meteorological conditions and atmospheric concentrations of many relevant trace gases.

3.2.1 Mace Head Atmospheric Research Station

Mace Head Atmospheric Research Station (MHD) in western Ireland was chosen as a flagship site in the AGAGE network due to its unique meteorological conditions and proximity to continental Europe. The synoptic situation at MHD features clean background air from the northern Atlantic Ocean about half of the time, mixed-source and polluted air from the UK and continental Europe ~35% of the time, and stagnant air masses sampling local sources for the remaining fraction (Potter, 2011).

Figure 3-1: Location of the AGAGE station (Prinn et al., 2000) at Mace Head, Ireland (Google Maps)

The station at MHD is also well placed to observe the delayed effects of stratospheric intrusions on surface air due to its middle/high latitude location (53° N) in the northern hemisphere. Direct observation of isotopically heavy N_2O in springtime (April-May) surface air following maximally active stratosphere-troposphere exchange events in February-March (Potter, 2011) could help disentangle stratospheric contributions to the local N_2O environment from those of other regional and global sources, especially when co-located high-frequency observations of other stratosphere tracer gases at MHD such as $CFCl_3$, CF_2Cl_2 and SF_6 (Nevison et al., 2007) are considered.

3.2.2 Observations from 2010

The first site-specific N_2O isotopic ratio observations made in the entire AGAGE network occurred in 2010, as part of the PhD thesis by Katherine Potter at MIT (Potter, 2011). These flask-based offline observations (Figure 3-2) were contextualized by simple computational modeling of the isotopic environment expected at MHD given the relative contribution of four aggregated N_2O source sectors (soil, ocean, burning, and industry; shown in Figure 2-6).

The infrequent nature of offline flask-based measurements means that some long-term patterns in N_2O isotopic ratios can be deduced from the timelines in Figure 3-2. However, after removal of all "non-baseline" observations as determined by the AGAGE standard "pollution flag" algorithm using tracers such as CO and CH_4 (Prinn et al., 2016), the remaining "baseline" measurements leave many gaps for deducing the contribution of well-mixed background tropospheric air to the N_2O isotopic ratios measured at the surface at MHD. The overall seasonal trends in N_2O isotopic ratios in a particular year of observations will largely depend on large-scale meteorological patterns such as the North Atlantic Oscillation (Chen and Prinn, 2005).

3.2.3 North Atlantic Oscillation

The NAO largely regulates transport phenomena that lead to surface emissions source signatures being measured at Mace Head, both in the model and in observed surface concentrations. The phase of the NAO has a well-documented effect on surface concentrations of CH_4 at Mace Head (Chen and Prinn, 2005), in which surface winds preferentially transported relatively clean air to MHD in positive phases of NAO and transported relatively polluted air from the European continent to MHD in negative phases of the NAO.

In addition, patterns of vertical transport and stratosphere-troposphere exchange influenced by the NAO (James et al., 2003) will have an impact on the observed N_2O isotopic ratios at the Northern Hemisphere surface in the late spring months after stratosphere-troposphere exchange reaches its maximum in early spring (Potter, 2011). Since the only observed N_2O isotopologue concentrations in this experiment are located in a mid-latitude

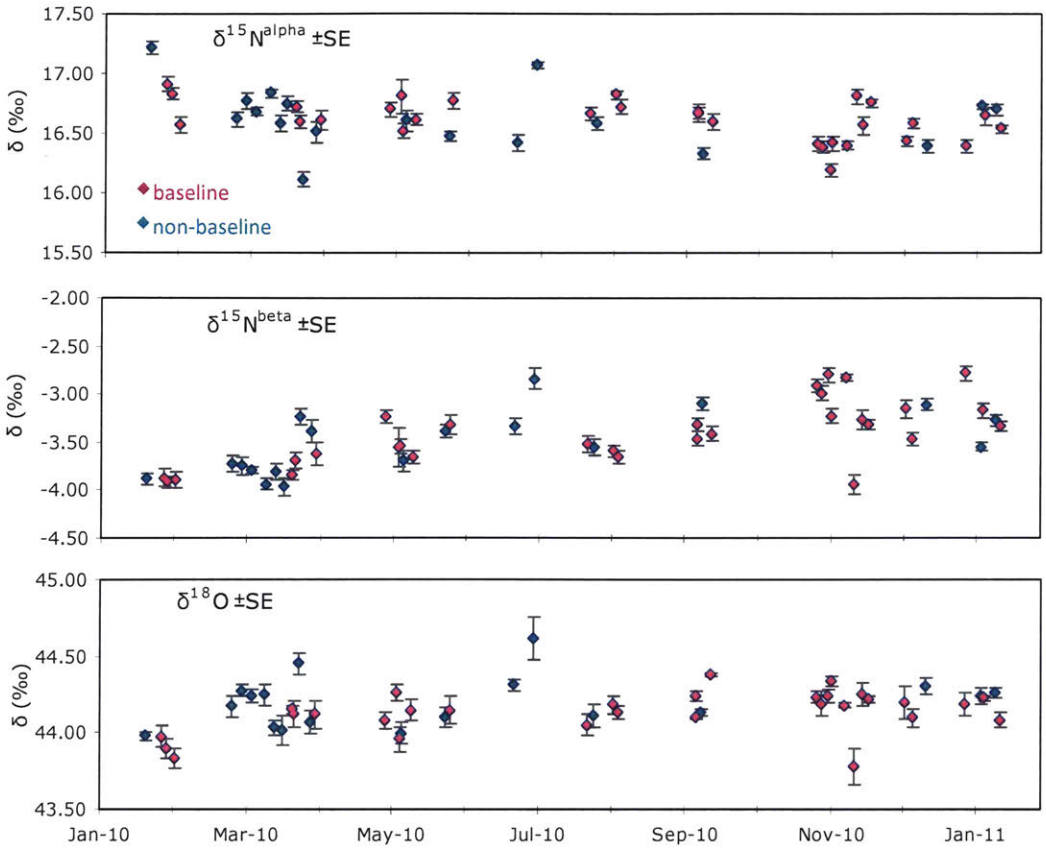

Figure 3-2: CF-IRMS N_2O isotopic ratio observations from 2010 at MHD, adapted with permission from Potter (2011) Figure 4.3

northern hemisphere site (MHD), the monthly averaged gross transport patterns experienced at MHD should have similar patterns in 2007-2008, 2011-2012, 2014-2015 due to alignment of their NAO index values (Figure 3-3) on monthly and daily timescales.

The CF-IRMS observations of N_2O isotopic ratios at MHD from Potter (2011) spanned January 2010 to January 2011 (48 samples in total). Due to the fact that these measurements were infrequent, made from "offline" analysis of flasks, and taken in a phase of NAO significantly different than that of 2014-2015, the seasonality and long-term trends in the resulting N_2O isotopic ratios are expected to be different in the high-frequency Stheno-TILDAS observations introduced in the following section.

3.3 Stheno-TILDAS Instrument

A new instrument capable of high-frequency measurements of site-specific N_2O isotope ratios at remote sites (Stheno-TILDAS (Harris et al., 2014), Figure 3) has recently been developed

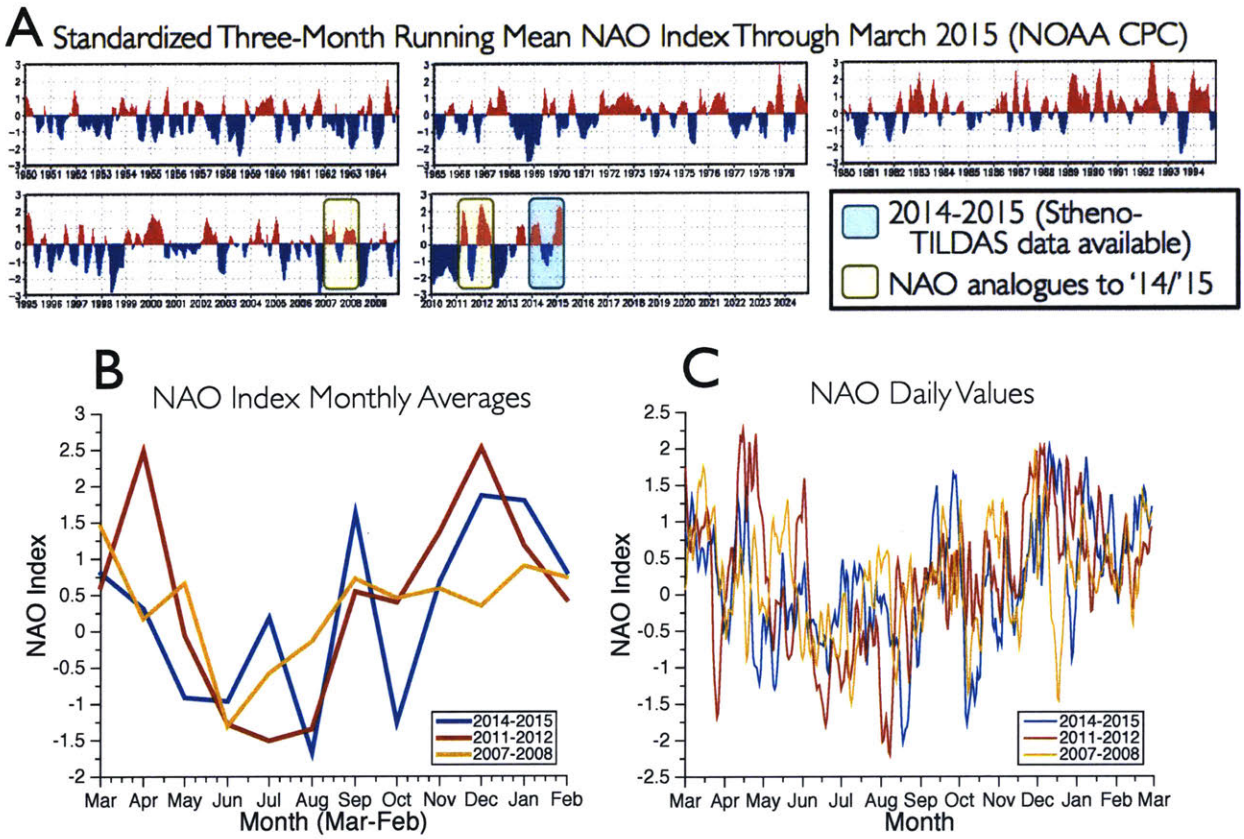

Figure 3-3: North Atlantic Oscillation index (NAO, from NOAA Climate Prediction Center) three-month running mean with 2014-2015 and closest analogues highlighted (panel A), monthly averages for 2014-2015, 2011-2012, and 2007-2008 (panel B), and daily values for the same time periods (panel C)

in a partnership between the laboratories of Ronald Prinn and Shuhei Ono at MIT, and David Nelson at Aerodyne Research. This instrument consists of a Stheno preconcentration system modified from Potter et al. (2013) (as described in Harris et al. (2014)) designed and built at MIT, combined with a tunable infrared laser direct absorption spectroscopy system (TILDAS) developed and built at Aerodyne Research. These measurements represent the first **real-time**, **high-frequency** isotopically-differentiated measurements of N_2O in the AGAGE network.

The Stheno-TILDAS instrument (Figure 3-4) pre-concentrates N_2O in dried ambient air by adsorption of N_2O, CO_2, and CO on DMCS-treated glass beads within a cold cryo-trap (Potter et al., 2013). Potentially interfering species such as nitrogen, oxygen, and other trace gases pass through the trap without adsorption. Spectroscopic analysis of N_2O at absorption bands at 2188 cm^{-1} and 2203 cm^{-1} (Harris et al., 2014) follows upon desorption of the concentrated sample from the trap (Figure 3-5). Pre-concentration is necessary due to the low atmospheric concentration of heavy-substituted N_2O isotopologues (**456**, **546**,

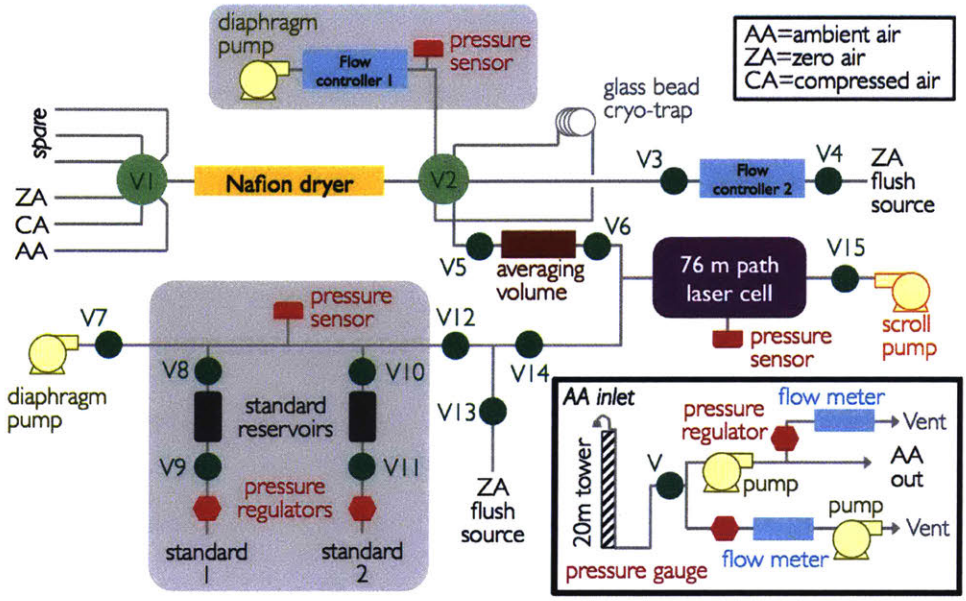

Figure 3-4: Schematic of Stheno-TILDAS instrument (after (Harris et al., 2014), Figure 1)

and **448**) compared to species that absorb in the same infrared (IR) bands. Additionally, the signal strength of N_2O absorption in the TILDAS laser cell is greatly enhanced after pre-concentration, allowing for more precise curve-fitting (Harris et al., 2014) of N_2O spectral features, which leads to greatly improved precision of N_2O isotopologue concentration calculations.

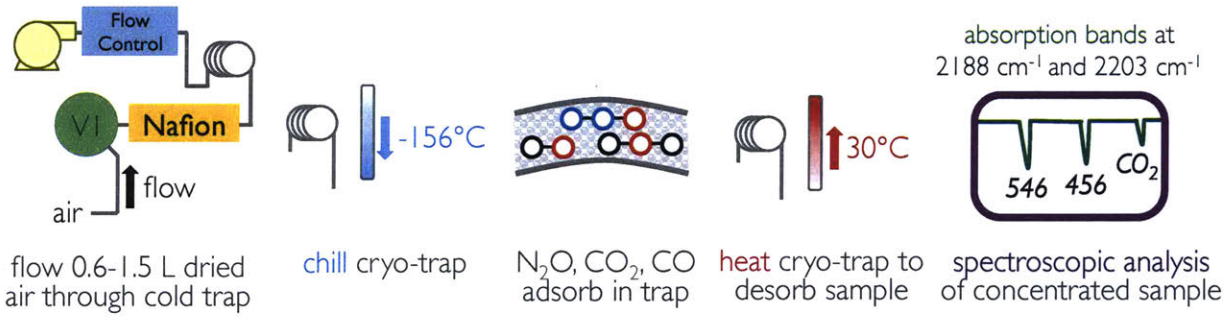

Figure 3-5: Preconcentration and analysis procedure for Stheno-TILDAS

Extensive testing in the initial development phase of the Stheno-TILDAS instrument (Harris et al., 2014) has led to development of built-in methods accounting for spectroscopic peak broadening (pressure and Doppler) and parameterization of the Dicke-narrowing factor (Demtroeder, 2008). Stheno-TILDAS produces highly precise isotopic ratio measurements in each analysis cycle (28 minutes required, typical precisions: 0.32 ‰ for $\delta^{18}O$, 0.17 ‰ for $\delta^{15}N^{\alpha}$, 0.19 ‰ for $\delta^{15}N^{\beta}$, and 0.16 ‰ for $\delta^{15}N^{bulk}$ (Harris et al., 2014)); for repeat analysis of flasks, the precision improves to <0.10 ‰ for all isotopologues in as few as 11 analysis cycles (approximately 5.1 hours) (Harris et al., 2014). The combination of high precision and

a rapid sampling duty cycle can allow for measurements made with Stheno-TILDAS to be linked to rapidly shifting meteorological conditions and intermittent N_2O source dynamics.

With the recent development of compact laser spectroscopy systems and cryogen-free preconcentration systems such as Stheno (Potter et al., 2013), a derivative of the preconcentration component of the Medusa instrument (Miller et al., 2008) used in the AGAGE network, highly precise site-specific N_2O isotopic ratios can be measured quickly at ambient concentrations without the need for consumable liquid cryogens such as liquid nitrogen. These advances allow for installation of analytical instrumentation such as Stheno-TILDAS and the similar P-QCLAS instrument (Harris et al., 2017) at remote sites, leading to high-frequency *in situ* direct measurements of N_2O isotopic ratios without confounding factors discussed above such as ion scrambling and chromatographic co-elution.

Given dense enough spatial and temporal coverage of site-specific N_2O isotopic measurements, the current uncertainty associated with N_2O source budgets could drastically decrease as new data streams are introduced in computational models of N_2O emission, chemical destruction, and transport dynamics.

3.3.1 Experimental Procedure

Long-term records of ambient N_2O isotopic ratios are calculated using calibrations from pure N_2O standards (Potter et al., 2013; Harris et al., 2014) after measurements have been corrected to account for unstable sample pressure/temperature and instrumental drift compared to a source of compressed air (Figure 3-6).

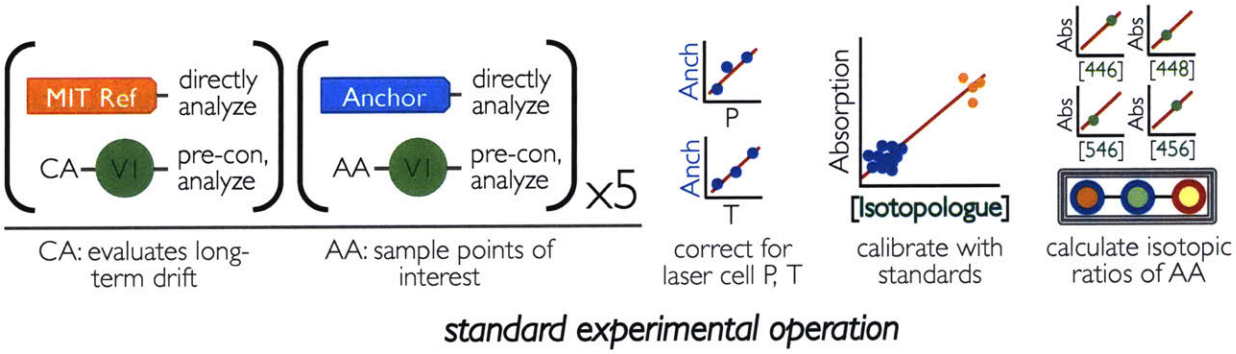

Figure 3-6: Standard experimental procedure for long-term sampling, including preconcentration, of ambient air (AA) and compressed air "drift" standard (CA) with Stheno-TILDAS

Accurate measurement of N_2O isotopic ratios ultimately relies on calibration curves built using standards containing known N_2O isotopic ratios. The lack of a universal N_2O isotopic standard (Mohn et al., 2014) means that N_2O isotopologue analysis of the same sample must be repeatable, different standards notwithstanding. For this experiment, many N_2O standards (Table 3.1) are available, including MIT working standards (Harris et al.,

2014; Potter et al., 2013; Potter, 2011) and EMPA intercomparison standards (Mohn et al., 2014).

Isotopic Ratios of Standard Gases			
* indicates ratios measured only with Stheno-TILDAS † indicates externally verified by S. Toyoda at Tokyo Institute of Technology			
Standard Gas	δ^{18}O (**448**)	δ^{15}N$^{\alpha}$ (**456**)	δ^{15}N$^{\beta}$ (**546**)
Only at Mace Head			
Ref P (MHD Anchor)*	39.8	2.2	1.3
MHD Compressed Air*	41.6	16.6	-2.56
At MHD and MIT			
MIT Ref I†	40.14	-0.44	1.50
MIT Ref II†	40.43	-0.78	0.30
EMPA S1†	35.16	15.70	-3.21
EMPA S2†	32.73	5.55	-12.87
EMPA Target†	42.43	12.10	-7.02
Only at MIT			
MIT Ref III (MIT Anchor)	Not Yet Measured		
MIT Compressed Air	Not Yet Measured		

Table 3.1: Isotopic standards available for use in Stheno-TILDAS experiments at Mace Head, Ireland and at MIT

The "anchor" standards mentioned above are large air tanks containing zero air (nitrogen and oxygen in tropospheric proportions, without other trace gases), 8% CO_2, and 65 ppm N_2O, premixed by the vendor (Airgas or Air Products); the isotopic ratios of the N_2O added to these anchor standards are not known *a priori*, but can be measured using Stheno-TILDAS or other techniques (isotope ratio mass spectrometry, IRMS, for example (Potter et al., 2013)). Anchor standards serve as the primary working standard and are used to determine drift in the laser system due to temperature, pressure, N_2O concentration, and other factors. MIT Ref I/II and EMPA S1/2 are pure tanks of N_2O that are diluted to 65 ppm in zero air with 8% CO_2 in small batches as needed for experiments. At 65 ppm N_2O, the N_2O heavy-substituted isotopologues are concentrated enough for direct analysis in the TILDAS laser cell without passing through the Stheno pre-concentration system. Additional tanks of compressed air, with ambient concentrations of N_2O, are sampled in order to assess the stability of the combined pre-concentration/analysis process (Harris et al., 2014).

3.4 Experimental Best Practices

Due to the reliance on various standard gases to produce calibrations for all types of N_2O isotopic ratio instrumentation, there must be some degree of alignment across all experi-

mental setups in order for the results to be comparable. In the N_2O isotopic measurement community, two "best practice" procedures help ensure that N_2O isotopic ratios that are reported from one instrument are reasonably similar to isotopic ratios that may have been reported by any other instrument.

3.4.1 Isotopic Standard Gases

Without a globally accepted standard gas mixture that can be used by every laboratory making N_2O isotopic ratio observations, one way that measurements can be compared is by using standards that have been thoroughly analyzed by other research groups. Due to the pioneering early work involving N_2O isotopic ratios (Yoshida and Matsuo, 1983) at Tokyo Institute of Technology, numerous instruments use gases first analyzed by the researchers at that institution (Mohn et al., 2014; Harris et al., 2014; Potter, 2011) in order to have a calibration scale that may be traced back to a common source.

The standard gases listed in Table 3.1 with a dagger (†) have been analyzed externally by Sakae Toyoda at Tokyo Institute or Technology, allowing for Stheno-TILDAS observations made using these standards to be traceable to a shared source, even if the same gases themselves are not shared among different groups conducting N_2O isotopic measurements.

3.4.2 Instrument Intercomparisons

A more rigorous method that can account for differences among instruments is through a blind intercomparison study such as that conducted by Joachim Mohn and collaborators at EMPA (Mohn et al., 2014). In this experiment, ten laboratories with optical spectroscopy and IRMS instruments were allowed to follow their own analytical procedure, but were given two designed standard gas mixtures with known N_2O isotopic ratios and a blind "target" gas that was to be analyzed and reported. Stheno-TILDAS was originally expected to participate in this intercomparison, but unfortunately, the instrument was not operable at the time that the analyses were to be completed. Future *post hoc* inclusion of Stheno-TILDAS in this intercomparison campaign may be possible following analysis of reserves of the standard gases provided by EMPA to MIT (Harris et al., 2014).

3.5 Observations at Mace Head, Ireland (Summer 2014)

The new Stheno-TILDAS instrument (Figure 3-4) was installed as part of the AGAGE network at Mace Head Atmospheric Research Station, Ireland (MHD) between 2014 and 2015. The data obtained by this instrument in its first field campaign starting in June 2014 represent the very first real-time measurements of any isotopic ratios in ambient air in the

entire twelve-site AGAGE network.

The N_2O isotopic ratio observations collected by Stheno-TILDAS at Mace Head, spanning roughly five months in two separate periods (summer 2014 and winter 2014-2015), represent a significant step for the entire AGAGE observation network: introduction of high-frequency *in situ* isotopic ratio observation of a major greenhouse gas. The timeline of observations (Figure 3-7) has rich features that will be explored further using observations of other trace gases at Mace Head (Prinn et al., 2016) and using computational atmospheric chemical transport models.

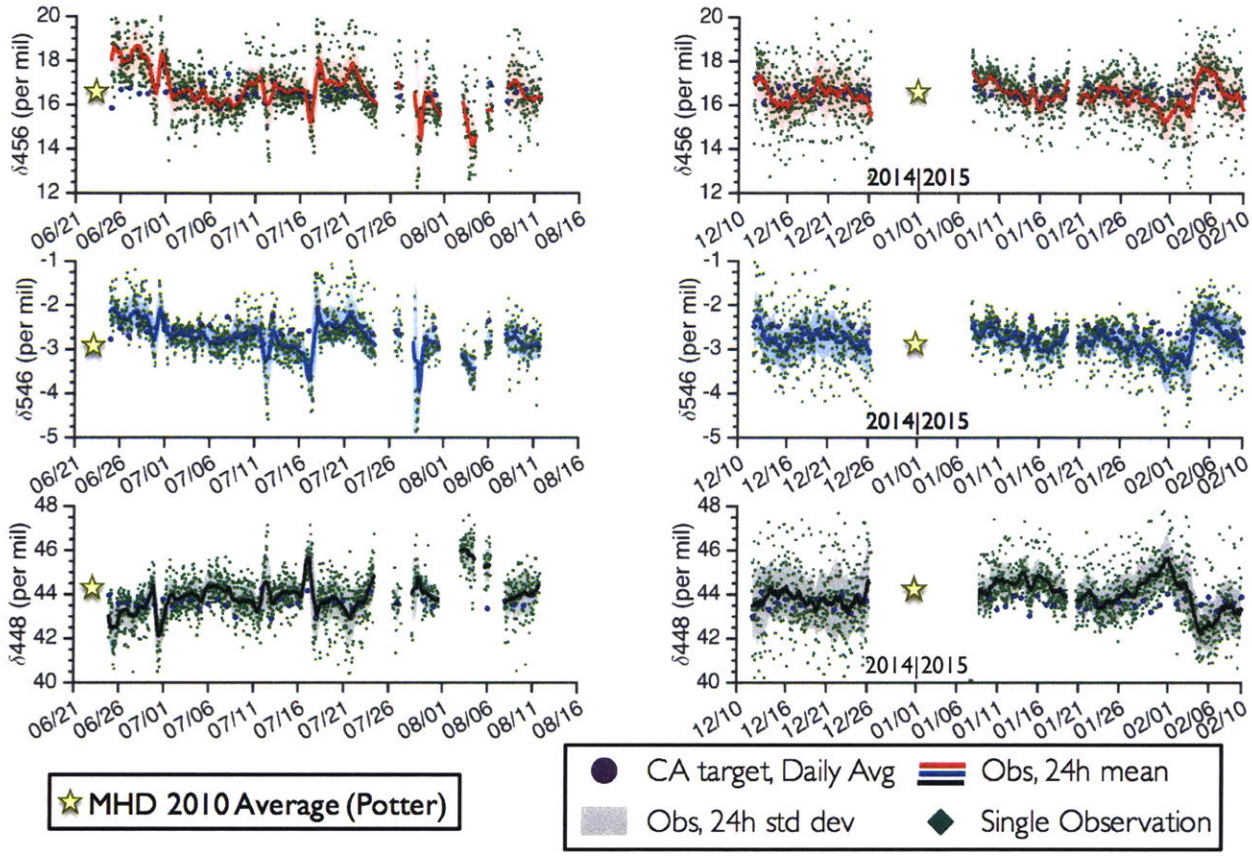

Figure 3-7: Timeline of N_2O isotopic ratios measured at MHD in the first year of Stheno-TILDAS operation; green points indicate actual measurements, the thick line indicates a 24-hour running mean, the translucent bounds represent the standard deviation of isotopic measurements of contemporaneously-measured compressed air "drift" standard, large purple points are daily average measurements of the "drift" standard, and yellow stars indicate the annual average of flask-based isotopic ratio observations made at MHD in 2010 (Potter et al., 2013)

The two seasons sampled in Figure 3-7 exhibit behavior previously seen in past observations of both N_2O isotopic ratio (Figure 3-2) and mole fraction (Figure 1-2), whereby the magnitude of excursions from the well-mixed baseline is smaller in winter than in summer.

As shown in the yellow star and purple dots in Figure 3-7, representing the average of all observations made by Potter (2011) and the daily average of the compressed air "drift" standard sampled by Stheno-TILDAS, the Stheno-TILDAS observations from 2014-2015 are in the range expected at Mace Head.

3.5.1 Interpretation of Stheno-TILDAS Timelines

The timeline of Stheno-TILDAS observations in Figure 3-7 contains, on each axis, numerous plot features that indicate the precision and accuracy of the ambient N_2O isotopic ratios measured at Mace Head. As described in the legend and in the caption of Figure 3-7, the following features are contained in the Stheno-TILDAS timeline:

- Individual Stheno-TILDAS observations (green dots): Each green dot represents one individual observation made from preconcentration and analysis of approximately 1L ambient air, as described in more detail in Figures 3-5 and 3-6.
- Running 24-hour mean of observations (thick solid lines): In order to better understand trends in the observations, a 24-hour running mean of all observations (green dots) is shown as a thick solid line for each N_2O isotopic ratio measured.
- Daily average of compressed air "drift" standard (purple dots): The daily average of the measurements made using the compressed air "drift" standard, which is preconcentrated and analyzed using the same procedure as for ambient samples (Figure 3-5). Ideally, these measurements would all align to the same value due to the singular source from which they are drawn. Differences between the long-term average of the isotopic ratios from the "drift" standard and any given daily average of "drift" measurements indicate potential effects on measured N_2O isotopic ratios due to a variable not currently directly accounted for in the Stheno-TILDAS analysis procedure. Variables such as outdoor temperature and barometric pressure (instead of laser cell temperature and pressure, currently included in the calibration procedure from Harris et al. (2014)) or mole fraction of chemical species that have absorption features in the Stheno-TILDAS infrared regions (such as of CO or CO_2) could be examined in a future controlled experiment for use in new Stheno-TILDAS calibration and analysis procedures.
- Running 24-hour standard deviation of compressed air "drift" standard (translucent bounds around thick lines): The thickness of the colored translucent bounds indicate the running 24-hour standard deviation of the compressed air "drift" standard. This spread gives a sense of the repeatability of measurements made following preconcentration of an air sample. This measure of repeatability correlates well with the "spread" in individual ambient observations (green dots); higher variance in compressed air "drift" standards tends to occur at time periods when the ambient observations also show higher variance (such as December 2014, compared to early January 2015 in Figure 3-7).

- Annual average of measurements at Mace Head from Potter (2011) (yellow stars): The annual long-term averages of N_2O isotopic ratios from the flask-based measurements made in Potter (2011) are near the values observed using Stheno-TILDAS in 2014-2015, indicating that the analysis and calibration procedures for Stheno-TILDAS are compatible with past observations using different instrumentation.

Similar features will appear in timelines for observational and computationally modeled data in later chapters; therefore, an understanding of all the components of Figure 3-7 is necessary to contextualize additional supporting data from other sources.

3.5.2 Experimental Issues from 2014-2015

As seen in the gaps throughout Figure 3-7, in the first year of Stheno-TILDAS operation at Mace Head, there were several mechanical setbacks that interrupted standard operation of the instrument. Before June 2014, the uninterruptible power supply into which Stheno-TILDAS was wired at Mace Head was inoperable. From August to November 2014, a critical pump had failed, preventing operation of valves. After February 2015, a section of the wiring inside the cryotrap housing failed, burning up the insulation surrounding the trap feedthroughs, which led to leaks of lab air into the analytical system. As a new instrument in the field for the first time, many of the issues that arose were unexpected; conditions leading to much of the downtime in 2014-2015 will be mitigated in future campaigns. Instrumental problems notwithstanding, measurements of isotopic ratios in ambient air at Mace Head were possible in two distinct periods (Figure 3-7) in 2014-2015: summer 2014, and winter 2014-2015.

Once longer periods of Stheno-TILDAS operability are possible at Mace Head, the N_2O isotopic ratios measured by Stheno-TILDAS will be used in combination with modeling experiments in order to further probe the dynamics and emissions regimes that led to the observed conditions. In addition, the observed isotopic ratios from future datasets will be compared with local and regional meteorological data (Potter, 2011) and fine-scale regional models such as NAME (Manning et al., 2011) in order to characterize the local N_2O source environment.

3.6 Future Operation of Stheno-TILDAS

After the initial field experiment of Stheno-TILDAS at MHD completed in March 2015, the instrument returned to MIT for the next phase of its experimental life. Due to the advantages in N_2O observation at MHD caused by the synoptic situation in western Ireland, Stheno-TILDAS will most likely continue to analyze air samples from MHD, but more likely from flasks periodically collected at the station. In its new experimental phase, likely collecting

high-frequency samples while stationed at MIT, Stheno-TILDAS can sample flasks from AGAGE stations, from external collaborators, and from flask archives (such as the Cape Grim Air Archive sampled in Park et al. (2012)). After Stheno-TILDAS receives numerous upgrades to its electrical components and control mechanisms, the datasets produced by Stheno-TILDAS will be longer and more consistent than the interrupted timeline presented in Figure 3-7. Future datasets will have fewer gaps associated with malfunctioning parts.

The entire analytical procedure, from air sampling to spectroscopic analysis to calibration, has many areas that can be improved in the future given the opportunity for highly controlled experiments in the laboratory. The current calibration procedure (described above and in Harris et al. (2014)) does not currently account for any dynamics in humidity or mole fraction of potentially interfering gases (notably, CO_2 and CO). Although the in-line Nafion dryer (Figure 3-4) and cold trap largely dry the ambient air samples, and the infrared absorption features of CO and CO_2 do not overlap with key N_2O isotopologue absorption features, any improved calibration procedure will have the goal of reducing the unaccounted variability seen in some regions of the "drift" standard Stheno-TILDAS measurements in Figure 3-7.

3.7 Summary

This chapter introduced the first observations of N_2O isotopic ratios made using the new Stheno-TILDAS instrument (Harris et al., 2014) outside of a controlled laboratory environment. The precisions of the Stheno-TILDAS site-specific N_2O isotopic ratio observations made at Mace Head, although not quite as good as those reported in the initial testing phase of the instrument at MIT in Harris et al. (2014) (0.32 ‰ for $\delta^{18}O$, 0.17 ‰ for $\delta^{15}N^{\alpha}$, 0.19 ‰ for $\delta^{15}N^{\beta}$, and 0.16 ‰ for $\delta^{15}N^{bulk}$), were reasonable enough (Figure 3-7) for notable temporal trends in observed N_2O isotopic ratios to emerge. These trends, which will be analyzed using various means in future chapters in this thesis, have the potential to help attribute the dynamics in N_2O isotopic ratios observed at Mace Head to distinct N_2O source sectors in the region.

This chapter also discusses opportunities for improvement in experimental procedures for Stheno-TILDAS and similar instruments currently being used to conduct high-frequency observations of N_2O isotopic ratios. Continued development of experimental best practices and isotopic standard gases (Mohn et al., 2014) will help reduce the reliance on "secondary" and "tertiary" working standards produced by analyzing off-the-shelf commercial gas mixtures containing N_2O as compared to a handful of other gas mixtures containing (ideally) slightly different mean N_2O isotopic ratios.

Chapter 4

Analysis of 2014-2015 Stheno-TILDAS Observations

This chapter introduces the methods by which the Stheno-TILDAS N_2O isotopic ratio observations made at Mace Head, Ireland in 2014-2015 (as described in the previous chapter) are analyzed in order to better understand the N_2O emissions in the region near the station. Measurement of other atmospheric trace gases at Mace Head—such as CO, CH_4, and $CHBr_3$ measured on the AGAGE GC-ECD and Medusa instruments (Prinn et al., 2016)—can provide additional information on likely sources of the air sampled at the station due to the distinctness of source sectors that induce high-concentration "spikes" in their mole fraction timelines.

The N_2O isotopic trends in observations made at Mace Head show short-term variability that can be traced to diverse N_2O source sectors using surface emission sensitivities ("footprints") from the Numerical Atmospheric-dispersion Modelling Environment (NAME III v6.5; Manning et al. (2011)), a dispersion model that tracks the trajectories of individual Lagrangian particles as they move through a three-dimensional field of reanalysis meteorology.

In the two seasons of Stheno-TILDAS operation at Mace Head, summer 2014 and winter 2014-2015, features in N_2O isotopic ratio timelines indicate shifts from well-mixed North Atlantic tropospheric "background" air to enhanced contribution from nearby soil-based, oceanic, agricultural, and industrial sources. These changes in source dynamics are supported by NAME footprints (Manning et al., 2011) and show promise for the ability of more complex inverse modeling and statistical techniques (Saikawa et al., 2014; Rigby et al., 2011; Huang et al., 2008) to disentangle contributions of regional N_2O sources to the observed conditions at Mace Head.

4.1 Comparison to Past Analysis at MHD

Prior to the high-frequency Stheno-TILDAS data presented in Figure 3-7, occasional flask sampling at MHD with GC-CFIRMS (gas chromatography/continuous flow isotope ratio mass spectrometry, as in Potter et al. (2013)) analysis was used to measure longer-term averages of N_2O isotopic composition at this site (Potter, 2011).

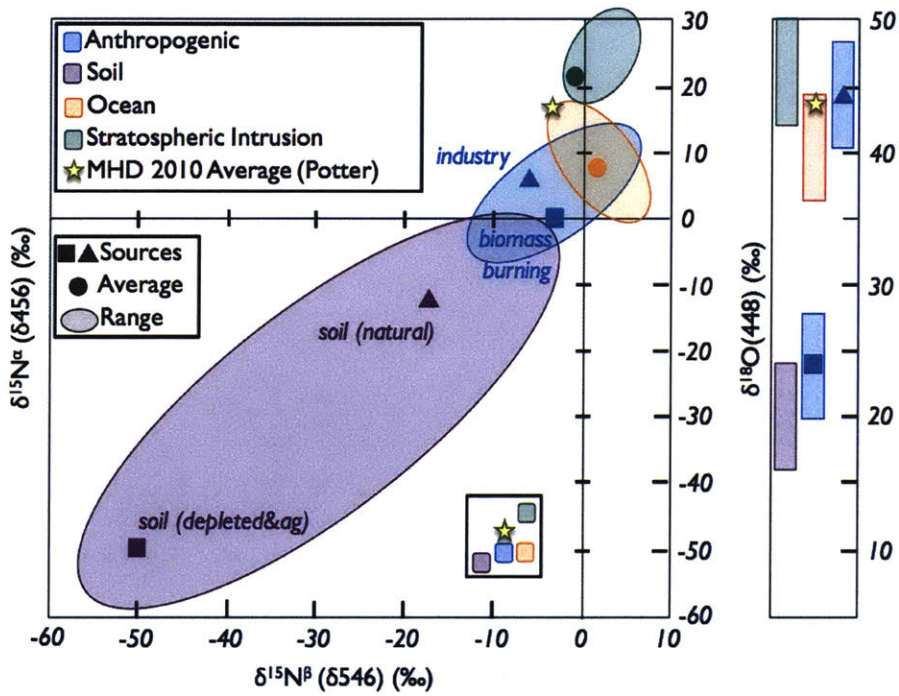

Figure 4-1: Ranges of site-specific ^{15}N and ^{18}O isotopic ratios for various N_2O sources potentially impacting measurements at Mace Head, Ireland (adapted with permission from Potter (2011), Figure 3.5), with a simplified diagram of the $\delta456$-$\delta546$ phase space of source signatures (inset).

The colored regions in Figure 4-1 (adapted from Potter (2011), Figure 3.5) enclose results from previous studies in which N_2O isotopic signatures were measured directly at the locations of the various indicated sources (with averages calculated in Potter (2011)). While this gives a sense of the variability of isotopic signatures within a given source type, great care must be exercised in using these source signatures to interpret ambient observations. For example, the yellow star in Figure 4-1 represents long-term average observations at MHD in 2010 that are influenced by different combinations of the indicated source types added on top of long-term trends in the isotopic composition of well-mixed tropospheric air (Park et al., 2012; Potter, 2011; Harris et al., 2017). In other words, simply placing observations on the same plot does not indicate that these measurements sample pure N_2O from a singular source. However, by graphically plotting source signatures alongside observations, one can intuit

that enrichment in $^{15}N-N_2O$ ("bulk" ^{15}N) indicates a combination of source signatures that includes less contribution from the relatively ^{15}N-depleted sources (depleted/agricultural and natural soils) and more contribution from relatively ^{15}N-enriched sources (industry, biomass burning, and oceanic biotic activity).

Divergence between the two positions of ^{15}N ($\delta 456$ and $\delta 546$, commonly shown as Site Preference as in Figure 2-4) can be particularly useful in separating sources with similar bulk $\delta^{15}N$ (oceanic and anthropogenic sources). Measurements of $\delta^{18}O$ allow for a third axis of variability for source identification, allowing for differentiation between ^{18}O-depleted sources (soils and anthropogenic sources) and relatively ^{18}O-enriched sources (oceanic sources).

4.2 Trace Gas Measurements

In standard operation of Stheno-TILDAS at MHD, measurements requiring pre-concentration (including all ambient air observations) were made every 28 minutes. Individual measurements and 24-hour running means of N_2O isotopic ratios observed at MHD using Stheno-TILDAS in summer 2014 and winter 2014-2015 are shown in Figure 3-7. In addition to the Stheno-TILDAS data, Figure 4-2 also shows measurements of bulk N_2O mole fraction and concentrations of three notable trace gases, measured using the GC-ECD and Medusa AGAGE network instruments at MHD, that can help elucidate the origin of air ultimately sampled at the station: carbon monoxide (CO), methane (CH_4), and bromoform ($CHBr_3$).

The bottom portion of Figure 4-2 shows distinct pollution events and other features in measured mole fractions of four trace gases that can be used to help determine the emissions sources most likely sampled:

- Nitrous oxide, N_2O: while somewhat tautological in the sense that "spikes" of N_2O mole fraction indicates enhanced sampling of surface sources of N_2O, the timeline of N_2O mole fraction can be used to indicate the contrast between largely well-mixed "background" air and air containing enhanced contributions from local N_2O sources

- Carbon monoxide, CO: this gas is produced from incomplete combustion and can be used as an indicator of transportation and other industrial activity. There are numerous major sources of CO that do not emit similarly large amounts of N_2O, such as light-duty and passenger vehicles; therefore, while CO may be used as a tracer for anthropogenic or industrial contribution to the contents of a given air sample, it may not always indicate enhanced contribution of industrially-produced N_2O

- Methane, CH_4: this potent greenhouse gas is emitted to the atmosphere in many of the same processes that create N_2O in the agricultural sector; however, any anthropogenic release of CH_4 into the atmosphere (such as from natural gas extraction) would likely not be paired with enhanced N_2O emission. Therefore, while CH_4 can be used as an

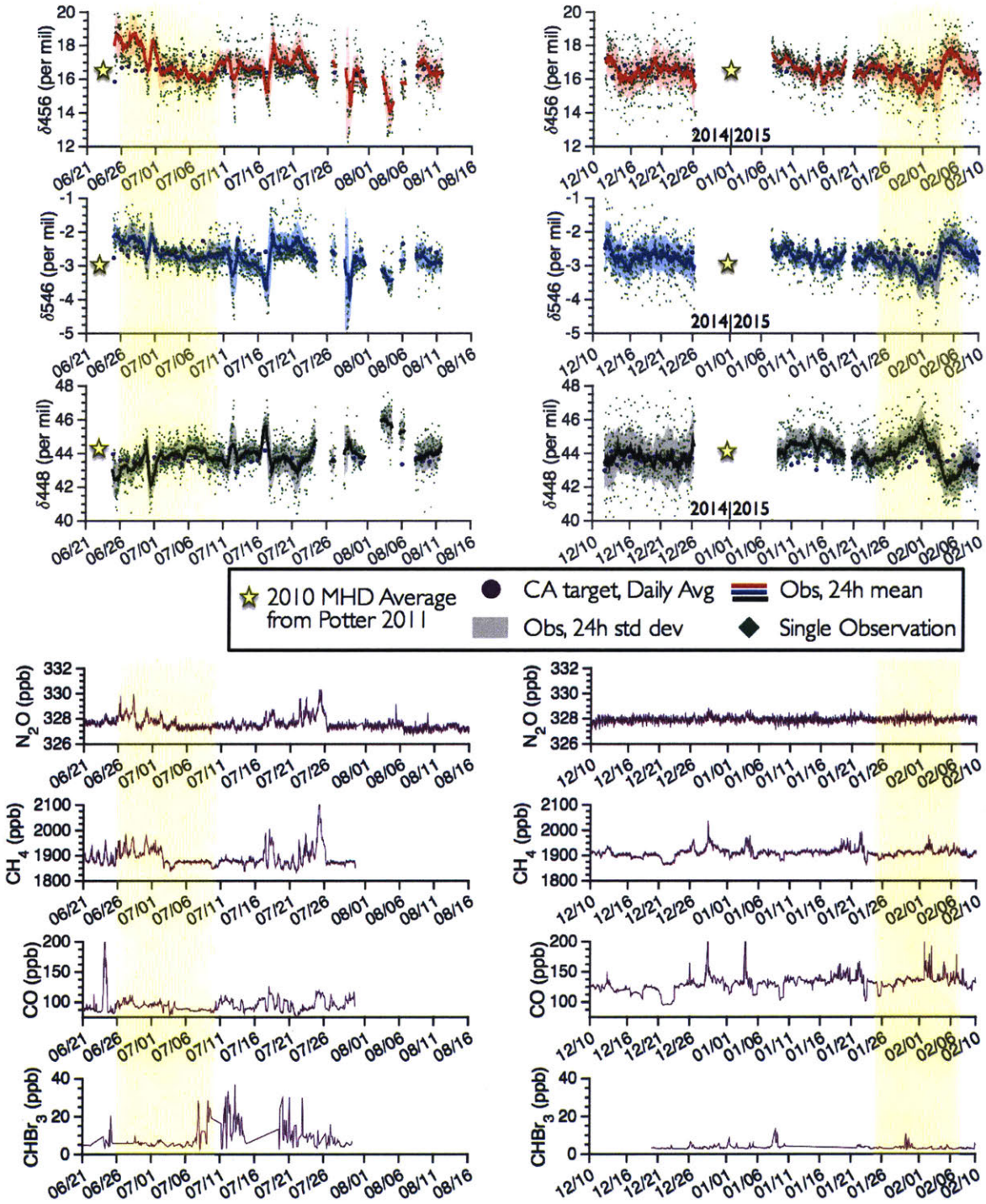

Figure 4-2: Timeline of N_2O isotopic ratios (Stheno-TILDAS), as described in Figure 3-7, and mole fractions of trace gases (Medusa and ECD) measured at MHD in the first year of Stheno-TILDAS operation in 2014-2015. The two highlighted regions, spanning 26 June-9 July 2014 and 26 January-9 February 2015 are analyzed in further detail in the following sections.

indicator of industrial or agricultural sectors, enhanced measured N_2O mole fractions would likely only correspond to enhanced CH_4 mole fractions when agricultural sectors are being sampled in an enhanced manner

- Bromoform, $CHBr_3$: this halogenated gas is used industrially as a chemical solvent, but is also produced by oceanic algae (Palmer and Reason, 2009). While this ocean-based source of $CHBr_3$ can be used to indicate enhanced sampling of coastal or oceanic regions, the surface waters in which algae produce $CHBr_3$ and the low-oxygen regions of the ocean in which N_2O is chiefly produced (Babbin et al., 2015) lead to a potential spatial and temporal mismatch between the source dynamics of N_2O and $CHBr_3$.

In some cases, multiple trace gas measurements can be used together to help understand the surfaces sources most likely being sampled. For example, a "spike" in the $CHBr_3$ mole fraction timeline may indicate enhanced sampling of an oceanic source if CO is contemporaneously low, or an industrial source if CO is abnormally high. Anomalously low CH_4 and N_2O could indicate stratospheric origin of the air, which can be further supported with anomalously low concentrations of certain anthropogenic gases.

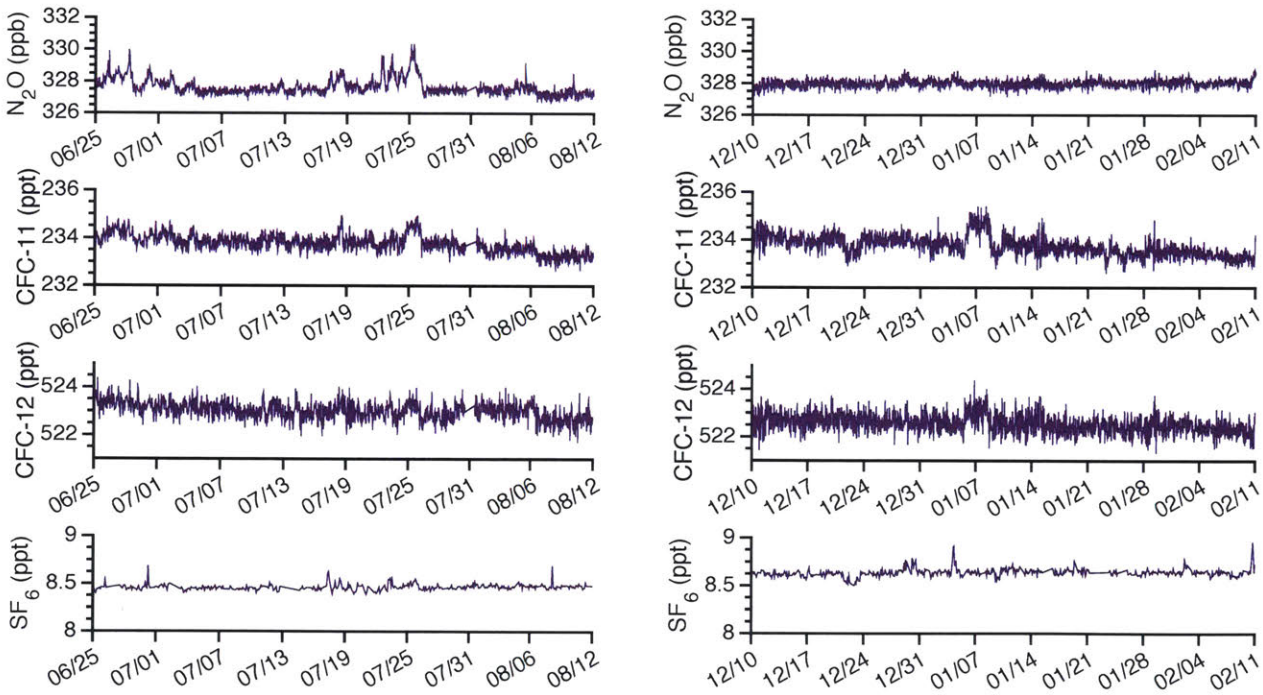

Figure 4-3: Stratospheric tracer mole fractions (AGAGE GC-ECD and Medusa) at MHD contemporaneous with Figure 4-2

In order to indicate the presence of strong stratospheric air contributions to surface conditions, mole fractions of CFC-11, CFC-12, SF_6, and bulk N_2O would all be expected to be anomalously low in a brief excursion from the seasonal baseline. A low-concentration

anomaly in the mole fractions of these gases would indicate a parcel of "old" (compared to initial release at the surface) air that had traversed high-altitude regions of the stratosphere where these gases may be destroyed by high-energy solar radiation and short-lived atomic species (such as $O(^1D)$). As shown in Figure 4-3, no significant CFC mole fraction features were present in the MHD Medusa data contemporaneous with Figure 4-2. While this does not definitively preclude any distinct stratospheric influence on the observations made at MHD, there are no distinct features in the 2014-2015 Stheno-TILDAS timeline that exhibit qualities of a relatively undiluted stratospheric intrusion at the surface.

4.3 Source Attribution from Isotopic Composition Observations

Using a quantitative approach based on Figure 4-1 (and its simplified inset), one can compare the relative contributions from various sources to the isotopic features highlighted in two regions within the timeline in Figure 4-2. All three site-specific N_2O isotopic ratios can be used in this manner. Stheno-TILDAS observations can also be compared to co-located, contemporaneous measurements of dozens of trace gases at MHD as part of the AGAGE network, as shown in Figure 4-2.

These two particular sections of the Stheno-TILDAS timeline were chosen for detailed analysis due to the following shared characteristics: completeness of accompanying GC-ECD and Medusa trace gas observations, no gaps in data coverage lasting more than a few hours (as seen in late July and early August 2014), and interesting features in N_2O isotopic ratio timelines that correspond to features in trace gas observations.

Each section of the Stheno-TILDAS data further explored in Figures 4-4 and 4-5 has five individual events (A-E for summer and V-Z for winter) that represent significantly different conditions sampled at MHD. The N_2O isotopic ratio and trace gas mole fraction observations at these events indicate that the following sources are likely being sampled:

- Event A (25 June 2014)
  - Trace gases: High-concentration "spike" in $CHBr_3$, indicating enhanced sampling of oceanic sources
  - $\delta 456$-$\delta 546$ (^{15}N) Space: Relatively enriched in both ^{15}N positions, indicating low contribution from soil-based sources
  - $\delta 448$ (^{18}O): Relatively depleted, which would typically indicate influence from soil-based or industrial sources
  - **Primary Source**: Coastal/ocean, with contribution from industrial sources possible

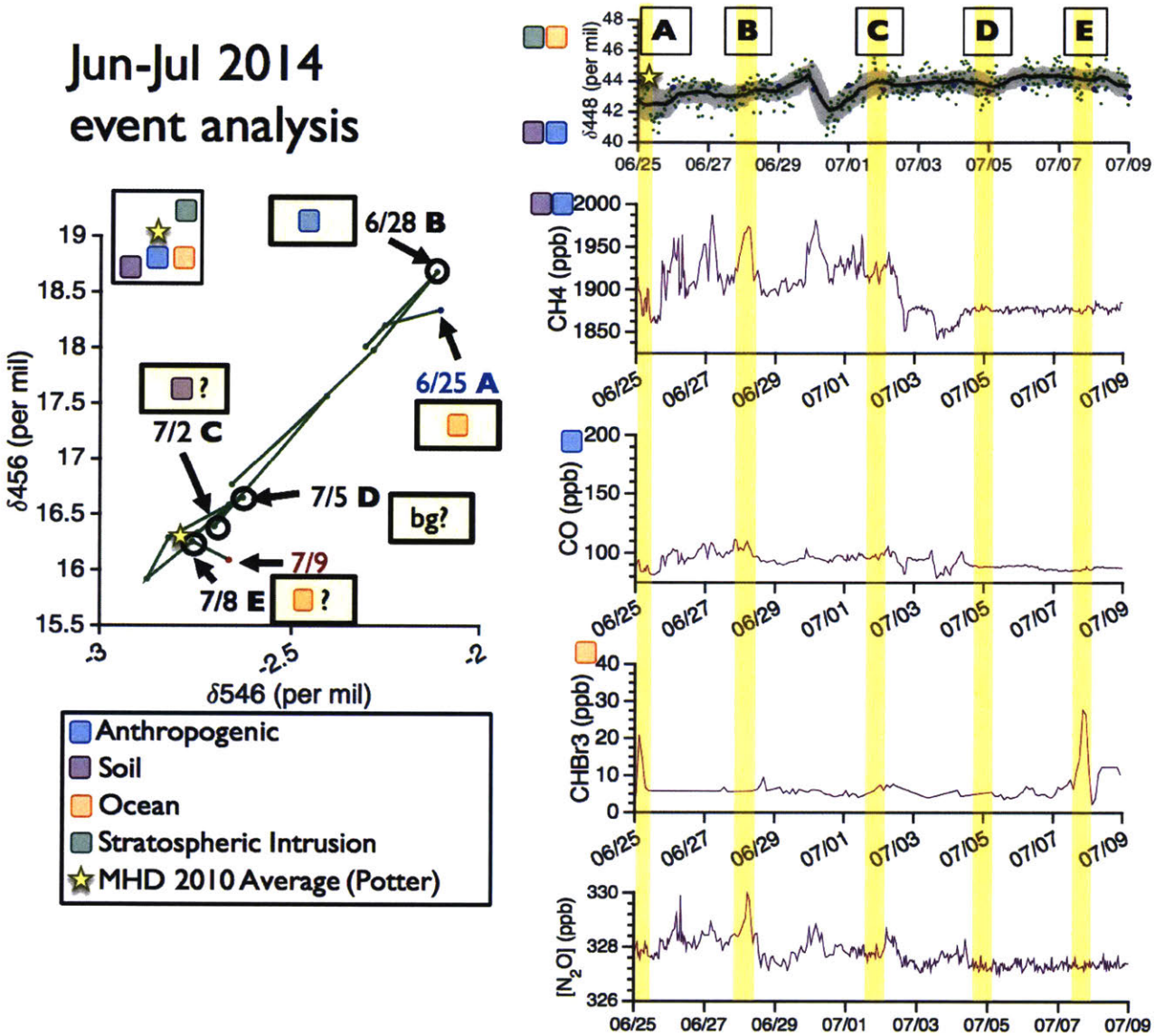

Figure 4-4: Stheno-TILDAS N_2O isotopic ratios and trace gas measurements at MHD in the first highlighted region from Figure 4-2, with year-long average observations at MHD from 2010 represented by the yellow star (average of all flask samples from 2010 in Potter (2011)). Events marked by the letters A-E are notable events within the highlighted time window, each of which bears a provisional source assignment (or indication of well-mixed background air) based on N_2O isotopic ratios (see the inset from Figure 4-1) and trace gas mole fractions.

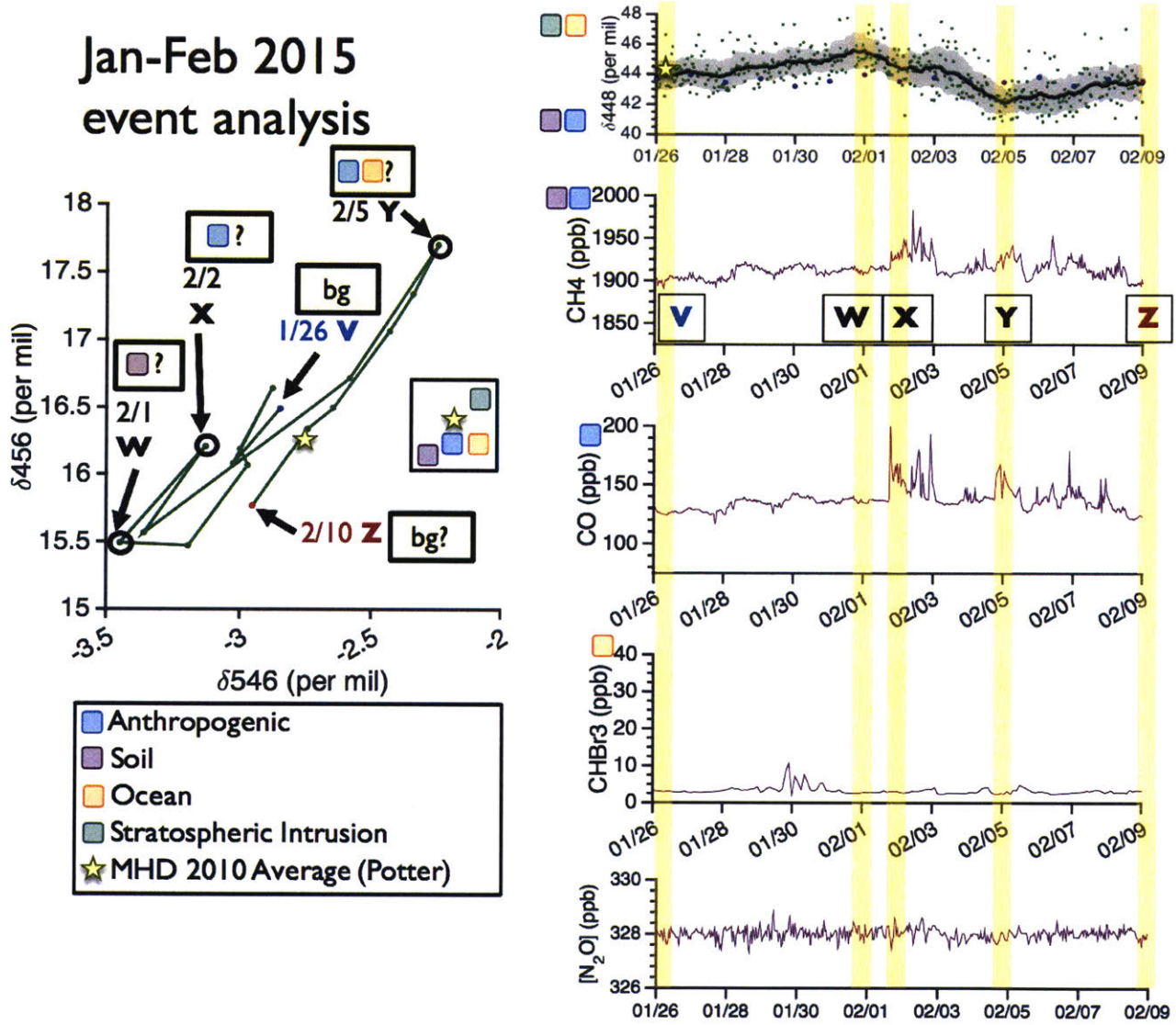

Figure 4-5: Stheno-TILDAS N_2O isotopic ratios and trace gas measurements at MHD in the second highlighted region from Figure 4-2, with year-long average observations at MHD from 2010 represented by the yellow star (average of all flask samples from 2010 in Potter (2011)). Events marked by the letters V-Z are notable events within the highlighted time window, each of which bears a provisional source assignment (or indication of well-mixed background air) based on N_2O isotopic ratios (see the inset from Figure 4-1) and trace gas mole fractions.

- Event B (28 June 2014):
  - Trace gases: High-concentration "spike" in CH_4 and CO, indicating enhanced sampling of industrial/anthropogenic sources
  - δ456-δ546 (^{15}N) Space: Relatively enriched in both ^{15}N positions, indicating low contribution from soil-based sources
  - δ448 (^{18}O): Near the 2010 MHD average (yellow star), indicating a mixture of sources or sampling well-mixed background air
  - **Primary Source**: Industrial
- Event C (2 July 2014):
  - Trace gases: Elevated CH_4 mole fraction, indicating contribution from industrial/anthropogenic or agricultural sources; CO mole fraction slightly above baseline, possibly indicating industrial/anthropogenic contribution
  - δ456-δ546 (^{15}N) Near the 2010 MHD average (yellow star), indicating a mixture of sources or sampling well-mixed background air
  - δ448 (^{18}O): Near the 2010 MHD average (yellow star), indicating a mixture of sources or sampling well-mixed background air
  - **Primary Source**: Unclear; a possible mixture of sources, likely including agricultural soil or other areas with CH_4 emissions
- Event D (5 July 2014):
  - Trace gases: Near the baseline for all trace gases
  - δ456-δ546 (^{15}N) Space: Slightly enriched in both ^{15}N positions from the 2010 MHD average (yellow star), indicating a mixture of sources or sampling well-mixed background air, perhaps with additional oceanic contribution
  - δ448 (^{18}O): Near the 2010 MHD average (yellow star), indicating a mixture of sources or sampling well-mixed background air
  - **Primary Source**: Likely well-mixed background air
- Event E (8 July 2014)
  - Trace gases: High-concentration "spike" in $CHBr_3$, indicating enhanced sampling of oceanic sources
  - δ456-δ546 (^{15}N) Space: Very close to the 2010 MHD average (yellow star), indicating a mixture of sources or sampling well-mixed background air
  - δ448 (^{18}O): Near the 2010 MHD average (yellow star), indicating a mixture of sources or sampling well-mixed background air

- **Primary Source**: Likely ocean, with additional contribution from well-mixed background air

- Event V (26 January 2015)
  - Trace gases: Near the baseline for all trace gases
  - δ456-δ546 (^{15}N) Space: Near the 2010 MHD average (yellow star), indicating a mixture of sources or sampling well-mixed background air
  - δ448 (^{18}O): Very close to the 2010 MHD average (yellow star), indicating a mixture of sources or sampling well-mixed background air
  - **Primary Source**: Well-mixed background air

- Event W (1 February 2015)
  - Trace gases: Near the baseline for all trace gases
  - δ456-δ546 (^{15}N) Space: Depleted in both ^{15}N positions, likely indicating contribution from soil-based emissions
  - δ448 (^{18}O): Slightly enriched compared to 2010 MHD average, potentially indicating contribution from oceanic sources
  - **Primary Source**: Likely soil-based, with some contribution from well-mixed background air

- Event X (2 February 2015)
  - Trace gases: High-concentration "spike" in CO, elevated CH_4 mole fraction, indicating industrial/anthropogenic sources
  - δ456-δ546 (^{15}N) Space: Depleted in δ546 compared to 2010 MHD average, potentially indicating a mixture of sources
  - δ448 (^{18}O): Near the 2010 MHD average (yellow star), indicating a mixture of sources or sampling well-mixed background air
  - **Primary Source**: Likely industrial, with contribution from well-mixed background air

- Event Y (5 February 2015)
  - Trace gases: Elevated mole fraction in CH_4 and CO, indicating anthropogenic/industrial sources; near minor features in $CHBr_3$
  - δ456-δ546 (^{15}N) Space: Enriched in both ^{15}N positions, possibly indicating contributions from oceanic and anthropogenic sources
  - δ448 (^{18}O): Depleted compared to the 2010 MHD average (yellow star), indicating anthropogenic/industrial or soil-based sources

- **Primary Source**: Industrial, with potential contribution from oceanic sources

- Event Z (10 February 2015)
  - Trace gases: Near the baseline for all trace gases
  - δ456-δ546 (^{15}N) Space: Near the 2010 MHD average (yellow star), indicating a mixture of sources or sampling well-mixed background air
  - δ448 (^{18}O): Very close to the 2010 MHD average (yellow star), indicating a mixture of sources or sampling well-mixed background air
  - **Primary Source**: Well-mixed background air

Although this method allows for some identification of potential N_2O sources sampled at MHD, there remains great uncertainty in this qualitative approach largely due to the overlap of some source signatures (Figure 4-1) and the small range of variability in ambient N_2O isotopic ratios (with source contributions being folded into well-mixed "background" air) compared to those of emissions directly from individual sources.

Seasonal dynamics of N_2O sources, in which soil-based and oceanic N_2O-producing microbes are less active during colder seasons, lead to a diminished magnitude of the ranges in observed N_2O mole fraction and isotopic ratios. These dynamics lead to different challenges in source assignment in the two regions explored in Figures 4-4 and 4-5 (Summer 2014 and Winter 2014-2015).

4.4 NAME Inert Tracer Sensitivity "Footprints"

NAME (Jones et al., 2007) is a Lagrangian particle model that is driven by output from numerical weather prediction and meteorological reanalysis products. In this particular case, the three-dimensional results from the United Kingdom Met Office's Unified Model III (Cullen, 1993) version 6.5 are used. Originally developed to help respond to emergencies, following the nuclear disaster at the Chernobyl Nuclear Power Plant in Ukraine in 1986, the model has been repurposed for many scientific and planning purposes in which a general Lagrangian dispersion model can provide useful insights (Manning et al., 2011).

Emissions "footprints" of inert chemical tracers from the Lagrangian NAME model run in "backward mode" (Manning et al., 2011) can provide additional insights into the source regions that most likely affected MHD chemical and isotopic observations during the active operation of Stheno-TILDAS. These emissions footprints express the sensitivity of mole fractions (mol tracer/mol air) at an observing station to emissions (mol/m^2/s) from the surrounding regions (Figure 4-6).

For the purposes of these modeling experiments, N_2O can be approximated as an inert tracer due to its long lifetime and the limited extent of the NAME European spatial do-

$$\frac{\textbf{(mol-tracer / mol-air)}}{\textbf{(mol-tracer m}^{-2}\textbf{ s}^{-1}\textbf{)}} \quad \text{MHD mole fraction caused by regional emissions} \qquad \boldsymbol{H} = \frac{\partial \boldsymbol{y}}{\partial \boldsymbol{x}} \qquad h_{ij} = \frac{\partial y_i}{\partial x_j}$$

Figure 4-6: Calculation of sensitivity of NAME "footprints" and its relation to the matrix **H** used in Bayesian inverse methods, with **y** representing a vector of observations and **x** representing a vector of emissions, with i representing a particular time at which an observation is made and j representing a particular grid cell from which emissions originate

main (Manning et al., 2011). The resulting footprints can then be used to gain additional certainty in assigning relative contributions from regional N_2O sources to the isotopic and correlative trace gas observations made at MHD. This analysis can connect Stheno-TILDAS observations to meteorological conditions and source dynamics more objectively than the qualitative assessment in the previous section based on small variations in ambient air as they relate to previously reported N_2O isotopic source signatures.

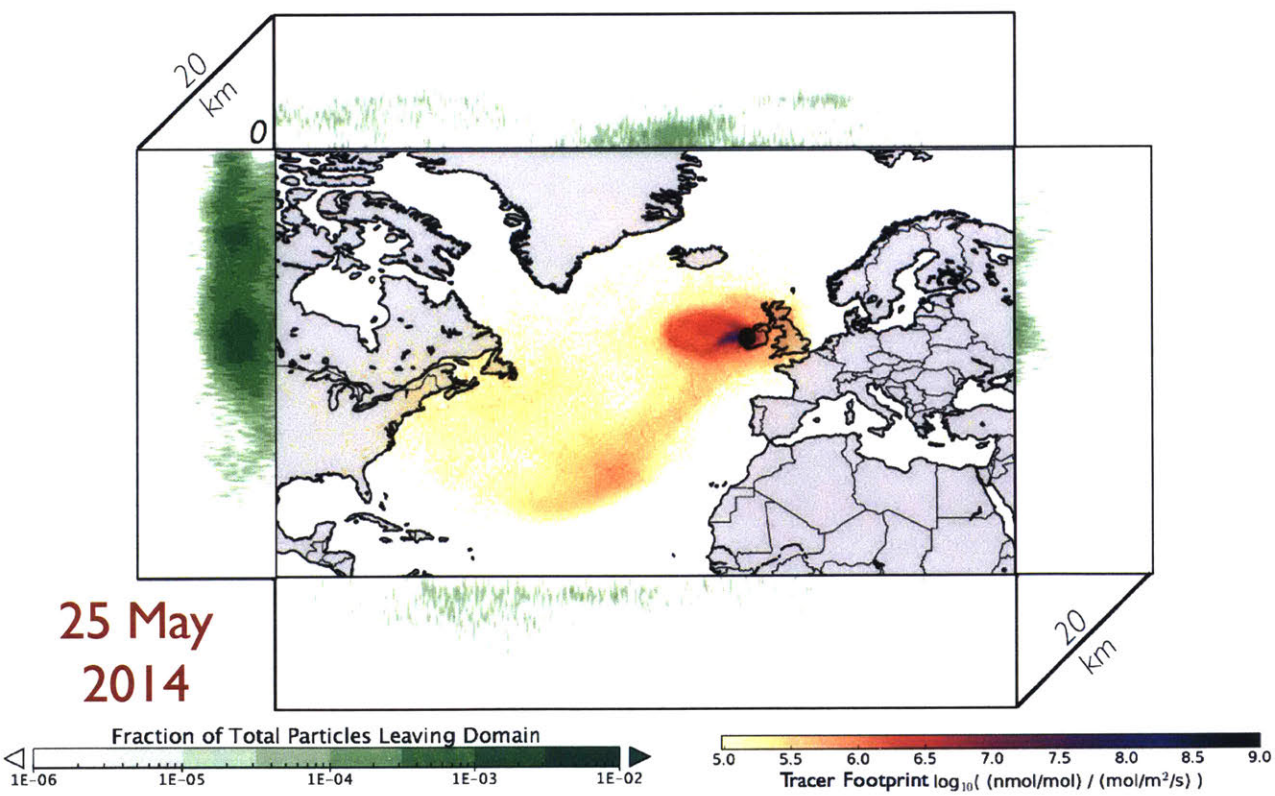

Figure 4-7: A sample NAME surface sensitivity "footprint" for MHD on 25 May 2014

The NAME surface sensitivity map in Figure 4-7 is calculated at the time of interest by

releasing 36,000 inert particles from 10 meters above ground level at MHD and tracking their "backward mode" trajectories for 30 days or until they intercept the surface level or the four bounding walls (20 km height) of the NAME Europe domain (Manning et al., 2011). These footprints can then statistically indicate the source regions that had the strongest effect on observations above "background" mean conditions in the model domain.

Use of "footprints" similar to Figure 4-7 for event analysis involves attributing small excursions from background mean N_2O isotopic ratios at MHD to emissions from within the domain (from red to purple areas with high density of particles impacting the surface before exiting the domain) or from long-range transport (from green areas with high density of particles leaving the domain before impacting the surface).

4.5 Source Attribution using NAME Lagrangian Footprints

Following the general approach described in Tables 1 and 2 within Manning et al. (2011), NAME footprints can be classified according to the surface and boundary wall regions to which observations of an inert tracer at MHD have the most sensitivity.

In this particular case, the NAME footprints in 4-8 can be used to confirm or update the provisional N_2O source sector assignments made using isotopic ratio and trace gas mole fraction observations (Figures 4-4 and 4-5).

- Event A (25 June 2014)
  - NAME Footprint: Largely oceanic, with the surface sensitivity spread throughout the North Atlantic
  - **Best Source Estimate (NAME + Observations)**: Ocean
- Event B (28 June 2014)
  - NAME Footprint: Largely industrial/anthropogenic, with the surface sensitivity concentrated over England (including London); significant contribution from the boundary walls at the northeast corner of the NAME domain
  - **Best Source Estimate (NAME + Observations)**: Industrial
- Event C (2 July 2014)
  - NAME Footprint: Surface sensitivity largely samples Ireland and the United Kingdom
  - **Best Source Estimate (NAME + Observations)**: Anthropogenic mixture; possibly agricultural soil and industry

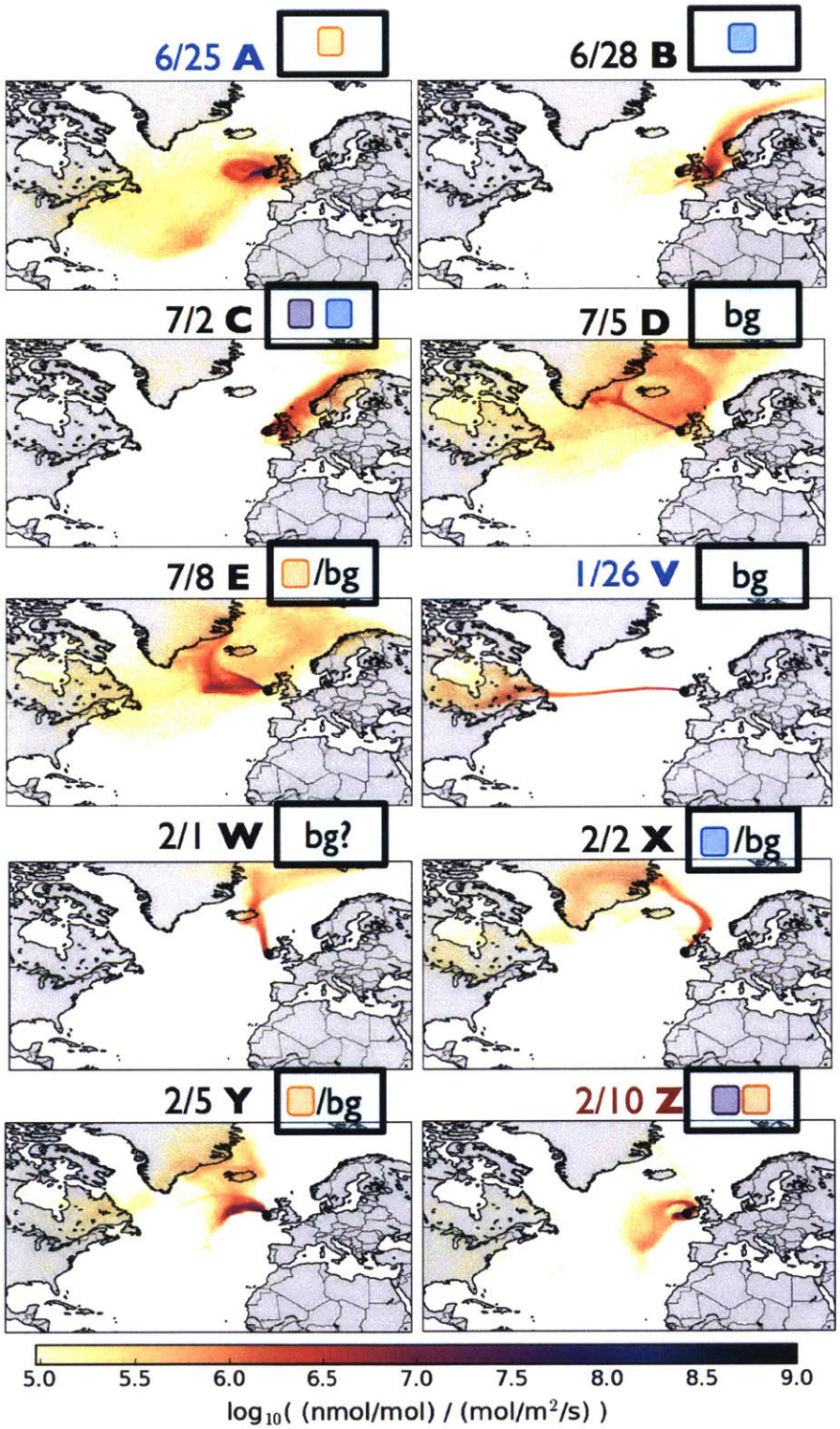

Figure 4-8: NAME emissions footprints calculated for 10 meters above ground level at MHD at events (A-E, V-Z) explored in Figures 4-4 and 4-5

- Event D (5 July 2014)
  - NAME Footprint: Well-mixed, with surface contributions from the entire North Atlantic region and domain boundary contributions from the north and west
  - **Best Source Estimate (NAME + Observations)**: Well-mixed background
- Event E (8 July 2014)
  - NAME Footprint: Similar to Event D, with strong additional sensitivity to oceanic areas near Ireland
  - **Best Source Estimate (NAME + Observations)**: Ocean and well-mixed background
- Event V (26 January 2015)
  - NAME Footprint: Virtually all sensitivity comes from the western domain wall
  - **Best Source Estimate (NAME + Observations)**: Well-mixed background
- Event W (1 February 2015)
  - NAME Footprint: Most sensitivity comes from the northern domain wall, indicating a different well-mixed profile than other events due to significant sampling of polar (not mid-latitude) air
  - **Best Source Estimate (NAME + Observations)**: Well-mixed background; may feature a different mixture of sources by sampling polar air
- Event X (2 February 2015)
  - NAME Footprint: Most sensitivity comes from the northern and western domain boundaries, with additional surface sensitivity to eastern Ireland and Scotland
  - **Best Source Estimate (NAME + Observations)**: Industry and well-mixed background air
- Event Y (5 February 2015)
  - NAME Footprint: Similar to event E, surface contributions from the North Atlantic and oceanic areas near Ireland, plus well-mixed contribution from the western boundary
  - **Best Source Estimate (NAME + Observations)**: Ocean and well-mixed background air
- Event Z (10 February 2015)
  - NAME Footprint: Surface sensitivity to Ireland and nearby oceanic areas

- **Best Source Estimate (NAME + Observations)**: Mixture, likely from soil and oceanic sources, including well-mixed background air

At best, the NAME footprints conclusively support the original assignments from Figures 4-4 and 4-5. In some cases, NAME footprints show sensitivity to multiple sources or strong contributions from the well-mixed domain boundary walls; often, the initial source assignment was similarly uncertain or mixed. In all cases explored in Events A-E and V-Z, the NAME footprints add information on the most likely source profile without directly disputing any provisional assignments made using isotopic ratios and trace gases alone.

4.6 Limitations of Event-Based Analysis

Ultimately, any quantitative analysis based on discrete events will be most illustrative when the events are chosen to represent significantly different observation regimes. Such an analysis will not be useful for evaluating transitions between such events or in situations where there is great uncertainty to the human eye. A more quantitative analysis, in which every observation can be used regardless of its "purity" in sampling relatively singular emissions sources, will be introduced in the chapters to follow.

4.7 Summary

This chapter introduces three methods to apportion contributions from various N_2O source sectors to conditions observed at Mace Head, Ireland at discrete points in time. The first such method, using observations of atmospheric "trace gas" mole fractions, allows for an understanding of N_2O source sectors most likely sampled due to the co-location of N_2O emission sources and emission sources of CO, CH_4, and $CHBr_3$. In some cases, however, there may be features in trace gas mole fraction timelines that do not correspond to a similar change in the source mixture of N_2O being sampled; notably, while $CHBr_3$ and N_2O both have significant ocean-based emissions, sources of the two gases have different spatial and temporal distributions. The second method involves analyzing movement within the δ**456**-δ**546**-δ**448** phase space as increased activity of various sources perturb isotopic ratios observed at Mace Head from well-mixed North Atlantic "background" isotopic conditions. This method has its own shortcomings owing to the fact that small isotopic perturbations in observed N_2O isotopic ratios may be difficult to assign to a particular source sector when multiple regional source sectors are sampled or when long-range transport of well-mixed air dominates. The third method uses a Lagrangian particle dispersion model (NAME) to statistically estimate the origin of air sampled at Mace Head. NAME-based analysis of events observed at Mace Head has the capability of clarifying the difficult scenarios discussed above (multiple sources being sampled, dominance of long-range transport), and therefore, NAME surface sensitivity

"footprints" will constitute a major component of more quantitative methods introduced in Chapter 6.

This chapter also shows the ranges in N_2O isotopic ratios and trace gas mole fractions that can be expected at Mace Head in various regimes that either preferentially sample particular source sectors or feature long-range transport of well-mixed air to the station. The periods in the Stheno-TILDAS N_2O isotopic ratio timelines that most strongly indicate sampling of background air, as corroborated by disperse NAME surface sensitivity footprints and major contributions from the bounding wall of the model domain, feature N_2O isotopic ratios very close to the long-term average of observations made at Mace Head in 2010 (Potter, 2011).

Chapter 5

Global Atmospheric Chemical Transport Modeling

This chapter will introduce modifications made to a chemical transport model, MOZART-4, in order to simulate N_2O isotopic chemistry on a global scale. Because of the discrete molecule-by-molecule nature of emission, transport, and destruction processes in atmospheric chemistry, atmospheric mole fractions of the four main N_2O isotopologues must be tracked within the model. In modeling these processes that govern the N_2O earth system, trade-offs must be made in spatial and time resolution in order to use available input data sources and to keep computational resource costs reasonable.

Other global chemical transport models, such as GEOS-Chem, WRF-Chem, and NCAR CESM could have been used to conduct this portion of the thesis. In order to expand upon the extensive modeling work done by Eri Saikawa on source-specific N_2O emissions estimates, the same model (MOZART-4) was chosen. In extending the MOZART-4 model runs conducted in Saikawa et al. (2014), the simulated mole fractions of N_2O were reasonably close to observations made in the AGAGE network with only minor adjustments needed. This allowed for a good representation of bulk N_2O chemistry in the model at the years of interest (2014-2015, concurrent with Stheno-TILDAS measurements at Mace Head) before adding isotopic chemistry into the model. Once isotopic chemistry was added to the model, and after a spin-up period for the surface and stratospheric influences on surface N_2O isotopic ratios to stabilize, the modeled N_2O isotopic ratios in Europe were near those expected from observations at Mace Head, Ireland in 2010 and in 2014-2015.

5.1 Chemical Transport Models

Chemical transport models (CTMs) can provide concentrations of atmospheric trace gases, including climate-relevant greenhouse gases (GHGs), that are continuous in time and space

despite the temporally and spatially sparse nature of observations of meteorology and chemical concentrations. "Forward modeling" of expected atmospheric trace gas mole fractions can aid in future instrumental development (e.g. site selection) and to test dynamics and chemistry built into the model. Once a sufficient volume of observational data has been collected, global CTMs can be used as one component of Bayesian "inverse modeling" in which an initial emissions estimate (*a priori*) and a forward model are used to determine an optimized emissions estimate that can best explain experimental observations (Huang et al., 2008; Hirsch et al., 2006).

5.1.1 MOZART-4 Model

For the modeling portion of this experiment, a modified version of MOZART-4 (Model for OZone and Related Tracers, version 4 (Emmons et al., 2010)) is used for the global domain. All major computations—many of which produce large result datasets and require supercomputer resources—are executed using computational clusters on the Discover system hosted by the NASA Center for Climate Simulation (NCCS).

MOZART is a global chemical transport model developed at the National Center for Atmospheric Research (NCAR) that was originally designed to evaluate concentrations and transport dynamics of both highly reactive and long-lived chemical species in the troposphere (Emmons et al., 2010). As an "offline" model with respect to meteorology, the meteorological conditions used to drive transport within the model domain must be provided from an outside source. The standard MOZART-4 model includes 85 gas-phase chemical species and 12 aerosol components, but chemical species may be added and removed by the user. In addition, photolysis and chemical reactions may be added and removed as needed.

5.1.2 Input Data for MOZART-4 N_2O Modeling

In order to simulate the N_2O Earth system using MOZART-4, the following model drivers are required:

- Meteorological data, in three-dimensional fields
- Initial conditions for all chemical species of interest, in a three-dimensional field
- Emissions for all chemical species of interest, as two-dimensional surfaces that change with time
- Chemical destruction equations and kinetic rate constants, and three-dimensional concentration fields of any chemical reactants (may be calculated interactively or provided as an "offline climatology")

5.1.3 Model Output Interpretation

Full forward modeling "production runs" are created once the model inputs (including spun-up three-dimensional initial conditions) are mature enough to simulate the portion of the Earth system of interest. Forward model runs, especially those that span multiple years, are often diagnostic of unrealistic or non-physical inputs to the model. In order for Bayesian inverse modeling experiments to begin, a well-conditioned forward model must first exist in order to accurately determine the sensitivity of the modeled Earth system to perturbations in emissions and other surface fluxes.

5.2 Modeling Atmospheric N_2O

For the eventual goal of comparing model-produced isotopically-differentiated N_2O conditions to observations made by Stheno-TILDAS, the years of 2014-2015 must first be simulated reasonably well. The inverse modeling experiment conducted in Saikawa et al. (2014) led to source-specific N_2O emissions estimates in 1995-2008 by simulating three-dimensional global mole fractions of N_2O in those years and comparing them to existing estimates of N_2O emissions. For modeling bulk N_2O in 2014-2015 using MOZART-4, the experimental setup from Saikawa et al. (2014) was extended beyond its final model year of 2008 as described in the sections below.

5.2.1 Meteorological Inputs

Transport dynamics in an offline model are wholly driven by meteorological dataset inputs. Since vertical transport of isotopically enriched N_2O in stratosphere-troposphere exchange plays such a key role in the isotopic ratios measured at the surface, the meteorological input data sets used in MOZART model runs must be able to reproduce realistic vertical transport. In these MOZART model runs, three different reanalysis meteorological datasets are used in order to obtain results from a variety of reanalysis schemes: NCEP/NCAR, MERRA, and GEOS-5.

The resolution of the meteorological input dataset (Table 5.1) determines the maximum spatial resolution of the corresponding MOZART model runs (Emmons et al., 2010); these reanalysis sets could be regridded to coarser resolution, but attempting to regrid them to a finer resolution could lead to nonphysical transport results. In addition to the spatial resolution, the reanalysis resolution also determines the minimum time resolution of the model runs by the Courant condition,

$$\Delta t = \frac{\Delta x}{\vec{u}}, \tag{5.1}$$

where Δt represents the maximum timestep, Δx represents the horizontal length of one grid box, and $\vec{u}$ represents the maximum zonal wind speed in the reanalysis dataset. The Courant condition ensures that advected chemical species do not move across an entire gridbox into another in the span of one time step (Holton, 2004).

Resolution of MOZART Reanalysis Meteorological Sets				
Dataset	Latitude	Longitude	Vertical	Gridboxes
NCEP/NCAR	64	128	28	229,376
MERRA	96	144	56	744,144
GEOS-5	96	144	56	744,144

Table 5.1: Resolution of NCEP/NCAR, MERRA, and GEOS-5 reanalysis meteorological datasets with variables needed to run MOZART-4

Each MERRA and GEOS-5 reanalysis time period (6-hourly) features an orography variable that serves as a land mask (Figure 5-1) differentiating areas of water, land, and ice (ice produces a negligible amount of N_2O).

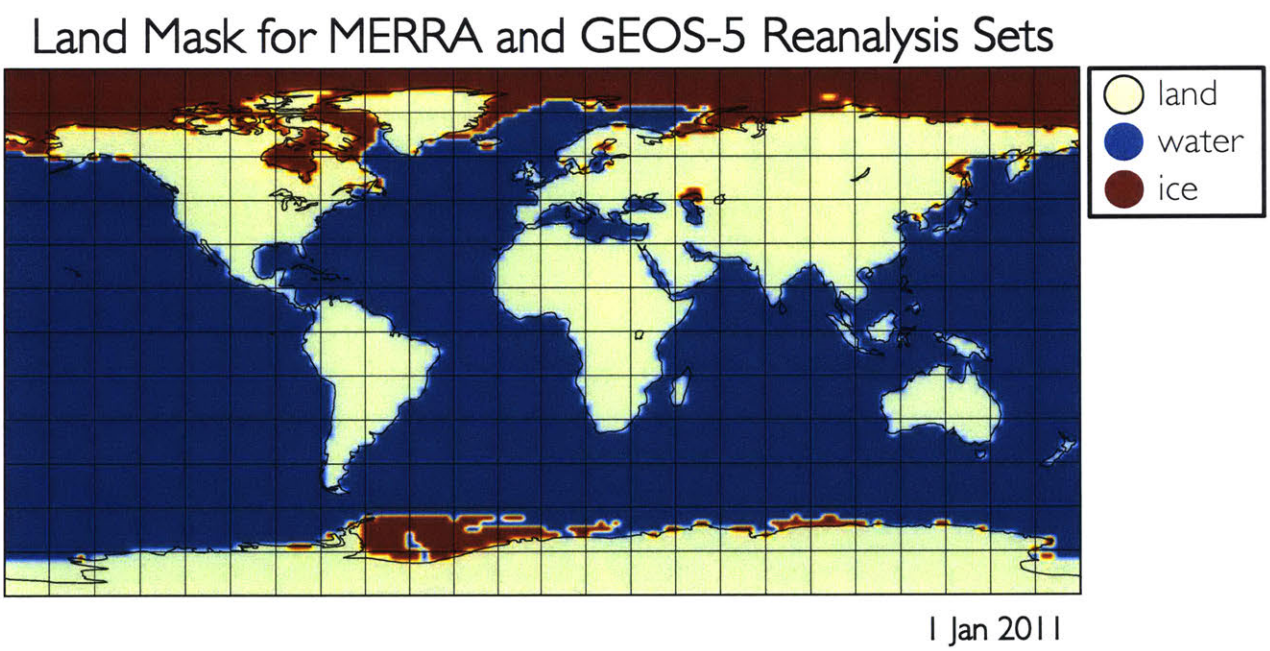

Figure 5-1: Sample MERRA/GEOS-5 land mask for 1 January 2011, featuring surface gridboxes corresponding to land, water, and ice

These three environments all feature distinct N_2O sources, and can be used in addition to the source-specific distributions in emissions inventories to verify the geographic placement of distinct source types (e.g. no emissions from ice or oceanic sources in all-land grid boxes). This land mask can be particularly helpful in differentiating land and water when coarse emissions datasets are regridded to a relatively fine spatial resolution.

In order to maximize the resolution of N_2O emission and transport in MOZART model runs, the spatially coarse NCEP/NCAR reanalysis meteorology data sets were not used beyond initial experimentation with the MOZART-4 model setup. For most initial MOZART-4 model runs, both MERRA and GEOS-5 reanalysis meteorology data sets were used. However, the GEOS-5 reanalysis generally featured more realistic N_2O chemical lifetimes, indicating that the N_2O chemistry and stratospheric transport for model runs with GEOS-5 more accurately reflect the actual conditions of these important drivers for N_2O isotopic ratios throughout the atmosphere and at the surface. In addition, with the development of MERRA-2 reanalysis datasets for chemical transport models, which were not made available with the particular meteorological variables necessary to run MOZART-4, the lack of MOZART-ready MERRA reanalysis data for the second half of 2015 made its use difficult in an experiment analyzing Stheno-TILDAS observations from 2014-2015. For the isotopically-differentiated MOZART model runs, GEOS-5 was used alone for creating the "production run" to be used in the inverse modeling experiments described in the following chapter.

5.2.2 Initial Conditions

The initial conditions (Figure 5-2) used in this portion were simply taken from the three-dimensional N_2O mole fraction field from the end of the optimized simulation in Saikawa et al. (2014), as provided by Eri Saikawa. This field represents an instantaneous MOZART model output of simulated global N_2O mole fractions on January 1, 2009.

5.2.3 N_2O Emissions Estimates

In order to extend the optimized emissions estimates from Saikawa et al. (2014) beyond the final modeled year of 2008, while retaining seasonal cycles and multiyear trends, the monthly emissions were linearly extrapolated by month and source sector to future years (Figure 5-3).

The extrapolation process in Figure 5-3 allows for preservation of persistent seasonal trends by extrapolating separately for each of the five emissions source sectors (agriculture, natural soil, oceans, industry, and biomass burning) and for each month (e.g. extrapolating future January emissions linearly from past January emissions).

The N_2O emissions map in Figure 5-4 shows small areas of active N_2O source activity, broad regions of diffuse N_2O emission, and swaths of N_2O net dissolution into the ocean likely moderated somewhat by simultaneous modest source production. Globally, the total global magnitude of the N_2O emissions inputs from these linearly extended emissions estimates are close in magnitude to estimates made from previous inverse modeling approaches (Saikawa et al., 2014; Huang et al., 2008).

In order to add more detail into the global distribution of source types, the location of the gridboxes on the map can be used to break global net surface fluxes into subsets for

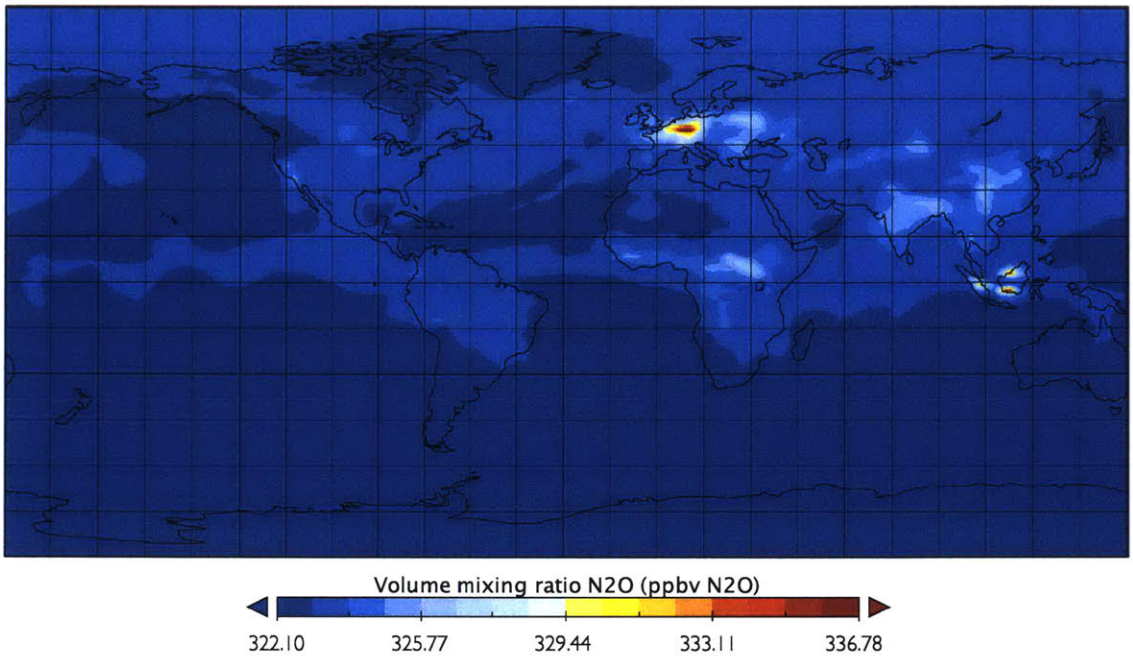

Figure 5-2: N_2O mole fraction initial conditions at the surface for January 1, 2009, from the end of Saikawa et al. (2014)

land and water (as shown in Saikawa et al. (2014)). However, decoupling the effects of small oceanic sources from the net atmospheric N_2O losses in cold ocean water will pose a challenge given the current emissions dataset. Surface flux behaviors (ocean-based emission vs. oceanic uptake, etc.) are not easily differentiated in the net flux fields used in MOZART; any physical dissolution or deposition and subsequent release of dissolved N_2O cannot be expected *a priori* to follow the trends of co-located emissions sources. Further study on dissolution and surface deposition of N_2O, and potential isotopic fractionation in these processes, will be discussed in the Future Work section of the final chapter.

5.2.4 Chemical Destruction of N_2O

Following the same approach used in Saikawa et al. (2014), three-dimensional offline fields corresponding to $O(^1D)$ and ultraviolet radiation (Figure 2-1) were used instead of interactively calculating concentrations of $O(^1D)$ and photon ($h\nu$) density. The offline fields used do not directly correspond to either chemical quantity ($O(^1D)$ concentration or photon density), but instead correspond to the **reaction rate** for N_2O in a bimolecular reaction with $O(^1D)$ or photolysis. As described in Saikawa et al. (2014), these fields are used in MOZART-4 as a "concentration" of an offline chemical species with a reaction rate **constant** of one, equivalent to specifying the **reaction rate** for the two reactions within every grid box.

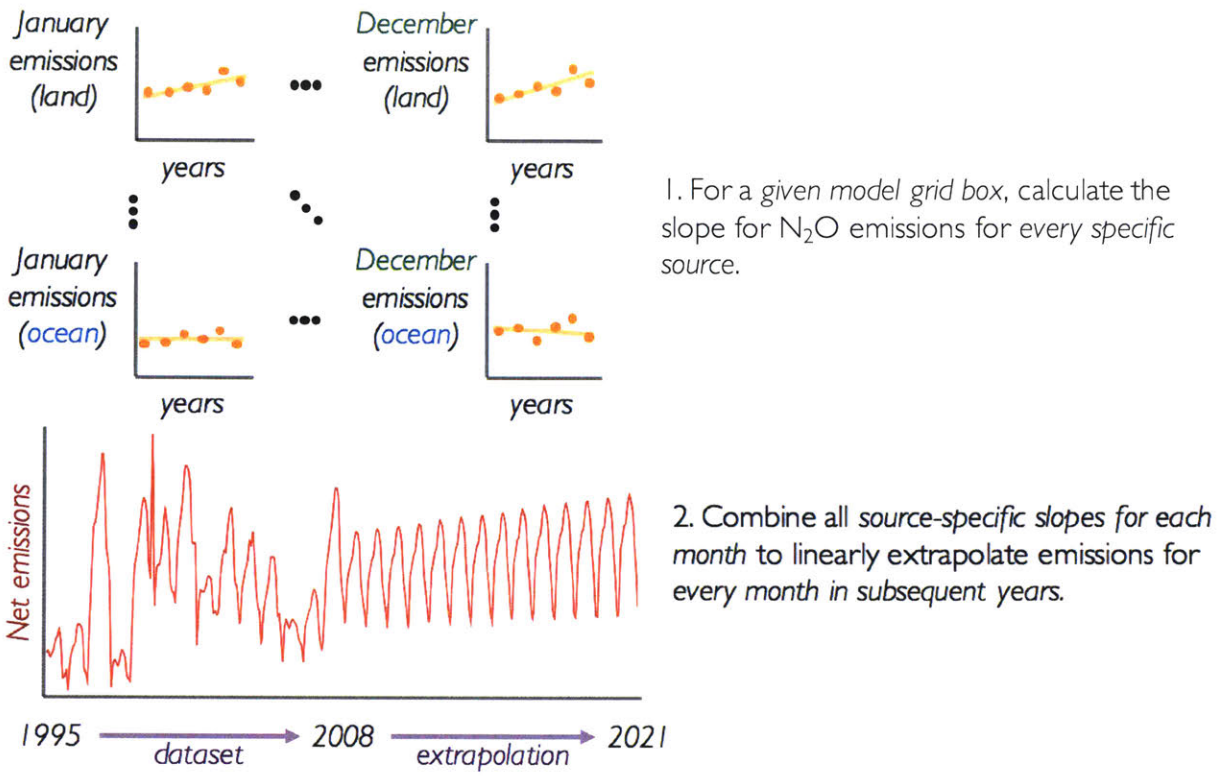

Figure 5-3: Linear extrapolation of monthly optimized emissions for years outside of the original experiment ending in 2008 (Saikawa et al., 2014)

5.2.5 Results from Saikawa et al. (2014) Extension to 2014-2015

Extending the MOZART-4 modeling runs from Saikawa et al. (2014) into the years of interest, 2014-2015, allows for direct comparison of the model output to the N_2O mole fraction observations made at Mace Head.

As shown in Figure 5-6, the linear extrapolation of emissions from Saikawa et al. (2014) combined with the initial conditions and chemical destruction fields from Saikawa et al. (2014) described above leads to a reasonable simulation of N_2O mole fraction at Mace Head in 2014-2015. The slight misalignment between the model and observations in the seasonal trends is likely caused by two major processes. First, the average over the entire grid box containing Mace Head causes a large model "representation error" (Prinn, 2000; Rigby et al., 2012) as conditions far from the station itself are included in the average presented in Figure 5-6. Second, the linear extrapolation of the source-specific N_2O emissions from Saikawa et al. (2014) necessarily smooths out interannual variability, as is evident by the transition from jagged peaks to an increasing periodic pattern in global N_2O emissions as seen in Figure 5-3. Both of these limitations can be addressed by the combined NAME-MOZART modeling approach introduced in the following chapter, which uses a significantly finer spatial grid

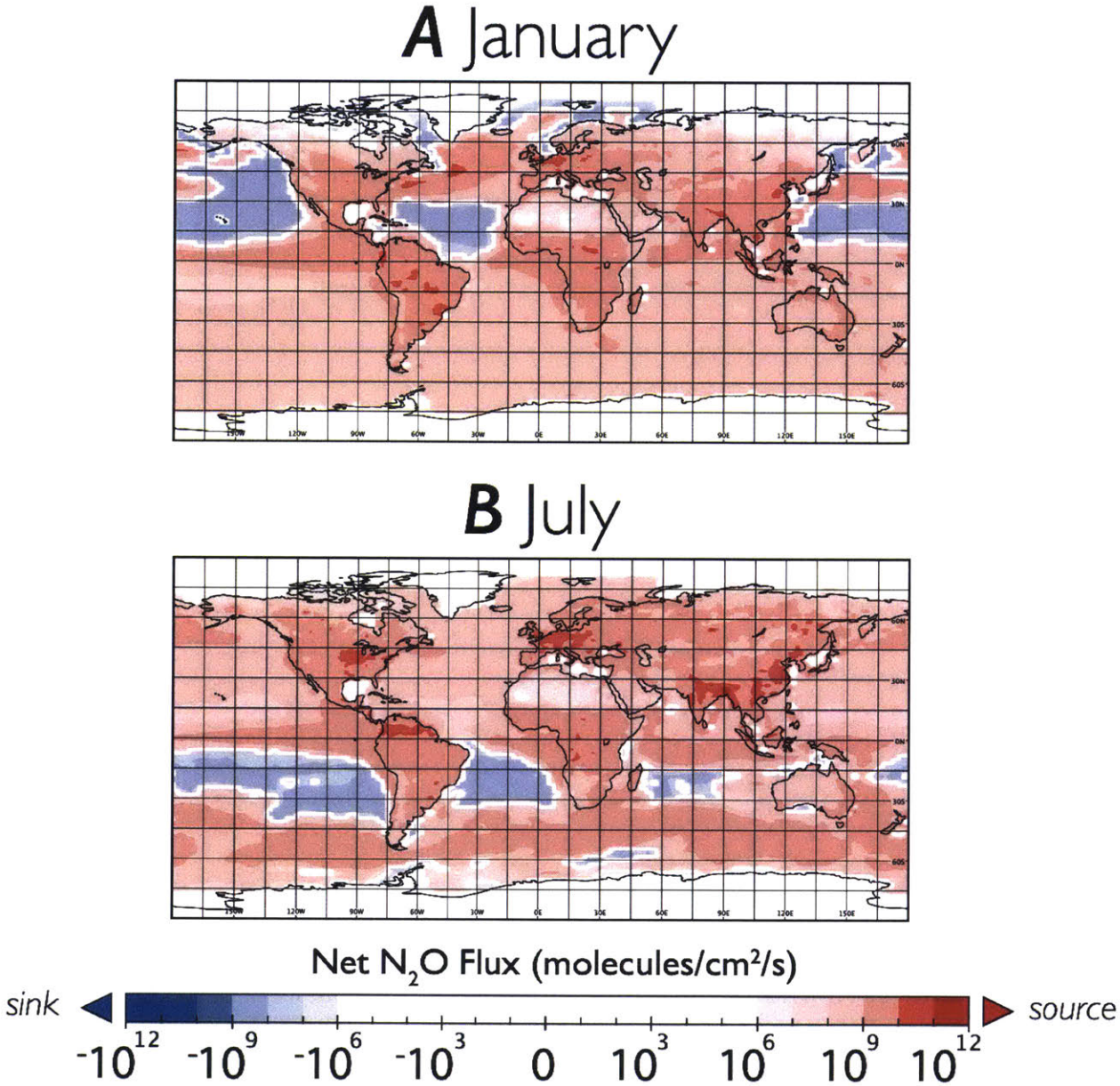

Figure 5-4: Optimized net N_2O flux estimates for 2008 (A) in January and (B) in July (Saikawa et al., 2014)

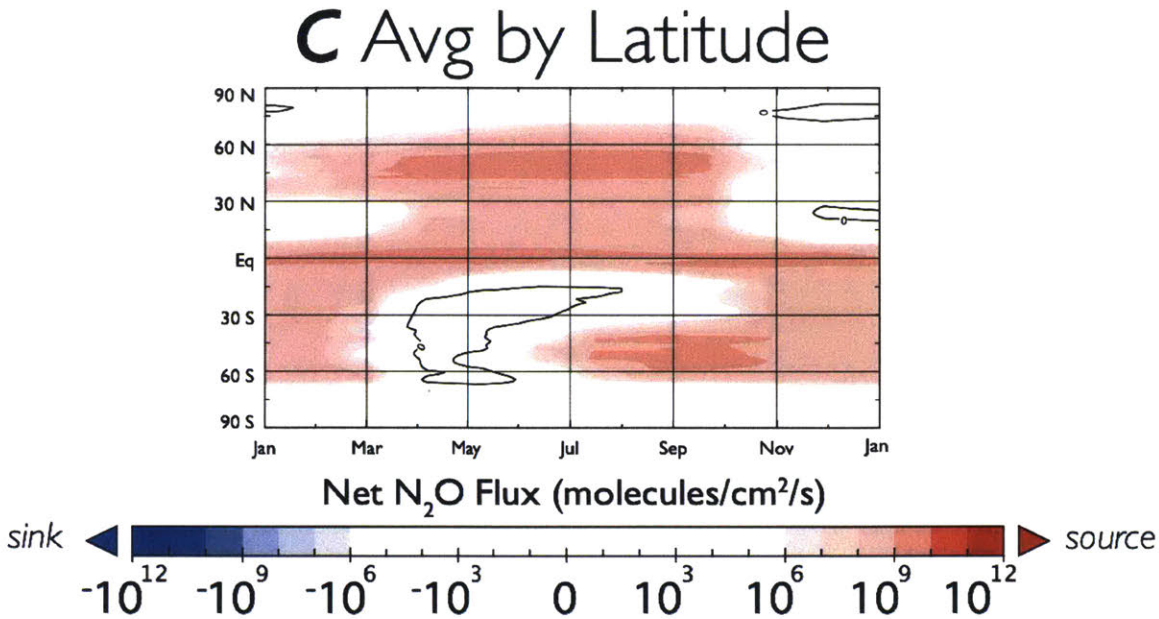

Figure 5-5: Meridionally averaged N_2O surface flux estimates from Figure 5-4

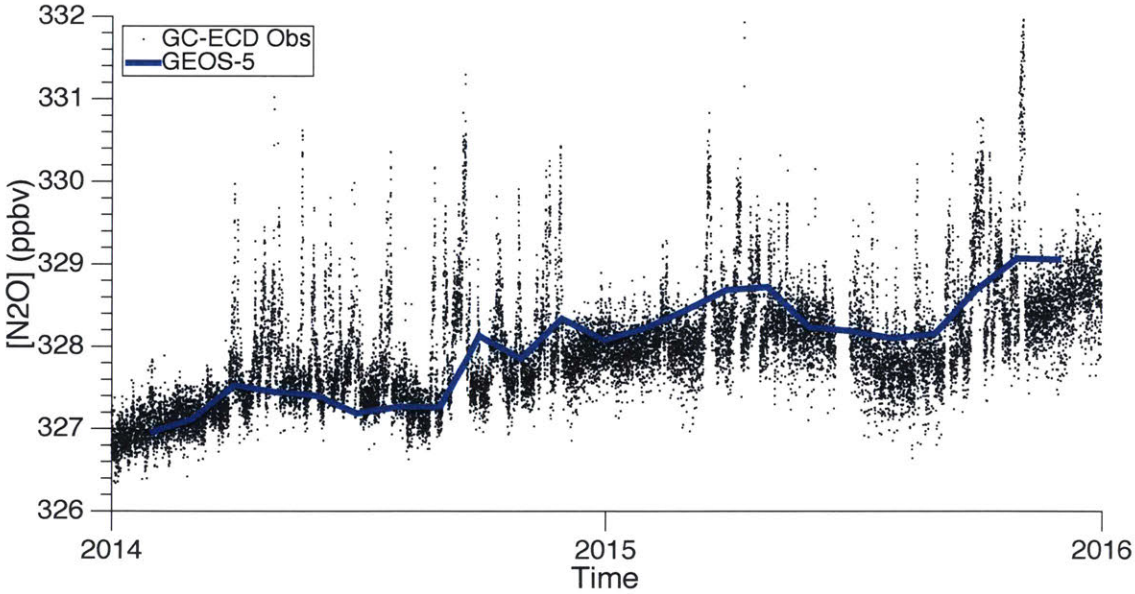

Figure 5-6: MOZART-4 simulated monthly average N_2O mole fraction in the grid box containing Mace Head (using GEOS-5 reanalysis meteorology), as compared to GC-ECD observations at the station in 2014-2015

near the station (reducing representation error) and allows for adjustment of N_2O emissions to more accurately represent the actual conditions at Mace Head after Bayesian inverse

modeling experiments are conducted.

5.3 Addition of Isotopic Chemistry

As shown in the previous section, extension of the experimental procedure from Saikawa et al. (2014) can reproduce the general trends in N_2O mole fraction at Mace Head. In order to use MOZART-4 to help interpret the Stheno-TILDAS N_2O isotopic ratio observations made at Mace Head, the model and its inputs will need to be adapted to simulate the N_2O isotopic environment at Mace Head.

The modifications made to the MOZART standard chemistry, described below, show promise for realistic isotopic fractionation in the stratosphere. Given a sufficiently long model realization, N_2O isotopic signatures of stratospheric air (slightly enriched in $^{15}N^{\beta}/\mathbf{546}$ and $^{18}O/\mathbf{448}$, significantly enriched in $^{15}N^{\alpha}/\mathbf{456}$) eventually propagate to the surface, especially in areas of the meteorological dataset featuring robust downward outflow from the stratosphere. After sufficient "spin-up" time for the highly idealized model initial conditions to become more realistic, the isotopically differentiated N_2O MOZART simulations should be comparable to Stheno-TILDAS and other isotopic N_2O measurements at global monitoring sites.

5.3.1 Isotopically Differentiated Initial Conditions

In order for the spin-up process to yield realistic atmospheric conditions in a timely fashion, the initial conditions for the MOZART model runs should be as close to the actual expected conditions as possible. Very few vertical profiles of N_2O isotopic ratios have been collected, but the few *in situ* experiments available (Toyoda et al., 2013) can be used to create the vertical gradients in the initial conditions for MOZART model runs (Figures 5-7 and 5-8).

The jagged piecewise tropopause imposed in the initial conditions (Figure 5-7) does not realistically represent the meridional smoothness of the actual atmospheric tropopause. However, due to the rapid mixing in the free troposphere and the vertical transport in the stratosphere (Seinfeld and Pandis, 2006), this imposed shape will rapidly conform to a realistic vertical structure of the atmosphere as described by the meteorological inputs used in any given model run. Within a few months, the MOZART model outputs show a convergence of the vertical gradient of N_2O isotopic ratios with the tropopause height and planetary boundary layer height variables built into the GEOS-5 and MERRA reanalysis meteorological datasets.

In MOZART model runs, the N_2O isotopic ratios themselves are not "transported" in the model; molecules of each N_2O isotopologue are transported and the ratios of their concentrations are used to calculate isotopic ratios (Figure 2-4) after a particular model

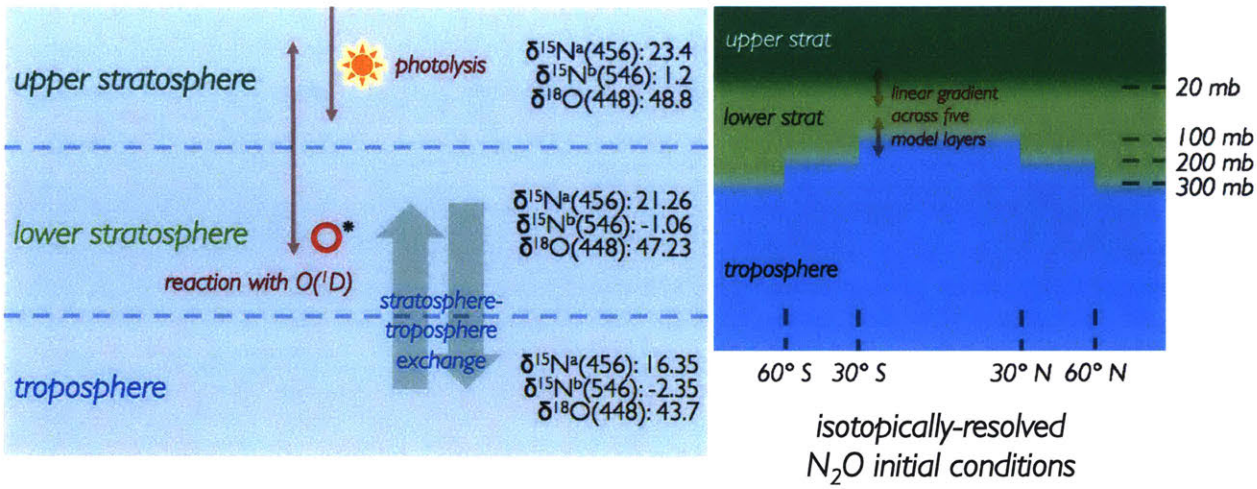

Figure 5-7: Initial conditions for the first spin-up year for distribution of N_2O isotopic ratios from averaged *in situ* vertical profiles (Toyoda et al., 2013); ratios are applied equally in the zonal dimension to standard MOZART initial conditions for whole-gas N_2O at the spring equinox of 2011

run has concluded. Therefore, the delta-values associated with the zonally-averaged initial conditions (Figure 5-7) are only applied to the N_2O mole fraction initial conditions for the first model run in any particular spin-up "family" of model runs, with continuity of N_2O isotopic ratio simulation in the model spin-up described below.

5.3.2 Isotopically Differentiated Emissions

Source-specific optimized N_2O emissions estimates (combined net emissions for January and July 2008 shown in Figure 5-4) produced in Saikawa et al. (2014) allowed for separation of five main sources of atmospheric N_2O: agriculture, biomass burning, industry, oceanic biotic activity, and natural land-based biotic activity. By combining source-specific isotopic ratio signatures with source-specific N_2O emissions estimates, an initial estimate of isotopically-differentiated N_2O emissions can be built for MOZART model runs.

Addition of Isotopic Ratios to *Saikawa 2014* N_2O Emissions

In order to use the best possible representation of isotopically differentiated *a priori* N_2O emissions distributions in the MOZART modeling framework, both source-specific isotopic ratio signatures and source-specific whole-gas N_2O emissions are combined. Optimized N_2O emissions estimates from Saikawa et al. (2014) are broken into five sectors: natural soil, agriculture, industry, biomass burning, and ocean. Therefore, the mean isotopic ratios associated with each source sector must be known in order to assign their contributions to emissions

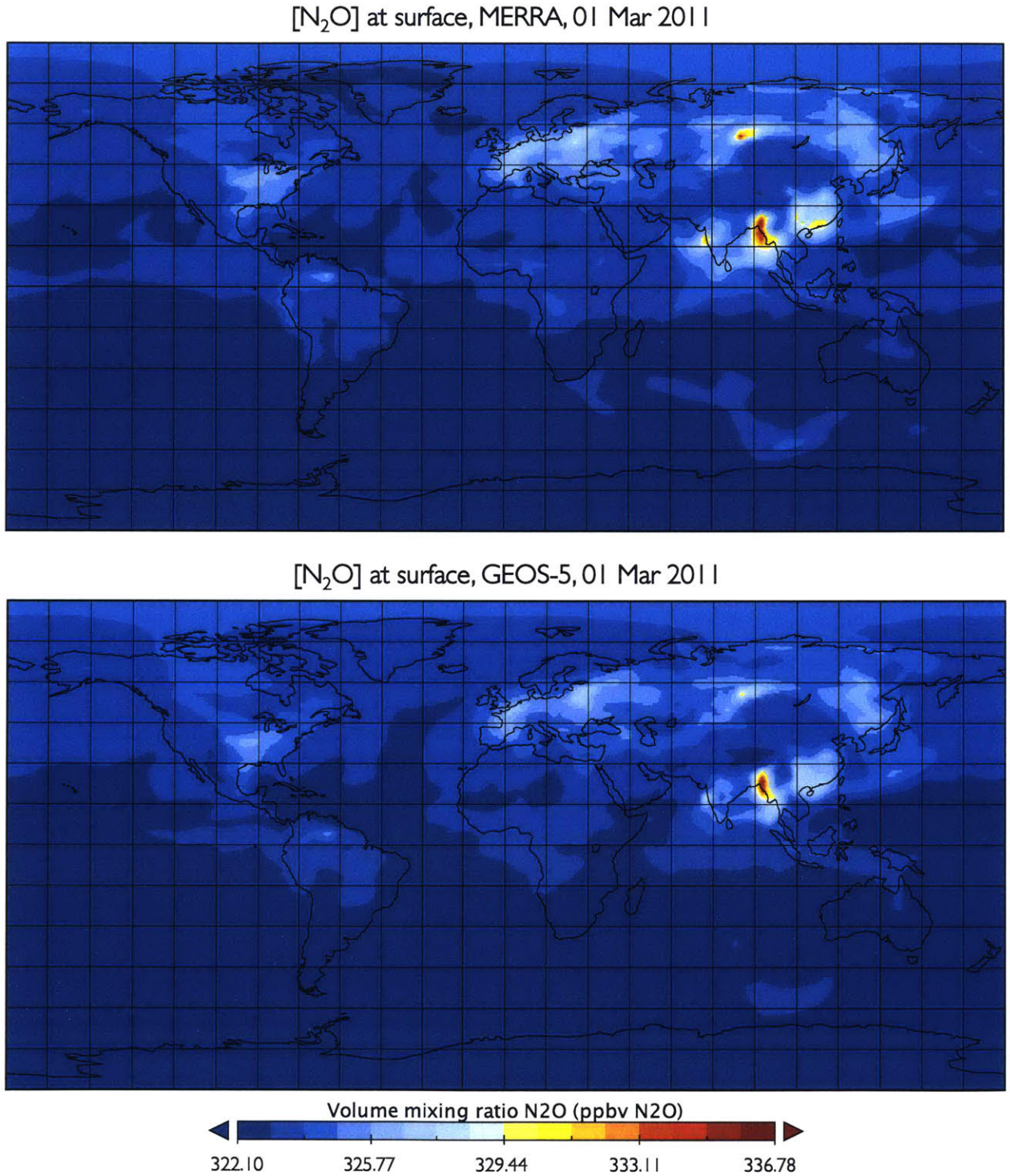

Figure 5-8: MOZART-4 simulated surface N_2O mole fraction for March 1, 2011, the fields to which the isotopic ratios in Figure 5-7 are applied to create initial conditions for isotopically-differentiated MOZART-4 model runs)

of each of the four major N_2O isotopologues. By combining averages of N_2O isotopic ratio measurements from each source sector (Figure 5-9) with emissions maps of each source type, an estimated set of isotopically-differentiated emissions can be created.

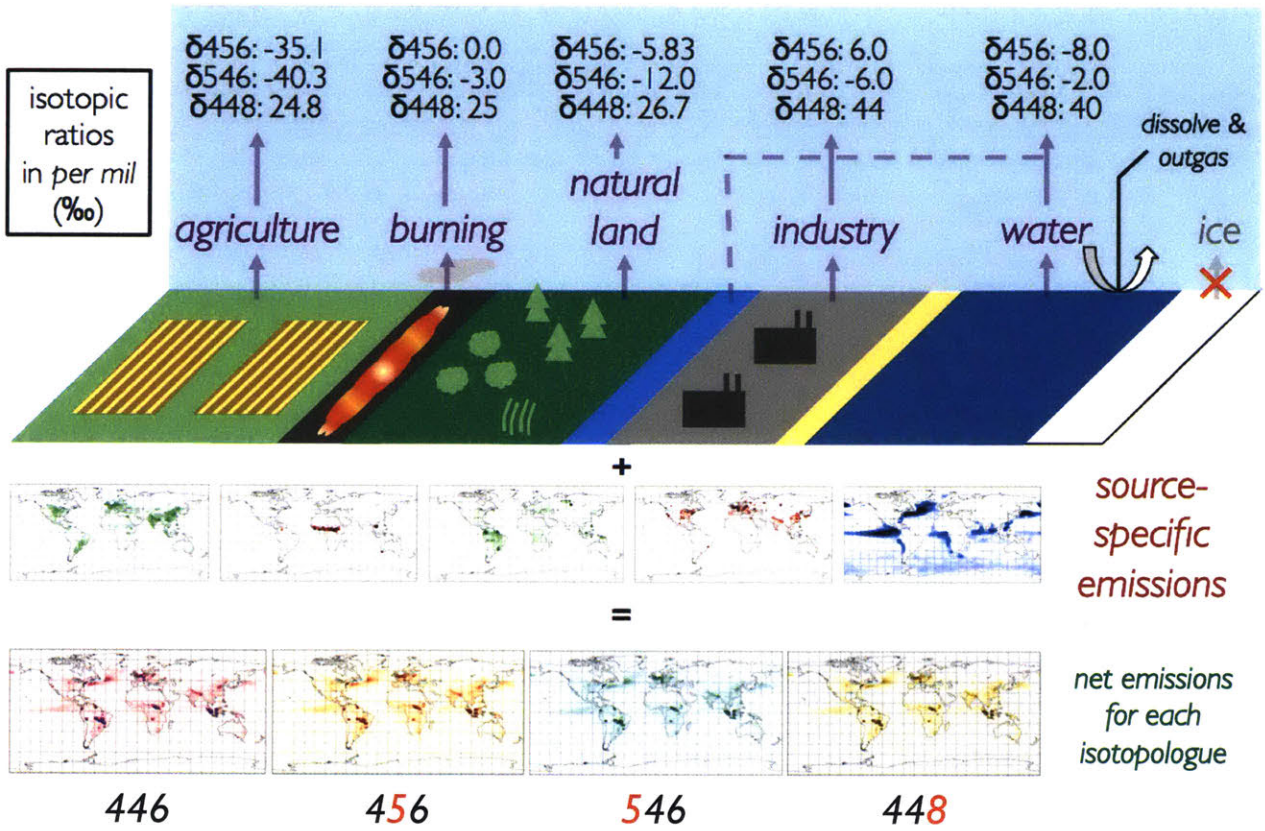

Figure 5-9: Creation of isotopically differentiated emissions using optimized N_2O emissions (Saikawa et al., 2014) and mean isotopic signatures of N_2O sources (Potter, 2011; Pérez et al., 2001; Whalen and Yoshinari, 1985)

The precisions of these modeled N_2O isotopic ratios could be greatly improved by conducting additional *in situ* and laboratory measurements of source signatures. In addition, a better representation of variables such as crop type, for example, could be built into the existing emissions inventory in order to capture the differences in N_2O production from different agricultural sectors. Future experiments of this type, which would greatly enhance the verisimilitude of N_2O isotopic ratio simulation in chemical transport models, are further discussed in the Future Work section of the final chapter.

5.3.3 Isotopically Differentiated Chemical Destruction

Each N_2O isotopologue was introduced as a separate chemical species, and new photolysis rates and bimolecular $O(^1D)$ reaction rates were calculated from laboratory and *in situ*

tropospheric experiments (Röckmann et al. (2001) and Kaiser et al. (2002a), as listed in Figure 2-8). For each isotopologue, the reaction rate constants for the two destruction processes were changed from one (as described above for bulk N_2O MOZART-4 simulation) to the fractionation factors φ in Figure 2-8, reproduced in Table 5.2.

Fractionation Factors φ for Chemical Destruction of N_2O		
Isotopologue	φ_1 (photolysis)	φ_2 ($O(^1D)$ reaction)
446	1	1
456	0.9488	0.998
546	0.9786	0.991
448	0.9669	0.986

Table 5.2: Fractionation factors φ for each N_2O chemical destruction process, drawn from Figure 2-8

5.3.4 Spin-up with Isotopic Chemistry

As the MOZART model runs progress, the effects of emissions, N_2O destruction processes, and vertical/horizontal transport from meteorological conditions all work to shift the modeled N_2O isotopic ratios away from the zonally-averaged piecewise initial conditions (Figure 5-7) used in the very first model run. When a model begins with unrealistic initial conditions, there are often drastic changes in the first few years as transport and chemistry drive species concentration distributions and gradients toward values that are more consistent with the expected values given a certain meteorological dataset. The re-alignment of these species concentration gradients is called a "spin-up" period (Saikawa et al., 2014; Rigby et al., 2011); the length of the spin-up depends on the average lifetime of the species of interest. In this case, N_2O destruction only occurs in the stratosphere, so many years may pass before circulation between the surface and the stratosphere establishes realistic vertical gradients of N_2O isotopologue concentrations.

For the first model run in a given spin-up "family" of model runs, the three-dimensional zonally-averaged isotopic ratio fields from Figure 5-7 are applied to the bulk N_2O mole fraction fields from January 1, 2011 in the extension of the experiment conducted by Saikawa et al. (2014) described above (the dotted box within Figure 5-10). At the end of each five-year spin-up model run, the final N_2O isotopic ratios of the five-year model run are applied to the initial bulk N_2O mole fractions from 2011 (the double-lined box in Figure 5-10). These new initial conditions have the same bulk N_2O mole fraction fields as the original MOZART-4 model runs without N_2O isotopic ratios, but the N_2O isotopic ratios are five years "older" than those from the immediately preceding spin-up run.

The spin-up process follows two separate tracks according to the two meteorological reanalysis datasets used. Both begin with the same MOZART standard initial conditions

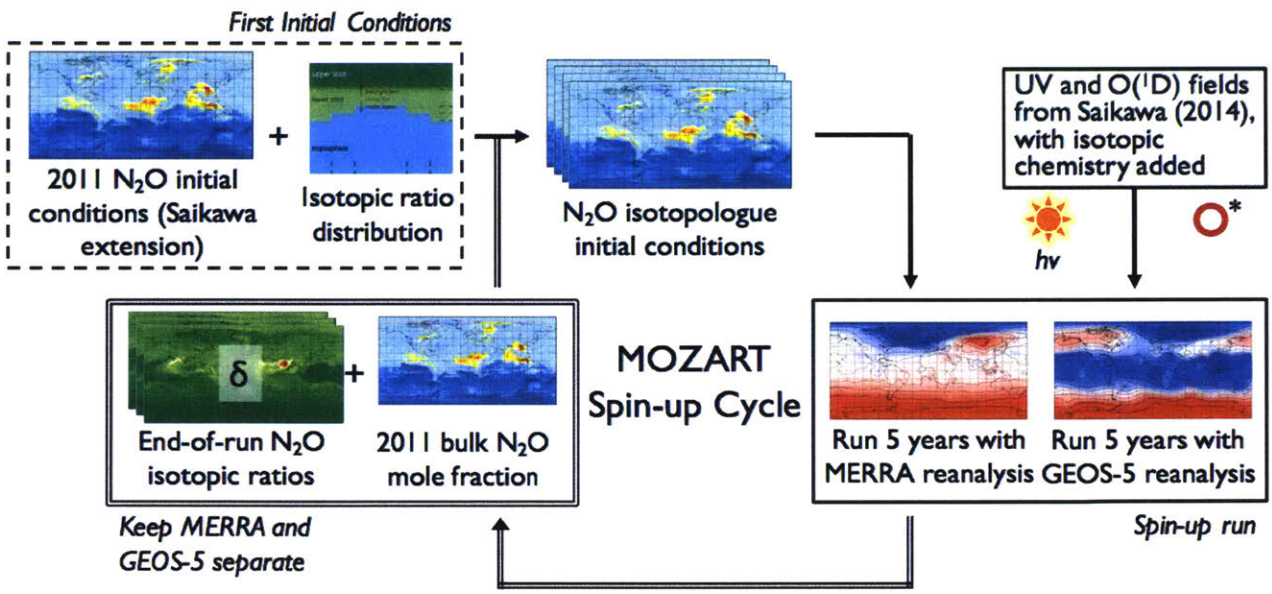

Figure 5-10: Procedure for advancing the spin-up phase of the N_2O isotopologue MOZART experiment, starting with the initial conditions described in Figure 5-7 and continuing with the model output, scaled to the initial surface concentration of N_2O from MOZART chemical forecasts

(with N_2O isotopologues added) but diverge due to differences in the transport associated with different realizations of meteorological dynamics in GEOS-5 and MERRA.

5.3.5 MOZART-4 Simulated N_2O Isotopic Ratios in 2014-2015

Due to the long atmospheric lifetime of N_2O (Prather et al., 2015; IPCC, 2013), a long spin-up period is needed in order to establish patterns of vertical transport and to stabilize concentration gradients. After 60 years of spin-up (Figure 5-10), the N_2O isotopic ratios at Mace Head had stabilized at levels near the initial flask sampling CF-IRMS N_2O isotopic ratio observation experiment conducted at Mace Head in 2011 (Potter, 2011).

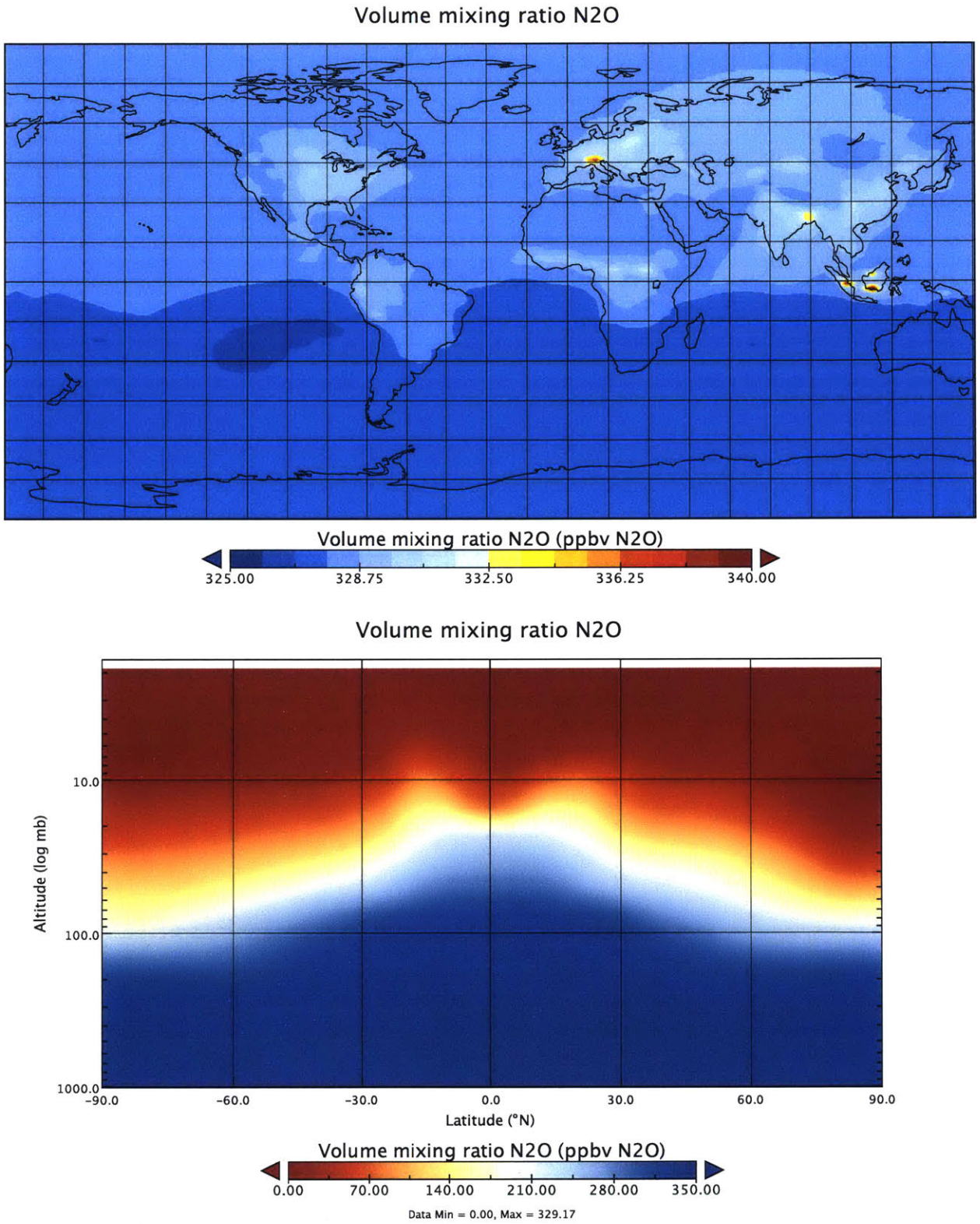

Figure 5-11: MOZART-4 surface (top) and zonal average (bottom; latitude-altitude plot) N_2O mole fraction on January 1, 2015

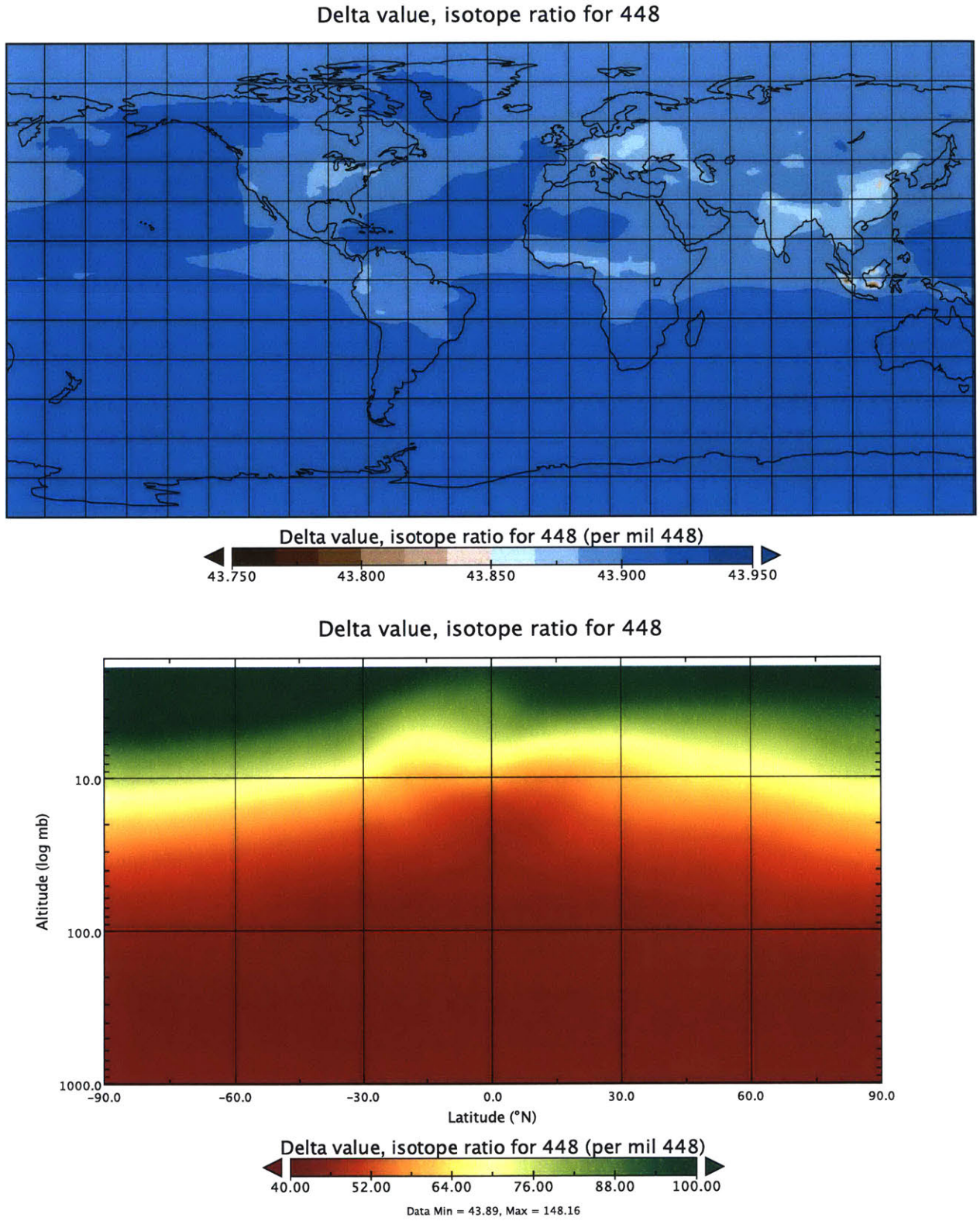

Figure 5-12: MOZART-4 surface (top) and zonal average (bottom; latitude-altitude plot) δ**448** (per mil) on January 1, 2015

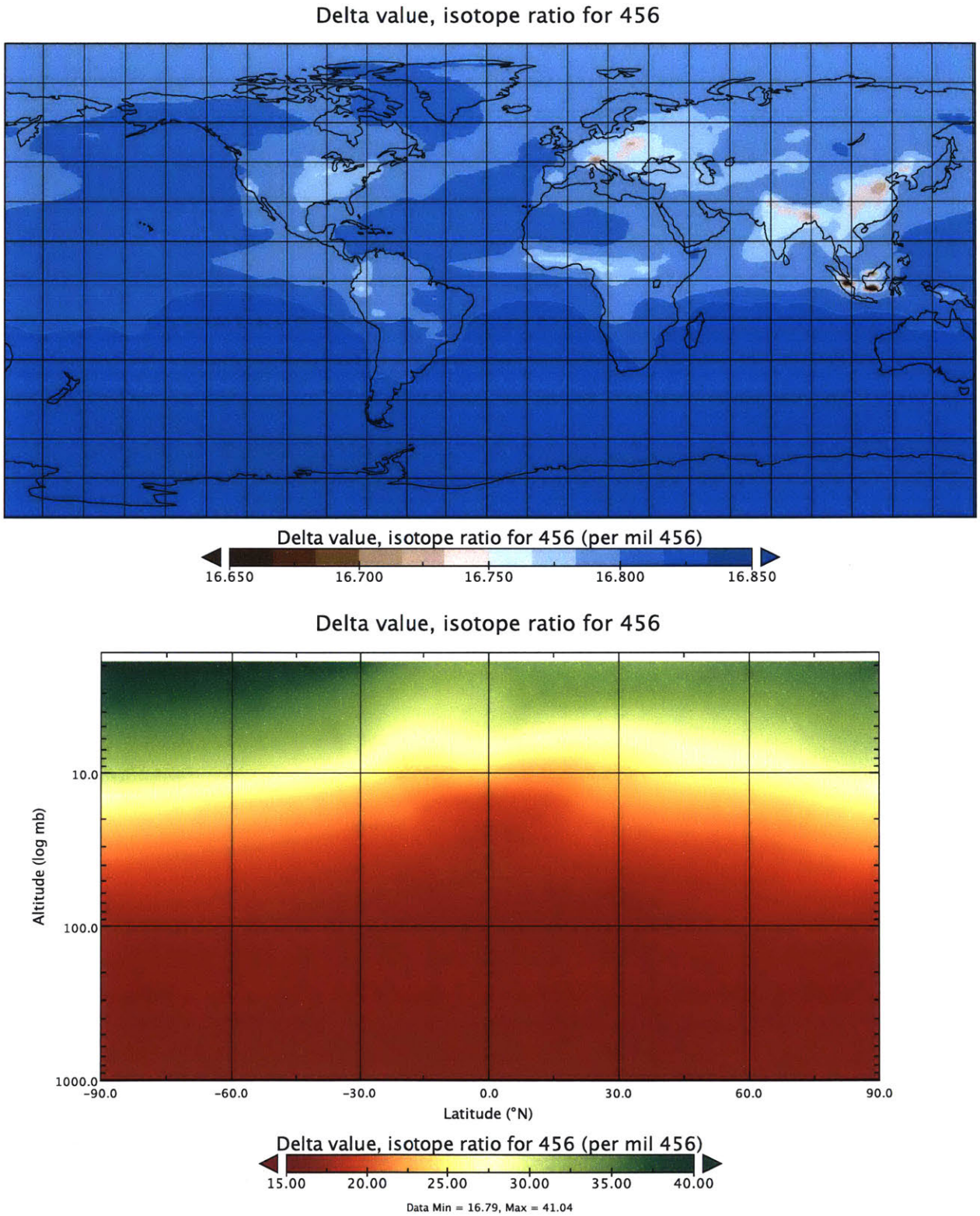

Figure 5-13: MOZART-4 surface (top) and zonal average (bottom; latitude-altitude plot) δ**456** (per mil) on January 1, 2015

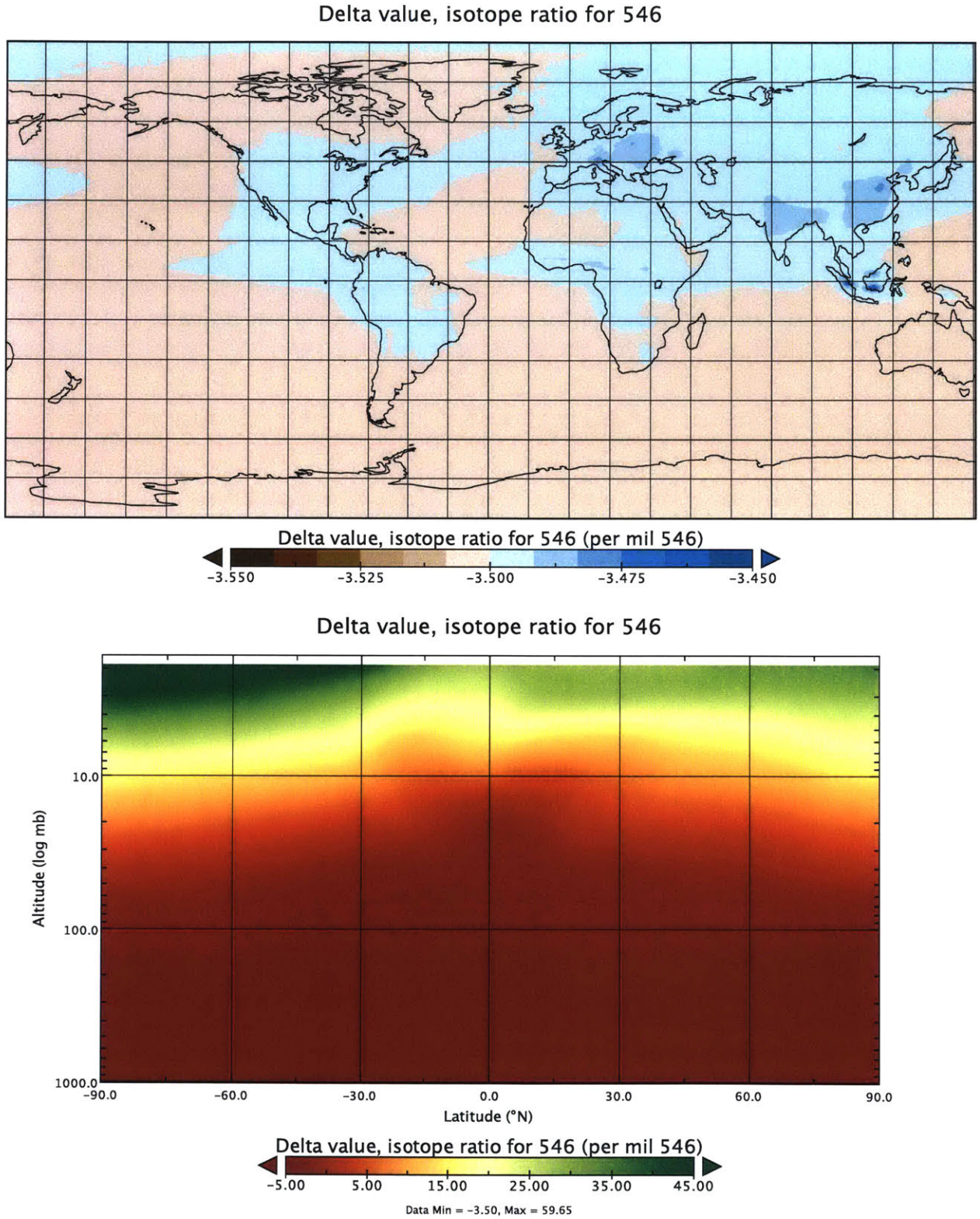

Figure 5-14: MOZART-4 surface (top) and zonal average (bottom; latitude-altitude plot) δ**546** (per mil) on January 1, 2015

With a dearth of N_2O isotopic ratio vertical gradient observations at multiple latitude bands, there is no straightforward "cut-off" point in the model spin-up process that leads to high certainty that the current representation of all three N_2O isotopic ratios cannot be further improved. The surface maps of N_2O isotopic ratios at January 1, 2015 (Figures 5-12 through 5-14; top panels) show relatively good qualitative agreement with patterns in N_2O emissions source signatures; for example, areas with more depleted δ**456** sources appear in brown in the Figure 5-12. However, fine-scale regional patterns or seasonal trends in N_2O isotopic ratios may not be correctly captured due to the relatively coarse resolution used in this model setup.

In the vertical extent, the modeled N_2O isotopic ratios are quite close to past balloon-based observations made by collecting air samples for analysis on the ground (Toyoda et al., 2004). Each of the three N_2O isotopic ratios (Figures 5-12 through 5-14; bottom panels) show a sharp gradient above the tropopause as N_2O isotopic ratios become highly enriched in areas where N_2O is chemically destroyed. As shown in Figure 1 of Toyoda et al. (2004) for balloon launches in Japan in 1999-2001, the observed atmospheric isotopic ratios at the tropopause (δ448 near 45 ‰, δ456 near 20 ‰, and δ546 near 0 ‰) become enriched at a height of 15 km above the tropopause (δ448 near 70 ‰, δ456 near 40 ‰, and δ546 near 15 ‰). The cross-sections for Figures 5-12 through 5-14 show a vertical gradient in all three isotopic ratios with approximately the same values.

Further exploration of global N_2O isotopic ratio modeling will be possible with greater spatial coverage of N_2O isotopic ratio observations, one of the top priorities for continued Stheno-TILDAS experiments as outlined in the Future Work section of the final chapter. Absent additional observations to constrain the N_2O isotopic ratios presented in this section, the reasonable ranges seen in MOZART-4 simulated N_2O isotopic ratios for 2014-2015 (Figures 5-12 through 5-14) indicate their potential to be used as boundary conditions within the NAME-MOZART modeling framework introduced in the next chapter.

5.4 Summary

This chapter expands on the global N_2O modeling experiment described in Saikawa et al. (2014) by extending that experiment through 2015 and by adding in treatment of N_2O isotopic ratios by including each major N_2O isotopologue as a new chemical tracer in the model. The results of this experiment, which used the global chemical transport model MOZART-4 as its base, show that laboratory studies of kinetic isotope effects in stratospheric chemical and photolytic destruction processes can be used directly to realistically model the kinetics of stratospheric N_2O isotopic fractionation in MOZART-4. In addition, the optimized five-sector (agriculture, biomass burning, industry, natural soil, ocean) global surface N_2O emissions estimates from Saikawa et al. (2014) are shown to lead to realistic modeled surface N_2O isotopic ratios when combined with the mean site-specific N_2O isotopic ratios for each of the five sectors calculated in Potter (2011). These advances in modeling global atmospheric

N_2O isotopic ratios notwithstanding, there remain opportunities for expanded observation campaigns such as those described in Toyoda et al. (2013) to better inform the spatial and temporal gradients of N_2O isotopic ratios, especially in air far from the surface.

Chapter 6

Inverse Modeling

This chapter will largely draw from the inverse modeling experiment from Rigby et al. (2012) in which methane isotopic ratio synthetic "pseudodata" (produced from a chemical transport model and subsampled with the frequency of established CH_4 isotopic ratio measurement techniques) was used to show that uncertainty of source-specific emissions estimates can be decreased when δD (deuterium, ^{2}H) and δ^{13}C measurements are added to observations of CH_4 mole fraction alone. The procedure used in this chapter will show the decreased uncertainty in source-specific N_2O emissions estimates when N_2O isotopic ratio observations are added to an "inversion" using AGAGE GC-ECD N_2O mole fraction observations alone.

The increased precision in magnitude and seasonality of N_2O emissions in the NAME Europe region resulting from addition of N_2O isotopic ratio observations validates the approach developed in Rigby et al. (2012), despite the lack of actual CH_4 isotopic ratio observations in that study. Once Stheno-TILDAS observations are extensive enough in time and space through new high-frequency and flask sampling experiments, Bayesian inverse modeling methods such as that described in this chapter will be employed on a global scale to drastically reduce the uncertainty in global and regional N_2O budgets.

6.1 Bayesian Inverse Methodology

The basis for Bayesian inverse modeling is creation of the best estimate of a state vector (N_2O emissions, $\mathbf{x}$) given a set of observations (N_2O concentrations or isotopic ratios, $\mathbf{y}$) and finding the most likely state vector values that can explain the observations (maximizing $P(\mathbf{x}|\mathbf{y})$) in Bayes' theorem (Prinn, 2000):

$$P(x|y) = \frac{P(y|x)P(x)}{P(y)} \tag{6.1}$$

A linear forward model (**F**) is used to populate the Jacobian (sensitivity) matrix **H** (Prinn, 2000), which contains elements corresponding to differences in modeled concentrations (y) given changes in emissions used in the forward model (x):

$$\mathbf{H} = \nabla_x \mathbf{F} = \frac{\partial \mathbf{y}}{\partial \mathbf{x}} \tag{6.2}$$

This Jacobian matrix (**H**) can then be used to maximize the PDF P(**x**|**y**) in order to determine the best estimate of emissions. If the forward model or observations are low-quality or inconsistent with each other, the "optimized" *a posteriori* emissions determined from the inverse model will be mostly determined by the *a priori* estimates originally passed to the model. Another way of posing this inverse problem is to minimize a cost function J such that the discrepancies between modeled and observed concentrations, and between the prior and optimized emissions sets, are minimized taking into account the uncertainty in each variable.

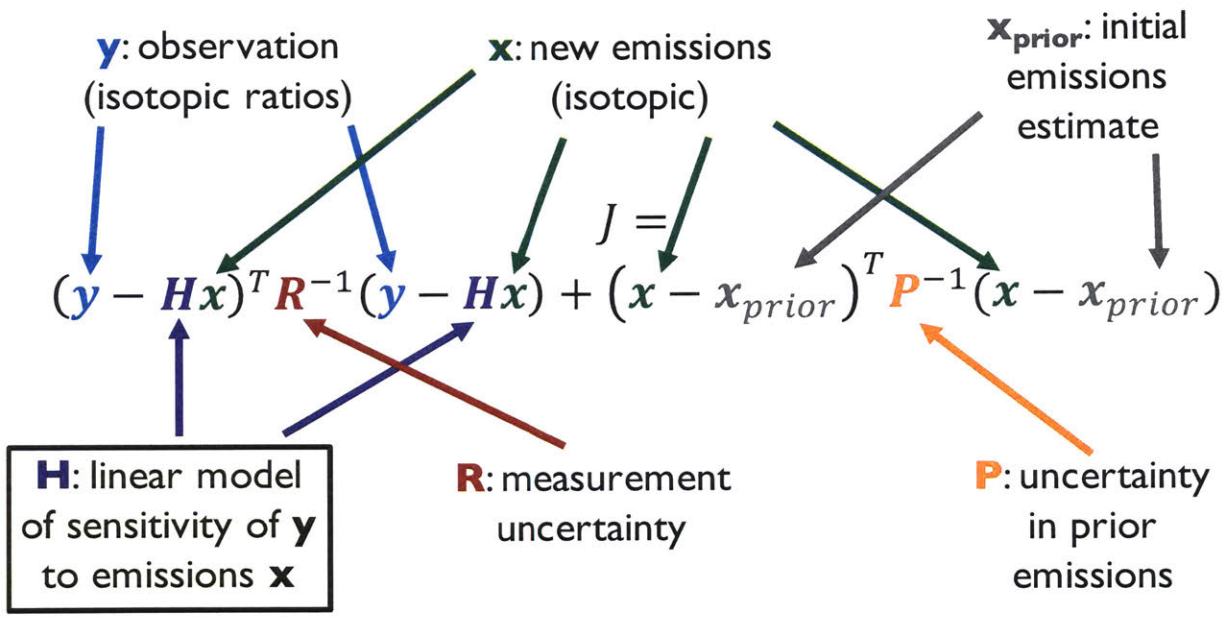

Figure 6-1: Formulation of the cost function J, which is minimized by finding the emissions estimate vector **x** that best explains the observations vector **y** given uncertainties within the matrices **R** and **P**, using a linear model **H**

Inverse modeling to determine surface fluxes and sources (Saikawa et al., 2014; Huang et al., 2008; Rigby et al., 2011) involves (a) a robust forward model, (b) observational data, and (c) an *a priori* best estimate of emissions (Prinn, 2000). Necessary in all three of these datasets is an understanding of the errors and uncertainties associated with each. As shown in Rigby et al. (2012), the uncertainty matrix of the posterior estimate (P_{opt}) derived from a "bulk inversion" as described above can be calculated (Equation 3.38, Tarantola (1987)) as

follows:

$$\mathbf{P}_{opt} = (\mathbf{H}^T\mathbf{R}^{-1}\mathbf{H} + \mathbf{P}^{-1})^{-1} \tag{6.3}$$

In order to improve the uncertainty of the optimized posterior estimate of N_2O emissions, there must be sufficient precision in data (represented by $\mathbf{R}$ above) in order for the linearly modeled results to add constraint to the prior emissions estimate $\mathbf{x}_{prior}$ and its uncertainty $\mathbf{P}$. In the paradigm described in Tarantola (1987), the square matrix $\mathbf{R}$ can contain the uncertainty of more than the repeatability of the observations alone; use of a chemical transport model leads to representation and modeling errors that can be included within $\mathbf{R}$ as the precision of all data used to constrain the estimate of the emissions $\mathbf{x}$. As described in Rigby et al. (2012) for inverse modeling with CH_4 isotopic ratios, the individual precision values σ that are squared to make the diagonal of $\mathbf{R}$ are calculated as follows:

$$diag(\mathbf{R}) = \sigma^2 \tag{6.4}$$

$$\sigma = \sqrt{\sigma_M^2 + \sigma_{RE}^2 + \sigma_{SF}^2 + \sigma_{SIR}^2} \tag{6.5}$$

where uncertainties σ are calculated for each observation type (N_2O mole fraction, and the three isotopic ratios measured). Using this method for uncertainty quantification, σ_M represents the measurement repeatability uncertainty, σ_{RE} represents the model-data representation error, σ_{SF} represents the sampling frequency uncertainty, and σ_{SIR} represents the errors from the estimates of N_2O source isotopic signatures (Rigby et al., 2012). Following Rigby et al. (2012), these individual components σ are calculated in the following ways:

- σ_M: determined from the operating procedure of each instrument; the procedure for calculating measurement repeatability for Stheno-TILDAS using a compressed air standard is discussed in Chapter 2
- σ_{RE}: because NAME-MOZART relies on the NAME Lagrangian Particle Dispersion Model footprints to calculate surface conditions at one location, one cannot use the typical method of averaging the grid cells surrounding the station (Chen and Prinn, 2005); therefore, error is estimated by the standard deviation of the variability of the modeled quantity within the averaging period of the observations
- σ_{SF}: calculated as the variability of observations within the averaging period divided by the square root of the number of observations within the period
- σ_{SIR}: only included in inversions using isotopic ratio observations, calculated by conducting NAME-MOZART iterations in which the isotopic ratio of each of the five source sectors from Saikawa et al. (2014) are perturbed to be at each extreme of the uncertainty ranges from the estimates presented in Table 6.1 drawn from Harris et al. (2017) and Potter (2011)

Therefore, in order to maximize the utility of this powerful statistical technique in constraining N_2O emissions estimates by source sector, the Bayesian framework using N_2O isotopic ratio observations and modeled conditions from NAME and MOZART must be implemented with the highest-quality data sources possible for both observations and prior emissions estimates. The power to identify source-specific emissions of N_2O ultimately relies on the ability to combine experimental measurements and computational models of site-specific isotopically-resolved N_2O concentrations. Global inverse models require spatially and temporally distributed data and a realistic forward model in order to improve initial emissions estimates; however, emissions estimates in a particular region can be improved by using observations at a small number of sites.

6.2 NAME-MOZART N_2O Isotopic Simulation

Bayesian inverse modeling experiments have the capability of comparing global N_2O isotopic ratio observations to outputs of well-conditioned CTM runs in order to produce optimized N_2O emissions maps for each source type. Due to the diffuse nature of N_2O sources and the mixing into the troposphere of isotopically-enriched N_2O from stratospheric intrusions, the effects of each constituent of the N_2O earth system must be well constrained in order to realistically model the results from the many competing global factors.

The first step in conducting an inverse modeling experiment is to create a linear model $\mathbf{H}$ that can use emissions $\mathbf{x}$ to produce expected concentrations ($\mathbf{Hx}$ or $\mathbf{y}_{model}$) to be compared with actual observations $\mathbf{y}$. In this experiment, the NAME-based analysis framework described in Rigby et al. (2011) is used to simulate mole fractions of each N_2O isotopologue at Mace Head, Ireland. Modeling results using the MOZART-4 global chemical transport model, described in the previous chapter, are also used to provide regional boundary conditions in this combined framework, referred hereafter as NAME-MOZART.

6.2.1 Input Data for NAME-MOZART N_2O Modeling

In order to simulate the N_2O Earth system using NAME-MOZART, the following model drivers are required:

- Inert tracer "footprints" calculated from NAME model runs forced by a three-dimensional meteorological field (described in Chapter 4)
- Boundary conditions at the edges of the NAME domain, produced in this case by MOZART global model runs spanning the same time (described in Chapter 5)
- Emissions for N_2O, as two-dimensional surfaces that ideally change in time with seasonality and interannual changes

- *Optionally*, observations (with uncertainties) for comparison to model-produced simulated observations

The computationally intensive inputs in the NAME-MOZART framework, created by running the NAME model to produce the inert tracer footprints and running the global MOZART chemical transport model, do not necessarily need to be recalculated for each NAME-MOZART iteration. Rather, as shown in Figure 6-2, adjustments to emissions in the NAME domain or the MOZART-produced domain boundary conditions directly cause changes in the simulated observed conditions at the location of interest, Mace Head, Ireland.

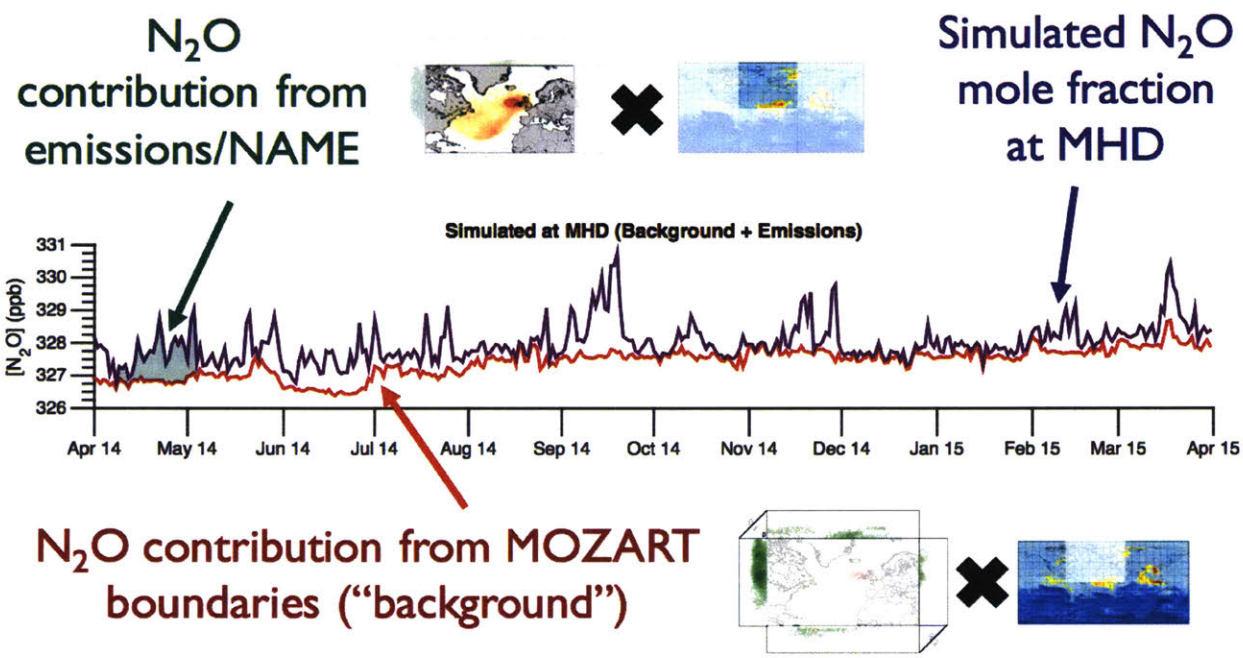

Figure 6-2: Simulated timeline of N_2O mole fraction (purple line) at Mace Head, Ireland in 2014-2015, separated into contribution from MOZART boundaries (red line) and contribution from surface emissions within the domain (space between red and purple lines, shaded green in April 2014)

This NAME-MOZART framework allows for rapid simulation of N_2O mole fractions expected at Mace Head given perturbed sets of emissions. These perturbed model iterations are used to populate the linear model matrix $\mathbf{H}$, which describes the sensitivity of observations $\mathbf{y}$ to any number of factors related to emissions $\mathbf{x}$.

6.2.2 NAME-MOZART with Bulk N_2O Mole Fraction

The first step in using the Stheno-TILDAS N_2O isotopic ratio observations within the NAME-MOZART inverse modeling framework described above is to understand how well

the NAME-MOZART method does in reproducing trends in bulk N_2O mole fraction at Mace Head. This section will describe the construction of the various input data sources used to produce the simulated N_2O mole fraction timeline above in Figure 6-2.

Observations

The bulk N_2O mole fraction observations used to compare with NAME-MOZART model results are from the Gas Chromatography-Electron Capture Detector (GC-ECD) instrument installed as part of the AGAGE station at Mace Head, Ireland.

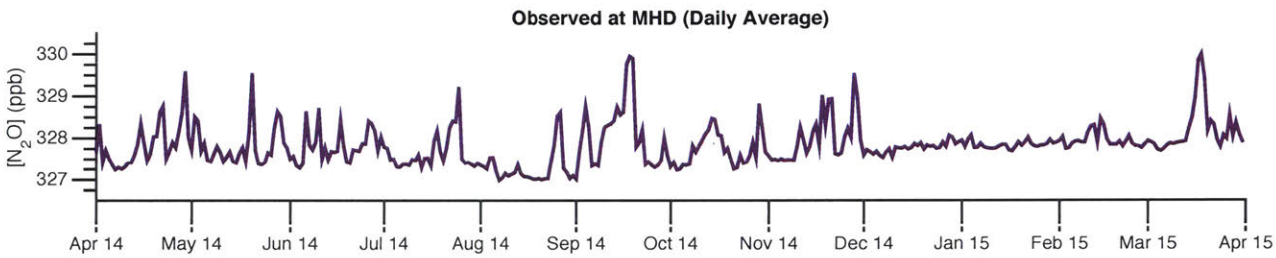

Figure 6-3: N_2O mole fraction observations at Mace Head, Ireland, as measured using the AGAGE GC-ECD instrument

The timeline of N_2O mole fraction at Mace Head (Figures 1-2 and 6-3) shows short-lived high-concentration excursions from a steadily increasing baseline influenced by seasonal trends. A high-quality model realization of N_2O mole fraction at Mace Head will need to capture both long-term trends and short-term "pollution events" in order to have value in constraining emissions estimates through inverse modeling.

NAME Inert Tracer Footprints

The NAME surface emissions sensitivity fields used in NAME-MOZART are the same as those described in Chapter 4. Again, the NAME surface sensitivity "footprints" (as in Figure 4-7) are created by releasing 36,000 inert particles from 10 meters above ground level at Mace Head and tracking their "backward mode" trajectories for 30 days or until they intercept the surface level or the four bounding walls (20 km height) of the NAME Europe domain (Manning et al., 2011). The particles that leave the domain largely represent well-mixed "background air" and the particles that strike the surface can statistically indicate the areas within the NAME region where surface emissions contribute to the mole fractions observed at Mace Head. This computationally intensive analysis does not need to be performed for every iteration of NAME-MOZART due to the inert nature of N_2O in the NAME domain and the lack of chemistry included in this particular NAME setup.

MOZART Boundary Conditions

The MOZART boundary conditions used in Figure 6-2 were those from the final isotopic model run (after 60 years of spin-up), as described in the previous chapter. In order for the raw MOZART-4 outputs to be used in NAME-MOZART, the three-dimensional fields of N_2O mole fraction must be regridded to the resolution of NAME-MOZART. In addition, the two-dimensional "slicing" process used to create the four bounding walls of the NAME Europe domain may interpolate within the 3-D MOZART field when boundaries fall between between adjacent grid boxes in the raw model output.

Emissions

The bulk N_2O emissions used in the NAME-MOZART simulation were drawn from multiple sources, each of which represents the best available estimate of emissions from the five sectors described in Saikawa et al. (2014): agriculture, biomass burning, industry, natural soil, and ocean. For biomass burning, natural soil, and oceanic emissions, the linearly extrapolated N_2O emissions used in MOZART (Figure 5-3) were regridded to the fine resolution used in NAME. Agricultural and industrial N_2O emissions were drawn from the EDGAR v4.3.2 inventory (Janssens-Maenhout et al., 2017), with the month-by-month breakdown of each constituent sector from 2010 applied to the annual average from 2014 and 2015. This leads to monthly N_2O emissions for the period spanning April 2014 to March 2015 in which there are two full seasons of Stheno-TILDAS observations.

The emissions estimates in Figure 6-4 are shown as the total amount of N_2O emitted within the NAME Europe domain during each month. These total emissions rates were calculated by multiplying the surface area (m^2) of each grid box by the emissions rate within each box (originally in moles/m^2/s, converted to Tg N_2O/m^2/month) and summing the monthly mass of N_2O emitted within each box of the domain.

NAME-MOZART Bulk N_2O Simulation

The simulated timeline of N_2O mole fraction at MHD (Figure 6-2) lines up well with actual observations at MHD from the AGAGE GC-ECD instrument, including timing and magnitude of short-lived events that depart from the "background" baseline.

Notably, the simulated N_2O mole fraction has a bias (Figure 6-5, bottom panel) of approximately +1 ppb in late summer/fall (August-November 2014). The rest of the model-observation comparison, however, aligns with little systematic bias.

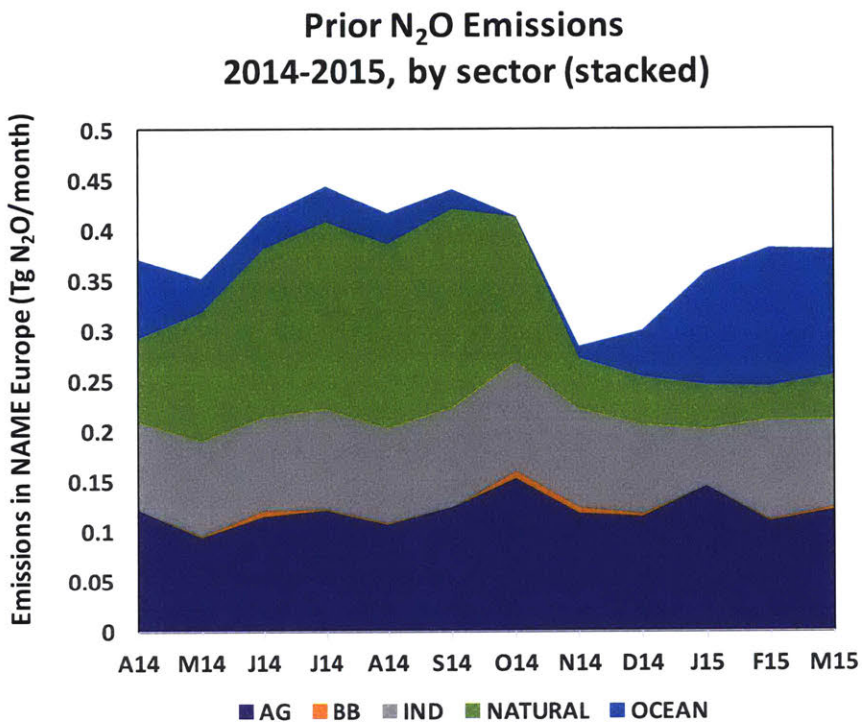

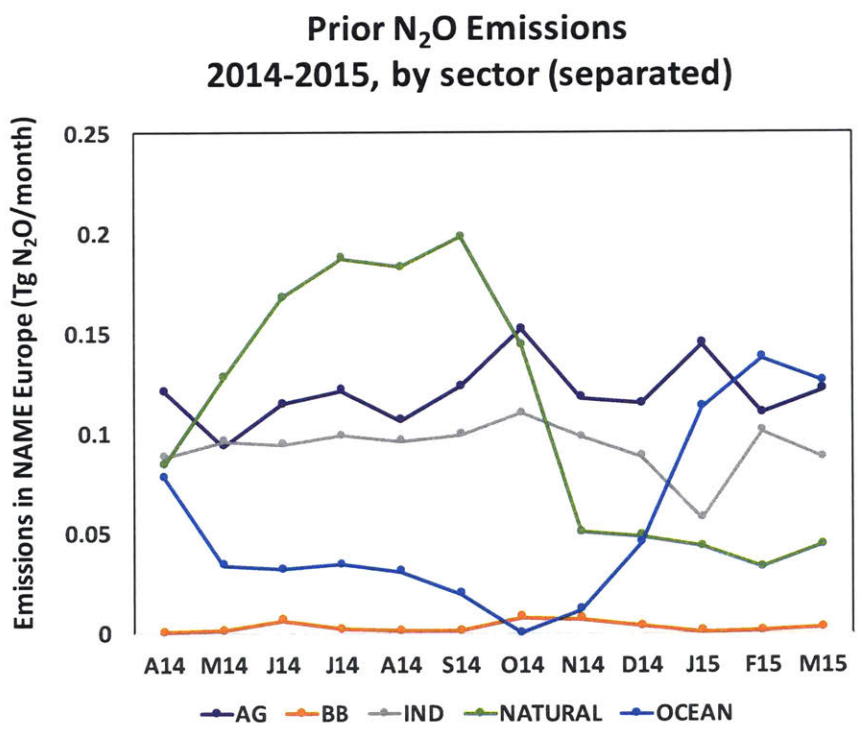

Figure 6-4: Prior emissions for inverse modeling, with sectors stacked to show net emissions (top) and separated by sector to show relative magnitude (bottom)

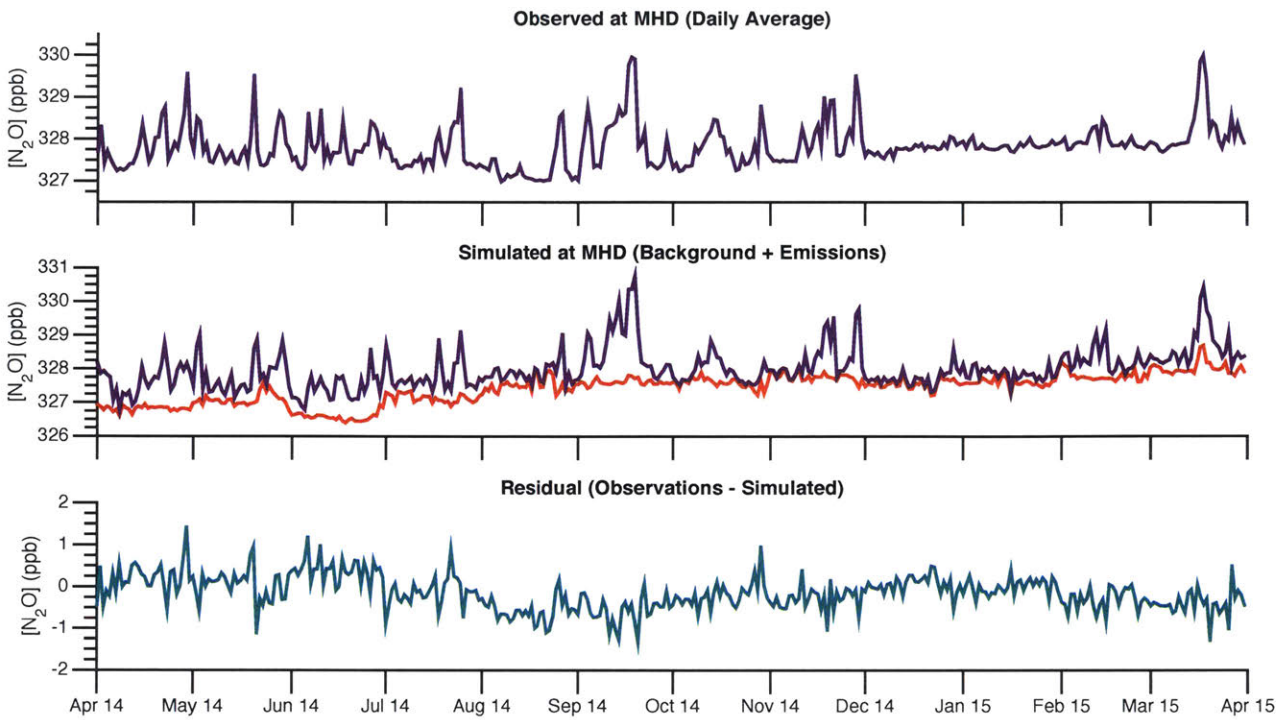

Figure 6-5: AGAGE GC-ECD N_2O mole fraction observations at Mace Head (top), NAME-MOZART simulated N_2O mole fraction (center; from Figure 6-2), and residual (bottom)

6.2.3 Isotopically Differentiated NAME-MOZART

In order to add isotopic ratios to the simulation described above, the same process of creating boundary conditions and emissions datasets must be replicated for all isotopic variants of N_2O (using the convention described in Chapter 2, **446**, **456**, **546**, and **448**). Rather than devising a way to "transport" physical measurement ratios (such as delta-value isotopic ratios) within the model, each isotopologue is treated as a separate species with its own boundary conditions, emissions estimates, and mole fraction observations. Due to the inertness of all N_2O isotopologues in the lower atmosphere, the inert tracer "footprints" used for bulk N_2O will be applicable to all of its isotopologues without any modification.

Observations

The mole fraction observations of each N_2O isotopologue are calculated by interpolating the bulk N_2O AGAGE GC-ECD mole fraction observations to the same time resolution as Stheno-TILDAS N_2O isotopic ratio observations, and then applying the Stheno-TILDAS isotopic ratios (Figure 4-2) to the interpolated bulk N_2O mole fraction timeline.

Ideally, Stheno-TILDAS would be capable of making mole fraction observations for all

four N_2O isotopologues, with the bulk N_2O mole fraction being a sum of the four isotopologues. However, for the 2014-2015 Stheno-TILDAS observation campaign at Mace Head, the absolute mole fractions of N_2O in the standard gases were not precisely known well enough to calibrate the instrumental response to bulk N_2O concentration. Regardless of this shortcoming, Stheno-TILDAS still allows for isotopic ratios to be calculated at a high level of precision due to the calculation of the relative ratios of the four major isotopologues. In future experimental campaigns using Stheno-TILDAS, this shortcoming will be corrected by quantifying the bulk N_2O mole fraction in the standard gas mixtures before use as working standards.

MOZART Boundary Conditions

As with the bulk N_2O NAME-MOZART simulation described in the previous section, the MOZART boundary conditions used in simulating N_2O isotopic ratios at Mace Head are from the final isotopic model run of MOZART-4 (after 60 years of spin-up), as described in the previous chapter. The raw model outputs can be regridded and "sliced" in the same fashion as bulk N_2O mole fractions due to the same implementation in MOZART of N_2O isotopologues as separate chemical tracers (Chapter 5).

Emissions

The isotopically differentiated emissions used in NAME-MOZART begin with the same five-sector monthly N_2O emissions described in the previous section for bulk N_2O NAME-MOZART simulation.

In order to add isotopic source signatures into the emissions used by NAME-MOZART, the isotopic ratios reported in Harris et al. (2017) and Potter (2011) (reproduced in Table 6.1) were incorporated in the following process:

- Start with the bulk five-sector N_2O emissions described in the previous section, for 2014-2015
- For each of the five sectors, apply source-specific isotopic signatures to produce emissions rates for each N_2O isotopologue as follows:
  - **Agriculture**: For the AGSOIL and AGBURN EDGAR sectors, apply the isotopic ratios from Harris et al. (2017) in the proportions AGSOIL and AGBURN appear in EDGAR v4.3.2 as a percentage of agricultural emissions in each grid box
  - **Biomass Burning**: For biomass burning, apply the average isotopic ratios used in the previous chapter for biomass burning N_2O emissions

EDGAR Anthropogenic N_2O Source Isotopic Signatures from Harris et al. (2017)			
Abbreviation	**δ456**	**δ546**	**δ448**
ENERGY	12.7 ± 2.9	-4.9 ± 2.9	35.9 ± 13.1
TRANS	-26.6 ± 3.8	-30.8 ± 3.8	28.6 ± 9.9
CARS	-5.1 ± 2.5	-9.3 ± 2.5	40.3 ± 3.7
HEAT	7.25 ± 6.3	3.75 ± 6.3	40.3 ± 10.0
INDUSTRY	-6.7 ± 11	-10 ± 11	29.1 ± 18.8
MANURE	-14.3 ± 6.5	-20.8 ± 6.5	23.9 ± 3.8
AGSOIL	-14.2 ± 6	-21.4 ± 6	29 ± 3.7
AGBURN	0.4 ± 3.4	-2.4 ± 3.4	25 ± 3.7
WASTE	-6.4 ± 13	-16.9 ± 13	31.5 ± 14.1
INDIRECT	-14.2 ± 6	-21.4 ± 6	29 ± 3.7
N_2O Source Isotopic Signatures from Chapter 5			
Source	**δ456**	**δ546**	**δ448**
Biomass Burning	0 ± 8	-3 ± 5	25 ± 10
Natural Soil	-5.8 ± 15	-12 ± 15	26.7 ± 10
Ocean	8 ± 8	2 ± 6	45 ± 10

Table 6.1: Site-specific N_2O isotopic signatures for EDGAR anthropogenic industrial and agricultural sources (Harris et al., 2017), and for the remaining three source sectors (Potter, 2011); any isotopic ratios originally reported in terms of ^{15}N and Site Preference have been converted to **δ456** and **δ546**

  - **Industry**: For CARS, ENERGY, HEAT, INDUSTRY, INDIRECT, MANURE, TRANSPORT, and WASTE EDGAR sectors, apply the isotopic ratios from Harris et al. (2017) in the proportions that each sector appears in EDGAR v4.3.2 as a percentage of industrial sources in each grid box
  - **Natural Soil**: For natural soil emissions, apply the average isotopic ratios used in the previous chapter for natural N_2O emissions
  - **Ocean**: For oceanic emissions, apply the average isotopic ratios used in the previous chapter for oceanic N_2O emissions

- Sum the N_2O isotopologue emissions from each of the five sectors, ensuring that emissions of the four isotopologues add to the bulk N_2O emissions

Using this approach allows EDGAR-based estimates of seasonality in individual agricultural and industrial sources to impact the net isotopic signatures of those two N_2O emission sectors in each month. Future inverse modeling experiments based on EDGAR source estimates could keep each source type separate, rather than aggregating industrial and agricultural sources, for additional insight into the changing trends in each EDGAR source.

Isotopically Differentiated Simulation

After addition of N_2O isotopic ratios to the necessary model input data sets, NAME-MOZART can be used to produce simulated isotopic ratio observations at Mace Head.

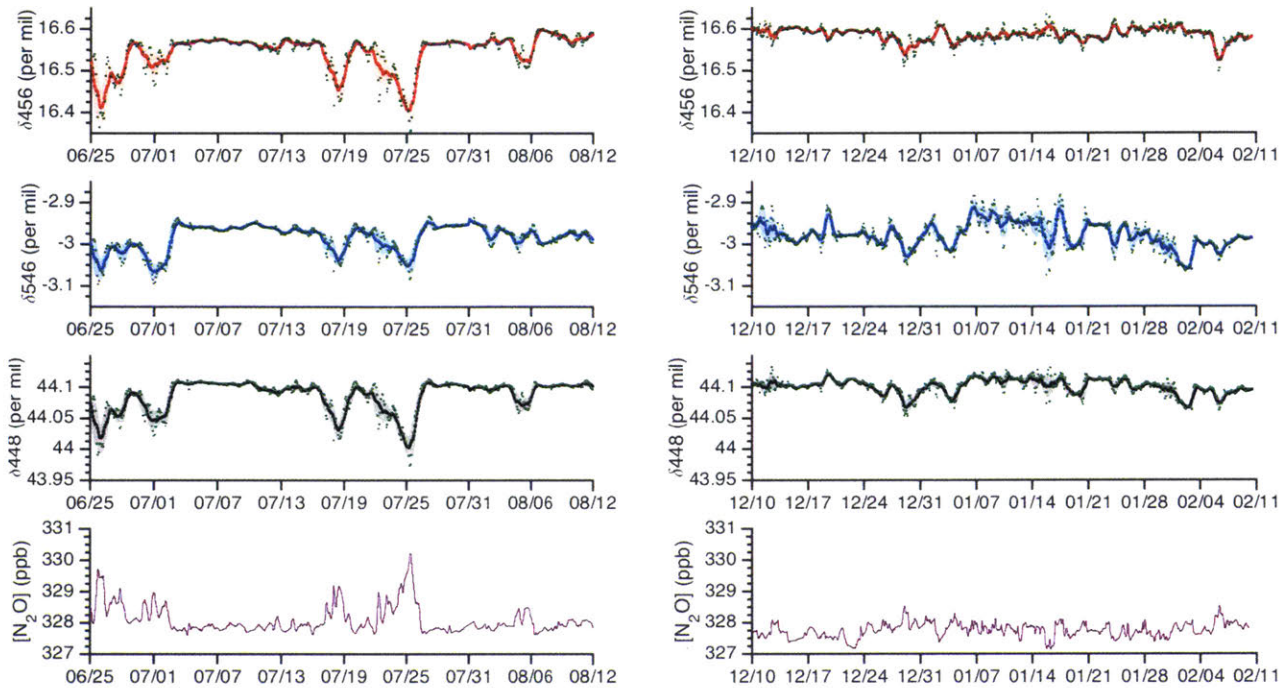

Figure 6-6: NAME-MOZART simulation of N_2O isotopic ratios and mole fraction, shown in the same time periods as Stheno-TILDAS observations in Figure 3-7; green points indicate simulated measurements, the thick line indicates a 24-hour running mean of simulated measurements, the translucent bounds represent the uncertainty in the simulated isotopic ratios

Notwithstanding a few discrepancies (exact event timing and magnitude of pollution events and short-term excursions), NAME-MOZART combined model results largely capture general patterns in N_2O isotopic ratio dynamics at MHD. There are, however, a few notable differences between the Stheno-TILDAS observed (Figure 3-7) and NAME-MOZART simulated (Figure 6-6) N_2O isotopic ratio timelines. First, the range of isotopic ratios in the simulation is significantly smaller than the range seen in the observations. Also, in high-N_2O "pollution events" such as that seen between 7/17-7/26, the simulated isotopic ratios all move in the same direction, as opposed to the general trend of anti-correlation between ^{15}N and ^{18}O seen in Stheno-TILDAS observations.

There are some aspects of the initial NAME-MOZART simulated data that compare well with Stheno-TILDAS observations. Both simulated and observed isotopic ratios have "calm" regions where the majority of the air being sampled comes from well-mixed background conditions (from the domain boundary walls in the simulation), corroborated by the

transition from peaks to baseline in the N_2O mole fraction timeline. Also, in most cases, the simulated 24-hour moving averages (thick line with 1-sigma uncertainty bounds in lightly shaded region) of the simulated isotopic ratios fall within the uncertainty ranges of the observations. Both of these aspects indicate that by optimizing the emissions using a Bayesian inverse method, the simulated N_2O isotopic ratio timelines may be able to more closely match the Stheno-TILDAS observations.

6.3 Inverse Modeling with NAME-MOZART

With NAME-MOZART model realizations that either use N_2O bulk mole fraction observations alone or add N_2O isotopic ratio observations, inverse modeling can be used to show the improved precision of N_2O emissions estimates after high-frequency isotopic observations are included. The linear model $\mathbf{H}$ used in the inverse model cost function (Figure 6-1) is made by systematically perturbing the surface emissions to assess the sensitivity of observations made at Mace Head to different aspects of N_2O emissions in the NAME Europe domain.

In this section, the inverse model realizations ("inversions") will show an optimized estimate for N_2O emissions ($\mathbf{x}_{opt}$) and a decrease in the uncertainty ($\mathbf{P}_{opt}$) from the prior emissions estimate ($\mathbf{P}$). The following parameters will be perturbed in order to determine the optimal N_2O emissions to explain the Stheno-TILDAS and GC-ECD observations at Mace Head:

- Location of total bulk N_2O emissions, with the NAME Europe domain split into the European subregion (centered on continental Europe) and four long-range regions within the large NAME Europe domain (Figure 6-7)
- Distribution of total N_2O emissions to the five emissions sectors used in Saikawa et al. (2014) (agriculture, biomass burning, industry, natural soil, ocean), using bulk N_2O mole fraction and N_2O isotopic ratios; assumes the isotopic signatures from Harris et al. (2017) for Dübendorf, Switzerland are also applicable to emissions sampled at Mace Head

For each inversion experiment, the linear model matrix $\mathbf{H}$ is first computed by perturbing emissions and noting the linear response in the simulated observation of interest at Mace Head (N_2O mole fraction or isotopic ratio). Once all variables necessary to produce the cost function J (Figure 6-1) are calculated, the optimized N_2O emissions are determined using Equation 3.37 from Tarantola (1987):

$$\mathbf{x}_{opt} = (\mathbf{H}^T\mathbf{R}^{-1}\mathbf{H} + \mathbf{P}^{-1})^{-1}(\mathbf{H}^T\mathbf{R}^{-1}\mathbf{y}_{obs} + \mathbf{P}\mathbf{x}_{prior}) \tag{6.6}$$

Although the first inversion experiment, in which bulk N_2O observations are used to constrain the spatial distribution of net N_2O emissions, does not take advantage of N_2O isotopic

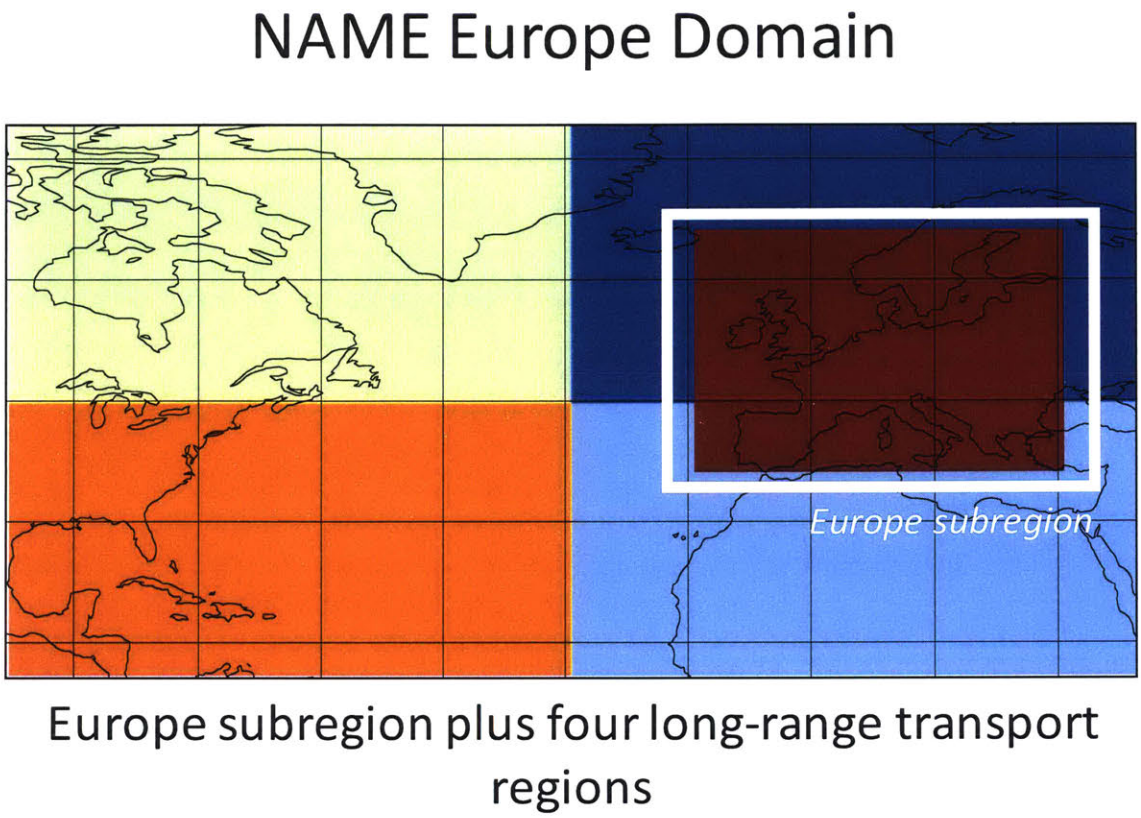

Figure 6-7: Basis functions for inversion of gridded bulk N_2O emissions, with four long-range sectors and a high-resolution (at the native NAME grid resolution) within continental Europe

ratio observations, the other inversion makes good use of the added isotopic measurements made at Mace Head. In addition, the N_2O isotopic ratio observations at Dübendorf, Switzerland (Harris et al., 2017) can be added into the inversion to further constrain the emissions sectors to which the conditions at the Dübendorf station are most sensitive.

While a novel use of this inverse method would be constraining the N_2O isotopic signatures for each source using observations (see an initial setup for this experiment in Appendix B), the best method of improving uncertainty in N_2O source signatures will be to conduct intensive field and lab sampling of distinct N_2O production processes. A dense enough network of N_2O isotopic ratio observations could help indicate seasonality or geographic variation in N_2O source isotopic signatures, but those so-far unconstrained aspects of the N_2O earth system will be better understood with additional experiments outside the scope of this thesis (described in the Future Work section in the final chapter).

6.3.1 Inversion by Spatial Location

The first application of the NAME-MOZART N_2O simulation to inverse modeling is to use bulk N_2O observations to constrain N_2O emissions by location. For the two seasons of Stheno-TILDAS observation, summer 2014 (JJA) and winter 2014-2015 (DJF), there are sufficient high-frequency GC-ECD observations of N_2O mole fraction to provide a basic understanding of N_2O source seasonality in the NAME Europe domain.

In this experiment, cost function **J** to be minimized (Figure 6-1) contains the following variables:

- n: number of GC-ECD observations used (no time averaging)
- m: number of basis function zones (four long-range sectors plus 16130 native-resolution grid points, as shown in Figure 6-7)
- $\mathbf{y}$ (n x 1): N_2O mole fraction observations
- $\mathbf{H}$ (n x m): sensitivity of mole fractions $\mathbf{y}$ to emissions $\mathbf{x}$, created by perturbing emissions in each basis function zone and looking for linear response
- $\mathbf{x}$ (m x 1): emissions from each basis function zone; trying to optimize this variable
- $\mathbf{R}$ (n x n): Combined uncertainty in data (measurements and model, as discussed pertaining to Equation 6.5 above), as diagonal on a sparse square matrix
- $\mathbf{x}_{prior}$ (m x 1): prior estimate of emissions from each sector
- $\mathbf{P}$ (m x m): Uncertainty in the *a priori* emissions estimate as a diagonal in a sparse matrix, with the global total N_2O emission uncertainty from 2008 in Saikawa et al. (2014) uniformly applied to all model grid cells

Results

The inversion to constrain bulk N_2O emissions by NAME grid cells within the Europe sub-region of the entire NAME domain leads to significant uncertainty reduction in both seasons near Mace Head with modest change and small uncertainty reduction far from the station (Figures 6-8 and 6-9). The model grid cells with the largest reduction in uncertainty are found in the regions of highest density in the seasonal average NAME surface sensitivity footprints in Figure 6-10.

This inversion shows that using one station alone to constrain emissions by model grid cell in an entire continent (spanning over 10,000 grid cells), especially when the *a priori* emissions estimates came from an inverse modeling experiment (Saikawa et al., 2014) using numerous high-frequency and flask-based measurement locations in the same domain, will be a challenge. However, by adding an additional observation station (Dübendorf, Switzerland) into the inverse modeling framework and by reducing the dimensionality of the emissions

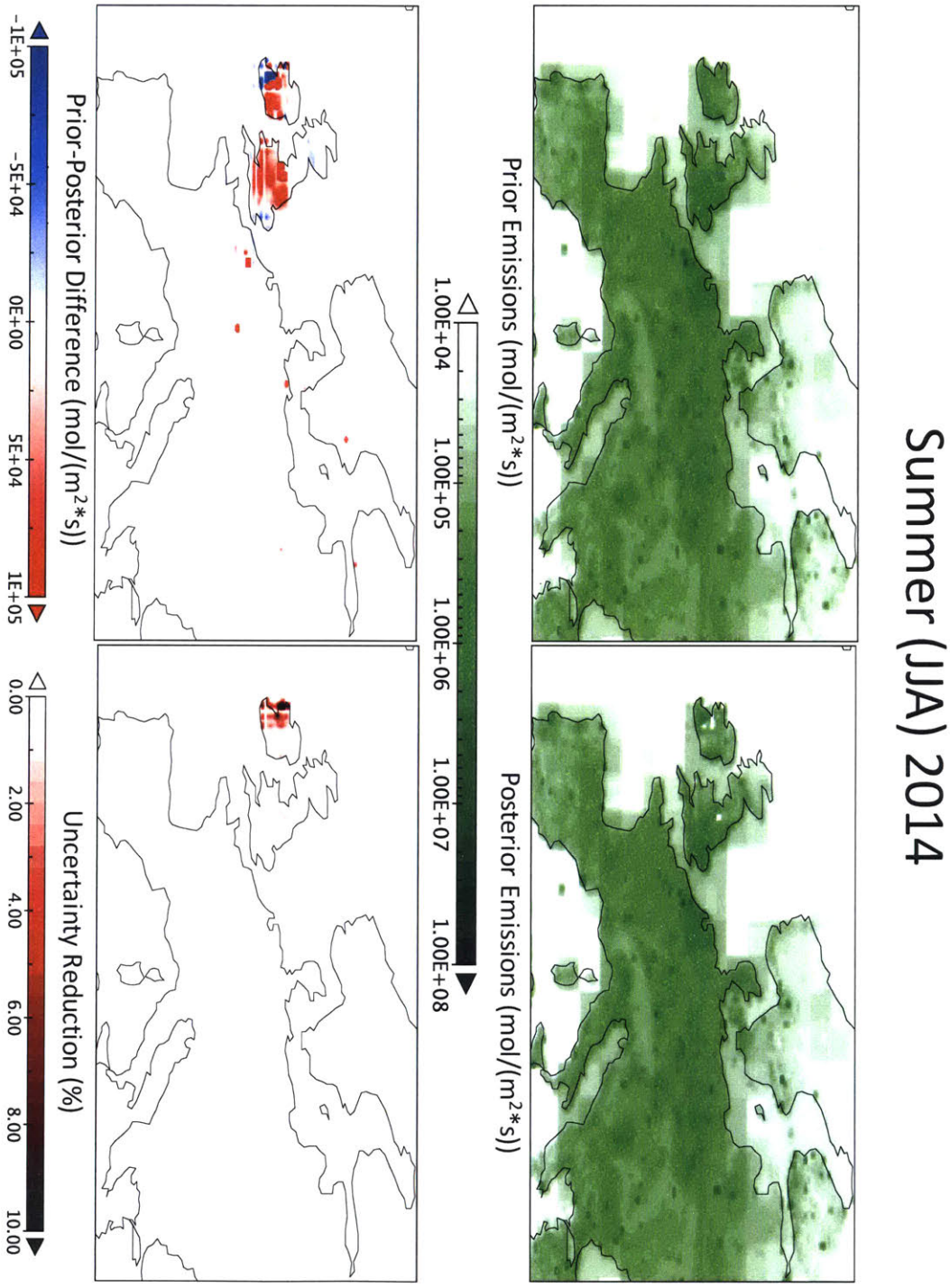

Figure 6-8: Prior emissions estimate, posterior emissions estimate, prior-posterior difference, and uncertainty reduction for summer (JJA) N_2O emissions, using basis function from Figure 6-7

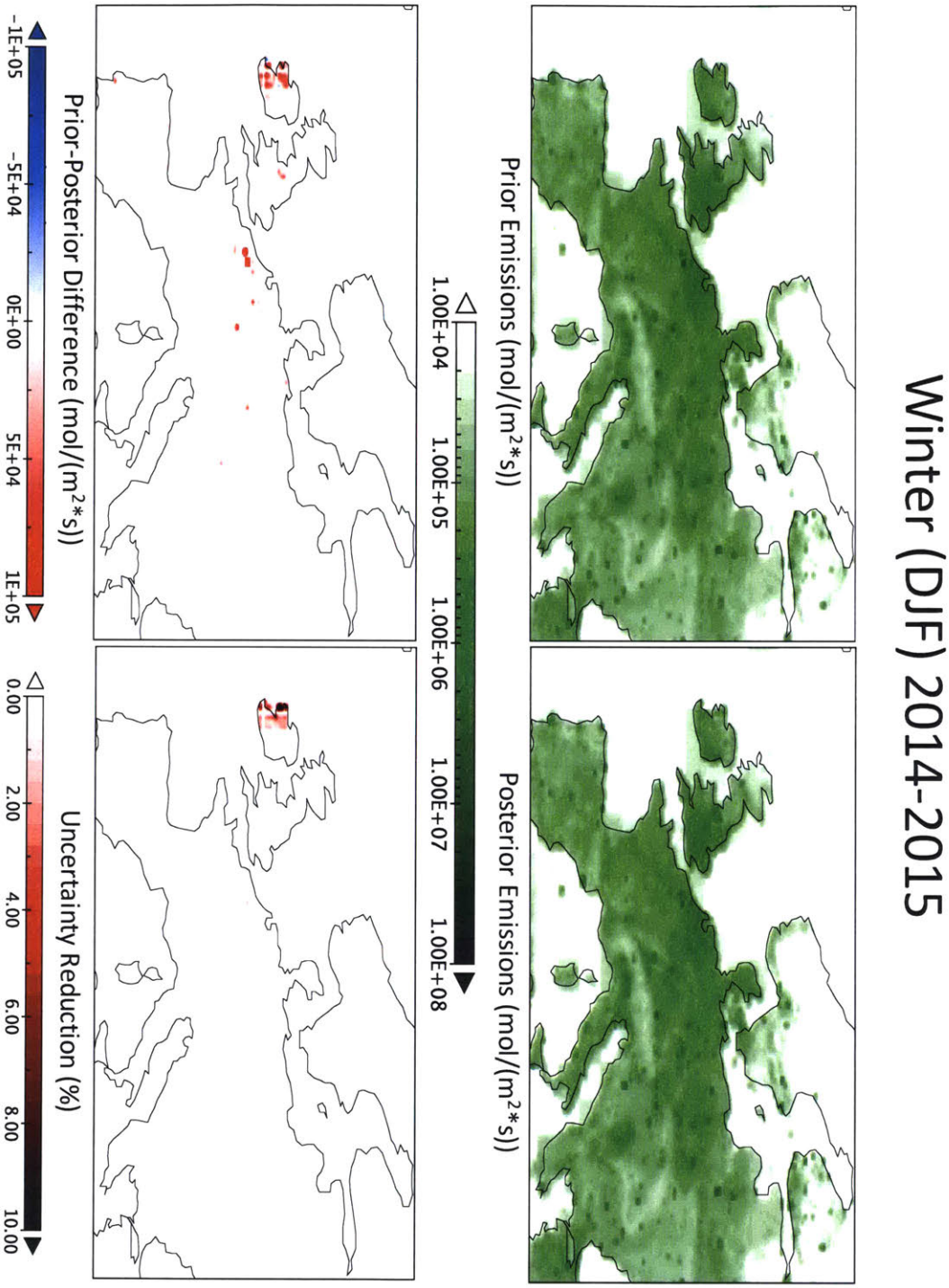

Figure 6-9: Prior emissions estimate, posterior emissions estimate, prior-posterior difference, and uncertainty reduction for winter (DJF) N_2O emissions, using basis function from Figure 6-7

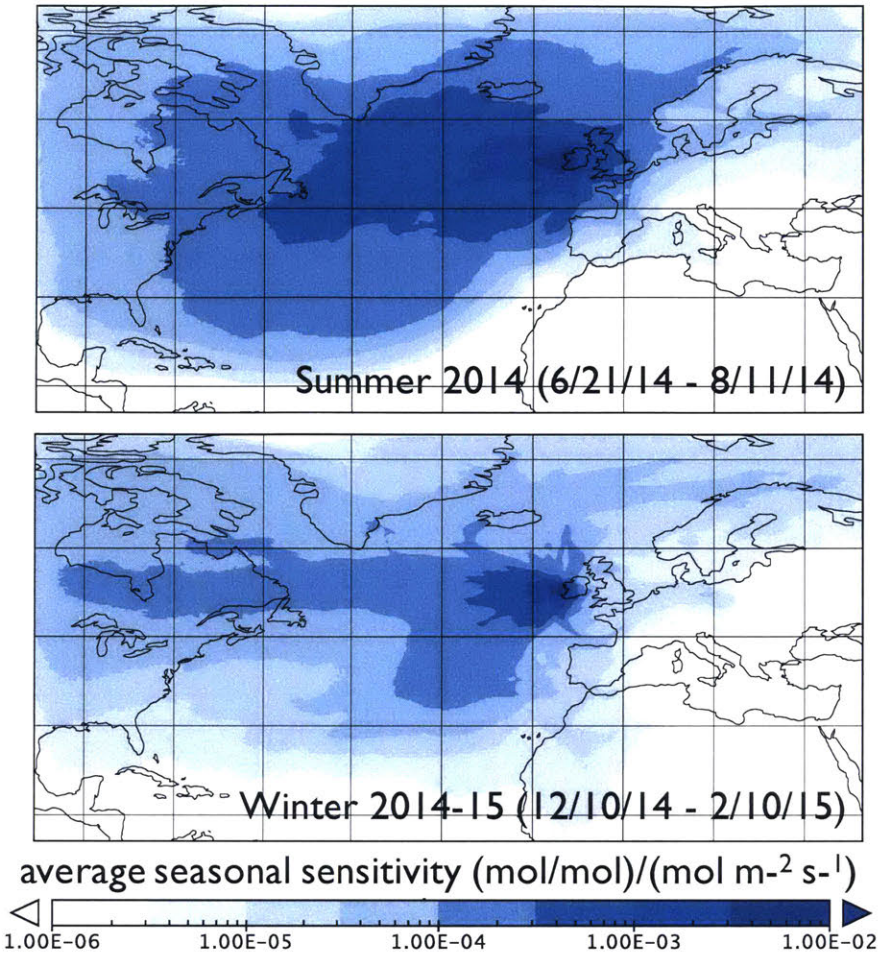

Figure 6-10: Average seasonal NAME surface sensitivity "footprints" at Mace Head for periods with Stheno-TILDAS observations during Summer (JJA) 2014 and Winter (DJF) 2014-2015

vector $\mathbf{x}$ being optimized, there will likely be a useful degree of uncertainty reduction in estimates of the five N_2O emission sectors being optimized in the inversion described in the following section.

6.3.2 Inversion by Emissions Sector

Addition of N_2O isotopic ratio observations to a NAME-MOZART inverse modeling framework can help constrain the emissions magnitudes of each of the five sectors that have the most significant impact on the N_2O isotopic environment at Mace Head. This particular inversion will compare the emissions estimates of the five N_2O emissions sectors described in Saikawa et al. (2014) for each three-month season in which Stheno-TILDAS observations were made (June-August 2014 and December-February 2014-2015). The total mass of N_2O

emitted from each sector in each month, and resulting uncertainties, will be compared among the prior estimate, an inversion using N_2O bulk mole fraction alone, and a combination of N_2O mole fraction and isotopic ratios. In addition, the N_2O isotopic ratio observations made using the P-QCLAS laser spectroscopy instrument at Dübendorf, Switzerland in 2014-2016 (Harris et al., 2017) can be added to further constrain the isotopic environment in continental Europe.

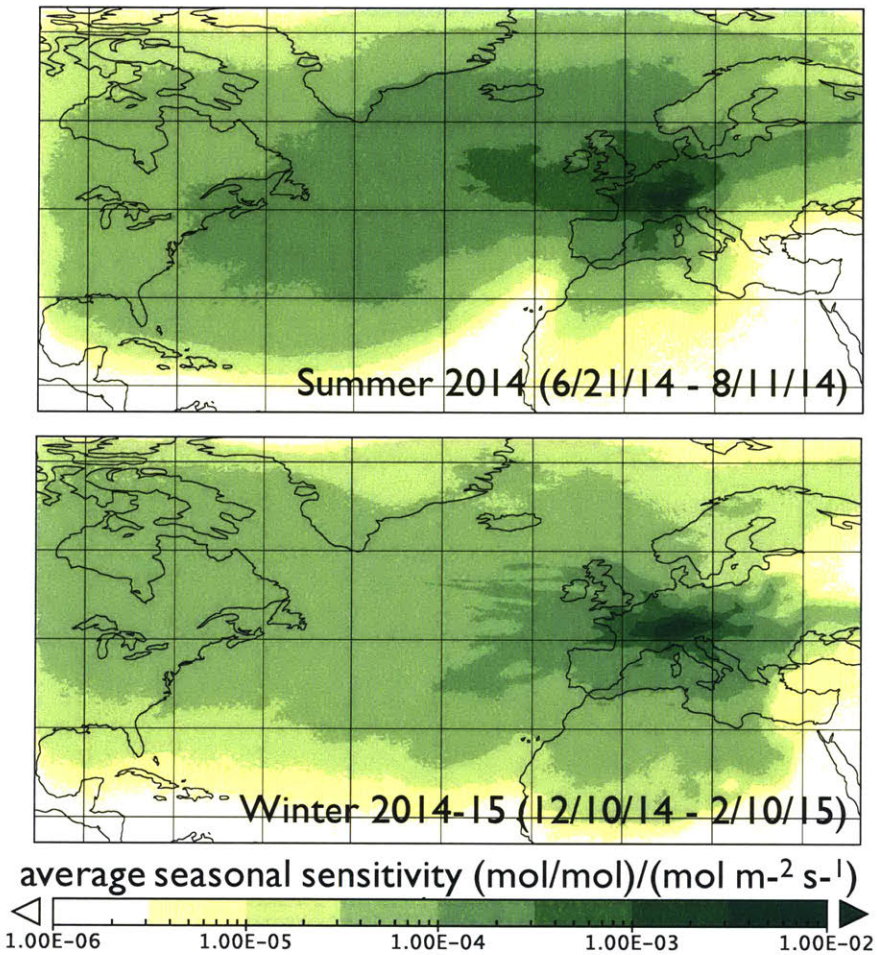

Figure 6-11: Average seasonal NAME surface sensitivity "footprints" at Dübendorf for periods concurrent with Stheno-TILDAS observations during Summer (JJA) 2014 and Winter (DJF) 2014-2015

As discussed above, the sensitivity of N_2O isotopic conditions at Mace Head (and, similarly, at Dübendorf) will not be high for emissions areas within the NAME Europe domain that are far from each station. Therefore, in addition to separating the prior estimates of N_2O emissions into five activity sectors, the prior emissions will be further divided into the continental Europe subregion and one combined rest-of-domain region consisting of the four long-range regions in Figure 6-7. This leads to a total of ten effective emissions sectors whose

magnitudes in summer 2014 and winter 2014-2015 will be optimized.

For the inversion using bulk N_2O mole fractions alone, the cost function **J** to be minimized (Figure 6-1) contains the following variables:

- n: number of GC-ECD observations used (1-hourly average)
- m: number of emissions sectors being perturbed in the two domains plus contribution from the boundary conditions (2*5+1=11)
- **y** (n x 1): mole fraction of N_2O at each time point
- **H** (n x m): sensitivity of N_2O mole fractions **y** to emissions **x**, created by perturbing each emissions sector by +/- 10 % and looking for linear response
- **x** (m x 1): emissions from each of the five sectors in the two domains plus contributions from the domain walls; trying to optimize this variable
- **R** (n x n): Combined uncertainty in data (measurements and model, as discussed pertaining to Equation 6.5 above), as diagonal on a sparse square matrix
- $\mathbf{x}_{prior}$ (m x 1): prior estimate of emissions from each sector
- **P** (m x m): Uncertainty in each emissions sector as a diagonal in a sparse square matrix, with the European (for land-based sources) or North Atlantic (for oceanic emissions) N_2O emissions uncertainties from 2008 in Saikawa et al. (2014) for each of the five Europe subregion sectors and with the North American (for land-based sources) or Atlantic (for oceanic emissions) N_2O emissions uncertainties from 2008 in Saikawa et al. (2014) for each of the five rest-of-domain sectors

For the inversion adding in N_2O isotopic ratios (either Stheno-TILDAS alone or Stheno-TILDAS plus P-QCLAS), the cost function **J** to be minimized (Figure 6-1) contains the following variables:

- n: number of observations used (1-hourly average)
- m: number of emissions sectors in the two domains being perturbed plus contribution from the boundary conditions (2*5+1=11)
- **y** ($4n$ x 1): mole fraction of N_2O and "raw" isotopic ratios (Figure 2-4) R_{456}, R_{546}, and R_{448} (vertically stacked, each with length n) at each observation time point
- **H** ($4n$ x m): sensitivity of observations (mole fraction and isotopic ratios) **y** to emissions **x**, created by perturbing each emissions sector by +/- 10 % and looking for linear response
- **x** (m x 1): emissions from each sector in the two domains plus contributions from the domain walls; trying to optimize this variable
- **R** ($4n$ x $4n$): Combined uncertainty in data (measurements and model, as discussed pertaining to Equation 6.5 above), as diagonal on a sparse square matrix

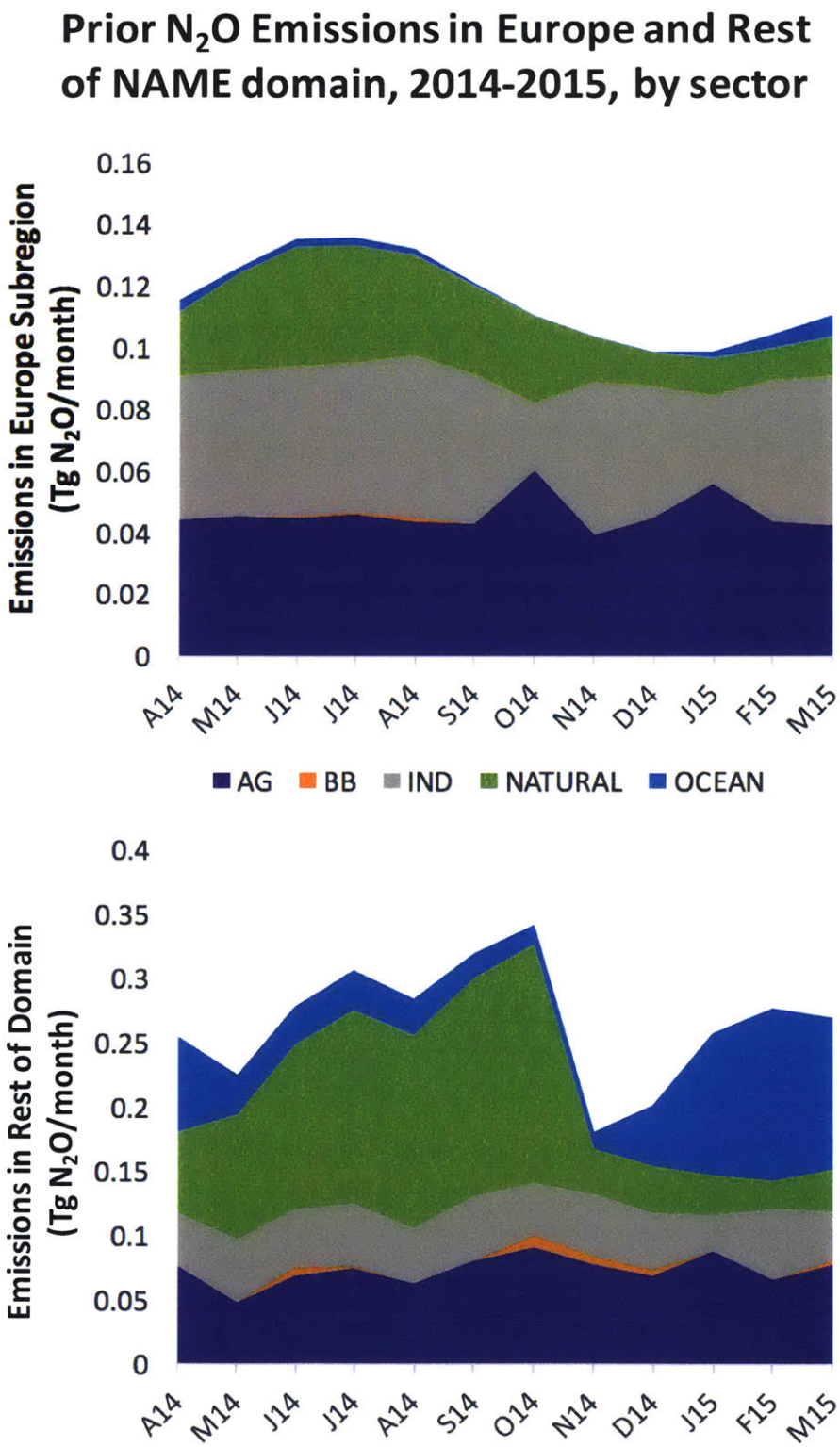

Figure 6-12: Prior emissions for inverse modeling within the NAME Europe domain from Figure 6-4, separated into the Europe subregion (top) and the rest-of-domain region (bottom)

- $\mathbf{x}_{prior}$ (m x 1): prior estimate of emissions from each sector
- $\mathbf{P}$ (m x m): Uncertainty in each emissions sector as a diagonal in a sparse square matrix, with the European (for land-based sources) or North Atlantic (for oceanic emissions) N_2O emissions uncertainties from 2008 in Saikawa et al. (2014) for each of the five Europe subregion sectors and with the North American (for land-based sources) or Atlantic (for oceanic emissions) N_2O emissions uncertainties from 2008 in Saikawa et al. (2014) for each of the five rest-of-domain sectors

Adding in the N_2O isotopic ratio observations leads to a significantly larger linear model matrix $\mathbf{H}$, and a corresponding increase in computational resources necessary to determine the optimal distribution of N_2O emissions by sector. However, in many month/sector combinations, the uncertainty in the emissions estimate is significantly decreased with the addition of N_2O isotopic ratio observations to the inversion.

Results

For each of the five N_2O emissions sectors, the total magnitude of emissions within the NAME Europe domain is optimized by using N_2O mole fraction alone (red features in the plots) and by using mole fraction and isotopic ratios (black features for Stheno-TILDAS alone; turquoise for Stheno-TILDAS plus P-QCLAS). In Figures 6-15 through 6-14, the two panels show the optimized emissions (including the prior estimate as blue features) with uncertainty as error bars, and a bar graph showing the magnitude of the uncertainty for each of the four cases (prior, bulk only, MHD Stheno-TILDAS, MHD plus DUB P-QCLAS). Each figure shows insights into the seasonality and overall magnitude of regional N_2O emissions trends, with some notable findings available only by adding in N_2O isotopic ratios to the inversion.

Natural soil: For natural soil N_2O emissions, the magnitude in the optimized emissions estimate is significantly lower in the European subregion and slightly enhanced in the rest-of-domain region (Figure 6-13). While the addition of N_2O isotopic ratio observations at Mace Head helps reduce the uncertainty in the Europe subregion, addition of P-QCLAS isotopic ratio data from Dübendorf does not further reduce the uncertainty in this sector. This is likely a reflection of the prevailing synoptic situation at Dübendorf and its urban location; as discussed in Harris et al. (2017), the emissions most often sampled at Dübendorf throughout the entire 2014-2016 P-QCLAS observation experiment are anthropogenic and from the immediate vicinity.

Ocean: Similar to the natural soil sector, the inversions indicate that the oceanic emissions within the Europe subregion (a small fraction of the total oceanic emissions in the entire NAME Europe domain) should be slightly reduced from the prior emissions, while the rest-of-domain emissions are modestly increased. In addition, the P-QCLAS observations at Dübendorf do not further reduce the uncertainty from the inversion using Stheno-TILDAS

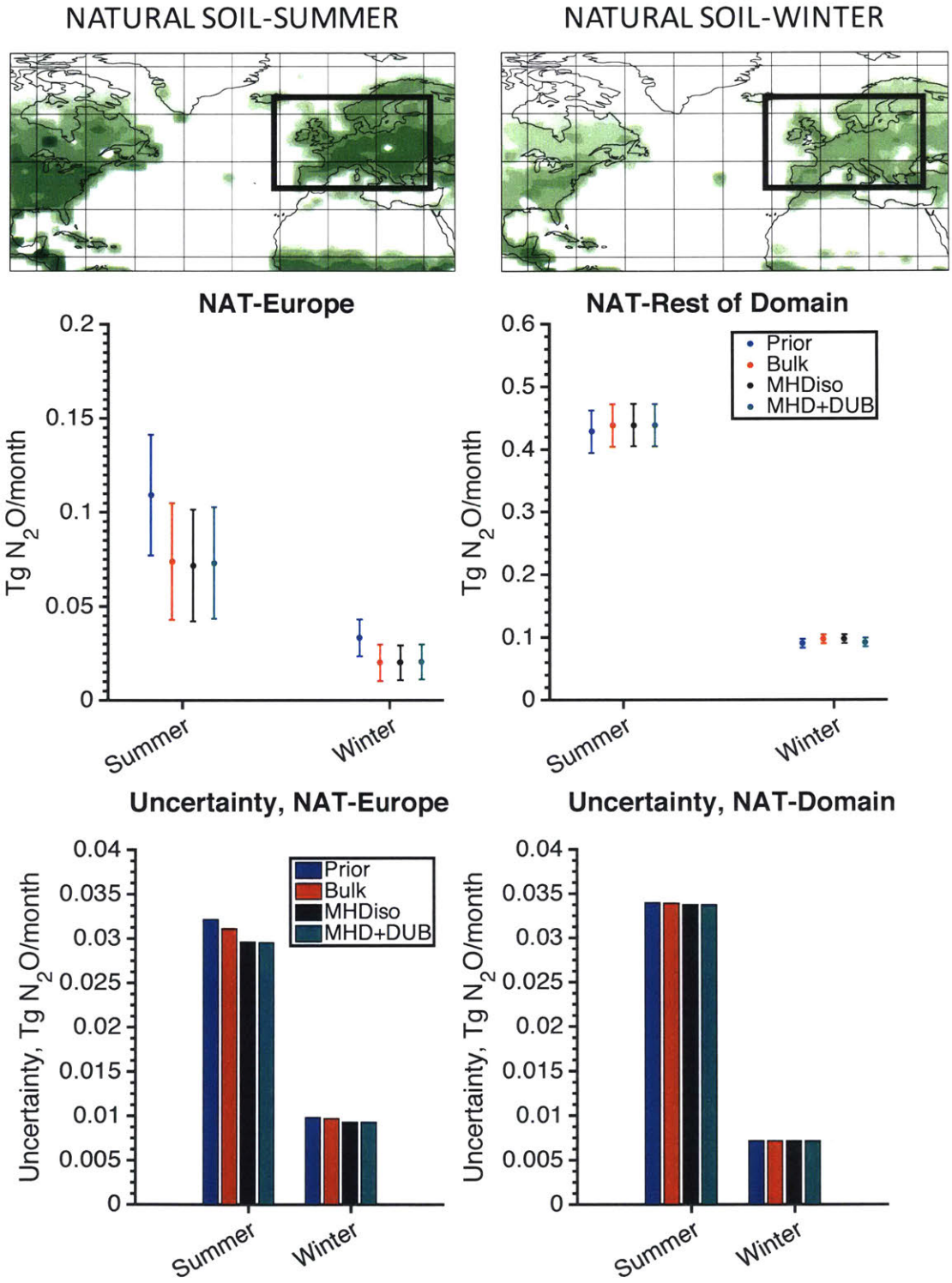

Figure 6-13: NAME-MOZART inverse modeling results in the two regions for natural soil emissions, with geographic distribution of prior emissions (top), changes in magnitude (center), and changes in uncertainty (bottom)

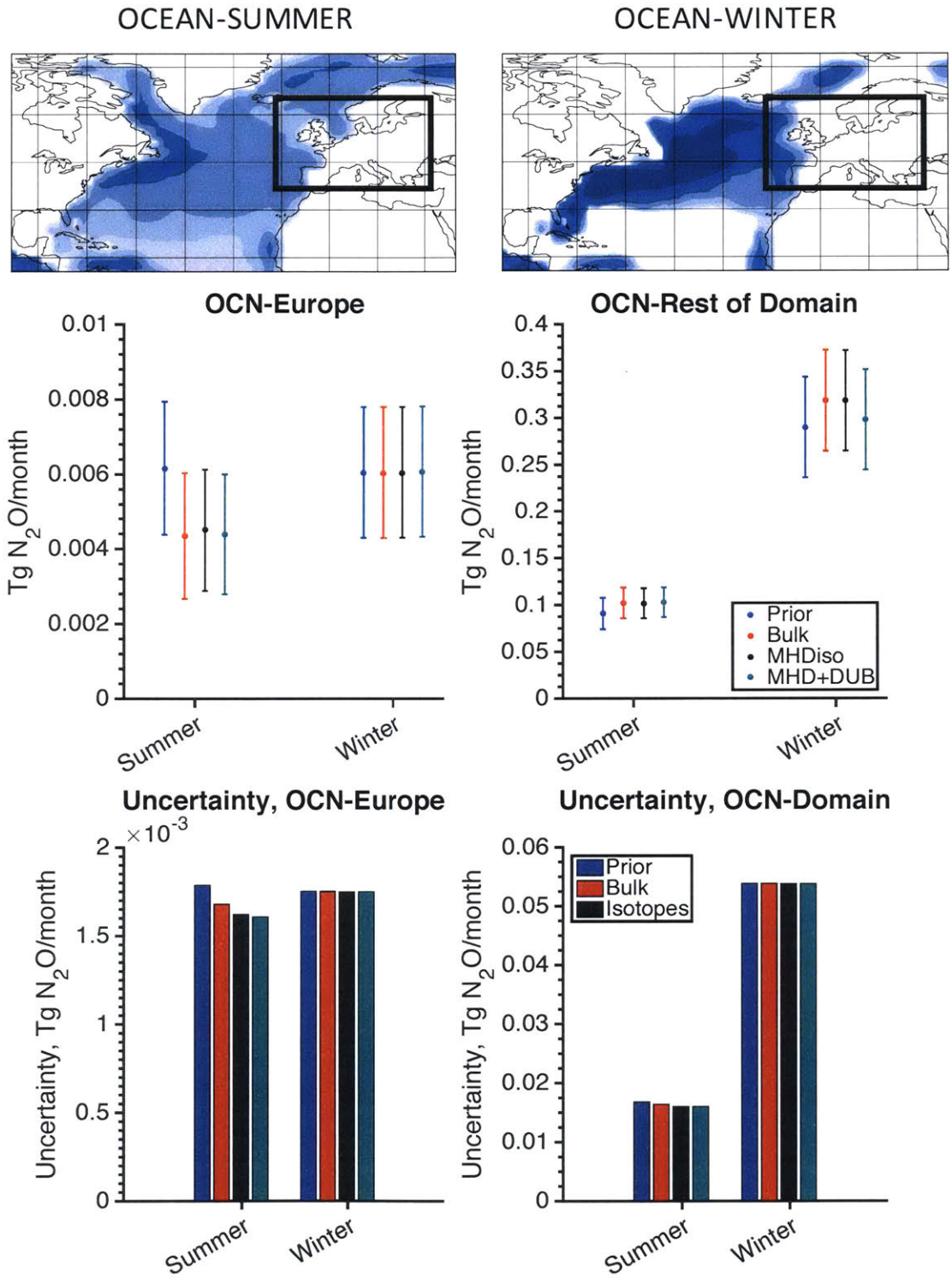

Figure 6-14: NAME-MOZART inverse modeling results in the two regions for oceanic emissions, with geographic distribution of prior emissions (top), changes in magnitude (center), and changes in uncertainty (bottom)

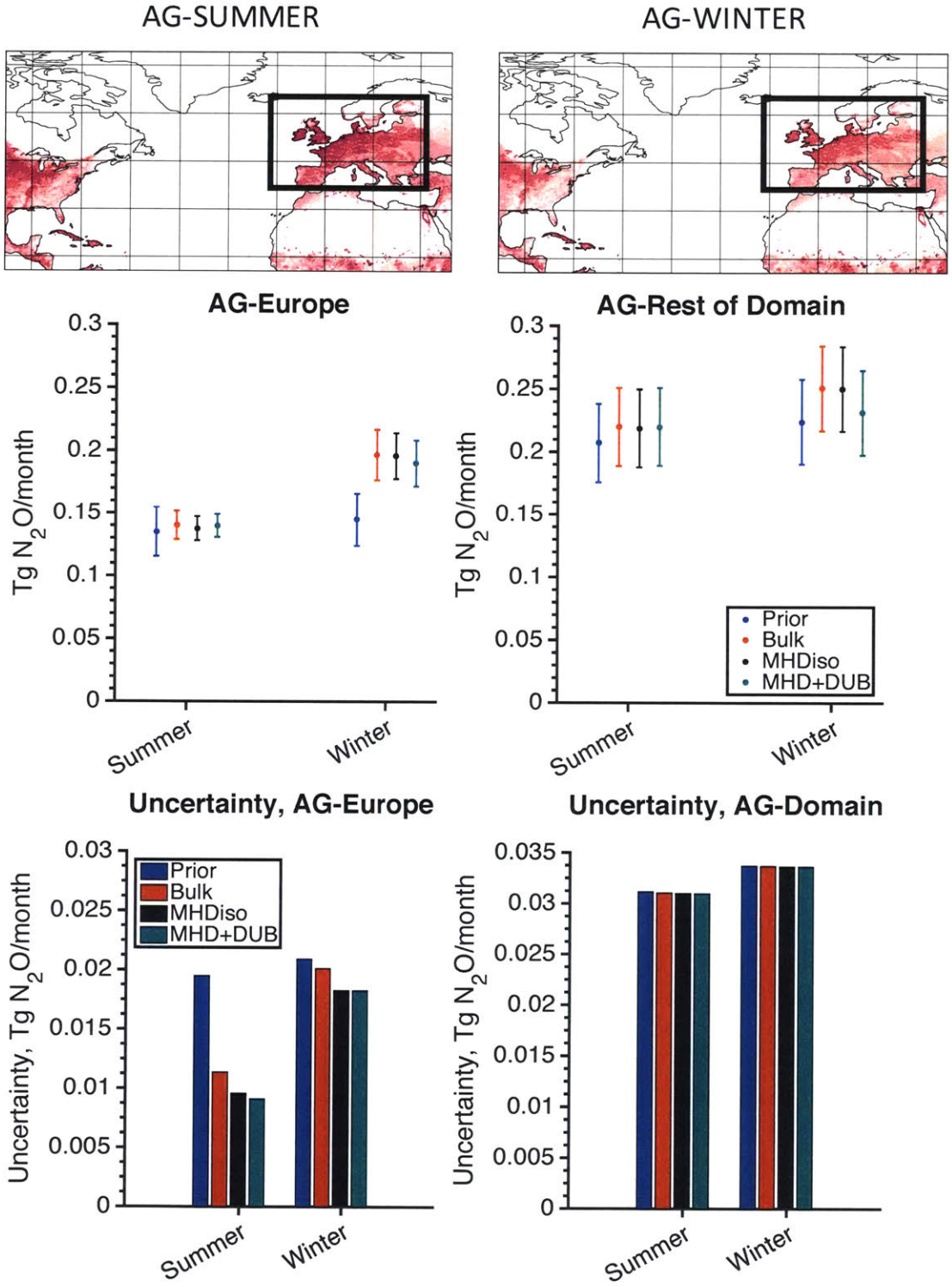

Figure 6-15: NAME-MOZART inverse modeling results in the two regions for agricultural emissions, with geographic distribution of prior emissions (top), changes in magnitude (center), and changes in uncertainty (bottom)

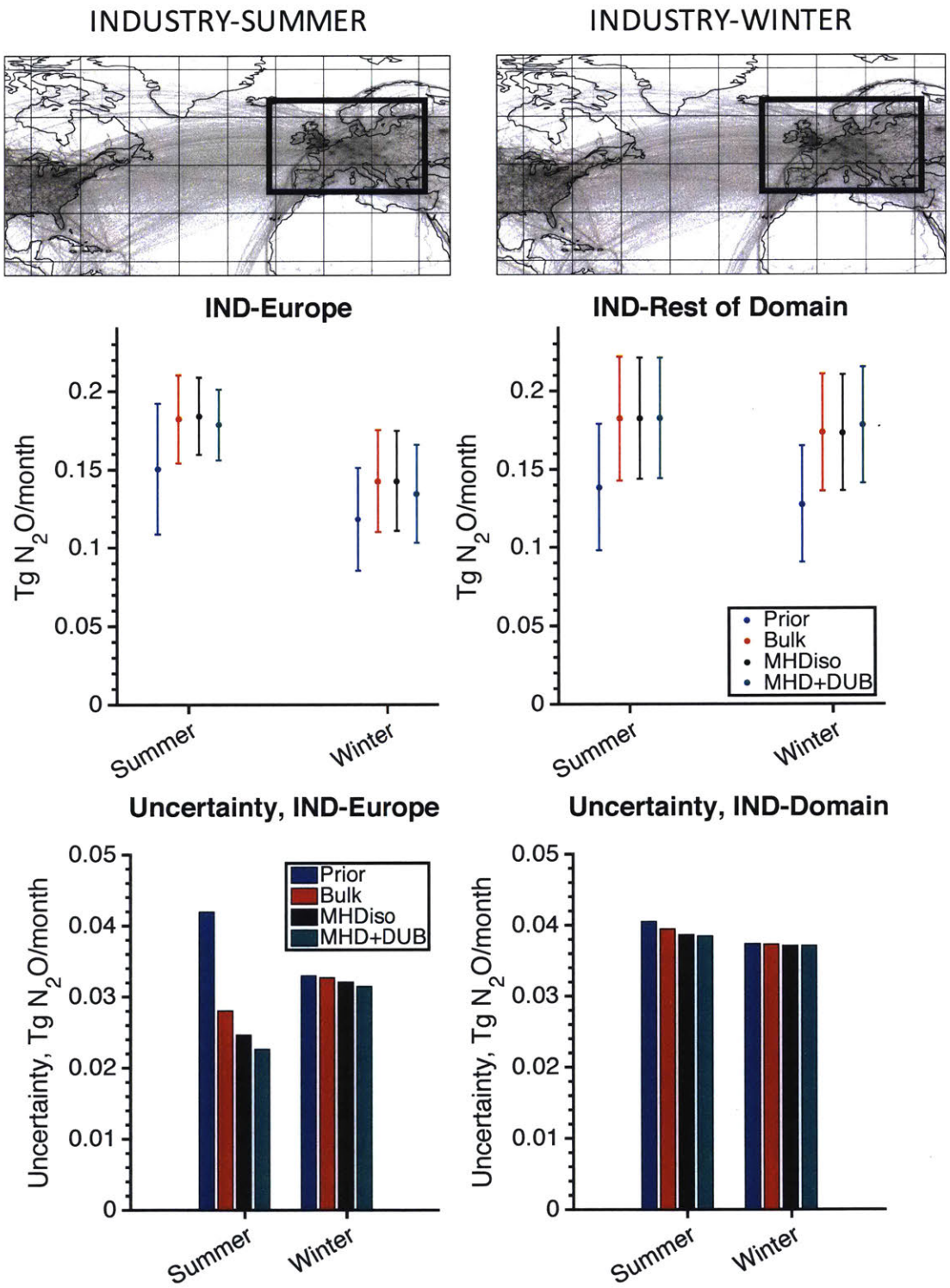

Figure 6-16: NAME-MOZART inverse modeling results in the two regions for industrial emissions, with geographic distribution of prior emissions (top), changes in magnitude (center), and changes in uncertainty (bottom)

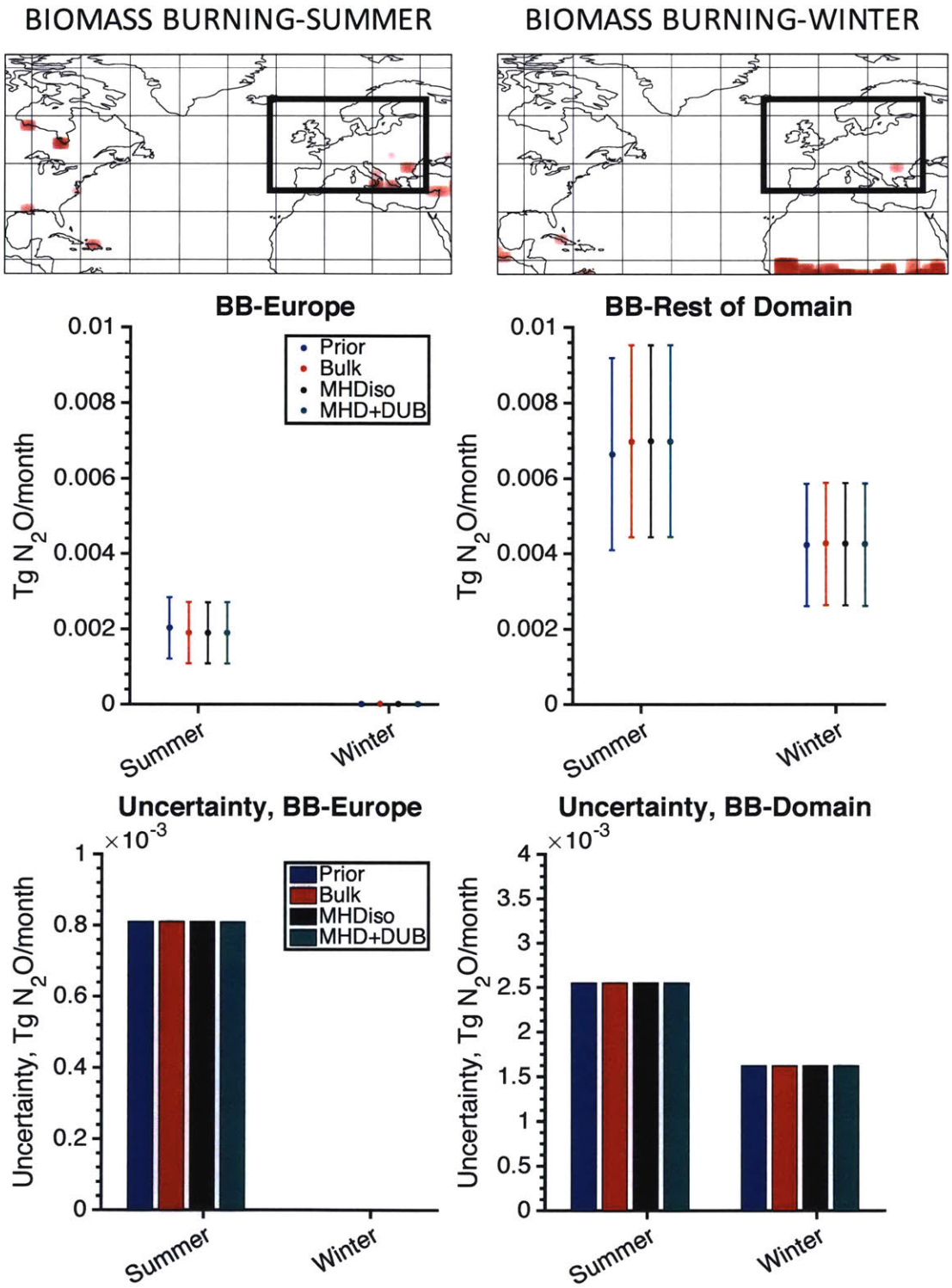

Figure 6-17: NAME-MOZART inverse modeling results in the two regions for biomass burning emissions, with geographic distribution of prior emissions (top), changes in magnitude (center), and changes in uncertainty (bottom)

observations alone, indicating once again that the emissions sampled at Dübendorf are significantly more local than those sampled at Mace Head (Figures 6-10 and 6-11). A complicating factor when optimizing oceanic N_2O emissions is that the *a priori* estimates combine emission from biotic activity in the ocean (likely occurring throughout the entire domain) and dissolution (also occurring throughout the entire domain). Separation of these phenomena, and only scaling the emissions while leaving unperturbed the physical uptake of gas-phase N_2O into water, would likely lead to better uncertainty reduction in the winter, where dissolution and emission are both enhanced. Further targeted experiments and ship-based observations could help differentiate between these competing processes affecting the N_2O earth system and the observations made at Mace Head and Dübendorf.

Agriculture: In summer, the optimized *a posteriori* emissions estimates for agriculture in the European subregion remain close to the prior estimates, as seen in the small variations in emissions magnitude for that season. However, in winter, all inversions point to a drastic underestimate of N_2O emissions from agricultural soil. The distinction between emission from actively growing agricultural regions and dormant previously-fertilized soil may be difficult to distinguish from regions where natural soil and agricultural soil have significant overlap; however, as seen in Figure 6-15, N_2O isotopic ratios for agricultural soil (significantly more depleted in both ^{15}N positions) can help differentiate these two sectors. For the agricultural N_2O emissions in the rest-of-domain region, there is almost no reduction in uncertainty due to the significant distance to the only other significant area of agricultural N_2O emissions in North America.

Industry: In both summer and winter, and in both the Europe subregion and in the rest of the NAME domain, industrial N_2O emissions are likely higher than those in the *a priori* estimate (Figure 6-16). For all four season/region combinations, there is a decrease in uncertainty as more observational data sources (bulk N_2O mole fraction, MHD isotopic ratios alone, both MHD and DUB isotopic ratios) are added. Due to the unique combination of the isotopic ratio signatures (Figure 2-6) that are most common in the various industrial N_2O sources (Table 6.1), there is the capability to greatly reduce the uncertainty in emissions estimates of this sector by adding in isotopic observations, especially from more than one site. While the reduction in uncertainty in the rest-of-domain region is more modest than for the Europe subdomain, as shown in Figure 6-10, the distant areas with the highest density of industrial N_2O sources (e.g. North America) are not highly sampled at Mace Head or Dübendorf during the two periods of interest.

Biomass burning: Compared to other N_2O emissions sectors, biomass burning represents a very small fraction of the overall N_2O emitted within the NAME Europe domain (as seen in the y-axis scales of Figure 6-17). In addition, largely due to the low sensitivity of observations at Mace Head and Dübendorf to biomass burning emissions, there is virtually no decrease in uncertainty when isotopic ratios are added into the inversion.

Overall, each of the five N_2O sectors have unique characteristics (spatial distribution and N_2O isotopic signatures) that allow for improvement in emissions estimates when bulk

N_2O mole fractions and isotopic ratios from two sites are added to a NAME-MOZART inverse modeling framework. Longer observation campaigns will allow for better constraints in other parts of the year, and observations at additional locations will help address the limitations of long-term sampling at stations (Mace Head and Dübendorf) that are not highly sensitive to emissions changes in all parts of the NAME model domain.

6.4 Future Improvements to Inverse Modeling

When comparing the Stheno-TILDAS and GC-ECD observations of N_2O isotopic ratios (Figure 3-7) to NAME-MOZART simulations, the model runs using *a posteriori* optimized emissions estimates for the five sectors feature slightly closer alignment to the observed conditions than those using *a priori* emissions estimates, as shown by the decreased magnitude of the residuals in Figure 6-18.

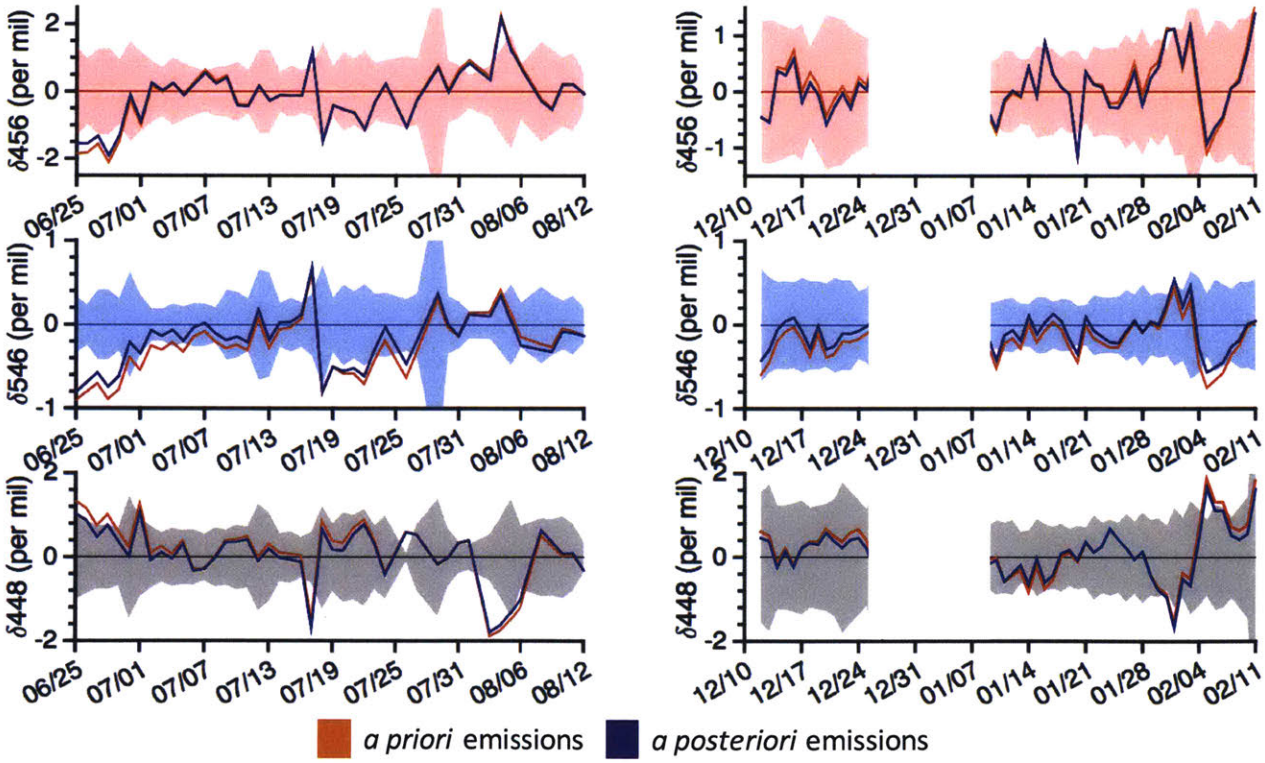

Figure 6-18: Timeline of residual (simulated-observed) between Stheno-TILDAS N_2O isotopic ratio observations and NAME-MOZART simulations (orange representing simulation with *a priori* emissions estimates and purple representing simulation with *a posteriori* emissions estimates), with Stheno-TILDAS observation uncertainty in shown in shading (as in Figure 3-7)

The small magnitude of the improvements in measurement-model alignment given the optimized emissions estimates indicate that there remain many opportunities to further improve the NAME-MOZART model setup introduced in this chapter. In general, the simulated isotopic ratios remain relatively flat near a stable long-term mean, as seen in the simulated isotopic ratios from Harris et al. (2017). The dominance of this long-term trend, on which small-magnitude features exist, shows that there remain many challenges in accurately simulating the dynamics of atmospheric N_2O isotopic ratios seen in observations.

One way to improve future optimized sector-specific N_2O emissions sets using NAME-MOZART is to reduce the uncertainty in the observational and model-based uncertainty σ that constitutes the diagonal of the square matrix $\mathbf{R}$ used in the inverse method described above (Figure 6-1). The relative contribution of the four factors σ for the two periods of Stheno-TILDAS data coverage (Figure 6-19) indicate that the two major contributors to $\mathbf{R}$ for simulations including N_2O isotopic ratios are the repeatability of Stheno-TILDAS observations (σ_M) and the uncertainty in the isotopic signatures associated with each source sector (σ_{SIR}).

The patterns in Figure 6-19 indicate that the relative contributions from σ_{SIR} are lower in the winter than in the summer. This can likely be explained by the significantly diminished magnitude of natural soil and industrial emissions, the two major sectors with the largest uncertainties in their site-specific isotopic signatures, in the winter season (Figures 6-13 and 6-16).

In order to further reduce σ_M, further refinement of the instrumental procedure used in the field will be necessary. Development of a set of standard gases that span a large range of N_2O isotopic ratios in all three isotopic positions can lead to a reliably robust two-point calibration for all expected conditions in the course of an observational campaign. The uncertainty in the Stheno-TILDAS N_2O isotopic ratio observations made at Mace Head was greater in all three isotopic ratios than the lab-based observations conducted in the testing phase of the instrument (Harris et al., 2014), indicating that improvement is possible from the performance of the instrument in its first field campaign. In order to further reduce σ_{SIR}, targeted field-based observations and lab-based experiments will be necessary to better understand the mean values and variability of isotopic signatures for various major N_2O sources.

In general, however, the narrow range of N_2O isotopic ratios that are sampled by the NAME-MOZART simulations, even with the optimized five-sector emissions estimates (Figures 6-13 through 6-17), indicate that some aspects of the NAME-MOZART modeling process not explicitly captured in the inverse modeling cost function (Figure 6-1) could stand to be improved. Given the lack of long-term N_2O isotopic ratio observations at various latitudes and altitudes, the MOZART component of the joint model may require improvements (such as finer spatial resolution in surface emissions) to better capture spatial and temporal dynamics in the model domain boundaries used by the NAME-based component of the experiment. While this shortcoming does not indicate that the method developed in Rigby

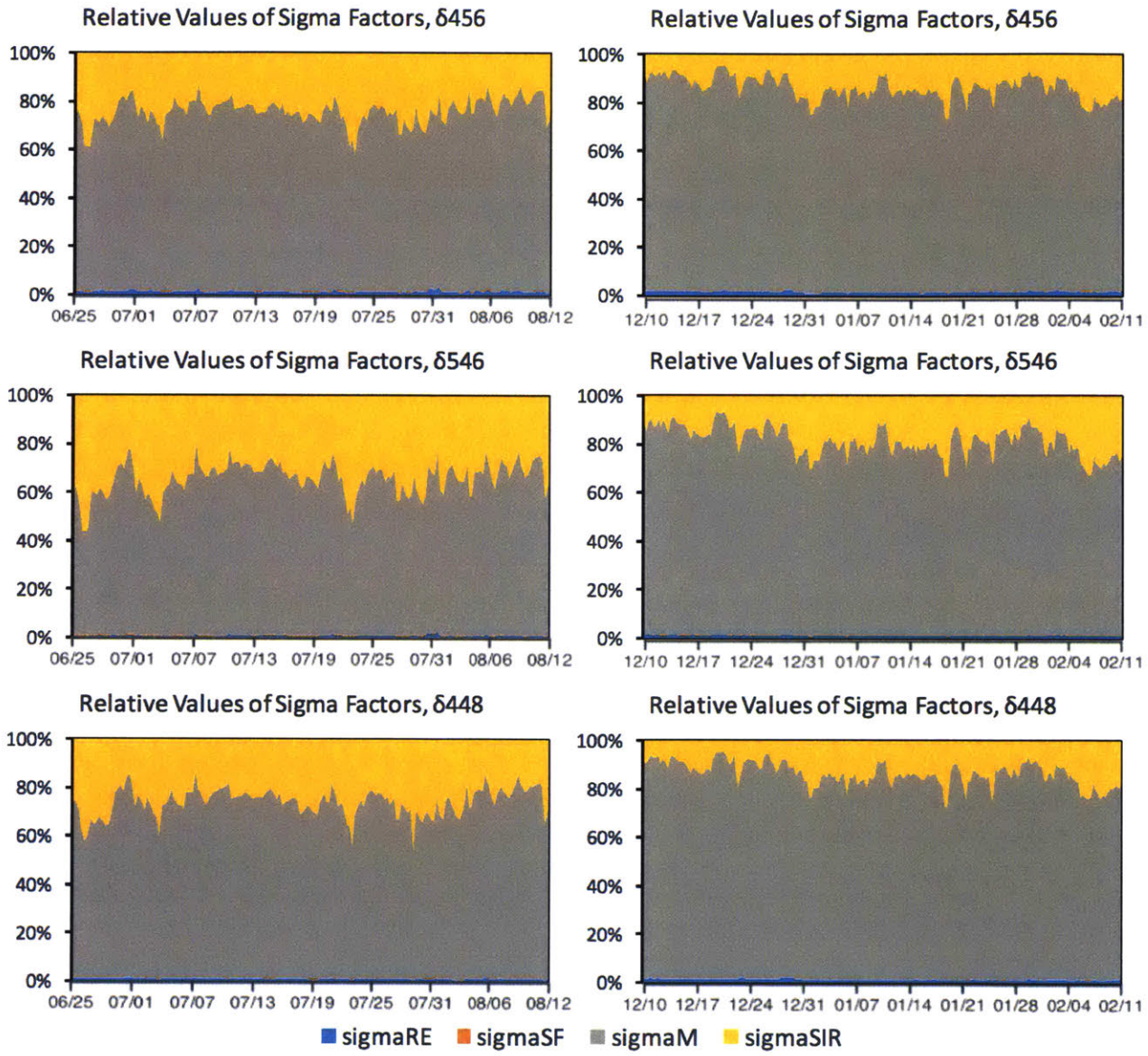

Figure 6-19: Relative contribution to σ^2 from the four factors σ_M, σ_{RE}, σ_{SF}, and σ_{SIR} for the three N_2O isotopic ratios

et al. (2012) is flawed for application to N_2O, the complexity of modeling three isotopic ratios with five largely overlapping isotopic signatures (as opposed to two isotopic ratios with four largely distinct isotopic signatures for CH_4 as in Rigby et al. (2012)) introduces new challenges not fully explored for a similar analysis of CH_4 isotopic ratios. Further high-resolution global modeling of N_2O isotopic ratios, combined with new global observations to validate the model setup in areas far from Mace Head, will potentially lead to more realistic model "boundary walls" that represent contribution by long-range transport to conditions observed at the station in the combined NAME-MOZART framework.

6.5 Summary

The NAME-MOZART inverse modeling experiments introduced in this chapter strongly validate the use of the approach proposed in Rigby et al. (2012) for actual N_2O isotopic observations. This framework, combining global three-dimensional model simulations of N_2O mole fraction and isotopic ratios (MOZART) with a Lagrangian particle dispersion model that can estimate the impact of local and regional European N_2O emissions on conditions observed at a single location (NAME), largely reproduces the N_2O mole fraction timelines observed at Mace Head, Ireland. This NAME-MOZART framework, with N_2O isotopic chemistry implemented as described in Chapters 5 and 6, can reproduce the long-term mean of N_2O isotopic ratios observed using the Stheno-TILDAS instrument at Mace Head but has opportunities for improvement in reproducing the short-term excursions and seasonal trends in N_2O source apportionment explored in Chapter 4.

Inverse modeling using the five-sector emissions estimates from Saikawa et al. (2014) linearly extrapolated to 2014-2015 as an *a priori* emissions set (x_{prior}) leads to improved *a posteriori* emissions estimates for each of the five sectors in summer 2014 and winter 2014-2015 with significant uncertainty reduction for European summertime emissions from four sectors (natural soil, ocean, industry, and agriculture) and modest to marginal uncertainty reduction in the remaining sectors and seasons. The optimized sector-specific emissions estimates from NAME-MOZART lead to better alignment between modeled and observed N_2O mole fractions and isotopic ratios; however, the *a posteriori* simulated N_2O isotopic ratios still do not replicate the magnitude of short-term trends seen in the observations.

More extensive Stheno-TILDAS observation campaigns will only further improve the inverse model results by reducing uncertainty in emissions estimates further than is possible using bulk N_2O mole fraction measurements alone. Additional global observations at varying latitudes and altitudes will help inform changes in the global modeling of N_2O isotopic ratios that will undoubtedly impact the contribution from "long-range transport" in the NAME-MOZART framework used in this chapter.

Chapter 7

Conclusions and Future Work

As shown in this thesis, there is great benefit in conducting long-term high-frequency nitrous oxide (N_2O) isotopic ratio observations in Europe, and by inference, in multiple locations around the world. Observations such as those conducted by the new Stheno-TILDAS instrument (Chapter 3) can alone help constrain our understanding of N_2O sources (Chapter 4), can be used as a benchmark for global chemical transport model performance in reproducing the isotopic features of the N_2O earth system (Chapter 5), and can be used as an input in Bayesian inverse modeling to constrain estimates of N_2O emissions in the regions near observation sites (Chapter 6). Each of these components of the comprehensive experiment described in this thesis have natural opportunities for extension in order to gain a more precise understanding of all aspects of the N_2O earth system.

7.1 Conclusions

The advances introduced in this thesis can be discussed in terms of directly advancing the work of five different recent experiments, the extensions of which are combined to provide new insights into global trends in N_2O emissions.

Chapter 3 expands on the development and initial testing of the Stheno-TILDAS instrument (Harris et al., 2014) by showing the ability of this new laser spectroscopy-based analytical instrument to produce high-frequency observations of site-specific N_2O isotopic ratios in the field. There were limitations to the Stheno-TILDAS experimental setup at the Mace Head, Ireland field site stemming from a difference in the standard gases available and leading to reduced precision in the isotopic ratio observations in 2014-2015; in addition, the failure of a few critical components in the Stheno preconcentration system led to large gaps in the N_2O isotopic ratio data coverage (notably, September-December 2014). This initial field campaign at Mace Head, however, provided crucial information about how to modify the Stheno-TILDAS instrument further in subsequent field campaigns for better reliability

and precision. Continued partnership with other laboratories and institutes to develop global standards for calibration and data reporting (Mohn et al., 2014) will further the overarching goal discussed within this thesis of using all available N_2O isotopic ratio observations to improve global and regional estimates of N_2O emissions.

Chapter 4 uses many of the general approaches for analyzing N_2O isotopic ratio observations introduced in Potter (2011) for the GC-CFIRMS instrument and Harris et al. (2017) for the P-QCLAS instrument, expanded through use of the NAME Lagrangian particle dispersion model. Addition of NAME model runs in the Europe domain provides statistical evidence to support the initial conclusions from event-based qualitative methods for apportioning contributions from various N_2O emissions sectors using observations at Mace Head. Co-located contemporaneous observations of mole fractions of other anthropogenic and natural trace gases (such as CO, CH_4, and $CHBr_3$) are shown, when combined with trends in all three N_2O isotopic ratios measured using Stheno-TILDAS, to largely explain individual events in which the atmospheric conditions at Mace Head are anomalously influenced by a particular N_2O source sector or by well-mixed "background air" transported to the station from great distances. These classifications can then be compared to the statistical surface sensitivity "footprint" maps produced by NAME to support apportionment of particular source sectors (when the footprints show high density in particular geographic areas within the domain) or well-mixed background air (when the footprints show high density on the model domain boundary walls). Similar methods, in which mole fraction observations of N_2O were combined with NAME footprints (Manning et al., 2011) have previously been shown to help explain the origin of atmospheric N_2O observed at Mace Head; the addition of other trace gases and isotopic ratio observations allow the methods used in this thesis to support and expand upon the findings of previous examinations of European N_2O emissions (Potter, 2011; Harris et al., 2014; Manning et al., 2011).

Chapter 5 uses the model environment developed for MOZART-4 for inverse modeling of global N_2O emissions by Eri Saikawa (Saikawa et al., 2014), extending that experiment to produce three-dimensional simulations of N_2O mole fractions through the end of 2015. In addition, this chapter shows that MOZART-4 can be used to simulate global distributions of N_2O isotopic ratios by implementing the results from controlled laboratory experiments on photolytic and chemical destruction kinetics of N_2O isotopologues into the chemical drivers within MOZART-4 used by Saikawa et al. (2014). By combining the optimized emissions (Saikawa et al., 2014) from the five major N_2O emission sectors (agriculture, biomass burning, industry, natural soil, ocean) with site-specific isotopic signatures (Potter, 2011) for the five sectors, new isotopically-differentiated surface fluxes are created that can be used in MOZART-4. Addition of isotopic chemistry into the emission and destruction processes of MOZART-4 leads to simulated global distributions of N_2O isotopic ratios that more closely match observed conditions at the surface than recent results from other global chemical transport model experiments (such as Bernath et al. (2017)). Future N_2O isotopic chemical transport model experiments featuring finer spatial resolution and improved source-specific isotopic signatures will have the potential to more closely recreate the seasonal and short-

term excursions and features seen in the Stheno-TILDAS timeline from Mace Head (Figure 3-7).

Chapter 6 uses all of the new findings discussed above in the framework proposed by Rigby et al. (2012) for inverse modeling of CH_4 emissions using hypothetical isotopically-differentiated observations and a chemical transport model. By combining the observations discussed in Chapter 3, the NAME surface sensitivity "footprints" introduced in Chapter 4, and the results from the MOZART-4 global chemical transport model runs described in Chapter 5, the resulting NAME-MOZART framework helps reduce the uncertainty in the *a priori* five-sector emissions estimates created by linearly extrapolating to 2015 the optimized estimates from Saikawa et al. (2014). Notably, the inclusion of N_2O isotopic ratio observations from Dübendorf, Switzerland (Harris et al., 2017) into the inverse framework already containing Stheno-TILDAS observations from Mace Head leads to decrease in uncertainty in European summertime N_2O emissions in the four largest N_2O emissions sectors (natural soil, ocean, industry, and agriculture). Future NAME-MOZART inverse modeling experiments will focus on improvement of simulating "well-mixed background" air from outside the continental subregion within the NAME Europe domain.

In isolation, each of the chapters discussed above provides new data or validates approaches related to one of three major questions related to the isotopic chemistry of atmospheric N_2O: how to measure ambient N_2O isotopic ratios, how N_2O source dynamics affect the local and regional isotopic environment, and how global distributions of N_2O isotopic ratios are changing. When combined, the experiments discussed in the preceding chapters help increase our understanding of the changing magnitudes of various N_2O emissions sectors in the European region. Future experiments expanding on the work presented in this thesis, discussed below, will further increase the ability of such a combined observation-model framework to constrain global N_2O emissions estimates.

7.2 Future Work

All future work outlined in this section will ultimately improve some aspect of the Bayesian inverse modeling from Chapter 6 in order to more precisely constrain estimates of N_2O emissions. Targeted measurements from new Stheno-TILDAS experiments, improvements to global CTM runs, and more comprehensive input data sets for MOZART and NAME can all be included in a new Bayesian inverse estimation experiment (Figure 7-1) encompassing the **global** N_2O earth system in addition to regional experiments (such as for Europe; Chapter 6).

7.2.1 Observations

Stheno-TILDAS can be used in three modes, each of which can be used in a larger experimental framework: online, *in situ* pre-concentration and analysis of ambient air in one location every ~30 minutes; offline flask analysis in which flasks are filled in many global locations with daily, weekly, or monthly frequency; and direct analysis of highly concentrated N_2O samples, such as standard gases created in a laboratory or from enclosures of controlled microbial experiments. This section will briefly describe potential expanded experiments involving each of these Stheno-TILDAS modes.

Flask Network

The major advantage of the Stheno-TILDAS instrument is the ability to produce high-frequency *in situ* measurements of ambient N_2O isotopic ratios. However, due to the number of unused inlet ports on the front of the Stheno pre-concentration system (Figure 3-4), flasks containing air from other locations could be sampled alongside *in situ* ambient air, or in a dedicated flask-only mode that could sample as many as four different flasks in series. Any new flask analysis experiment would expand the spatial coverage of N_2O isotopic ratio measurements without sacrificing the high-frequency operation of Stheno-TILDAS at one location.

A number of global sites could serve as flask sampling locations. The AGAGE network stations shown in Figure 1-8 would be ideal due to the co-location of high-frequency trace gas concentration measurements with Medusa, GC-ECD, and Picarro instruments (Prinn et al., 2000, 2018). In addition, sampling sites in the NOAA-ESRL-GMD measurement network could be considered due to their relatively high frequency and operational support by NOAA staff. Short-term flask sampling campaigns are also possible; field campaigns, such as those run AGAGE collaborators, could easily add a flask sampling setup with little additional work or cost.

Although flasks will lose the time resolution inherent in real-time *in situ* measurement using Stheno-TILDAS, the advantage gained by adding a flask sampling component to this experiment will be invaluable in apportioning isotopically-differentiated N_2O emissions in areas far from the future location of Stheno-TILDAS. This is made clear in the difference between high-frequency and flask-based synthetic "pseudodata" observations of CH_4 isotopic ratios in constraining CH_4 emissions estimates, as conducted by Rigby et al. (2012).

High-Altitude Samples

Stheno-TILDAS measurements and flask sampling events occur at or near Earth's surface. Although there are few N_2O isotopic ratio observations made at the surface, even fewer exist in high-altitude regions where chemistry and transport of N_2O are more important for

describing the local N_2O isotopic environment and are much less constrained. While high-frequency high-altitude measurements would pose a considerable experimental challenge, a small number of flasks collected at various altitudes and latitudes could give crucial insight into the isotopic N_2O dynamics in well-mixed "background" environments. These measurements will immediately improve the verisimilitude of CTM initial conditions of N_2O isotope ratios.

A flask-sampling component could be added to any existing high-altitude measurement campaigns such as those by the group of Dr. Jim Elkins at NOAA ESRL, or similar projects with collaborators at NASA GSFC. The modeled N_2O transport dynamics would be greatly improved by adding these flask measurements, and collection of flasks would come with minimal interruption to the operation of the collaborating campaign. Stheno-TILDAS and similar instruments would not be flight-ready, necessitating the need for flasks rather than making high-altitude online *in situ* N_2O isotopic observations.

A number of open-source tools, such as the Community Intercomparison Suite (cis-tools.net; CIS (2018)) written for Python, can be used to determine expected along-track observations for a flight campaign given various types of input data: three-dimensional chemical transport model output, two-dimensional and column-based satellite retrievals, and many more source types (see Appendix A for examples of CIS in use for a NASA flight campaign experiment in West Africa).

Investigation of Source Isotopic Signatures

Current estimates on the ranges of N_2O isotopic variation in emissions sources are poorly constrained, with disparate source types combined under large categories (e.g. all soil sources in purple in Figure 2-6 and exclusion of natural N_2O sources from EDGAR inventories). Collection of concentrated *in situ* and laboratory-based N_2O samples from distinct sources, alongside current sampling from oceanic N_2O sources conducted by Andrew Babbin at MIT (Babbin et al., 2015) and agricultural methane sources conducted by Shuhei Ono at MIT (Wang et al., 2015), could potentially lead to more distinct source types in the list of N_2O isotopic signatures (Figure 2-6), but with significantly more precise understanding of all constituent sources in each cluster.

In addition, combined measurement-modeling studies on relationships between variables such as soil moisture (using NASA Landsat, GPM, TRMM, and Aqua satellite data) and microbial N_2O activity could lead to fine-resolution relationships between surface conditions and N_2O source dynamics even where the isotopic signatures cannot be measured directly. This type of experiment has the potential to determine the variables that drive potential seasonality and spatial heterogeneity of N_2O isotopic signatures from the same source types (Appendix B).

7.2.2 Global Forward Modeling

The forward modeling experiments in Chapter 5 using the MOZART-4 chemical transport model have many opportunities for improvement to more accurately model actual global atmospheric conditions. In addition to improving the input data sets used in the model, as described in the previous section, the model itself could be improved going forward by taking advantage of recent chemical transport modeling advances.

NCAR CESM

As discussed in Chapter 5, challenges unexpectedly arose in obtaining MERRA meteorological reanalysis data sets for use with MOZART-4 concurrent with Stheno-TILDAS observations. This is unfortunately not surprising in hindsight due to the the discontinuation of official support by NCAR for MOZART-4, which has been subsumed into the larger NCAR Community Earth System Model (CESM). While MOZART has nearly all of the features necessary to conduct the modeling experiments in this thesis, new modeling frameworks with additional features could ensure long-term viability of N_2O modeling experiments that expand on the work presented in Chapter 5.

Potential alternative models include NCAR CESM (which currently uses MOZART source code to drive its atmospheric chemistry), GEOS-CHEM, WRF-CHEM, and others. Alternatively, existing reanalysis data sets could be modified to meet the parameters necessary to run MOZART; however, this plan carries the potential risk of creating nonphysical meteorological conditions in processing and re-gridding the new meteorological data. In any case, future use of CESM would require the fewest number of fundamental changes due to the shared source code between CESM and MOZART-4; in addition, the future versions of CESM will have features enabling native modeling of isotopic chemistry (personal communication with NCAR staff at the 2017 CESM summer tutorial) without the need for major adjustments outlined in Chapter 5.

7.2.3 Global Inverse Modeling

The regional inverse modeling experiment described in Chapter 6 is able to provide insights into the N_2O source environment within the NAME Europe domain, but observations from Stheno-TILDAS at Mace Head and other sites (e.g. P-QCLAS at Dübendorf, Switzerland) cannot, alone, do much to constrain N_2O emissions estimates outside the region. Developing a global Bayesian inverse framework that uses N_2O isotopic ratio observations to constrain emissions estimates will require, at minimum, a handful of additional observation sites. In addition, improving the uncertainty in input data sets such as isotopic source signatures will subsequently reduce uncertainty in the optimized *a posteriori* N_2O emissions estimates produced by an inverse framework such as that described in Figure 7-1.

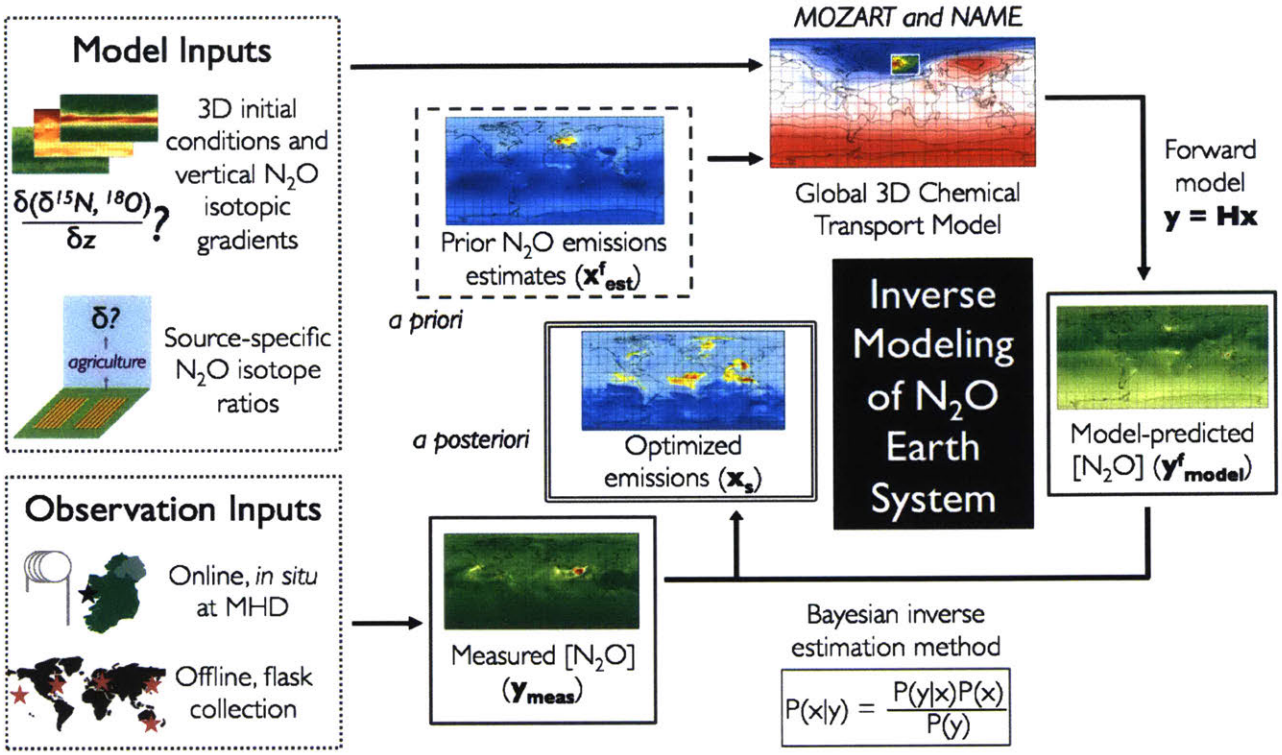

Figure 7-1: Schematic of Bayesian inverse modeling methodology, including measured concentrations, modeled concentrations, an *a priori* emissions estimate, and an optimized *a posteriori* emissions estimate

When isotopically differentiated N_2O data from Stheno-TILDAS field missions and flask samples are included in new modeling experiments, the magnitude of individual natural and anthropogenic N_2O sources could be much more constrained than at present. Accurate apportionment can lead to identification of novel/emerging sources and potential strategies for abatement of non-critical N_2O-emitting processes. A thorough understanding of N_2O budgets can inform policy in areas ranging from food security to global climate due to the indelible role of N_2O in many modern areas of life. Due to its ascendance as an increasingly important greenhouse and ozone-depleting gas in Earth's atmosphere, all phases of the N_2O budget must be studied further in order to understand its role in the changing global Earth system. A combined experiment using powerful analytical (Stheno-TILDAS) and computational (MOZART, NAME, and MOZART-NAME) tools is well-posed to contribute greatly to the understanding of the global effects of atmospheric N_2O and its rapidly changing emissions profile.

7.3 Closing Thoughts

This thesis introduces experimental work whose expanded potential future results have the capacity to advance human knowledge of the nitrogen cycle and greenhouse gas emissions, to lead to potential environmental changes that could abate N_2O emissions, and to improve the lives of those who may be affected by the potential damage to Earth's climate due to shifts in the radiative balance of the Earth system. In addition, further investigation of N_2O dynamics will directly improve understanding of changes in Earth's radiative balance and the ozone layer (due to the rapid destruction of ozone by nitric oxides produced from stratospheric N_2O). Once more-precise source-specific N_2O emissions maps are created, the inverse modeling experiments continuing from the work in this thesis will have utility in development of public policy that could reform industrial and agricultural processes and behaviors in order to produce far less N_2O.

The global monitoring component of the Stheno-TILDAS experiment already represents a new area of research for the AGAGE network, namely high-frequency isotopic measurements and their interpretation. Expansion of N_2O isotopic observation in the AGAGE network will improve the quality of the observational data used in experiments described in this thesis, greatly expanding the capability of the MOZART- and NAME-based inverse modeling experiments to produce improved global source-differentiated N_2O emission distributions. This thesis validates the approach developed in Rigby et al. (2012) for use in analyzing N_2O isotopic observations, and shows that regional N_2O emissions estimates can be improved even with isotopic observations from only one observation site. Future experiments that will greatly increase the precision of inputs used within a **global** Bayesian estimation framework, leading to significantly enhanced knowledge of N_2O source distributions, and potential abatement strategies for this potent greenhouse gas.

Bibliography

Acton, S. and Baggs, E.: Interactions between N application rate, CH4 oxidation and N2O production in soil, Biogeochemistry, 103, 15–26, 2011.

Arévalo-Martínez, D., Kock, A., Löscher, C., Schmitz, R., Stramma, L., and Bange, H.: Influence of mesoscale eddies on the distribution of nitrous oxide in the eastern tropical South Pacific, Biogeosciences, 13, 1105–1118, 2016.

Babbin, A., Bianchi, D., Jayakumar, A., and Ward, B.: Rapid nitrous oxide cycling in the suboxic ocean, Science, 348, 1127–1129, 2015.

Bernath, P. F., Yousefi, M., Buzan, E., and Boone, C. D.: A Near-Global Atmospheric Distribution of N2O Isotopologues, Geophysical Research Letters, 44, 10 735–10 743, 2017.

Boering, K. A., Jackson, T., Hoag, K. J., Cole, A. S., Perri, M. J., Theimens, M., and Atlas, E.: Observations of the anomalous oxygen isotopic composition of carbon dioxide in the lower stratosphere and the flux of the anomaly to the troposphere, Geophysical Research Letters, 31, 2004.

Bol, R., Toyoda, S., Yamulki, S., Hawkins, J. M. B., Cardenas, L. M., and Yoshida, N.: Dual isotope and isotopomer ratios of N2O emitted from a temperate grassland soil after fertiliser application, Rapid Commun. Mass Spectrom., 17, 2550–2556, 2003.

Breider, F., Yoshikawa, C., Abe, H., Toyoda, S., and Yoshida, N.: Origin and fluxes of nitrous oxide along a latitudinal transect in western North Pacific: Controls and regional significance, Global Biogeochemical Cycles, 29, 1014–1027, 2015.

Chen, Y. and Prinn, R.: Atmospheric modeling of high- and low-frequency methane observations: Importance of interannually varying transport, J. Geophys. Res., 110, 2005.

CIS: Community Intercomparison Suite, URL `http://www.cistools.net`, 2018.

Clough, T., Addy, K., Kellogg, D. Q., Nowicki, B. L., Gold, A. J., and Groffman, P. M.: Dynamics of nitrous oxide in groundwater at the aquatic–terrestrial interface, Global Change Biology, 13, 1528–1537, 2007.

Croteau, P., Atlas, E. L., Schauffler, S. M., Blake, D. R., Diskin, G. S., and Boering, K. A.: Effect of local and regional sources on the isotopic composition of nitrous oxide in the tropical free troposphere and tropopause layer, Journal of Geophysical Research, 115, 2010.

Cullen, M. J. P.: The Unified Forecast/Climate Model, Meteorol. Mag., 1449, 81–94, 1993.

Demtroeder, W.: Laser Spectroscopy: Basic Principles, Springer-Verlag, Berlin, 4th edn., 2008.

Denk, T. R., Mohn, J., Decock, C., Lewicka-Szczebak, D., Harris, E., Butterbach-Bahl, K., Kiese, R., and Wolf, B.: The nitrogen cycle: A review of isotope effects and isotope modeling approaches, Soil Biology and Biochemistry, 105, 121–137, 2017.

EDGARv4.3.2: EDGAR-Emissions Database for Global Atmospheric Research, URL `https://data.europa.eu/doi/10.2904/JRC_DATASET_EDGAR`, 2018.

Emmons, L., Walters, S., Hess, P., Lamarque, J., Pfister, G., Fillmore, D., Granier, C., Guenther, A., Kinnison, D., Laepple, T., Orlando, J., Tie, X., Tyndall, G., Wiedinmyer, C., Baughcum, S., and Kloster, S.: Description and evaluation of the Model for Ozone and Related Chemical Tracers, version 4 (MOZART-4), Geosci. Model Dev., 3, 43–67, 2010.

Frame, C. H., Deal, E., Nevison, C. D., and Casciotti, K. L.: N2O production in the eastern South Atlantic: Analysis of N2O stable isotopic and concentration data, Global Biogeochemical Cycles, 28, 1262–1278, 2014.

Giltrap, D. L., Li, C., and Saggar, S.: DNDC: A process-based model of greenhouse gas fluxes from agricultural soils, Agriculture Ecosystems and Environment, 136, 292–300, 2010.

Harris, E., Nelson, D., Olszewski, W., Zahniser, M., Potter, K., McManus, B., Whitehill, A., Prinn, R., and Ono, S.: Development of a Spectroscopic Technique for Continuous Online Monitoring of Oxygen and Site-Specific Nitrogen Isotopic Composition of Atmospheric Nitrous Oxide, Analytical Chemistry, 86, 1726–1734, 2014.

Harris, E., Zeyer, K., Kegel, R., Müller, B., Emmenegger, L., and Mohn, J.: Nitrous oxide and methane emissions and nitrous oxide isotopic composition from waste incineration in Switzerland, Waste Management, 35, 135–140, 2015.

Harris, E., Henne, S., Hüglin, C., Zellweger, C., Tuzson, B., Ibraim, E., Emmenegger, L., and Mohn, J.: Tracking nitrous oxide emission processes at a suburban site with semicontinuous, in situmeasurements of isotopic composition, Journal of Geophysical Research: Atmospheres, 122, 2017.

Hintsa, E. J., Boering, K. A., Weinstock, E. M., Anderson, J. G., Gary, B. L., Pfister, L., Daube, B. C., Wofsy, S. C., Loewenstein, M., Podolske, J. R., Margitan, J. J., and

Bui, T. P.: Troposphere-to-stratosphere transport in the lowermost stratosphere from measurements of H2O, CO2, N2O and O3, Geophysical Research Letters, 25, 2655–2658, 1998.

Hirsch, A. I., Michalak, A. M., Bruhwiler, L. M., Peters, W., Dlugokencky, E. J., and Tans, P. P.: Inverse modeling estimates of the global nitrous oxide surface flux from 1998–2001, Global Biogeochemical Cycles, 20, 2006.

Holton, J.: An Introduction to Dynamic Meteorology, Elsevier Academic Press, 4th edn., 2004.

Huang, J., Golombek, A., Prinn, R., Weiss, R., Fraser, P., Simmonds, P., Dlugokencky, E., Hall, B., Elkins, J., Steele, P., Langenfelds, R., Krummel, P., Dutton, G., and Porter, L.: Estimation of regional emissions of nitrous oxide from 1997 to 2005 using multi-network measurements, a chemical transport model, and a Kalman Filter, J. Geophys. Res., 113, 2008.

IPCC: In contribution of Working Group I to the Fourth Assessment Report of the Intergovernmental Panel on Climate Change, Tech. rep., Intergovernmental Panel on Climate Change, 2007.

IPCC: Working Group I Contribution to the Fifth Assessment Report, Tech. rep., Intergovernmental Panel on Climate Change, 2013.

James, P., Stohl, A., Forster, C., Eckhardt, S., Seibert, P., and Frank, A.: A 15-year climatology of stratosphere–troposphere exchange with a Lagrangian particle dispersion model 2. Mean climate and seasonal variability, J. Geophys. Res: Atmos, 208, 2003.

Janssens-Maenhout, G., Crippa, M., Guizzardi, D., Muntean, M., Schaaf, E., Dentener, F., Bergamaschi, P., Pagliari, V., Olivier, J. G. J., Peters, J. A. H. W., van Aardenne, J. A., Monni, S., Doering, U., , and Petrescu, A. M. R.: Global Atlas of the three major Greenhouse Gas Emissions for the period 1970-2012, Earth System Science Data, 2017.

Jones, A. R., Thomson, D. J., Hort, M. C., and Devenish, B.: The U.K. Met Office's nextâĂŘgeneration atmospheric dispersion model, NAME III, pp. 580–589, Air Pollution Modeling and Its Application XVII, Springer, New York, 2007.

Kaiser, J., Brenninkmeijer, C., and Röckmann, T.: Intramolecular 15N and 18O fractionation in the reaction of N2O with O(1D) and its implications for the stratospheric N2O isotope signature, J. Geophys. Res: Atmos, 107, 4214–4227, 2002a.

Kaiser, J., Röckmann, T., and Brenninkmeijer, C.: Temperature dependence of isotope fractionation in N2O photolysis, Phys. Chem. Chem. Phys., 4, 4420–4430, 2002b.

Kaiser, J., Rockmann, T., Brenninkmeijer, C. A. M., and Crutzen, P. J.: Wavelength dependence of isotope fractionation in N2O photolysis, Atmos. Chem. Phys., 3, 303–313, 2003.

Kaiser, J., Engel, A., Borchers, R., and Röckmann, T.: Probing stratospheric transport and chemistry with new balloon and aircraft observations of the meridional and vertical N2O isotope distribution, Atmos. Chem. Phys., 6, 3535–3556, 2006.

Liao, T., Camp, C. D., and Yunt, Y. L.: The seasonal cycle of N2O, Geophysical Research Letters, 31, 2004.

Lunt, M. F., Rigby, M., Ganesan, A. L., and Manning, A. J.: Estimation of trace gas fluxes with objectively determined basis functions using reversible-jump Markov chain Monte Carlo, Geoscientific Model Development, 9, 3213–3229, 2016.

Mandernack, K. W., Mills, C. T., Johnson, C. A., Rahn, T., and Kinney, C.: The Îť15N and Îť18O values of N2O produced during the co-oxidation of ammonia by methanotrophic bacteria, Chemical Geology, 267, 96–107, 2009.

Manning, A., O'Doherty, S., Jones, A., Simmonds, P., and Derwent, R.: Estimating UK methane and nitrous oxide emissions from 1990 to 2007 using an inversion modeling approach, J. Geophys. Res., 116, 2011.

Mathieu, O., Henault, C., Leveque, J., Baujard, E., Milloux, M.-J., and Andreux, F.: Quantifying the contribution of nitrification and denitrification to the nitrous oxide flux using 15N tracers, Environmental Pollution, 144, 933–940, 2006.

McLinden, C. A., Prather, M. J., and Johnson, M. S.: Global modeling of the isotopic analogues of N2O: Stratospheric distributions, budgets, and the 17O–18O mass-independent anomaly, Journal of Geophysical Research, 108, 4233, 2003.

Miller, B., Weiss, R., Salameh, P., Tanhua, T., Greally, B., Mühle, J., and Simmonds, P.: Medusa: A sample preconcentration and GC/MS detector system for in situ measurements of atmospheric trace halocarbons, hydrocarbons, and sulfur compounds., Anal. Chem., 80, 1536–1545, 2008.

Mohn, J., Wolf, B., Toyoda, S., Lin, C., Liang, M., Bruggemann, N., Wissel, H., Steiker, A., Dyckmans, J., Szwec, L., Ostrom, N., Casciotti, K., Forbes, M., Giesemann, A., Well, R., Doucett, R., Yarnes, C., Ridley, A., Kaiser, J., and Yoshida, N.: Interlaboratory assessment of nitrous oxide isotopomer analysis by isotope ratio mass spectrometry and laser spectroscopy: current status and perspectives, Rapid Commun. Mass Spectrom., 28, 1995–2007, 2014.

Morgan, C. G., Allen, M., Liang, M. C., Shia, R. L., Blake, G. A., and Yung, Y. L.: Isotopic fractionation of nitrous oxide in the stratosphere: Comparison between model and observations, Journal of Geophysical Research, 109, 2004.

Nevison, C., Mahowald, N., Weiss, R., and Prinn, R.: Interannual and seasonal variability in atmospheric N2O, Global Biogeochem. Cycles, 21, 2007.

Ogawa, M. and Yoshida, N.: Nitrous oxide emission from the burning of agricultural residue, Atmospheric Environment, 39, 3421–3429, 2005.

Palmer, C. J. and Reason, C. J.: Relationships of surface bromoform concentrations with mixed layer depth and salinity in the tropical oceans, Global Biogeochemical Cycles, 23, 2009.

Park, S., Atlas, E. L., and Boering, K. A.: Measurements of N2O isotopologues in the stratosphere: Influence of transport on the apparent enrichment factors and the isotopologue fluxes to the troposphere, Journal of Geophysical Research, 109, 2004.

Park, S., Perez, T., Boering, K. A., Trumbore, S. E., Gil, J., Marquina, S., and Tyler, S. C.: Can N2O stable isotopes and isotopomers be useful tools to characterize sources and microbial pathways of N2O production and consumption in tropical soils?, Global Biogeochemical Cycles, 25, 2011.

Park, S., Croteau, P., Boering, K., Etheridge, D., Ferretti, D., Fraser, P., Kim, K.-R., Krummel, P., Langenfelds, R., van Ommen, T., Steele, L., and Trudinger, C.: Trends and seasonal cycles in the isotopic composition of nitrous oxide since 1940, Nature Geoscience, 5, 261–265, 2012.

Pérez, T., Trumbore, E., Tyler, S., Matson, P., Ortiz-Monasterio, I., Rahn, T., and Griffith, D.: Identifying the agricultural imprint on the global N2O budget using stable isotopes, J. Geophys. Res: Atmos., 106, 9869–9878, 2001.

Popp, B. N., Westley, M. B., Toyoda, S., Miwa, T., Dore, J. E., Yoshida, N., Rust, T. M., Sansone, F. J., Russ, M. E., Ostrom, N. E., and Ostrom, P. H.: Nitrogen and oxygen isotopomeric constraints on the origins and sea-to-air flux of N2O in the oligotrophic subtropical North Pacific gyre, Global Biogeochemical Cycles, 16, 2002.

Potter, K.: Nitrous oxide (N2O) isotopic composition in the troposphere: instrumentation, observations at Mace Head, Ireland, and regional modeling., Ph.D. thesis, Massachusetts Institute of Technology, 2011.

Potter, K., Ono, S., and Prinn, R.: Fully automated, high-precision instrumentation for the isotopic analysis of tropospheric N2O using continuous flow isotope ratio mass spectrometry, Rapid Commun. Mass Spectrom., 27, 1723–1738, 2013.

Prather, M. J. and Hsu, J.: Coupling of Nitrous Oxide and Methane by Global Atmospheric Chemistry, Science, 330, 952–954, 2010.

Prather, M. J., Hsu, J., DeLuca, N. M., Jackman, C. H., Oman, L. D., Douglass, A. R., Fleming, E. L., Strahan, S. E., Steenrod, S. D., Sovde, O. A., Isaksen, I. S. A., Froidevaux, L., and Funke, B.: Measuring and modeling the lifetime of nitrous oxide including its variability, Journal of Geophysical Research: Atmospheres, 120, 5693–5705, 2015.

Prinn, R.: Measurement Equation for Trace Chemicals in Fluids and Solution of its Inverse, in: Inverse Methods in Global Biogeochemical Cycles, edited by Kasibhatla, P. et al., no. 114 in Geophysical Monograph, pp. 3–18, American Geophysical Union, 2000.

Prinn, R., Weiss, R., Fraser, P., Simmonds, P., Cunnold, D., Alyea, F., O'Doherty, S., Salameh, P., Miller, B., Huang, J., Wang, R., Hartley, D., Harth, C., Steele, L., Sturrock, G., Midgley, P., and McCulloch, A.: A history of chemically and radiatively important gases in air deduced from ALE/GAGE/AGAGE, J. Geophys. Res: Atmos., 105, 17 751–17 792, 2000.

Prinn, R., Weiss, R., Krummel, P., O'Doherty, S., Fraser, P., Muhle, J., Reimann, S., Vollmer, M., Simmonds, P., Maione, M., Arduini, J., Lunder, C., Schmidbauer, N., Young, D., Wang, H., Huang, J., Rigby, M., Harth, C., Salameh, P., Spain, T., Steele, L., Arnold, T., Kim, J., Hermansen, O., Derek, N., Mitrevski, B., and Langenfelds, R.: The ALE / GAGE / AGAGE Network, Tech. rep., Carbon Dioxide Information Analysis Center (CDIAC), Oak Ridge National Laboratory (ORNL), U.S. Department of Energy (DOE), 2016.

Prinn, R. G., Weiss, R. F., Arduini, J., Arnold, T., DeWitt, H. L., Fraser, P. J., Ganesan, A. L., Gasore, J., Harth, C. M., Hermansen, O., Kim, J., Krummel, P. B., Li, S., Loh, Z. M., Lunder, C. R., Maione, M., Manning, A. J., Miller, B. R., Mitrevski, B., Mühle, J., O'Doherty, S., Park, S., Reimann, S., Rigby, M., Saito, T., Salameh, P. K., Schmidt, R., Simmonds, P. G., Steele, L. P., Vollmer, M. K., Wang, R. H., Yao, B., Yokouchi, Y., Young, D., and Zhou, L.: History of chemically and radiatively important atmospheric gases from the Advanced Global Atmospheric Gases Experiment (AGAGE), Earth Syst. Sci. Data, 10, 985–1018, 2018.

Prokopiou, M., Matrinerie, P., Sapart, C. J., Witrant, E., Monteil, G., Ishijima, K., Bernard, S., Kaiser, J., Levin, I., Blunier, T., Etheridge, D., Dlugokencky, E., van de Wal, R. S. W., and Rockmann, T.: Constraining N2O emissions since 1940 using firn air isotope measurements in both hemispheres, Atmos. Chem. Phys., 17, 4539–4564, 2017.

Ravishankara, A., Daniel, J., and Portmann, R.: Nitrous oxide (N2O): the dominant ozone-depleting substance emitted in the 21st Century, Science, 326, 123–125, 2009.

Rigby, M., Manning, A., and Prinn, R.: Inversion of long-lived trace gas emissions using combined Eulerian and Lagrangian chemical transport models, tmos. Chem. Phys., 11, 9887–9898, 2011.

Rigby, M., Manning, A., and Prinn, R.: The value of high-frequency, high-precision methane isotopologue measurements for source and sink estimation, Journal of Geophysical Research, 117, 2012.

Röckmann, T., Kaiser, J., Brenninkmeijer, C., Crowley, J., Borchers, R., Brand, W., and Crutzen, P.: Isotopic enrichment of nitrous oxide (15N14NO, 14N15NO, 14N14N18O) in the stratosphere and in the laboratory, J. Geophys. Res: Atmos., 106, 10 403–10 410, 2001.

Saikawa, E., Prinn, R., Dlugokencky, E., Ishijima, K., Dutton, G., Hall, B., Langenfelds, R., Tohjima, Y., Machida, T., Manizza, M., Rigby, M., O'Doherty, S., Patra, P., Harth, C., Weiss, R., Krummel, P., van der Schoot, M., Fraser, P., Steele, L., Aoki, S., Nakazawa, T., and Elkins, J.: Global and regional emissions estimates for N2O, Atmos. Chem. Phys., 14, 4617–4641, 2014.

Schmidt, J. A. and Johnson, M. S.: Clumped isotope perturbation in tropospheric nitrous oxide from stratospheric photolysis, Geophysical Research Letters, 42, 3546–3552, 2015.

Seinfeld, J. H. and Pandis, S. N.: Atmospheric chemistry and physics: from air pollution to climate change, Wiley, Hoboken, N.J., 2nd edn., URL `http://www.knovel.com/knovel2/Toc.jsp?BookID=2126`, 2006.

Smemo, K. A., Ostrom, N. E., Opdyke, M. R., Ostrom, P. H., Bohm, S., and Robertson, P.: Improving process-based estimates of N2O emissions from soil using temporally extensive chamber techniques and stable isotopes, Nutr. Cycl. Agroecosyst., 91, 145–154, 2011.

Snider, D. M., Schiff, S. L., and Spoelstra, J.: 15N/14N and 18O/16O stable isotope ratios of nitrous oxide produced during denitrification in temperate forest soils, Geochimica et Cosmochimica Acta, 73, 877–888, 2009.

Snider, D. M., Venkiteswaran, J. J., Schiff, S. L., and Spoelstra, J.: Deciphering the oxygen isotope composition of nitrous oxide produced by nitrification, Global Change Biology, 18, 356–370, 2012.

Snider, D. M., Venkiteswaran, J. J., Schiff, S. L., and Spoelstra, J.: A new mechanistic model of d18O-N2O formation by denitrification, Geochimica et Cosmochimica Acta, 112, 102–115, 2013.

Sowers, T., Rodebaugh, A., Yoshida, N., and Toyoda, S.: Extending records of the isotopic composition of atmospheric N2O back to 1800 A.D. from air trapped in snow at the South Pole and the Greenland Ice Sheet Project II ice core, Global Biogeochemical Cycles, 16, 1129, 2002.

Tarantola, A.: Inverse Problem Theory: Methods for Data Fitting and Model Parameter Estimation, Elsevier, 1987.

Toyoda, S., Yoshida, N., Urabe, T., Nakayama, Y., Suzuki, T., Tsuji, K., Shibuya, K., Aoki, S., Nakazawa, T., Ishidoya, S., Ishijima, K., Sugawara, S., Machida, T., Hashida, G., Morimoto, S., and Honda, H.: Temporal and latitudinal distributions of stratospheric N2O isotopomers, Journal of Geophysical Research, 109, 2004.

Toyoda, S., Mutobe, H., Yamagishi, H., Yoshida, N., and Tanji, Y.: Fractionation of N2O isotopomers during production by denitrifier, Soil Biology and Biochemistry, 37, 1535–1545, 2005.

Toyoda, S., Yamamoto, S.-I., Arai, S., Nara, H., Yoshida, N., Kashiwakura, K., and Akiyama, K.-I.: Isotopomeric characterization of N2O produced, consumed, and emitted by automobiles, Rapid Commun. Mass Spectrom., 22, 603–612, 2008.

Toyoda, S., Kuroki, N., Yoshida, N., Ishijima, K., Tohjima, Y., and Machida, T.: Decadal time series of tropospheric abundance of N2O isotopomers and isotopologues in the Northern Hemisphere obtained by the long-term observation at Hateruma Island, Japan, J. Geophys. Res.: Atmos., 118, 3369–3381, 2013.

Wang, D., Gruen, D. S., Lollar, B. S., Hinrichs, K.-U., Stewart, L. C., Holden, J. F., Hristov, A. N., Pohlman, J. W., Morrill, P. L., Könneke, M., Delwiche, K. B., Reeves, E. P., Sutcliffe, C. N., Ritter, D. J., Seewald, J. S., McIntosh, J. C., Hemond, H. F., Kubo, M. D., Cardace, D., Hoehler, T. M., and Ono, S.: Nonequilibrium clumped isotope signals in microbial methane, Science, 348, 428–431, 2015.

Whalen, M. and Yoshinari, T.: Oxygen isotope ratios in N2O from different environments, Nature, pp. 780–782, 1985.

Wofsy, S. C., Boering, K. A., Daube, B. C., and McElroy, M. B.: Vertical transport rates in the stratosphere in 1993 from observations of CO2, N2O and CH4, Geophysical Research Letters, 21, 2571–2574, 1994.

Yamagishi, H., Westley, M., Popp, B., Toyoda, S., Yoshida, N., Watanbe, S., Koba, K., and Yamanaka, Y.: Role of nitrification and denitrification on the nitrous oxide cycle in the eastern tropical North Pacific and Gulf of California, J. Geophys. Res.: Biogeosci, 112, 2007.

Yamulki, S., Toyoda, S., Yoshida, N., Veldkamp, E., Grant, B., and Bol, R.: Diurnal fluxes and the isotopomer ratios of N2O in a temperate grassland following urine amendment, Rapid Commun. Mass Spectrom., 15, 1263–1269, 2001.

Yano, M., Toyoda, S., Tokida, T., Hayashi, K., Hasegawa, T., Makabe, A., Koba, K., and Yoshida, N.: Isotopomer analysis of production, consumption and soil-to-atmosphere emission processes of N2O at the beginning of paddy field irrigation, Soil Biology and Biochemistry, 70, 66–78, 2014.

Yoshida, N. and Matsuo, S.: Nitrogen isotope ratio of atmospheric N2O as a key to the global cycle of N2O, Geochemical Journal, 17, 231–239, 1983.

Appendix A

Community Intercomparison Suite

The Community Intercomparison Suite (CIS) (CIS, 2018) is an open-source tool written in Python by a team at the University of Oxford for combining disparate types of Earth Science data into one framework through various 3-D aggregation and co-location algorithms. The CIS tool can use input data from point sources (ground stations), 2-D and 3-D satellite retrievals, and 3-D "gridded" model outputs.

As part of the ACES (Advanced Computing in Earth Sciences) educational/research program sponsored by NASA and the University of Virginia, I used CIS extensively in a summer at NASA Goddard Space Flight Center (GSFC) with Dr. Charles Ichoku to simulate expected flight-based atmospheric data by interpolating data from satellite retrievals and chemical transport models onto flight tracks. This experiment was in anticipation of a future survey of air quality in West Africa, but the concepts from that experiment are equally applicable to help understand expected high-altitude N_2O isotopic measurements in a future flight campaign.

A.1 Simulation of Flight Data in West Africa

The data presented below show the power of CIS to create timelines of atmospherically relevant chemical species (black carbon and aerosol optical depth; Figures A-2 and A-3) that would be expected on a flight-based experiment in West Africa (Figure A-1), using satellite retrievals and three-dimensional model results as the underlying data sources.

The ability to convert a three-dimensional path of a plane into a timeline of expected chemical and physical measurements on board allows for many operational benefits in planning a future flight-based atmospheric experiment. Using the MOZART-4 model results from Chapter 5, one could construct a timeline of expected N_2O isotopic ratio observations that would be made from flasks aboard an operationally feasible flight track (as determined

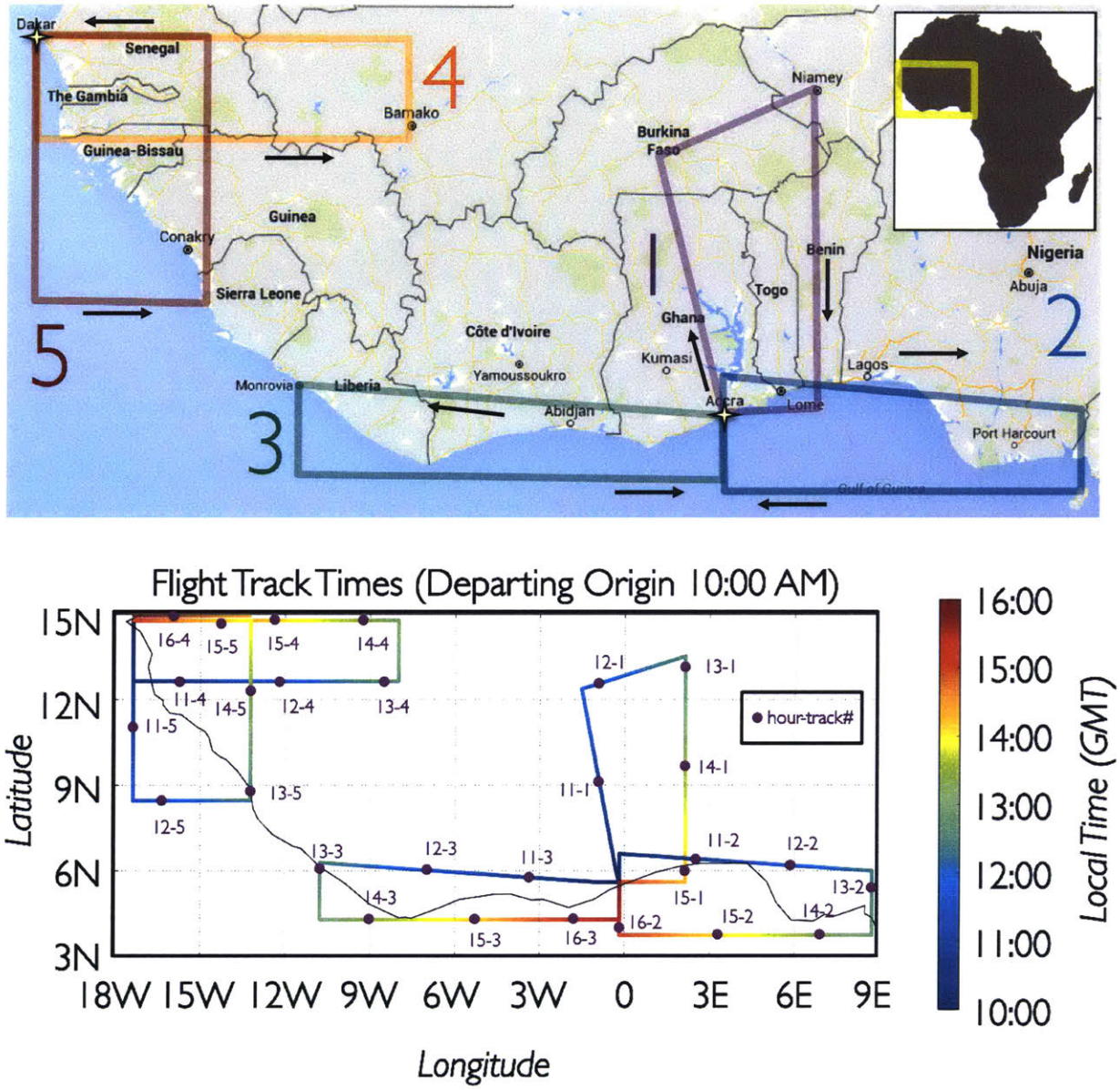

Figure A-1: Hypothetical flight tracks for a flight experiment on air quality in West Africa

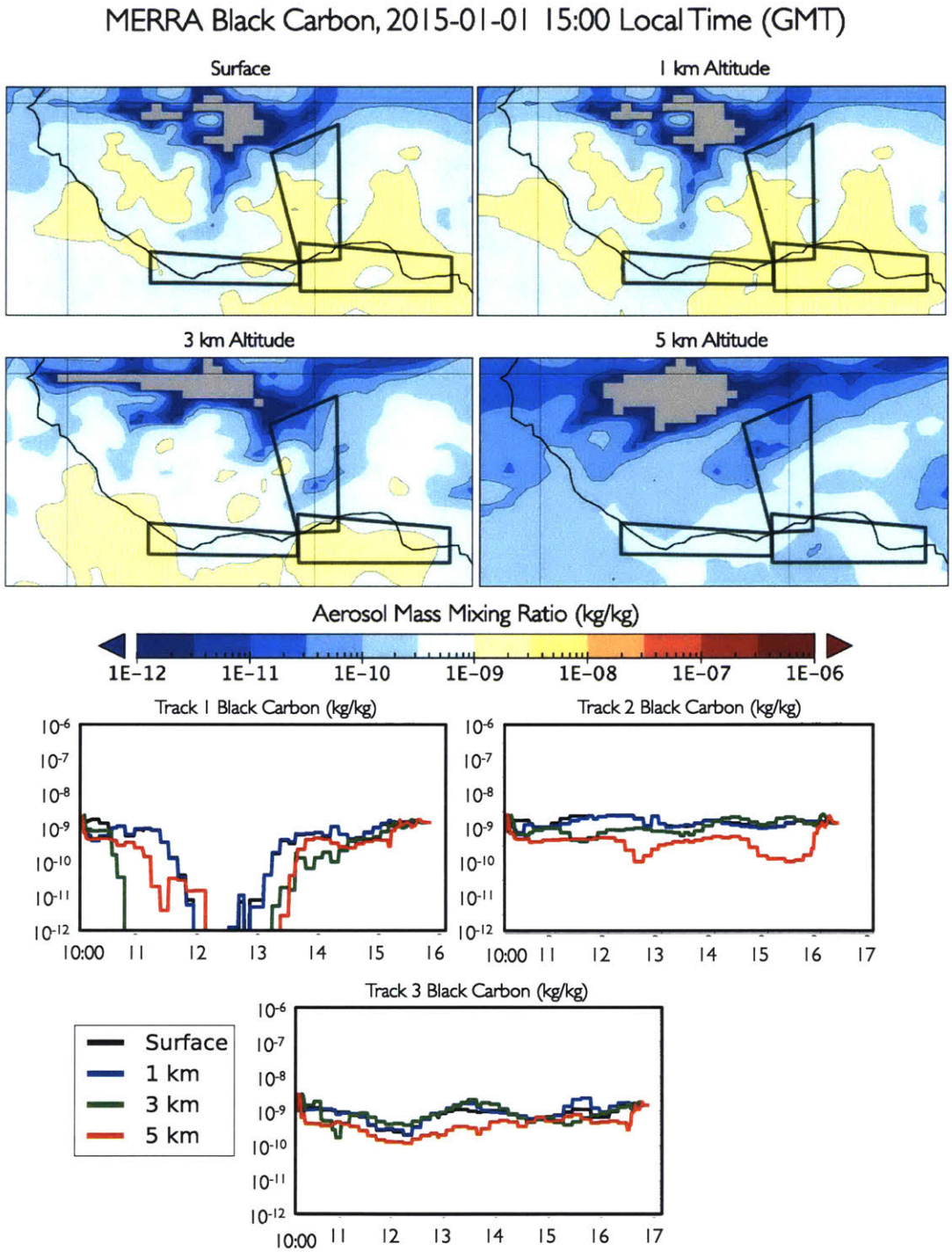

Figure A-2: Black carbon mass concentration timelines for flight tracks 1-3 at four altitudes on January 1 2015, as interpolated from MERRA black carbon fields

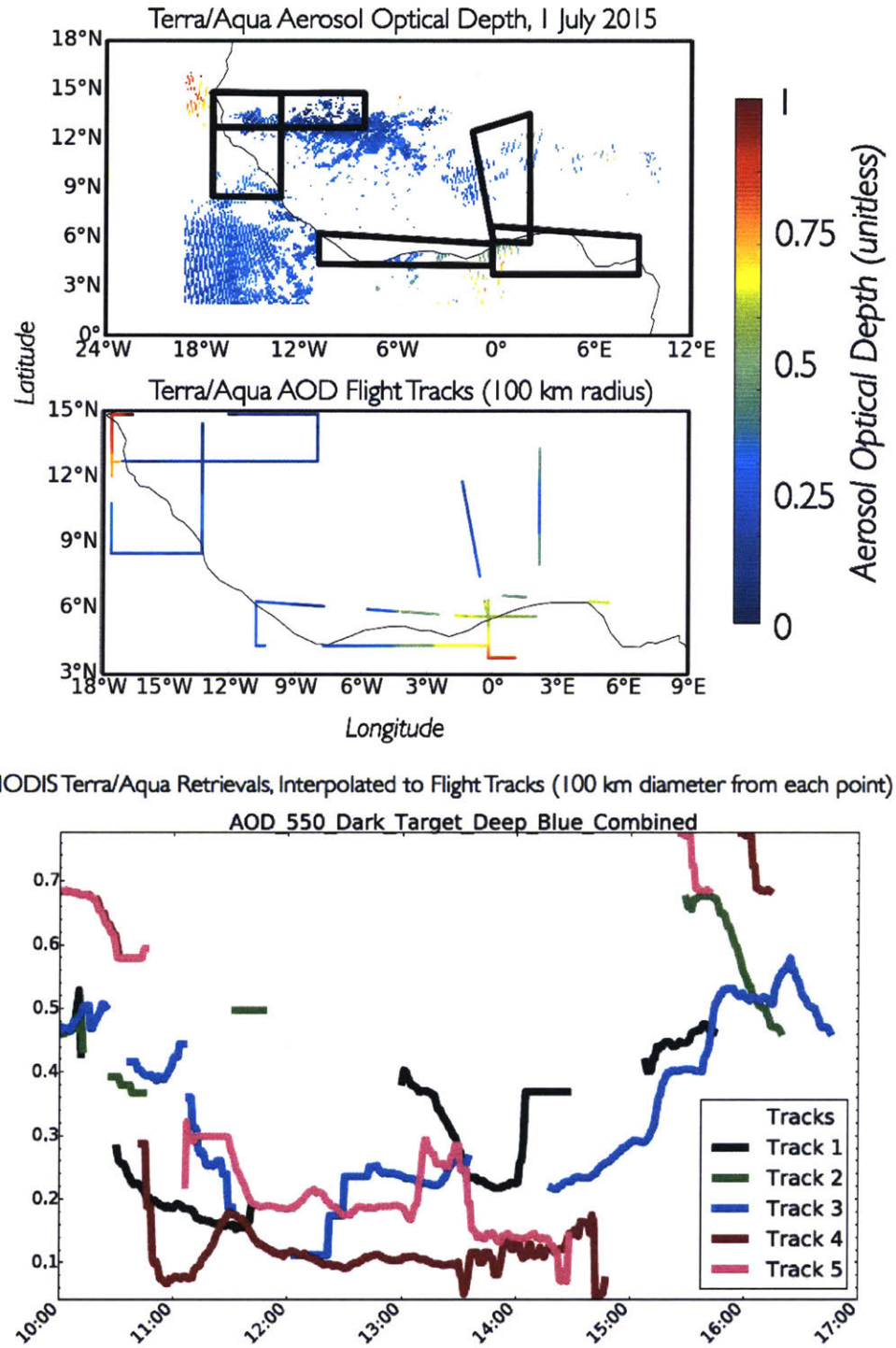

Figure A-3: Aerosol optical depth timelines for flight tracks 1-5 on July 1 2015, as interpolated from Terra/Aqua column satellite retrievals

by collaborators such as Dr. Jim Elkins at NOAA). While the global chemical transport modeling experiments with MOZART-4 would not conclusively be able to determine ahead of time the locations in which the most scientifically interesting N_2O isotopic features could be found, the general sense of latitude and altitude combinations from an exploratory analysis using CIS and MOZART-4 model output could help identify the areas statistically most likely to yield observations that could help constrain various aspects of the global N_2O earth system (similar to an OSSE, or Observing System Simulation Experiment).

Appendix B

Inversion by Source Sector Isotopic Signature

For any of the sectors being optimized with inclusion of N_2O isotopic ratio observations, large shifts from prior to posterior emissions estimates could be due to unrealistic *a priori* N_2O isotopic ratio "signatures" used in the simulation. In addition, spatial overlap could blend contributions from multiple sectors. For example, when there are large adjustments to natural soil and agricultural emissions in an inversion (Chapter 6), it could also indicate a mis-assignment of soil-based emissions as "agricultural" vs. "natural" due to their similar spatial distributions and similar isotopic signatures (as seen in the overlap in Figure 2-6).

As discussed in Chapter 6, the best way to constrain N_2O isotopic source signatures is to conduct intensive *in situ* and laboratory-based experiments in which relatively undiluted N_2O directly emitted from sources is sampled. However, there are still opportunities for a long-term observation experiment to provide data that could help constrain the source signatures implemented in models of the N_2O earth system.

B.1 Inversion Setup

As mentioned above, the best way to increase the precision of source-specific isotopic signatures is to make measurements of relatively pure N_2O near the sources, as previously published for many different source sectors. This initial setup for an inverse modeling experiment will use Stheno-TILDAS isotopic ratio observations alone to constrain the mean N_2O source signatures for the EDGAR sources described in Harris et al. (2017), plus natural and oceanic emissions (listed in 6.1).

In this experiment, the variables in the cost function to be minimized (Figure 6-1) are as follows:

- n: number of Stheno-TILDAS observations used
- m: number of emissions sources being perturbed (13; all EDGAR sources plus natural and oceanic emissions)
- $\mathbf{y}$ ($3n$ x 1): "raw" isotopic ratios (Figure 2-4) R_{456}, R_{546}, and R_{448} at each Stheno-TILDAS time point
- $\mathbf{H}$ ($3n$ x $3m$): sensitivity of isotopic ratio observations $\mathbf{y}$ to source isotopic signatures $\mathbf{x}$, created by perturbing each isotopic signature for each of the 12 sources by $\pm$ 10% and looking for linear response
- $\mathbf{x}$ ($3m$ x 1): each of three isotopic ratio signatures for all 12 sources; trying to optimize this variable
- $\mathbf{R}$ ($3n$ x $3n$): Combined uncertainty in data (measurements and model, as discussed pertaining to Equation 6.5, with the σ_{SIR} uncertainty replaced by a σ_{emis} variable in which the uncertainty bounds of the total emissions estimates for each source provide error as opposed to the source isotopic ratios being optimized), as diagonal on a sparse square matrix
- $\mathbf{x}_{prior}$ ($3m$ x 1): prior estimate of isotopic ratio signatures from each sector, from Harris et al. (2017) and the previous chapter
- $\mathbf{P}$ ($3m$ x $3m$): Uncertainty in each isotopic ratio signature for all 12 sources, as diagonal on a sparse square matrix (more on uncertainty below)

Results

Not surprisingly, the optimized isotopic ratios from this inversion are mostly quite close to the average EDGAR isotopic signatures calculated in Harris et al. (2017). In fact, the biomass burning sector, not shown in Figures B-1 and B-2, shows exactly zero change in the optimized isotopic signature and features vanishingly small uncertainty reduction. For all 12 source sectors pictured in Figures B-1 and B-2, the uncertainty in the estimates for isotopic signatures within the NAME Europe domain are modestly reduced. Three sectors stand out for having a significant change in the isotopic signature: AGSOIL, OCEAN, and NATURAL.

The fact that the natural soil emissions isotopic signature is optimized to be significantly more depleted, thereby bringing it closer to the average values of agricultural soil (which is also more depleted in all three positions for this inversion), aligns with a potential overlap of agricultural and natural emissions. Future investigation of this overlap could help separate the contributions from each sector. However, an inversion in which source signatures and sector emissions magnitudes are simultaneously optimized would entail a significantly more computationally expensive NAME-MOZART inverse framework, and the need for more extensive long-term N_2O isotopic observation at Mace Head would become significantly more apparent in order to further constrain any of the various emissions parameters.

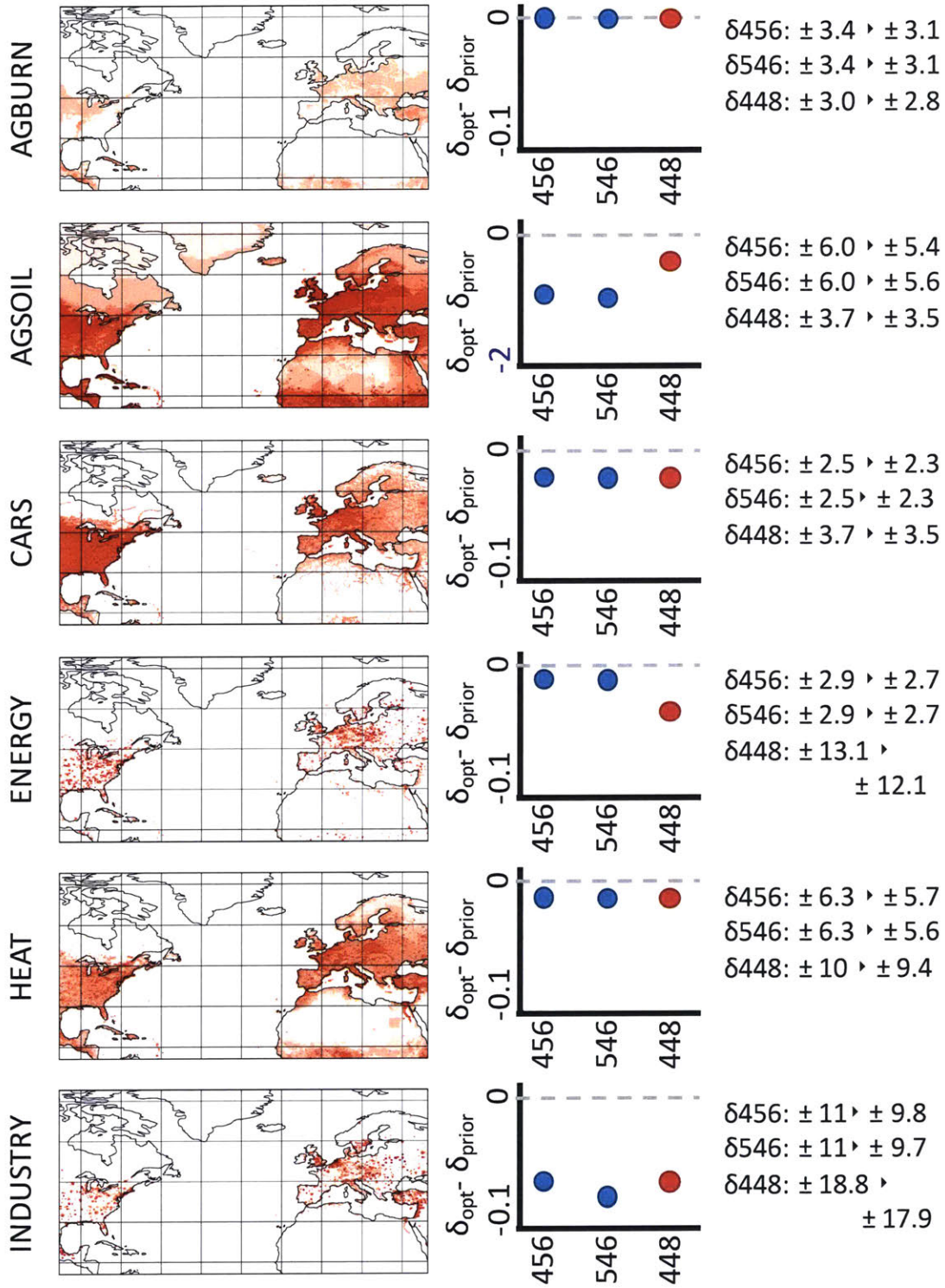

Figure B-1: Changes in isotopic signature "delta values" for EDGAR/ocean/natural sectors over the entire Stheno-TILDAS observation period, with uncertainty reduction from prior to optimized estimates (Part 1)

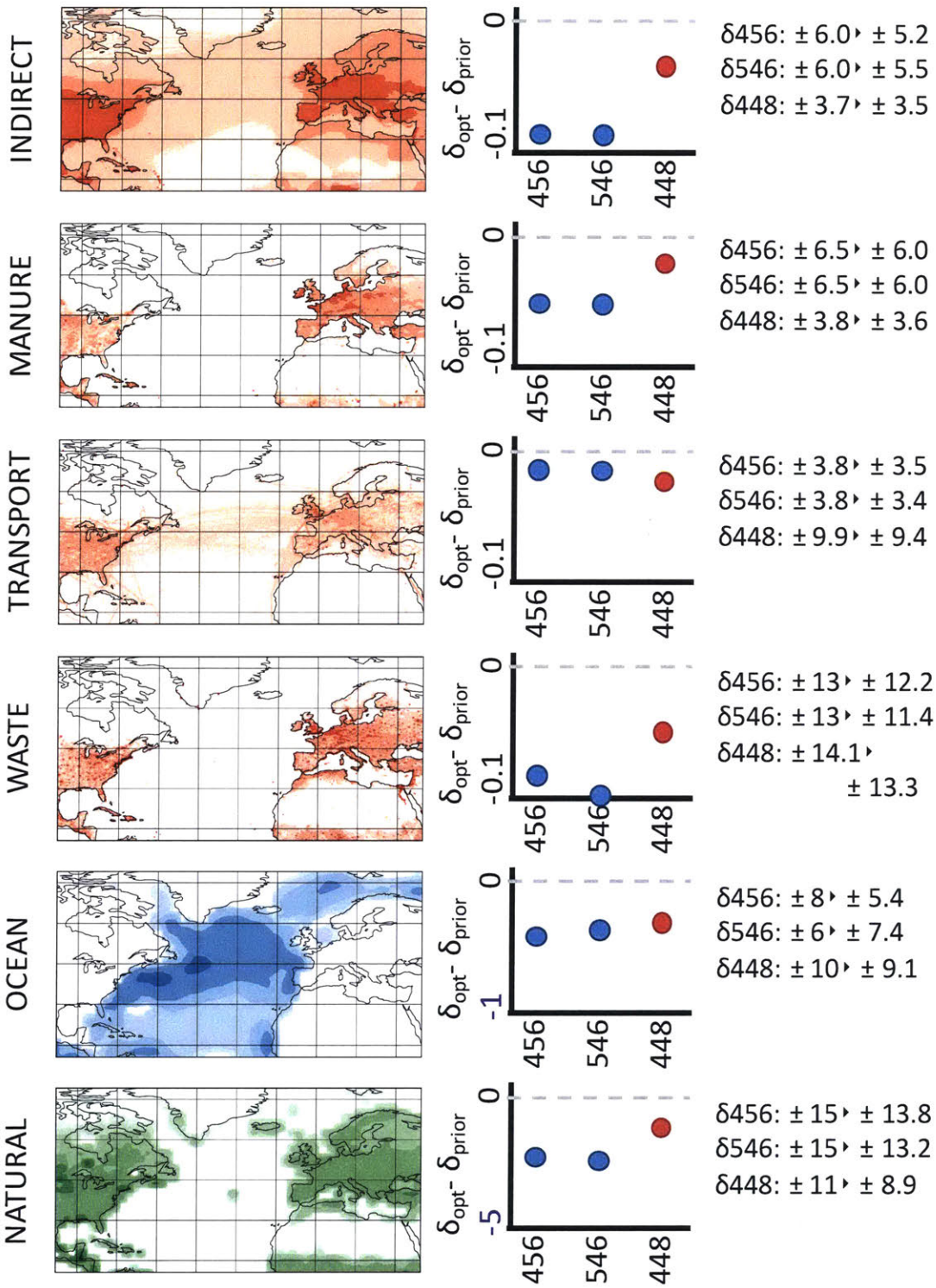

Figure B-2: Changes in isotopic signature "delta values" for EDGAR/ocean/natural sectors over the entire Stheno-TILDAS observation period, with uncertainty reduction from prior to optimized estimates (Part 2)